Geometry and Supersymmetry in Type II String Theory

Dissertation zur Erlangung des Grades
"Doktor der Naturwissenschaften"

am Fachbereich Physik, Mathematik und Informatik
der Johannes Gutenberg-Universität in Mainz

Isabel Koltermann
geboren in Mainz

Mainz, den 24. Mai 2016

Datum der mündlichen Prüfung: 22. Juli 2016

Abstract

My thesis is associated with the field of D6-brane model building in type IIA string theory, where the fractional D6-brane stacks are wrapped on special Lagrangian cycles in backgrounds of factorisable toroidal orientifolds $T^6/(\mathbb{Z}_2 \times \mathbb{Z}_{2M} \times \Omega\mathcal{R})$ with $2M = 2, 6, 6'$ and with discrete torsion. I develop an explicit formalism for complex structure deformations of the $\mathbb{Z}_2$ orbifold singularities and observe how the volumes of the special Lagrangian cycles change under deformations. I show that, depending on the concrete model, this procedure can be used to stabilise several or all twisted complex structure moduli, or that, alternatively, the sizes of gauge couplings can be varied.

As a starting point, I introduce the orientifold $T^6/(\mathbb{Z}_2 \times \mathbb{Z}_2 \times \Omega\mathcal{R})$ on square torus lattices, now expressed as hypersurface in a complex weighted projective space. I demonstrate the process of concrete deformations and discuss how explicit volumes of fractional cycles, bulk cycles, and exceptional cycles can be computed. These can be used to determine physical quantities like gauge couplings. My investigations also show if the cycles keep their special Lagrangian property under deformations. After that, I present the orientifold $T^6/(\mathbb{Z}_2 \times \mathbb{Z}_6' \times \Omega\mathcal{R})$ with underlying hexagonal tori, which is very interesting for model building with intersecting D6-brane stacks. For the concrete construction, I start again with $T^6/(\mathbb{Z}_2 \times \mathbb{Z}_2 \times \Omega\mathcal{R})$ and mod out an additional $\mathbb{Z}_3$ symmetry by hand, which implies that the deformation parameters are organised in $\mathbb{Z}_3$ and $\Omega\mathcal{R}$ invariant orbits. In this setup, new technical difficulties arise. In addition, I show first results for the phenomenologically very appealing orientifold $T^6/(\mathbb{Z}_2 \times \mathbb{Z}_6 \times \Omega\mathcal{R})$ on one rectangular and two hexagonal tori, whose underlying structure is much more complicated than in the previous examples. Hence, so far only local descriptions were found.

In concrete models, there exist stacks of N coincident D6-branes, wrapped on fractional cycles, which carry gauge groups $SO(2N)$, $USp(2N)$, and/or $U(N)$. I show that, depending on the model, the impact of the deformations can be divided into three different cases. Firstly, the brane stack does not couple to a certain deformation, which gives rise to a flat direction in the moduli space. Secondly, the branes couple only to the orientifold-even part of the deformed exceptional cycle, but not to the orientifold-odd part, in which case one can adjust the corresponding gauge couplings by changing the volume of the exceptional cycle. Thirdly, if the brane stack couples to the orientifold-odd part, one finds that the respective complex structure modulus is stabilised, which is a desirable property to find a unique vacuum. For D6-branes with $SO(2N)$ or $USp(2N)$ gauge group, by construction all orientifold-odd contributions are zero and no moduli are stabilised. On the other hand, in a Pati-Salam model with three particle generations and only $U(N)$ gauge groups all three cases can be observed, and actually ten out of 15 complex structure moduli can be stabilised at the orbifold point.

Contents

1   Introduction

The Standard Model of particle physics, which describes the fundamental particles of nature and their gauge interactions, includes three of the four fundamental forces of nature, i.e. the electromagnetic, the weak, and the strong force, and agrees with experiment up to very high precision [1, 2]. On the other side, the Standard Model has of the order of twenty free parameters, which have to be adjusted by hand, and gravity is not included. Hence, one is searching for a fundamental theory of quantum gravity, which is not only able to provide a unified framework, but also a deeper understanding of the underlying principles of nature. This search is furthermore motivated by the historical fact that the unification of theories always provided a more profound understanding. Among the most famous examples for that are the unification of the electric and magnetic force at the end of the 18th and beginning of the 19th century, with a major contribution by Maxwell in 1861 [3], or the unification that gave rise to the electroweak force in the late 1960s, for which Glashow [4], Salam [5], and Weinberg [6] received the Nobel Prize in Physics in 1979.

The best candidates so far for a theory of quantum gravity are the so-called superstring theories (see e.g. the more recent text books [7–10] for a comprehensive introduction), which are conjectured to be certain perturbative limits of an underlying even more fundamental (unique) theory, called M-theory [11]. The different superstring theories are connected by (partly conjectured and partly proven) dualities, and they incorporate supersymmetry as an underlying principle. They are only consistent in ten space-time dimensions, while M-theory and the associated supergravity theory (i.e. a supersymmetric version of general relativity that is also considered as the low-energy approximation to M-theory) live in eleven space-time dimensions.

Hence, all these theories have to be effective theories in the four-dimensional Minkowski space-time, and this can be achieved by "curling up" the six (or seven) extra dimensions into a compact space of tiny size. The mechanism that is used for the compactification is actually much older and was already developed by Kaluza and Klein in the 1920s [12, 13]. Inside the ten (or eleven) dimensions live closed and open strings with different properties, depending on the superstring theory that is considered. Their size, which is called the string length l_s (and which is at least of the order of the the Planck length l_P, see equation (1.1) below), is in fact the only dimensionful parameter in string theory. The oscillation modes of the strings give rise to the particle spectrum that can be observed in the four large space-time dimensions. These two characteristics imply that not only the free parameters of the Standard Model can in principle be fixed by geometrical properties, but also that gravity is naturally included, namely by the oscillation mode of a closed string.

The very first beginnings of string theory go back to the late 1960s and early 1970s, with e.g. the articles of Veneziano [14], Virasoro [15], Shapiro [16], Neveu and Schwarz [17, 18], and Ramond [19], where string theory was still believed to be a theory of strong interactions. Nevertheless, the mathematical formalism that was developed those days is the basis for all modern (super-)string theories, though they are now used in a somewhat different context. At the end of the seventies, after the articles of Scherk and Schwarz [20], and of Yonega [21] had appeared, it was realised that the low-energy behaviour of string amplitudes is in fact related to higher-dimensional gauge theories and gravity. This also implies that the characteristic length scale of strings should be at the order of (or slightly above) the Planck length l_P, defined as

$$l_P = \sqrt{\frac{\hbar G}{c^3}} \approx 1.616 \times 10^{-35} \text{m} \,. \tag{1.1}$$

This quantity is composed of fundamental physical constants that should appear in a theory of quantum gravity, namely the reduced Planck constant $\hbar$, the gravitational constant G, and the speed of light in vacuum c. Starting from this point, string theory became a promising candidate for the unification of quantum field theory and gravity.

In 1985, Green and Schwarz found a mechanism to cancel certain gauge and gravitational anomalies [22], which makes it possible to construct realistic string models that incorporate chiral matter. This discovery cleared the way to develop the framework of the three superstring theories called $E_8 \times E_8$ heterotic, $SO(32)$ heterotic, and type I (cf. [23] and the two text book volumes [24] and [25]), and many physicists started working in this field. In addition, the two superstring theories called type IIA and type IIB were already known, but the time was not yet ripe for model building in these theories.

The compactification of the six extra dimensions of these superstring theories was mathematically realised in form of Calabi-Yau manifolds [23], which I will introduce in detail in section 2.1. In particular, the two heterotic string theories were strongly developed these years, see for example [26], [27], and [28]. They are made of only closed *oriented* strings supporting the gauge groups $E_8 \times E_8$ or $SO(32)$, respectively. On the other hand, the type I string theory follows a different construction, which means that it incorporates *non-oriented* closed and open strings (i.e. the two orientations are identified), where the open strings come with a gauge group $SO(32)$. At the end of the 80s, also first models on strings on orbifolds appeared [29–35], see section 2.4 for more details about orbifolds.

Roughly ten years later, one can again set an important milestone in the development of string theory. At this point, people understood that, in fact, the five different superstring theories are related by so-called dualities [11], parts of which are closely related to the concept of mirror symmetry [36]. As already mentioned, this gave rise to the conjecture that

all five superstring theories are only different parts of a larger eleven-dimensional theory with the name M-theory [37]. In addition, it was discovered that the type IIA and type IIB string theories also involve higher-dimensional dynamical objects called Dp-branes [38–41]. These Dp-branes play a major role in both type IIA and type IIB string theories (and are also present in type I string theories), and will be introduced in section 3.2.2. They are defined as lower-dimensional subspaces in ten-dimensional space-time on which open strings end, and are therefore dynamical objects themselves. The observation that Dp-branes which intersect at generic angles can give rise to chiral fermions [42], residing at the intersection point, turned the type II string theories into an interesting playground for model building.

In addition, one introduces the non-dynamical Op-planes, which are called orientifold planes, and which have the effect that half of the particle spectrum is divided out. Models including both Dp-branes and Op-planes are called orientifold models. While one finds already first attempts of this kind starting in 1995 [43], it took several years to develop the full formalism of intersecting D-brane models [44–46], see also the models on specific orbifold backgrounds further down. Since then, people have constructed loads of orientifold models with intersecting D-branes, for which e.g. the article [47] provides a pedagogical introduction. Additionally, the more recent text books mentioned at the beginning of this chapter, the review article [48] or the review article [41] concentrating on the CFT framework can be consulted for more details.

For string theory, supersymmetry is always a desirable property because it ensures the stability of the models. Indeed, the first chiral *supersymmetric* model was published in 2001, for which a setup of $T^6/(\mathbb{Z}_2 \times \mathbb{Z}_2)$ type IIA orientifolds with D-branes intersecting at angles was used, cf. [49] and also [50] for a short overview. For my own work, I will use a similar setup, and therefore the concrete specifications of the $T^6/(\mathbb{Z}_2 \times \mathbb{Z}_2)$ orbifold and the additional orientifold action $\Omega\mathcal{R}$ will be discussed in section 3.1. Nevertheless, also non-supersymmetric models exist, which are very appealing at first sight since one can easily find spectra with amazing similarity to the standard model [51], but a closer look reveals their severe stability problems, see e.g. [52].

In [53], the authors demonstrated that in type II string theories the Calabi-Yau manifolds and the orbifolds, which are singular limits thereof, agree in terms of their topological properties. Thus, in the following years, many people constructed models in a similar manner as [49] on different kinds of so-called toroidal orbifolds (i.e. orbifolds where the basic objects are tori). For instance, model building on the $T^6/\mathbb{Z}_4$ orientifold [54] and on $T^6/\mathbb{Z}_6^{(\prime)}$ [55–62] was studied, but also $T^6/(\mathbb{Z}_N \times \mathbb{Z}_M)$ [63], $T^6/(\mathbb{Z}_4 \times \mathbb{Z}_2)$ [64], and orientifolds with the group $\mathbb{Z}_{12}$-II [65] were under consideration. Recently, also the $T^6/(\mathbb{Z}_2 \times \mathbb{Z}_6^{(\prime)})$ orientifolds were analysed in the context of semi-realistic model building [66–70], and more

details (like model building rules and consistency conditions, or the spectrum) of the models on $T^6/(\mathbb{Z}_2 \times \mathbb{Z}_2 \times \Omega\mathcal{R})$ [71] and on $T^6/(\mathbb{Z}_2 \times \mathbb{Z}_{2M} \times \Omega\mathcal{R})$ with discrete torsion [66] were derived. The concept of discrete torsion was first pointed out already in the late 80s [72, 35], and will reappear in section 3.1. In fact, to my best knowledge there exists only one article by Palti [73], where a setup similar to the one that is used in my thesis is presented, i.e. a global model with intersecting D6-branes wrapped on so-called *special Lagrangian* (*sLag*) submanifolds, cf. section 3.1.3, with embeddings into weighted projective spaces, see sections 2.2.3 and 2.2.4. An introduction to the mathematical formalism of special Lagrangian geometry can be found e.g. in [74], or in the shortened version [75].

In fact, in string theory there exist millions of consistent string vacua, which is known as the string theory landscape [76–79]. These are parametrised by flat directions of the dilaton and of geometric moduli, see section 3.2, which can be used to tune the parameters for the strengths of gauge and gravitational interactions, but on the other hand, these fields must obtain fixed values to find a unique vacuum. Hence, it is crucial to find mechanisms for (partial) moduli stabilisation. Over the years, many ways were considered, such as closed string background fluxes in type II orientifolds, which have the problem of back-reactions on the geometry (i.e. the compactified space is not Calabi-Yau or some singular limit thereof anymore), see the review article [80], and [81–83] for type IIA and type IIB orientifolds on T^6.

A different ansatz for moduli stabilisation are the so-called blow-ups or resolutions of orbifold singularities, which are very well-known in the literature, see for instance [36, 84–86], and also [87, 88], which are among the first articles with the subject of resolution of orbifold singularities in string theory. Applications of blow-ups in type IIB orientifold models can be found e.g. in the articles [89–91]. Furthermore, blow-ups in $T^6/(\mathbb{Z}_2 \times \mathbb{Z}_2)$ orientifolds *without* discrete torsion are described in [92], which are closely related to the $T^6/(\mathbb{Z}_2 \times \mathbb{Z}_2)$ orientifolds *with* discrete torsion, which I will use later for my concrete constructions. More recently, also blow-ups in heterotic orbifolds were considered, and complete resolutions of the singularities for all factorisable orbifolds could be realised [93–97]. An extensive analysis of the possible resolutions of toroidal orbifold models in heterotic string theory can be found in [98]. The formalism for blow-ups in heterotic orbifolds used in these papers has the same basic ideas as the ones that I will use here, but the concrete realisation looks quite different, in particular the mechanism to smoothen a singularity is not the same. Also with blow-ups the so-called Kähler moduli are stabilised, while in my thesis I will make use of complex structure moduli, cf. section 2.6.

The method for moduli stabilisation in type IIA string theory that I will apply is based on the auxiliary fields called D, which appear in supersymmetric theories in the vector multiplets [99]. These fields contribute to the scalar potential, which determines the ground

state of the theory, and can give rise to Fayet-Iliopoulos terms, which correspond to vacuum expectation values (*vev*s) of the massless moduli fields. From this follows that supersymmetry is broken unless the *vev* is zero, and hence the moduli are stabilised, see for instance the review articles [48, 53], or the text books presented at the beginning of this chapter. In fact, the idea to break supersymmetry via non-vanishing Fayet-Iliopoulos terms is not new, and there exist even text books only on this subject [100, 101]. For heterotic or type I string theory models, see e.g. [102, 103], and there also exist articles about complex structure deformations in heterotic orbifolds using F-terms [104–107]. However, the mechanisms used in these models are completely different from the one I will use here.

More concretely, the starting point here is the method that was sketched in [108], but which (to my best knowledge) was neither analysed further nor applied to concrete setups. Therefore, me and my collaborators, my supervisor Jun.-Prof. Dr. Gabriele Honecker and Dr. Michael Blaszczyk, were the first ones to study moduli stabilisation via complex structure deformations on *sLag* cycles of type IIA orientifolds models, in particular on the $T^6/(\mathbb{Z}_2 \times \mathbb{Z}_2 \times \Omega\mathcal{R})$ orientifold with discrete torsion [109], published in 2014, and on the technically more complicated orientifold $T^6/(\mathbb{Z}_2 \times \mathbb{Z}_6' \times \Omega\mathcal{R})$ with discrete torsion [110]. Additionally, based on my poster presentation, we contributed to the proceedings of "The String Theory Universe, 21st European String Workshop and 3rd COST MP1210 Meeting" in 2015 [111].

Though my thesis is based on the joint work of me and my collaborators [109–111], the content that I present here is oriented on my own contribution, for which I will give much more details on the concrete calculations compared to our publications. On the other hand, parts of our joint work in which I was not much involved, will be kept rather short and I will refer at the corresponding places to our respective article. In the conclusions (chapter 6), where I also summarise the findings of my work, I will point out in detail my personal contributions to our research that appeared in the publications [109–111]. I also revised and reordered our findings to create a consistent framework, which will make it easier to apply our results to different setups in the future. Additionally, I developed in my thesis some new tools to visualise the process of the deformations, which provide a better understanding of its structure. I will also present my first new results for deformations on the $T^6/(\mathbb{Z}_2 \times \mathbb{Z}_6 \times \Omega\mathcal{R})$ orientifold with discrete torsion, which are supposed to lead to a further publication [112]. This orientifold setup exhibits some unexpected technical difficulties, which prevented us so far from finding a global description. However, I could already study the local behaviour of the singularities under complex structure deformations and compute the volumes of some concrete D6-branes in this setup.

The structure of my thesis is as follows: In chapter 2, I review known facts of the mathematical literature that are important for the understanding of the following discussion. Here

I introduce complex manifolds and especially Calabi-Yau manifolds in detail, which are the underlying geometric objects for string theory compactifications. I discuss some relevant examples thereof and explain the mathematical language of hypersurfaces in weighted projective spaces in general and the application to two-tori T^2 in particular, which will be expanded to descriptions of certain toroidal orbifolds in chapter 4. This hypersurface language is necessary when deformations of one or several orbifold singularities are involved, and it provides the possibility to perform concrete calculations of certain physical quantities. Thereafter, I touch on orbifolds in general and postpone a more detailed explanation to section 3.1.1, where my specific orbifold setup is presented. Finally, the concepts of homology and cohomology are discussed, which give rise to the notions of Kähler and complex structure moduli together with the idea of metric deformations.

Chapter 3 gives an overview over the setup in string theory, where I collect the relevant definitions and explanations from different articles and books dealing with string theory. In the first part, I speak about the pure geometry which I impose on the internal six-dimensional space of type IIA string theory. I introduce the (factorisable) toroidal orbifolds $T^6/(\mathbb{Z}_2 \times \mathbb{Z}_{2M})$ with $2M = 2, 6, 6'$ and explain the geometrical effect when the additional symmetry $\Omega\mathcal{R}$ is introduced, which turns the just mentioned orbifolds into orientifolds. On these orientifolds, one can consider certain lower-dimensional closed subspaces, called cycles, which should at this point already be familiar to the reader from section 2.5 about homology. These cycles, especially the so-called *special Lagrangian (sLag)* cycles, are the geometrical objects on which the aforementioned Dp-branes are wrapped and which play a major role throughout my thesis.

In chapters 4 and 5 I present my own work. Chapter 4 treats Lagrangian cycles and their deformations, where at first I discuss which characteristics the *(s)Lag* cycles introduced before have when described in terms of the aforementioned hypersurface language. As a warm-up, I consider in the following section local deformations on the non-compact orbifolds $\mathbb{C}^2/\mathbb{Z}_2$ and $\mathbb{C}^3/(\mathbb{Z}_2\times\mathbb{Z}_2)$, and I explain which *special Lagrangian (sLag)* cycles appear. After that, I come to toy models on $T^4/\mathbb{Z}_2$ orbifolds, where the hypersurface language is applied to orbifolds and where the characteristics of deformations of orbifolds become apparent. These toy models reappear later as certain special cases when deformations on T^6 orbifolds are discussed. The following section treats deformations of $T^6/(\mathbb{Z}_2 \times \mathbb{Z}_2)$, where the underlying torus is chosen to have the simplest possible shape (i.e. a "square torus lattice"). This leads over to the technically more complicated $T^6/(\mathbb{Z}_2 \times \mathbb{Z}_6')$ orbifold with hexagonal two-tori, for which I will also introduce some new visualisation tools that give a better understanding of the structure of certain deformations. Finally, I give some first new results on the $T^6/(\mathbb{Z}_2 \times \mathbb{Z}_6)$ orbifold which features the combination of two hexagonal and one rectangular (or square) torus.

Concrete global models are studied in chapter 5. Here I start again with the toy models on $T^4/\mathbb{Z}_2$. Then I go over to $SO(2N)$ and $USp(2N)$ models as well as to a $U(N)$ model, which is a Pati-Salam model, on the $T^6/(\mathbb{Z}_2 \times \mathbb{Z}_6')$ orbifold. I will show that in these concrete configurations, the moduli stabilisation mechanism works as expected and that indeed a large number of moduli can be stabilised. Moreover, there can exist flat directions which can be used to adjust the values of gauge couplings by slightly changing the volumes of the fractional cycles wrapped by D6-branes. I conclude with a summary and an outlook in chapter 6. In appendix A, I present some rather technical computations of certain correction terms, which are necessary in order to obtain global models under deformations, and where a concrete description might be helpful when different models are studied in the future. Appendix B gives some hints on how I implemented my findings in Mathematica, which might also be quite useful in order to reproduce my results and for possible future work.

2 Mathematical Preliminaries

In this chapter, I recapitulate known mathematical facts that are needed as a basis for the following string theory constructions in the present work. In section 2.1, I introduce Calabi-Yau manifolds, which are usually the underlying mathematical objects for the six-dimensional internal space of string theory due to their special characteristics. The subsequent section 2.2 deals with concrete examples of manifolds that will all prove to be useful for the later discussions, and especially various descriptions of the torus will be considered in more detail in section 2.3. The next section 2.4 deals with the mathematical objects called orbifolds, which will reappear in section 3.1 in much more detail as concrete string theory backgrounds for the six-dimensional internal space. In section 2.5, the concepts of homology and cohomology are presented, which make it possible to define certain topological invariants on a manifold. In addition, one can build equivalence classes of closed subspaces of a manifold, the so-called cycles, that are used in order to build concrete models in type II string theories, and which reappear in this context in section 3.1.3. In the last part of this chapter, the ideas of the moduli space and metric deformations are introduced (section 2.6), which play a major role in my own analysis of string theory backgrounds.

Good references in a rather compact shape, written by string theorists, are for example the articles [113] and [114]. For more details, one can consult e.g. [25], [115], [116], [84], or [36], as well as [85].

2.1 Calabi-Yau manifolds

For the following considerations, I assume that the reader is familiar with basic knowledge of real differentiable manifolds and complex analysis. The combination of both will give rise to complex manifolds, which can be further restricted to the so-called Calabi-Yau manifolds [117, 118]. These will be the subject of my discussion since they proved to be especially suitable as internal space for string theory models, see e.g. [23, 25], due to their properties of being compact, complex, Kähler and with $SU(n)$ holonomy.

2.1.1 Complex manifolds

A complex manifold M of n complex dimensions is a differentiable manifold with coordinate charts (U_α, ϕ_α), where the U_α are open subsets covering M and where the coordinate maps $\phi_\alpha : U_\alpha \to \phi_\alpha(U_\alpha) \subset \mathbb{C}^n$ are defined in such a way that the transition functions $\psi_{\beta\alpha} = \phi_\beta \circ \phi_\alpha^{-1}$

from $\phi_\alpha(U_\alpha \cap U_\beta) \subset \mathbb{C}^n$ to another coordinate system $\phi_\beta(U_\alpha \cap U_\beta) \subset \mathbb{C}^n$ are holomorphic maps for all α, β.

The definition of a complex manifold implies that it resembles locally $\mathbb{C}^n$, and in case that the manifold can be covered by a finite number of open subsets U_α it is also compact. The holomorphic transition functions ensure that all analytic considerations are the same independent of what coordinate system is used. Furthermore, the combination of local complex coordinates together with the holomorphic transition functions $\psi_{\beta\alpha}$ from one coordinate system to another gives rise to a so-called complex structure on the manifold M, which is not necessarily unique. To be more precise, the complex structures of two complex manifolds M and N can be identified if there exists a biholomorphic map $f : M \to N$ and $f^{-1} : N \to M$.

In fact, every complex manifold can be expressed as a real manifold with $2n$ real dimensions, but not the other way round. Therefore, it is always possible to write the complex coordinates in terms of real ones, i.e. $z_\mu^\alpha \equiv x_\mu^\alpha + i x_{n+\mu}^\alpha$ (with $1 \le \mu \le n$) for the chart (U_α, ϕ_α).

2.1.2 Tangent and cotangent spaces

Since each complex manifold is also a $2n$-dimensional real manifold, let me first recall the notion of the ordinary tangent space $T_p M$ at a point $p \in M$, for which a basis is usually constructed via partial derivatives of the real coordinates,

$$T_p M : \left\{ \left. \frac{\partial}{\partial x^1} \right|_p, \dots, \left. \frac{\partial}{\partial x^{2n}} \right|_p \right\} . \tag{2.1}$$

The tangent space can be interpreted as the space which is the closest flat approximation at p of the manifold M and is the vector space of all tangent vectors $v = \sum_k v^k \left. \frac{\partial}{\partial x^k} \right|_p$ with v^k real numbers.

One can easily expand this definition to complexified tangent spaces $T_p M^{\mathbb{C}}$ on complex manifolds. Rearranging the basis vectors of $T_p M$ in terms of so-called holomorphic and antiholomorphic coordinates such that

$$\frac{\partial}{\partial z^\mu} \equiv \left(\frac{\partial}{\partial x^\mu} + i \frac{\partial}{\partial x^{n+\mu}} \right), \quad \frac{\partial}{\partial \overline{z}^{\overline{\mu}}} \equiv \left(\frac{\partial}{\partial x^\mu} - i \frac{\partial}{\partial x^{n+\mu}} \right) \qquad (1 \le \mu \le n) , \tag{2.2}$$

the basis of the complexified tangent space at point p reads

$$T_p M^{\mathbb{C}} : \left\{ \left. \frac{\partial}{\partial z^1} \right|_p, \dots, \left. \frac{\partial}{\partial z^n} \right|_p, \left. \frac{\partial}{\partial \overline{z}^1} \right|_p, \dots, \left. \frac{\partial}{\partial \overline{z}^n} \right|_p \right\} . \tag{2.3}$$

This also implies that a vector v has now complex components v^k. For later constructions of Calabi-Yau manifolds it will be useful to split the definition of the complexified tangent space into the holomorphic and antiholomorphic directions by writing

$$T_p M^{\mathbb{C}} = T_p M^{(1,0)} \oplus T_p M^{(0,1)} \,, \tag{2.4}$$

where the holomorphic tangent space $T_p M^{(1,0)}$ is spanned by the first n basis vectors of equation (2.3) and the antiholomorphic tangent space $T_p M^{(0,1)}$ by the second set of n basis vectors. Since this decomposition holds true for all points $p \in M$, one can define the complexified tangent bundle as

$$T M^{\mathbb{C}} = T M^{(1,0)} \oplus T M^{(0,1)} \,, \tag{2.5}$$

with holomorphic and antiholomorphic tangent bundles $T M^{(1,0)}$ and $T M^{(0,1)}$, respectively.

From the notion of real differentiable manifolds, the reader should furthermore be familiar with the idea of dual tangent spaces at points $p \in M$, usually given by the basis

$$T_p^* M : \left\{ \mathrm{d}x^1 \big|_p, \dots, \mathrm{d}x^{2n} \big|_p \right\} . \tag{2.6}$$

The one-forms $\mathrm{d}x^k$ are linear maps $\mathrm{d}x^k : T_p M \to \mathbb{R}$ (with $1 \le k \le 2n$) which satisfy $\mathrm{d}x_p^k(\frac{\partial}{\partial x^l}\big|_p) = \delta_l^k$. The construction of a complexified cotangent space $T_p^* M^{\mathbb{C}}$ works completely analogous as for the complexified tangent space $T_p M^{\mathbb{C}}$, i.e. one can form the differentials

$$\mathrm{d}z^\mu = \mathrm{d}x^\mu + i\mathrm{d}x^{n+\mu}, \qquad \mathrm{d}\bar{z}^{\bar{\mu}} = \mathrm{d}x^\mu - i\mathrm{d}x^{n+\mu} \qquad (1 \le \mu \le n) \tag{2.7}$$

and write the complexified basis of $T_p^* M^{\mathbb{C}}$ as

$$T_p^* M^{\mathbb{C}} : \left\{ \mathrm{d}z^1 \big|_p, \dots, \mathrm{d}z^n \big|_p, \mathrm{d}\bar{z}^1 \big|_p, \dots, \mathrm{d}\bar{z}^n \big|_p \right\} . \tag{2.8}$$

In the same manner as for the complexified tangent spaces, one finds also for $T_p^* M^{\mathbb{C}}$ the decomposition into holomorphic and antiholomorphic parts,

$$T_p^* M^{\mathbb{C}} = T_p^* M^{(1,0)} \oplus T_p^* M^{(0,1)} \,, \tag{2.9}$$

with the assignment of the basis vectors similar to $T_p M^{\mathbb{C}}$. This structure is given for all points p of the complex manifold, and therefore

$$T^* M^{\mathbb{C}} = T^* M^{(1,0)} \oplus T^* M^{(0,1)} \tag{2.10}$$

is the complexified cotangent bundle of M.

2.1.3 Tensors and differential forms

A tensor of type (k, l) on a real differentiable manifold can be easily constructed as the product of the basis tangent vectors $\frac{\partial}{\partial x^a}$ and of the cotangent vectors $\mathrm{d}x^b$, see equations (2.1) and (2.6), respectively, such that

$$T \equiv T^{a_1,\dots,a_k}_{b_1,\dots,b_l} \, \mathrm{d}x^{b_1} \otimes \dots \otimes \mathrm{d}x^{b_l} \otimes \frac{\partial}{\partial x^{a_1}} \otimes \dots \otimes \frac{\partial}{\partial x^{a_k}} \, . \tag{2.11}$$

With the notions of complexified tangent and cotangent spaces, one can easily generalise to complex-valued tensors.

Based on the definition in equation (2.11), on complex manifolds M one can define totally antisymmetric forms in two different ways. Firstly, the complexified q-forms are smooth sections of the space $\Lambda^q T^* M^{\mathbb{C}}$, i.e. the wedge product of q complexified cotangent bundles, see equation (2.10). In particular, a q-form can be expressed as

$$\omega = \omega_{k_1 \dots k_q} \mathrm{d}x^{k_1} \wedge \mathrm{d}x^{k_2} \wedge \dots \wedge \mathrm{d}x^{k_q} \, , \tag{2.12}$$

and is an element of the vector space $\Gamma(\Lambda^q T^* M^{\mathbb{C}})$. Secondly, the wedge product of complexified cotangent bundles can be decomposed into a tensor product of holomorphic and antiholomorphic cotangent bundles,

$$\Lambda^q T^* M^{\mathbb{C}} = \bigoplus_{r=0}^{q} \Lambda^r T^* M^{(1,0)} \otimes \Lambda^{q-r} T^* M^{(0,1)} \equiv \bigoplus_{r=0}^{q} \Lambda^{r,q-r} M \, , \tag{2.13}$$

with the definition $\Lambda^{r,s} M \coloneqq \Lambda^r T^* M^{(1,0)} \otimes \Lambda^s T^* M^{(0,1)}$. Taking a section of $\Lambda^{r,s} M$, one obtains an (r, s)-form

$$\omega^{r,s} = \omega_{\mu_1 \dots \mu_r \bar{\nu}_1 \dots \bar{\nu}_s} \mathrm{d}z^{\mu_1} \wedge \dots \wedge \mathrm{d}z^{\mu_r} \wedge \mathrm{d}\bar{z}^{\bar{\nu}_1} \wedge \dots \wedge \mathrm{d}\bar{z}^{\bar{\nu}_s} \, , \tag{2.14}$$

with r holomorphic and $s = q - r$ antiholomorphic indices. The (r, s)-forms are elements of the vector space $\Gamma(\Lambda^{r,s} M)$. With that notion, one can express a q-form as

$$\omega = \sum_r \omega^{r,q-r} \, . \tag{2.15}$$

For a complex manifold M one can decompose the usual exterior differential as $\mathrm{d} = \partial + \bar{\partial}$ with $\partial : \Gamma(\Lambda^{r,s} M) \to \Gamma(\Lambda^{r+1,s} M)$ and $\bar{\partial} : \Gamma(\Lambda^{r,s} M) \to \Gamma(\Lambda^{r,s+1} M)$ such that

$$\begin{aligned}
\mathrm{d}\omega^{r,s} &= \frac{\partial \omega_{\mu_1 \dots \mu_r \bar{\nu}_1 \dots \bar{\nu}_s}}{\partial z^{\mu_0}} \mathrm{d}z^{\mu_0} \wedge \mathrm{d}z^{\mu_1} \wedge \dots \wedge \mathrm{d}z^{\mu_r} \wedge \mathrm{d}\bar{z}^{\bar{\nu}_1} \wedge \dots \wedge \mathrm{d}\bar{z}^{\bar{\nu}_s} \\
&+ \frac{\partial \omega_{\mu_1 \dots \mu_r \bar{\nu}_1 \dots \bar{\nu}_s}}{\partial \bar{z}^{\bar{\nu}_0}} \mathrm{d}z^{\mu_1} \wedge \dots \wedge \mathrm{d}z^{\mu_r} \wedge \mathrm{d}\bar{z}^{\bar{\nu}_0} \wedge \mathrm{d}\bar{z}^{\bar{\nu}_1} \wedge \dots \wedge \mathrm{d}\bar{z}^{\bar{\nu}_s} \, .
\end{aligned} \tag{2.16}$$

In case that $\mathrm{d}\omega = 0$, one says that ω is a closed form. If in addition one can write $\omega = \mathrm{d}\beta$ with β being a $(q-1)$-form, one calls ω an exact form. These two properties will be crucial for the definition of cohomology groups, cf. section 2.5.

2.1.4 Kähler manifolds

On a complex manifold M, the metric can be naturally extended to the bilinear map

$$g : T_p M^{\mathbb{C}} \times T_p M^{\mathbb{C}} \to \mathbb{C} , \tag{2.17}$$

for which I can define components by e.g. $g_{\mu\nu} = g \left(\frac{\partial}{\partial z^{\mu}}, \frac{\partial}{\partial z^{\nu}} \right)$ or $g_{\mu\bar{\nu}} = g \left(\frac{\partial}{\partial z^{\mu}}, \frac{\partial}{\partial \bar{z}^{\bar{\nu}}} \right)$. Thus, I find $g_{\mu\nu} = g_{\nu\mu}$, $g_{\mu\bar{\nu}} = g_{\bar{\nu}\mu}$ similar to the ordinary real metric defined on $T_p M$, and $\overline{g_{\mu\nu}} = g_{\bar{\mu}\bar{\nu}}$, $\overline{g_{\mu\bar{\nu}}} = g_{\bar{\mu}\nu}$. One can show that on each complex manifold there exists a so-called Hermitian metric

$$g = g_{\mu\bar{\nu}} \mathrm{d}z^{\mu} \otimes \mathrm{d}\bar{z}^{\bar{\nu}} + g_{\bar{\mu}\nu} \mathrm{d}\bar{z}^{\bar{\mu}} \otimes \mathrm{d}z^{\nu} \tag{2.18}$$

on $T_p M^{(1,0)} \otimes T_p M^{(0,1)} \to \mathbb{C}$, which possesses the additional restriction $g_{\mu\nu} = g_{\bar{\mu}\bar{\nu}} = 0$, for details see e.g. [115, 85].

Based on the Hermitian metric, one can build a closed two-form of degree $(r,s) = (1,1)$, namely the Kähler form, defined by

$$J_{1,1}^{\mathrm{K\ddot{a}hler}} = i g_{\mu\bar{\nu}} \, \mathrm{d}z^{\mu} \wedge \mathrm{d}\bar{z}^{\bar{\nu}} \qquad \text{with} \qquad \mathrm{d}J_{1,1}^{\mathrm{K\ddot{a}hler}} = 0 , \tag{2.19}$$

which has only real values. If such a Kähler form exists, one says that the manifold is Kähler. In that case, the Levi-Civita connection and the Christoffel symbols, known from general relativity, become very simple due to the restriction $\mathrm{d}J_{1,1}^{\mathrm{K\ddot{a}hler}} = 0$. This implies that also the Riemann curvature tensor and the Ricci tensor are highly restricted.

2.1.5 Holonomy

For a real differentiable m-dimensional manifold (M, g) with Levi-Civita connection, the parallel transport of a vector $v \in T_p M$ along a closed curve $\mathcal{C}$ with starting and ending point p results generally in a differently orientated vector v' (cf. for instance [115] for the definitions of a Levi-Civita connection and parallel transport of vectors, which I assume as basic knowledge in the context of real manifolds). In case M is orientable, which holds true for all complex manifolds of $m \equiv 2n$ real dimensions, the transformation $v' = A_{\mathcal{C}} v$ is realised by an $SO(m)$ matrix $A_{\mathcal{C}}$. In a next step, one finds that the matrices for all closed curves $\mathcal{C}$ that run through a single point p form a subgroup of $SO(m)$. Combining now these subgroups of all points $p \in M$, one obtains the so-called *holonomy group* of the manifold M.

For example, if the manifold is flat, tangent vectors do not change upon parallel transport and thus the holonomy group is the identity. For a Kähler manifold with $\dim_{\mathbb{R}} M = m = 2n$,

the holonomy group is $U(n)$ because the restrictions on the connection imply that parallel transport does not mix holomorphic and antiholomorphic components of the vectors $v \in T_pM^{\mathbb{C}} = T_pM^{(1,0)} \oplus T_pM^{(0,1)}$. The even smaller subgroup $SU(n)$ is obtained for the Calabi-Yau manifolds, which are defined in the next section 2.1.6. For the Calabi-Yau manifolds that appear in string theory, one uses $SU(3)$ holonomy groups in order to obtain $m = 2n = 6$ dimensions of the compact internal space. The advantage of this holonomy group becomes clear in the following argument, which shows that manifolds of $SU(3)$ holonomy admit exactly two covariantly constant spinor fields in type II string theories [8] (and only one spinor for type I and the heterotic string theories). This corresponds to unbroken $\mathcal{N} = 2$ supersymmetry in the four-dimensional Minkowski space-time for type II string compactifications. Let me remark that this $\mathcal{N} = 2$ supersymmetry will be broken to $\mathcal{N} = 1$ by an additional symmetry that will later be imposed on the six-dimensional internal space. This symmetry is known as orientifold projection and will be explained in section 3.1.2 in terms of its geometric properties, but also the implications on the particle spectrum will be discussed in section 3.2.

To start with, in the ten-dimensional flat Minkowski space-time one finds 32 conserved supercharges, which correspond to two Majorana-Weyl spinors with 16 real components that transform as spinors of the group $SO(1,9)$. Note that these spinors have opposite chirality in type IIA string theory and the same chirality in type IIB string theory. Separating now into a four-dimensional Minkowski space-time $\mathbb{R}^{1,3}$ and six compactified dimensions with the structure of a compact complex manifold M_6, the spinors can be split into the components $SO(1,3) \times SO(6)$, where $SO(1,3)$ is the four-dimensional Lorentz group. The six-dimensional spinors transform as $\mathbf{4}$ or $\bar{\mathbf{4}}$ under the group $SO(6) \simeq SU(4)$ (with the bar denoting opposite chirality), which rotates all supercharges under parallel transport. This implies that no supercharge is globally well-defined, and the four-dimensional supersymmetry is completely broken.

Hence, one takes the subgroup $SU(3) \subset SU(4)$, which has the representations $\mathbf{3} + \mathbf{1}$ or $\bar{\mathbf{3}} + \mathbf{1}$, where only the $\mathbf{1}$'s contribute to the four-dimensional spectrum. For example in [84], there exists a table with all possible decompositions of the group $SO(6)$, where one finds that manifolds of $SU(3)$ holonomy group are indeed the only ones with the desired property of a four-dimensional covariantly constant spinor. To summarise, the decomposition reads

$$
\begin{array}{ccccc}
SO(1,9) & \to & SO(1,3) \times SO(6) & \to & SO(1,3) \times SU(3) \\
\mathbf{16} & & (\mathbf{2}, \mathbf{4}) + (\mathbf{2'}, \bar{\mathbf{4}}) & & (\mathbf{2}, \mathbf{3}) + (\mathbf{2'}, \bar{\mathbf{3}}) + (\mathbf{2}, \mathbf{1}) + (\mathbf{2'}, \mathbf{1})
\end{array} , \tag{2.20}
$$

where the parts $(\mathbf{2}, \mathbf{1})$ and $(\mathbf{2'}, \mathbf{1})$ are the two covariantly constant spinors with $\mathbf{2}$ and $\mathbf{2'}$ referring to the left- and right-handedness under the four-dimensional Lorentz group $SO(1,3)$.

14

2.1.6 Calabi-Yau manifolds

A Calabi-Yau manifold M (with $\dim_{\mathbb{C}} M = n$) is a compact Kähler manifold with additional properties that can be stated in many different ways. These different statements are related in interesting ways, and depending on the concrete situation, the one or the other expression proved to be especially useful. Four equivalent definitions, which are of interest in the context of my work, are the following ones:

1. The first Chern class vanishes.

2. The metric is Ricci-flat, i.e. the Ricci tensor vanishes.

3. M has a Levi-Civita connection with $SU(n)$ holonomy.

4. There exists a nowhere vanishing holomorphic $(n,0)$-form Ω_n that is globally defined.

The first definition involves the so-called first Chern class, which is a topological invariant that is very easy to compute. Therefore, this property is mostly used to prove if a manifold is Calabi-Yau. For my discussion, the knowledge of Chern classes is not needed and therefore I will not introduce them here, but the interested reader will easily find their definition in the literature, e.g. in [115]. Historically, in 1957 Calabi conjectured that for vanishing first Chern class, there exists a metric of a compact Kähler manifold which is Ricci-flat, and this was proved by Yau in 1978. The $SU(n)$ holonomy stated in the third item is crucial for the construction of physical models because it ensures the existence of one covariantly constant spinor (and its CPT conjugate), cf. table 0.1 in [84]. Finally, the last definition provides a useful tool in order to do integration on a Calabi-Yau manifold. Due to its properties, Ω_n can be taken as a volume element, of which I will make extensive use in chapter 4.

Because of their interesting characteristics, Calabi-Yau manifolds have been studied in much detail in the past. Especially in string theory, see e.g. [84, 36], they are important elements on which concrete theories can be built. On the other hand, for most Calabi-Yau manifolds it was not possible thus far to find the explicit expression of a Ricci-flat metric. Therefore, it makes sense to consider certain orbifolds, see sections 2.4 and 3.1, which are singular limits of the Calabi-Yau manifolds in question, and where it is easy to perform concrete calculations.

2.2 Relevant examples of complex manifolds

In the subsequent chapters, concrete complex manifolds of different appearance will turn up. Therefore, it will be useful for the reader to already familiarise him/herself with the following sample. The first examples are the Riemann surfaces that are introduced here in order to provide an easier understanding of the other examples. In addition, the basic objects of string theory, namely closed and open strings, can be perceived as two-dimensional worldsheets if not only the length of the string, but also the time component is considered (cf. section 3.2). These worldsheets are mathematically Riemann surfaces and are basic ingredients for the calculation of e.g. string scattering amplitudes (a subject which is not discussed further in the present work, consult for example the text books [9], [24], [25], [39], and [40] for more information). Also the fact that Riemann surfaces allow for a so-called conformally flat metric is important in string theory, which I will also not discuss further here (see for instance [115]).

The second example is the complex two-dimensional torus T^2, which is used as the basic object for a large number of string compactifications, as already mentioned in chapter 1, in particular for the so-called factorisable toroidal orbifolds (cf. section 2.4 about orbifolds in general). In section 3.1.1, I will introduce the concrete examples $(T^2 \times T^2 \times T^2)/(\mathbb{Z}_2 \times \mathbb{Z}_{2M})$ with $2M = 2, 6, 6'$. In addition, different descriptions of the torus that I will make use of later will be discussed in section 2.3.

In section 2.2.3, complex projective spaces $\mathbb{CP}^n$ will be discussed, whose knowledge is needed to understand in a next step the concept of compact submanifolds of these spaces $\mathbb{CP}^n$, i.e. hypersurfaces, see section 2.2.4. Some very specific choices of the six-dimensional internal space used in string theory, which is generally assumed to be a Calabi-Yau manifold, can be expressed as such hypersurfaces. The big advantage of such a description is the fact that not only the topology can be studied in detail and that concrete geometric quantities can be computed, but also the possibility to easily deform these hypersurfaces and to analyse their behaviour under such changes, cf. also section 2.6. This will be done in chapter 4 in great detail.

2.2.1 Riemann surfaces

Riemann surfaces are defined as being complex one-dimensional manifolds. All two-forms on Riemann surfaces are closed because the space has only two real dimensions, and therefore these manifolds are also Kähler. Furthermore, Riemann surfaces look locally like the complex plane, but globally they can be very different from $\mathbb{C}$. This different appearance

is owing to the construction of Riemann surfaces by performing branch cuts of the complex plane and then gluing the resulting sheets together again (consult e.g. [85] for the exact mathematical definitions).

As examples of Riemann surfaces, one can consider the complex plane or the Riemann sphere $\mathbb{C} \cup \{\infty\}$, which is compact. Furthermore, compact Riemann surfaces are equivalent to complex projective algebraic curves, which are generally defined as the zero locus of a polynomial $f(z^0, \ldots, z^n) = 0$ living in the complex projective space $\mathbb{CP}^n$, cf. section 2.2.3, where a concrete example is the torus, see section 2.3 for more details. Another example that I will use further down are the elliptic curves over the complex numbers, which are in fact homeomorphic to the complex torus.

2.2.2 Tori

The two-torus, usually denoted by T^2, is homeomorphic to the complex manifold $\mathbb{C}/\Lambda$, which endows the T^2 naturally with a complex structure. A lattice Λ on the complex plane $\mathbb{C}$ is given by

$$\Lambda = \{ m\zeta_1 + n\zeta_2 | m, n \in \mathbb{Z} \} , \tag{2.21}$$

with lattice vectors $\zeta_1, \zeta_2 \in \mathbb{C}$ such that $\operatorname{Im} \frac{\zeta_2}{\zeta_1} > 0$, i.e. considering only the complex upper half plane by a suitable sign choice of ζ_2. One can then define the complex structure parameter as $\tau := \frac{\zeta_2}{\zeta_1}$, which encodes the concrete shape of the torus. Due to the periodicity of the lattice, one can choose a fundamental parallelogram, which is usually given by the set $\{ s\zeta_1 + t\zeta_2 | 0, \leq s, t \leq 1 \}$, and to obtain a torus, opposite sides of this fundamental domain are identified. One should note that the torus is a flat space and has therefore trivial holonomy.

Between different complex structure parameters τ there exists an interesting relation. Two sets of basic lattice vectors (ζ_1, ζ_2) and $(\tilde{\zeta}_1, \tilde{\zeta}_2)$ give rise to the same complex structure τ if the sets are related by the transformation

$$\begin{pmatrix} \tilde{\zeta}_1 \\ \tilde{\zeta}_2 \end{pmatrix} = \begin{pmatrix} a & b \\ c & d \end{pmatrix} \begin{pmatrix} \zeta_1 \\ \zeta_2 \end{pmatrix} \qquad \text{with} \quad \begin{pmatrix} a & b \\ c & d \end{pmatrix} \in PSL(2, \mathbb{Z}) . \tag{2.22}$$

The *modular group* $PSL(2, \mathbb{Z}) \equiv SL(2, \mathbb{Z})/\mathbb{Z}_2$ has the effect that two matrices A and $-A$, which are both elements of $SL(2, \mathbb{Z})$, are identified, where the special linear group is defined in the following way,

$$SL(2, \mathbb{Z}) \equiv \left\{ \begin{pmatrix} a & b \\ c & d \end{pmatrix} \middle| a, b, c, d \in \mathbb{Z}, \, ad - bc = 1 \right\} . \tag{2.23}$$

Note that it is not always the group $PSL(2, \mathbb{Z})$ which is referred to as the modular group, but some authors take instead the larger group of $SL(2, \mathbb{Z})$. In addition, the complex structure parameters τ and τ' of two coinciding lattices are related by the modular transformation

$$\tau \mapsto \tau' = \frac{a\tau + b}{c\tau + d} \qquad \text{with } ad - bc = 1 \qquad (a, b, c, d \in \mathbb{Z}), \tag{2.24}$$

and one can show that the group of modular transformations is generated by $\tau \mapsto \tau + 1$ and $\tau \mapsto -1/\tau$, see for instance [115].

2.2.3   Complex projective spaces

The complex projective spaces $\mathbb{CP}^n$, which have n dimensions, are compact Kähler manifolds and are defined as

$$\mathbb{CP}^n \equiv (\mathbb{C}^{n+1} - \{0\})/ \sim . \tag{2.25}$$

Their main advantage is that they are very easy to handle. Concretely, the space $\mathbb{CP}^n$ describes lines running through the origin of the complex space $\mathbb{C}^{n+1}$, where a line is parametrised by homogeneous coordinates $[z_0, z_1, \ldots, z_n] \in (\mathbb{C}^{n+1} - \{0\})$, and with the equivalence relation

$$(z_0, \ldots, z_n) \sim \lambda(z_0, \ldots, z_n) \tag{2.26}$$

divided out (for $\lambda \in \mathbb{C}$, $\lambda \neq 0$). The notion of homogeneous coordinates means basically that one can use λ to scale one of the $n + 1$ coordinates to one. Thus, reducing to only n coordinates means going over to so-called inhomogeneous coordinates χ_i^j. In detail, one chooses a chart $U_j \subset (\mathbb{C}^{n+1} - \{0\})$ where $z_j \neq 0$ and defines $\chi_i^j \equiv z_i/z_j$ with $i \neq j$. The holomorphic maps $\psi_{jk} : \mathbb{C}^n \to \mathbb{C}^n$ on the underlying open subset $U_j \cap U_k$ translate the coordinate system χ_i^j to χ_i^k by a multiplication of $(\chi_k^j)^{-1}$.

As a concrete example one can consider $\mathbb{CP}^1$, which is the Riemann sphere $\mathbb{C} \cup \{\infty\}$ that can also be identified with the ordinary two-sphere S^2. Taking the homogeneous coordinates $[z_0, z_1] \in \mathbb{CP}^1$, one finds either $z_1 \neq 0$ and can choose $z_1 = 1$, or the other way round. Therefore, one has a complex plane due to $z_0 \in \mathbb{C}$ and an additional point $z_1 = 1$ (or with reversed coordiantes), as required for the definition of the Riemann sphere.

This formalism can be easily generalised to weighted projective spaces, where the equivalence relation has a different weight for each coordinate. Later on, I will use the

weighted complex projective space $\mathbb{CP}^2_{112}$ extensively, where I will always use the notation $(z_0, z_1, z_2) \equiv (x, v, y)$ for the homogeneous coordinates. $\mathbb{CP}^2_{112}$ is then defined by the equivalence relation

$$(x, v, y) \sim (\lambda x, \lambda v, \lambda^2 y). \tag{2.27}$$

In most cases, I will choose a chart where $v \neq 0$ and set $v \equiv 1$. It is important to note that contrary to $\mathbb{CP}^n$, weighted projective spaces may have singular points since there can appear non-trivial fixed points under the coordinate identification.

2.2.4 Hypersurfaces of complex projective spaces

In the subsequent chapters, I will use as basic mathematical objects compact submanifolds of complex (weighted) projective spaces. For my discussion it is crucial that these spaces are compact because otherwise they wouldn't be suitable backgrounds for the internal dimensions of string theory. The simpler examples of submanifolds of just complex spaces $\mathbb{C}^n$ are not useful here since a compact, connected and analytic submanifold of the complex space is just a single point, see [114, 116].

There exists an important theorem of Chow, cf. for example [113, 85], or the original article [119], which says that each submanifold of $\mathbb{CP}^n$ can be written as the zero locus of a finite number of homogeneous polynomial equations, expressed in terms of homogeneous coordinates $[z_0, \ldots, z_n] \in \mathbb{CP}^n$. Homogeneity of degree d of a polynomial f means that

$$f(\lambda z_0, \ldots, \lambda z_n) = \lambda^d f(z_0, \ldots, z_n), \tag{2.28}$$

and in the following discussions I will only need one such polynomial f, giving rise to a $(n-1)$-dimensional hypersurface of degree d of $\mathbb{CP}^n$

$$\{f(z_0, \ldots, z_n) = 0\} \subset \mathbb{CP}^n. \tag{2.29}$$

In the general case of k such polynomials $(f_i)_{i=1,\ldots,k}$, one would find an $(n-k)$-dimensional submanifold of the complex projective space. Contrary to $\mathbb{CP}^n$, the hypersurfaces do not possess a unique complex structure.

One can easily generalise equation (2.29) to using a product of weighted projective spaces, where only the equivalence relation has to be modified. Hypersurfaces of complex (weighted) projective spaces are algebraic objects, and as such they can be used for concrete mathematical calculations. In chapter 4, I will explicitly translate certain toroidal orbifolds into the hypersurface language of weighted projective spaces, and I will perform explicit calculations on them: such a description is especially useful in the context of deformations. The

singular points of the hypersurface are the solutions to $f = \mathrm{d}f = 0$ (except for the values $z_j = 0$ for all j, which do not belong to $\mathbb{CP}^n$). Hence, all partial derivatives of f must vanish at the singular points, which will be applied to the concrete examples in chapter 4.

2.3   Descriptions of the torus

As already mentioned, I will use concrete toroidal orbifolds in the following chapters, which are products of two-tori with an additional orbifold action. In this section, I provide the information about the concrete map from the ordinary torus description to the hypersurface expression, as introduced in the previous section, for which the Weiserstrass elliptic function is used.

2.3.1   Weierstrass elliptic function

The Weierstrass elliptic function is a special form of an elliptic function, for which a nice introduction can be found e.g. in [120] or [121]. The Weierstrass functions will prove to be a useful tool for translating between different descriptions of the torus, see section 2.3.2.

To start with, let me recall the notion of meromorphic functions f, which are defined on an open set of a complex manifold M, and where f is the quotient $f = g/h$ of two holomorphic functions g and h. Furthermore, f is called double periodic, i.e. periodic in two directions, on a period lattice $\Lambda = \{m\zeta_1 + n\zeta_2 | m, n \in \mathbb{Z}\}$ (cf. equation (2.21)) if

$$f(z + \zeta_1) = f(z) = f(z + \zeta_2) \qquad \forall z \in \mathbb{C}. \tag{2.30}$$

When $\tau \coloneqq \frac{\zeta_2}{\zeta_1}$ is chosen such that $\operatorname{Im}\tau > 0$, f is said to be an *elliptic function*. One can show that f has at least two simple poles (or one pole degenerated by degree two) in the fundamental domain.

As a very simple form of an elliptic function, one can define the *Weierstrass elliptic function*

$$\wp(z) = \frac{1}{z^2} + \sum_{\zeta \neq 0} \left(\frac{1}{(z - \zeta)^2} - \frac{1}{\zeta^2} \right), \tag{2.31}$$

with periods $\zeta \equiv m\zeta_1 + n\zeta_2$ $(m, n \in \mathbb{Z})$. One can see that $\wp(z)$ is invariant under the shifts $z \mapsto z + m\zeta_1 + n\zeta_2$ and that the poles lie at the coordinates $z = \zeta$. In addition, $\wp(z)$ has the important properties

$$\wp(z) = \wp(-z), \qquad \wp'(z) = -\wp'(-z), \tag{2.32}$$

which directly implies that the fixed points of $\wp(z)$, defined on the lattice, reside at the coordinates $z = 0, \frac{\zeta_1}{2}, \frac{\zeta_2}{2}, \frac{\zeta_3}{2}$ with $\zeta_3 \equiv \zeta_1 + \zeta_2$. These fixed points will play an important role for the discussion of concrete models. The elliptic function $\wp'(z)$ has three zeros, which are obtained when $z = \frac{\zeta_1}{2}, \frac{\zeta_2}{2}, \frac{\zeta_3}{2}$ is inserted.

The Weierstrass $\wp$-function has furthermore the property that it fulfils the differential equation

$$\wp'(z)^2 = 4\wp(z)^3 - g_2\wp(z) - g_3 \,, \tag{2.33}$$

which has the form of an elliptic curve. This means that the relation is expressed as a curve $y^2 = 4z^3 - az - b$, which has the property of being non-singular. Equation (2.33) will become quite important for later constructions of concrete models. The invariants g_2 and g_3 are defined as

$$g_2 = 60 \sum_{\zeta \neq 0} \zeta^{-4} \,, \qquad g_3 = 140 \sum_{\zeta \neq 0} \zeta^{-6} \,, \tag{2.34}$$

and can be combined into the following meromorphic function,

$$j(\tau) := \frac{g_2^3}{g_2^3 - 27g_3^2} \,. \tag{2.35}$$

This function has the name *Klein invariant* $j(\tau)$ and provides a one-to-one map to the complex structure τ. The dependency on the complex structure parameter is given by the relation $\tau := \frac{\zeta_2}{\zeta_1}$, and $j(\tau) \in \mathbb{R}$ because the parameters g_2, g_3 are real numbers by a rotation of the lattice.

One of the most interesting and quite useful characteristics of the Weierstrass $\wp$-function is the fact that there exists the following addition theorem, which reads

$$\wp(z_1 + z_2) = \frac{1}{4} \left\{ \frac{\wp'(z_1) - \wp'(z_2)}{\wp(z_1) - \wp(z_2)} \right\}^2 - \wp(z_1) - \wp(z_2) \,. \tag{2.36}$$

By this relation, the Weierstrass function at the coordinate z_1 is shifted to another coordinate $z_1 + z_2$. I will make use of this relation in section 4.1.

2.3.2 The torus as hypersurface in a complex projective space

So far, I presented in section 2.2.2 the definition of the two-torus that is probably the most well-known expression. An equivalent description as an elliptic curve in $\mathbb{CP}^2_{112}$ can be obtained with the help of the Weierstrass $\wp$-function as introduced in section 2.3.1.

For my later calculations, this second description will turn out to be more useful than the definition in section 2.2.2. The differential equation (2.33) together with the identifications $\wp(z) = x/v$ and $\wp'(z) = y/v^2$ directly leads to the elliptic curve.

The torus expressed as an elliptic curve E is given by the zero locus of a polynomial of degree four,

$$E = \{f := -y^2 + F(x, v) = 0\}, \tag{2.37}$$

with the definition

$$F(x, v) := 4vx^3 - g_2 v^3 x - g_3 v^4. \tag{2.38}$$

In subsequent calculations the factorised form of $F(x, v)$ will become important, which is

$$F(x, v) = 4v(x - \epsilon_2 v)(x - \epsilon_3 v)(x - \epsilon_4 v) \tag{2.39}$$

with the roots of x/v ($v \neq 0$) being at the positions ϵ_α ($\alpha = 2, 3, 4$) with $\sum_\alpha \epsilon_\alpha = 0$ and at $\epsilon_1 := \infty$. The parameters g_2 and g_3 in definition (2.38) can be reproduced by the relations $g_2 = 4 \sum_{\alpha < \beta} \epsilon_\alpha \epsilon_\beta$ and $g_3 = 4\epsilon_2 \epsilon_3 \epsilon_4$.

Using the identifications, the globally defined holomorphic one-form Ω_1 on the torus can also be written in terms of the homogeneous coordinates,

$$\Omega_1 := dz = \frac{d\wp}{\wp'} = \frac{v \cdot dx - x \cdot dv}{y} \xrightarrow{v \equiv 1} \frac{dx}{y}, \tag{2.40}$$

where in the last step I introduced the chart $v \equiv 1$ that I will often use for the calculations in the following chapters.

2.4   Orbifolds

An orbifold is defined as a manifold M divided by a discrete group Γ, i.e. M/Γ. There exist in general invariant points under Γ, and at the position of these fixed points one finds conical curvature singularities, which means that the curvature is a δ-function. As a simple example, take the orbifold $\mathbb{C}^2/\mathbb{Z}_2$, see section 4.2.1 for more details, where the discrete orbifold group $\mathbb{Z}_2$ generates a conifold singularity at the origin of $\mathbb{C}^2$. It is crucial that the orbifold group Γ does not act freely. For example, I explained in section 2.2.2 that the two-torus T^2, which is not an orbifold, can be described as the quotient $\mathbb{C}/\Lambda$. Since the action of Λ is free, there exist no fixed points, and T^2 is a flat space without singularities.

To set up concrete models in string theory, a good starting point is to consider those orbifolds which are singular limits of Calabi-Yau manifolds because, as mentioned in section 2.1.6, one can explicitly write down their metric. In addition, orbifolds are mathematically very well understood objects, which are easy to use for computations. More details on the concrete orbifold setup in string theory that I will use for my analysis are given in section 3.1.1. Concrete calculations on the non-compact orbifolds $\mathbb{C}^2/\mathbb{Z}_2$ and $\mathbb{C}^3/(\mathbb{Z}_2 \times \mathbb{Z}_2)$, as well as on the compact toroidal orbifolds $T^4/\mathbb{Z}_2$, $T^4/\mathbb{Z}_6$, $T^6/(\mathbb{Z}_2 \times \mathbb{Z}_2)$, $T^6/(\mathbb{Z}_2 \times \mathbb{Z}_6')$ and $T^6/(\mathbb{Z}_2 \times \mathbb{Z}_6)$ will be presented in chapter 4.

There exist different ways to "get rid" of the orbifold singularities in order to obtain a smooth Calabi-Yau manifold, which depend on the fact if a certain conifold singularity is degenerated in the Kähler or complex structure. In the context of conformal field theories, there exists a very interesting symmetry principle between these two kinds of singularities, known as mirror symmetry [36]. For the Kähler type, one usually applies the very well-known mechanism of a blow-up, which was analysed in the context of string theory in much detail, see e.g. [84, 36] and the literature presented in the introductory chapter. However, I will study singularities of the second kind, making use of the method known as complex structure deformations, cf. section 2.6. To my best knowledge, very few examples of such deformations that are relevant to string theory have been studied up to now and my collaborators and me were the first ones to analyse concrete models in type IIA string theory [109–111]. In chapter 4, I will present explicit complex structure deformations on orbifolds which are promising backgrounds for semi-realistic models.

In order to perform concrete deformations, I need the mathematical concepts known as homology and cohomology, introduced in the next section. These lead, amongst other things, to the notion of the moduli space, which is closely related to the deformations, see section 2.6.

2.5   Homology and cohomology

Homology and cohomology groups encode topological information of a manifold, independent of the chosen coordinates, and are therefore of major importance for the classification of manifolds in terms of their topologies. In order to group geometrical objects into equivalence classes, one needs the notion of (co)homology. This makes it possible to distinguish only between interesting classes of elements, where an arbitrary element can be chosen as representative. In the notion of homology, the topological objects called cycles are defined, which are the basic objects of my later constructions.

On a smooth connected manifold M, one can define a complex q-chain as sum over smooth oriented submanifolds N_k of dimension q,

$$a_q \equiv \sum_k c_k N_k \,, \tag{2.41}$$

where $c_k \in \mathbb{C}$ (analogously, one can write down real or integer q-chains). The oriented boundary of a manifold M is denoted by ∂ and maps a q-chain to a $(q-1)$-chain. ∂ has the property that the boundary ∂M of a manifold does not have a boundary,

$$\partial \partial M = 0 \,. \tag{2.42}$$

Within this notation, one says that a q-chain without a boundary, $\partial a_q = 0$, is a *cycle*. Furthermore, one calls c_q with the property $c_q = \partial d_{q+1}$ a q-boundary, and it is directly clear that for the q-boundaries the property $\partial c_q = 0$ is trivially fulfilled, i.e. c_q is a cycle. Hence, it makes sense to consider only such cycles which cannot be written as a boundary, and to define the q-th homology group

$$H_q(M, \mathbb{R}) \equiv \frac{\{a_q | \partial a_q = 0\}}{\{c_q | c_q = \partial d_{q+1}\}} \,. \tag{2.43}$$

Differently said, the group $H_q(M, \mathbb{R})$, which is also a vector space, is the group of non-trivial cycles, and its dimension is given by the Betti number $\mathbf{b}_q$. The elements of the q-th homology group are the equivalence classes $[a_q]$ of the cycles a_q, for which the representative can be chosen arbitrarily.

The basic ideas of homology apply in a similar fashion to cohomology. As already mentioned in section 2.1.3, there exist closed q-forms with $\mathrm{d}\omega = 0$, called cocycles, which may have the additional property of being exact, i.e. they can be expressed as coboundaries $\omega = \mathrm{d}\beta$. Since the exact forms provide only trivial solutions to $\mathrm{d}\omega = 0$ due to the property $d^2 = 0$ on all q-forms, it makes sense to define a group of closed q-forms, where the exact forms are divided out. This idea is realised in the q-th de Rham cohomology group $H_{dR}^q(M) \equiv H^q(M)$, which is the quotient space

$$H^q(M, \mathbb{R}) \equiv \frac{\{\omega | \mathrm{d}\omega = 0\}}{\{\alpha | \alpha = \mathrm{d}\beta\}} \tag{2.44}$$

with real q-forms ω and α. Analogously, one can define $H_{dR}^q(M, \mathbb{C})$ with complexified q-forms. The elements $[\omega] \in H_{dR}^q(M)$ are called equivalence classes with ω being an arbitrary representative of $[\omega]$.

De Rham proved that $H_q(M, \mathbb{R})$ and $H^q(M, \mathbb{R})$ (and $H_q(M, \mathbb{Z})$, $H^q(M, \mathbb{Z})$) are dual to each other, cf. for instance [8] for a compact presentation or [115] for more details, in the

sense that one can always choose a basis $\{(a_q)_i\}$ of q-cycles and a basis $\{(A_q)_j\}$ of q-forms with $i, j = 1, \ldots, \mathbf{b}_q$ such that

$$\int_{[(a_q)_i]} [(A_q)_j] = \delta_{ij} \,. \tag{2.45}$$

To show this one has to use Stokes' theorem $\int_{a_q} \mathrm{d}B_{q-1} = \int_{\partial a_q} B_{q-1}$ from which follows that it is sufficient to integrate over an arbitrary representative of the homology and cohomology classes. From *De Rham duality*, it is clear that the above introduced cycles and boundaries are the dual objects to the cocycles and coboundaries, respectively.

There exists a second relation between the homology and cohomology groups known as *Poincaré duality*. The integral $\int_M B_q \wedge A_{m-q}$ over a real m-dimensional manifold M is a map $H^q(M, \mathbb{R}) \times H^{m-q}(M, \mathbb{R}) \to \mathbb{R}$, and therefore $H^q(M, \mathbb{R})$ and $H^{m-q}(M, \mathbb{R})$ are considered as being dual, thus also the Betti numbers $\mathbf{b}_q = \mathbf{b}_{m-q}$. Using this property together with de Rham duality, one can identify $H^{m-q}(M, \mathbb{R})$ with $H_q(M, \mathbb{R})$, which means that each non-trivial q-cycle a_q corresponds to a non-trivial $(m-q)$-cocycle $\delta(a_q)$. With this relation, it is possible to rewrite integrals as $\int_{a_q} B_q = \int_M B_q \wedge \delta(a_q)$, i.e. one can extend the integration over a subspace to the integral over the whole manifold M. This makes it possible to define the topological intersection number between two homology classes,

$$[a_q] \circ [b_{m-q}] \equiv \int_M \delta(a_q) \wedge \delta(b_{m-q}) \,, \tag{2.46}$$

which is a crucial ingredient for model building in string theory.

For a complex manifold M, one can use the decomposition $\mathrm{d} = \partial + \bar{\partial}$ of the exterior derivative into operators acting only on the holomorphic or antiholomorphic components of a q-form, respectively, see equation 2.16. Thus, one can also define the (r, s)-th Dolbeault cohomology group,

$$H_{\bar{\partial}}^{r,s}(M, \mathbb{C}) \equiv \frac{\{\omega^{r,s} | \bar{\partial} \omega^{r,s} = 0\}}{\{\alpha^{r,s} | \alpha^{r,s} = \bar{\partial} \beta^{r,s-1}\}} \,, \tag{2.47}$$

which can similarly be expressed with ∂. For a Kähler manifold, one finds between the two definitions of equations (2.44) and (2.47) the relation

$$H_{dR}^q(M, \mathbb{C}) = \bigoplus_{q=r+s} H_{\bar{\partial}}^{r,s}(M, \mathbb{C}) \,, \tag{2.48}$$

i.e. the de Rham cohomology groups can be decomposed into Dolbeault cohomology groups.

To denote the dimensions of the cohomology groups, one uses, as for the homology groups, the Betti numbers, which are for the de Rham cohomology groups $H_{dR}^q(M, \mathbb{R})$ and $H_{dR}^q(M, \mathbb{C})$ defined as

$$\mathbf{b}^q \equiv \dim_{\mathbb{R}} H_{dR}^q(M, \mathbb{R}) = \dim_{\mathbb{C}} H_{dR}^q(M, \mathbb{C}) \,. \tag{2.49}$$

To encode the (complex) dimensions of the Dolbeault cohomology groups $H_{\bar{\partial}}^{r,s}(M,\mathbb{C})$, one introduces further quantities, namely the Hodge numbers

$$h^{r,s} \equiv \dim_{\mathbb{C}} H_{\bar{\partial}}^{r,s}(M,\mathbb{C}), \tag{2.50}$$

which play an important role in string theory and in my present work. The Hodge numbers have the properties

$$h^{r,s} = h^{n-r,n-s}, \qquad h^{r,s} = h^{s,r}, \tag{2.51}$$

where the second relation is only true on a Kähler manifold. If equation (2.48) is fulfilled, it is clear that for the Betti numbers one can write

$$\mathbf{b}^q = \bigoplus_{q=r+s} h^{r,s}, \tag{2.52}$$

and therefore the Betti numbers can be split into a sum over Hodge numbers.

For Calabi-Yau manifolds of complex dimension $n = 1, 2, 3$, the Hodge numbers are given in table 1, and the Hodge numbers of some concrete orbifolds that I will use in the subsequent chapters are summarised in table 2. The Hodge numbers play an important role in string theory, not only because they describe the topology of the internal six-dimensional space, but also because they reappear in the particle spectrum, where they count the numbers of certain fields (see section 3.2), and as parameters of the so-called moduli space, which will be introduced in the next section 2.6. These close relations of the Hodge numbers to physical quantities underline how much the geometry of the internal space influences the physics of the four-dimensional effective theory.

2.6 Moduli space and metric deformations

For Calabi-Yau manifolds M, the number of independent Hodge numbers is severely reduced, cf. also section 2.5, and I find the collections as shown in the Hodge diamonds of table 1. For $n = 1, 2$, there exists only one possible Calabi-Yau manifold, which is the two-torus T^2 and the $K3$ surface, respectively. In case that the complex dimension is larger, one finds families of Calabi-Yau manifolds with different Hodge numbers. Choosing a certain Calabi-Yau manifold, one can take a look at its so-called *moduli space*, which has $h^{1,1}$ real and $h^{2,1}$ complex dimensions. Changing one of the $h^{1,1}$ parameters with name Kähler moduli implies that the metric is deformed with respect to the Kähler structure, which is roughly speaking a change in the size of the manifold. On the other hand, a variation in one of the $h^{2,1}$ complex structure moduli corresponds to a deformation of the

Hodge diamonds for Calabi-Yau manifolds of complex dimension n	
$n = 1$	$\begin{matrix} & h^{0,0} & \\ h^{1,0} & & h^{0,1} \\ & h^{1,1} & \end{matrix}$ = $\begin{matrix} & 1 & \\ 1 & & 1 \\ & 1 & \end{matrix}$
$n = 2$	$\begin{matrix} & & h^{0,0} & & \\ & h^{1,0} & & h^{0,1} & \\ h^{2,0} & & h^{1,1} & & h^{0,2} \\ & h^{2,1} & & h^{1,2} & \\ & & h^{2,2} & & \end{matrix}$ = $\begin{matrix} & & 1 & & \\ & 0 & & 0 & \\ 1 & & 20 & & 1 \\ & 0 & & 0 & \\ & & 1 & & \end{matrix}$
$n = 3$	$\begin{matrix} & & & h^{0,0} & & & \\ & & h^{1,0} & & h^{0,1} & & \\ & h^{2,0} & & h^{1,1} & & h^{0,1} & \\ h^{3,0} & & h^{2,1} & & h^{1,2} & & h^{0,3} \\ & h^{3,1} & & h^{2,2} & & h^{1,3} & \\ & & h^{3,2} & & h^{2,3} & & \\ & & & h^{3,3} & & & \end{matrix}$ = $\begin{matrix} & & & 1 & & & \\ & & 0 & & 0 & & \\ & 0 & & h^{1,1} & & 0 & \\ 1 & & h^{2,1} & & h^{2,1} & & 1 \\ & 0 & & h^{1,1} & & 0 & \\ & & 0 & & 0 & & \\ & & & 1 & & & \end{matrix}$

Table 1: The table shows the so-called Hodge diamonds for the Calabi-Yau manifolds of complex dimension $n = 1, 2, 3$. The Hodge diamonds form a collection of all possible Hodge numbers, cf. section 2.5 for the definition and explanation of their properties, and therefore contain the information about the topological properties of the manifolds.

complex structure of the Calabi-Yau manifold, which can be interpreted as altering its shape. Table 1 reveals that all Calabi-Yau manifolds with $n = 1, 2, 3$ have at least one Kähler modulus $h^{1,1}$, but only for $n = 3$ there exist in addition complex structure moduli $h^{2,1}$. In chapter 4 I will perform concrete deformations of these complex structure moduli, but I will also use $K3$ manifolds as toy models, and one should keep in mind that here it is actually the hyper-Kähler structure which is deformed. Hyper-Kähler means here that the $K3$ manifold has a symplectic structure due to the property $SU(2) \simeq USp(2)$ of the holonomy group.

Since complex structure deformations (cf. for instance [113, 7, 84, 108]) are crucial for my work, I will give here some more detail. At first, take the possible perturbations of the metric g,

$$\delta g = \delta g_{\mu\bar{\nu}} \mathrm{d}z^{\mu} \wedge \mathrm{d}\bar{z}^{\bar{\nu}} + \delta g_{\mu\nu} \mathrm{d}z^{\mu} \wedge \mathrm{d}z^{\nu} + \text{c.c.} \,, \tag{2.53}$$

where for a Hermitian metric (see equation (2.18)) only the first type of transformation preserves the index structure. This is an infinitesimal deformation of the Kähler structure, i.e. the Kähler class $[J_{1,1}^{\text{Kähler}}]$ is transformed into a new element $[J_{1,1}^{\text{Kähler}}] \in H_{\bar\partial}^{1,1}(M)$. If the second type of perturbation is applied, the metric is not Hermitian anymore, but one can always redefine the coordinates by a non-holomorphic transformation in order to obtain again a metric in Hermitian form. Since the coordinate change is not holomorphic, one goes over to a different complex structure. Such complex structure deformations are associated to elements $\Omega_{\mu\nu\rho}\, g^{\rho\bar\gamma}\, \delta g_{\bar\gamma\bar\lambda}\, \mathrm{d}z^\mu \wedge \mathrm{d}z^\nu \wedge \mathrm{d}z^{\bar\lambda}$ of $H_{\bar\partial}^{2,1}(M)$ with $\Omega_{\mu\nu\rho}$ being the components of the holomorphic three-form, see section 2.1.6.

For the computations in chapter 4, I use concrete complex structure deformations as first introduced in [108] by Vafa and Witten. To be somewhat more precise, take the simple example

$$x_1^2 + x_2^2 + x_3^2 + x_4^2 = 0 \tag{2.54}$$

of a conifold singularity in a Calabi-Yau manifold of three dimensions, as presented in [108]. This singularity is removed by setting equation (2.54) equal to the complex structure deformation parameter ε,

$$x_1^2 + x_2^2 + x_3^2 + x_4^2 = \varepsilon\,. \tag{2.55}$$

In addition, Vafa and Witten briefly sketched how local and global complex structure deformations of the $T^6/(\mathbb{Z}_2 \times \mathbb{Z}_2)$ orbifold (with discrete torsion, see section 3.1.1) in principle would look like. Together with my collaborators, I took [108] as a starting point to develop for the first time an explicit method for performing such complex structure deformations. We studied several examples, also generalisations to the orbifold $T^6/(\mathbb{Z}_2 \times \mathbb{Z}_6')$, and additionally we analysed the effects of the deformations on the volumes and calibrations of three-cycles, as well as applications to concrete models, cf. [109–111].

More details and physical applications will be presented in chapter 4, as well as the new example of the $T^6/(\mathbb{Z}_2 \times \mathbb{Z}_6)$ orbifold. As a short hint to the physical interest of concrete deformations, let me remark that for instance the (squares of the) gauge couplings are (anti-)proportional to the volumes of three-cycles, and therefore, by continuous changes in the volumes, one can adjust the gauge couplings.

3 The Setup in String Theory

In the first part, I treat only the purely geometric properties of the concrete setup that I will use in my thesis for the internal six-dimensional space of type IIA string theory. The concrete structure of this background space and of certain subspaces thereof is crucial for my work, and this is why I will present the characteristics here at full length. After that, I summarise the physical quantities that appear in these backgrounds in type IIA string theory, i.e. bosonic and fermionic fields, generated by certain oscillation modes of closed and open strings. I will mostly restrict the discussion to the different kinds of massless bosonic fields since these have important implications for the deformations, and especially because these incorporate the aforementioned Kähler and complex structure moduli. In addition, the higher-dimensional physical Dp-branes and Op-planes will be introduced, as mentioned in the introductory chapter 1, which play a major role in string model building.

3.1 Geometry of the background and construction of subspaces

The mathematical objects that I use for the construction of the six-dimensional internal background space are factorisable toroidal orbifolds, i.e. special cases of the orbifolds that were presented in section 2.4. As discussed in the introductory chapter, orbifolds are a fruitful field for model building in string theory, and have many interesting properties. In section 3.1.2, I will describe an additional restriction that can be imposed on the background space, which leads to an orientifold. Note that I will explain here only the geometric target space part of this restriction, while the second contribution from the worldsheet will be discussed in section 3.2. Finally, I present in section 3.1.3 specific subspaces called cycles, which should already be familiar to the reader from section 2.5 about homology and cohomology. These cycles are the basic objects of my analysis in chapter 4, and therefore I give a lot of information on them.

3.1.1 The background space: factorisable toroidal orbifolds

As six-dimensional compact space I take a six-torus T^6, which I divide by a discrete group Γ, expressed as T^6/Γ. The resulting object is called toroidal orbifold, cf. section 2.4 for orbifolds and section 2.3 for mathematical descriptions of a torus. For the concrete form $T^6/(\mathbb{Z}_2 \times \mathbb{Z}_{2M})$, the orbifold has the generators θ, ω

$$\theta^p \omega^q : z_i \longmapsto e^{2\pi i(pv^i + qw^i)} z_i \qquad (i = 1, 2, 3) \qquad (3.1)$$

that act diagonally on the torus coordinates z_i with specifications

$$\vec{v} = \frac{1}{2}(1, -1, 0) \quad \text{for } \mathbb{Z}_2\,, \qquad \begin{aligned} \vec{w} &= \tfrac{1}{2}(0, 1, -1) & \text{for } \mathbb{Z}_{2M} \equiv \mathbb{Z}_2\,, \\ \vec{w} &= \tfrac{1}{6}(0, 1, -1) & \text{for } \mathbb{Z}_{2M} \equiv \mathbb{Z}_6\,, \\ \vec{w} &= \tfrac{1}{6}(-2, 1, 1) & \text{for } \mathbb{Z}_{2M} \equiv \mathbb{Z}_6'\,. \end{aligned} \qquad (3.2)$$

Each choice of $p \in \{0, 1\}$ and $q \in \{0, \ldots, 2M - 1\}$ gives rise to a so-called twisted sector. Furthermore, one has to take into account that the generator of $\mathbb{Z}_{2M}$ can act with sign $\eta := \pm 1$ on the other generator $\mathbb{Z}_2$, or the other way round. Orbifolds with sign choice $\eta = +1$ are called *without discrete torsion*, while those with opposite sign $\eta = -1$ are referred to as *with discrete torsion*. The structure of such toroidal orbifolds with generators as in equation (3.2), together with the implications on the particle spectrum, was studied in much detail in [66], and D6-brane model building on the $T^6/(\mathbb{Z}_2 \times \mathbb{Z}_2)$ orbifold with discrete torsion traces back to [71].

It is possible to treat the toroidal orbifolds presented above on non-factorisable tori, but since the more specialised setup of factorisable six-tori $T^6 \equiv T^2_{(1)} \times T^2_{(2)} \times T^2_{(3)}$, i.e. the product of three two-tori, is much easier to handle and has interesting properties, models on factorisable tori have been up to now more popular among string phenomenologists. The generators of equation (3.2) impose then the following conditions on the lattice vectors of T^6. For the $T^6/(\mathbb{Z}_2 \times \mathbb{Z}_2)$ orbifold I find an $SU(2)^6$ root lattice, where the lattice vectors are unrestricted in the sense that they can be chosen arbitrarily. In case of $T^6/(\mathbb{Z}_2 \times \mathbb{Z}_6)$, there is again no restriction on the first two-torus, while the second and third have a hexagonal shape due to the $\mathbb{Z}_3$ action thus corresponding to a $SU(2)^2 \times SU(3)^2$ root lattice. The orbifold $T^6/(\mathbb{Z}_2 \times \mathbb{Z}_6')$ provides three hexagonal lattices, and therefore it is clear that each has the properties of an $SU(3)^3$ root lattice.

For the orbifolds with discrete torsion ($\eta = -1$), which I am mostly interested in, at the positions of the orbifold fixed lines there appear curvature singularities of complex codimension two due to the orbifold action. These can be referred to as singular lines when speaking in terms of complex coordinates, or likewise as singular planes if the picture of real dimensions is used. The complex codimension two singularities can intersect, and for the orbifolds considered here, at all their intersection points one finds complex codimension three singularities.

The concrete structure of the orbifolds given in equations (3.1) and (3.2) is encoded in the Hodge numbers, cf. section 2.5, which are summarised in table 2. Each orbifold has three untwisted Kähler moduli, $h^{1,1}_{\text{unt}} = 3$, for the untwisted or bulk part. These refer to the size of each two-torus $T^2_{(i)}$ and can be chosen arbitrarily. On the contrary, the untwisted complex structure moduli $h^{2,1}_{\text{unt}}$, describing the shape of a two-torus $T^2_{(i)}$, differ for the above

									Hodge numbers of $T^6/(\mathbb{Z}_2 \times \mathbb{Z}_{2M})$ orbifolds
					$T^6/(\mathbb{Z}_2 \times \mathbb{Z}_2)$ with $\eta = +1$, root lattice: $SU(2)^6$					
	Bulk	$\mathbb{Z}_2^{(1)}$	$\mathbb{Z}_2^{(2)}$	$\mathbb{Z}_2^{(3)}$						$h_{\mathrm{unt}}^{l,m} + h_{\mathrm{tw},\mathbb{Z}_2}^{l,m}$
$h^{1,1}$	3	16	16	16						3 + 48
$h^{2,1}$	3	0	0	0						3 + 0
					$T^6/(\mathbb{Z}_2 \times \mathbb{Z}_2)$ with $\eta = -1$, root lattice: $SU(2)^6$					
	Bulk	$\mathbb{Z}_2^{(1)}$	$\mathbb{Z}_2^{(2)}$	$\mathbb{Z}_2^{(3)}$						$h_{\mathrm{unt}}^{l,m} + h_{\mathrm{tw},\mathbb{Z}_2}^{l,m}$
$h^{1,1}$	3	0	0	0						3 + 0
$h^{2,1}$	**3**	**16**	**16**	**16**						**3 + 48**
					$T^6/(\mathbb{Z}_2 \times \mathbb{Z}_6)$ with $\eta = -1$, root lattice: $SU(2)^2 \times SU(3)^2$					
	Bulk	$\mathbb{Z}_2^{(1)}$	$\mathbb{Z}_2^{(2)}$	$\mathbb{Z}_2^{(3)}$	$\mathbb{Z}_3$	$\mathbb{Z}_6: \omega, \theta\omega, \theta\omega^2$			$h_{\mathrm{unt}}^{l,m} + h_{\mathrm{tw},\mathbb{Z}_2}^{l,m} + h_{\mathrm{tw},\mathbb{Z}_3+\mathbb{Z}_6}^{l,m}$
$h^{1,1}$	3	0	0	0	8	0	4	4	3 + 0 + 16
$h^{2,1}$	**1**	**6**	**4**	**4**	2	2	0	0	**1 + 14 + 4**
					$T^6/(\mathbb{Z}_2 \times \mathbb{Z}_6')$ with $\eta = -1$, root lattice: $SU(3)^3$					
	Bulk	$\mathbb{Z}_2^{(1)}$	$\mathbb{Z}_2^{(2)}$	$\mathbb{Z}_2^{(3)}$	$\mathbb{Z}_3$	$\mathbb{Z}_6': \omega, \theta\omega, \theta\omega^2$			$h_{\mathrm{unt}}^{l,m} + h_{\mathrm{tw},\mathbb{Z}_2}^{l,m} + h_{\mathrm{tw},\mathbb{Z}_3+\mathbb{Z}_6}^{l,m}$
$h^{1,1}$	3	0	0	0	9	1	1	1	3 + 0 + 12
$h^{2,1}$	**0**	**5**	**5**	**5**	0	0	0	0	**0 + 15 + 0**

Table 2: This table is based on [66] and displays the Hodge numbers for the $T^6/(\mathbb{Z}_2 \times \mathbb{Z}_{2M})$ orbifolds, which are separated into the number of Kähler moduli $h^{1,1}$ and the number of complex structure moduli $h^{2,1}$. A further distinction between the untwisted (also called bulk) und twisted sectors is made, i.e. $h^{2,1} = h_{\mathrm{unt}}^{2,1} + h_{\mathrm{tw},\mathbb{Z}_2}^{2,1} + h_{\mathrm{tw},\mathbb{Z}_3+\mathbb{Z}_6}^{2,1}$, and similarly for $h^{1,1}$. The complex structure moduli $h^{2,1}$ in bold face are relevant for later discussions and the concrete generators for the twisted sectors can be found in equations (3.3) and (3.4).

orbifolds. While for $\mathbb{Z}_2 \times \mathbb{Z}_2$ the three tori can have an arbitrary shape, i.e. $h_{\mathrm{unt}}^{2,1} = 3$, in case of $\mathbb{Z}_2 \times \mathbb{Z}_6$ or $\mathbb{Z}_2 \times \mathbb{Z}_6'$ two or all three tori, respectively, are due to the additional $\mathbb{Z}_3$ symmetry restricted to have hexagonal shape, which means that these complex structure moduli have now a fixed value.

The twisted moduli appear at the positions of the orbifold fixed points, where curvature

singularities of codimension two emerge. At these singular points, one can glue in algebraic objects of zero volume that are called exceptional divisors. If their volume is changed and differs from zero, e.g. due to a deformation, the corresponding singularity vanishes and is replaced by a smooth patch. In case that the fixed line supports a twisted complex structure modulus $h_{\text{tw}}^{2,1}$, cf. table 2, the singularity can, roughly speaking, be *deformed* in its shape. If a twisted Kähler modulus $h_{\text{tw}}^{1,1}$ is apparent, the exceptional divisor at the singular point can change its size by a so-called *blow-up*. In section 3.1.3, I will explain the concept of exceptional *cycles* on $T^6/(\mathbb{Z}_2 \times \mathbb{Z}_{2M})$ orbifolds, which are basically exceptional divisors. In this context it will become clear that I am mainly interested in the twisted complex structure moduli $h_{\text{tw}}^{2,1}$ since these correspond to exceptional three-cycles, while the twisted Kähler moduli $h_{\text{tw}}^{1,1}$ imply the existence of exceptional two-cycles.

To understand better which twisted moduli exist for the orbifolds given above, I will look in more detail at the twisted sectors, see equations (3.1) and (3.2). For a combination of the $\mathbb{Z}_2$ generators I obtain the $\mathbb{Z}_2^{(i)}$ twisted sectors, where the label (i) refers to the torus that stays invariant under the action of equation (3.1),

$$\mathbb{Z}_2 \times \mathbb{Z}_2: \qquad \mathbb{Z}_2^{(1)} \leftrightarrow \omega, \quad \mathbb{Z}_2^{(2)} \leftrightarrow \theta\omega, \quad \mathbb{Z}_2^{(3)} \leftrightarrow \theta. \tag{3.3}$$

Each $\mathbb{Z}_2^{(i)}$ twisted sector gives rise to 4×4 fixed points $(\alpha\beta) \in T_{(i)}^4 \equiv T_{(j)}^2 \times T_{(k)}^2$ with labels $\alpha, \beta \in \{1, 2, 3, 4\}$ and (ijk) a permutation of (123), see also figure 1. Table 2 reveals that both orbifolds $T^6/(\mathbb{Z}_2 \times \mathbb{Z}_2)$ have the maximal number of $3 \times 4 \times 4 = 48$ twisted moduli at these fixed points, but the choice of discrete torsion $\eta = \pm 1$ determines if one finds only twisted Kähler moduli $h_{\text{tw},\mathbb{Z}_2}^{1,1}$ ($\eta = +1$) or twisted complex structure moduli $h_{\text{tw},\mathbb{Z}_2}^{2,1}$ ($\eta = -1$). For the orbifolds $T^6/(\mathbb{Z}_2 \times \mathbb{Z}_6^{(\prime)})$ with $\eta = -1$ the number $h_{\text{tw},\mathbb{Z}_2}^{2,1}$ is reduced due to fixed point identifications under the additional $\mathbb{Z}_3$ symmetry, see the discussion below.

The generators of the orbifold group $\mathbb{Z}_2 \times \mathbb{Z}_6^{(\prime)}$ give rise to more sectors due to the additional $\mathbb{Z}_3$ symmetry on the tori that have hexagonal shape,

$$\begin{aligned} \mathbb{Z}_2 \times \mathbb{Z}_6^{(\prime)}: \qquad & \mathbb{Z}_2^{(1)} \leftrightarrow \omega^3, & \mathbb{Z}_2^{(2)} \leftrightarrow \theta\omega^3, & \mathbb{Z}_2^{(3)} \leftrightarrow \theta, \\ & \mathbb{Z}_3 \leftrightarrow \omega^2, \\ & \mathbb{Z}_6^{(\prime)} \leftrightarrow \omega, \theta\omega, \theta\omega^2, \end{aligned} \tag{3.4}$$

and the 4×4 fixed points per $\mathbb{Z}_2^{(i)}$ twisted sector are no longer independent owing to the $\mathbb{Z}_3$ symmetry. Furthermore, there arise twisted moduli for the $\mathbb{Z}_3$ and $\mathbb{Z}_6^{(\prime)}$ twisted sectors, which are different for the two orbifolds. Since the effect of $\mathbb{Z}_3$ is here basically to restrict the $\mathbb{Z}_2 \times \mathbb{Z}_2$ fixed points and their moduli, I will later express the $\mathbb{Z}_2 \times \mathbb{Z}_6^{(\prime)}$ orbifolds as $(T^6/(\mathbb{Z}_2 \times \mathbb{Z}_2))/\mathbb{Z}_3$, where I take $T^6/(\mathbb{Z}_2 \times \mathbb{Z}_2)$ and divide out the symmetry $\mathbb{Z}_3$ by hand.

Orbifold group $\mathbb{Z}_2 \times \mathbb{Z}_6'$:   Here the $\mathbb{Z}_3$ action has the same effect on all two-tori $T^2_{(i)}$, due to which all $\mathbb{Z}_2 \times \mathbb{Z}_2$ fixed points are identified in orbits as

$$T^2_{(i)}: \qquad 1 \overset{\mathbb{Z}_3}{\longmapsto} 1\,, \quad 3 \overset{\mathbb{Z}_3}{\longmapsto} 2 \overset{\mathbb{Z}_3}{\longmapsto} 4 \overset{\mathbb{Z}_3}{\longmapsto} 3 \qquad (i = 1,2,3)\,. \tag{3.5}$$

This implies that the number of complex structure moduli $h^{2,1}_{\mathrm{tw},\mathbb{Z}_2}$ shown in table 2 is reduced. More concretely, one can observe the following fixed point orbits:

$$\mathbb{Z}_2 \times \mathbb{Z}_6': \qquad \begin{bmatrix} (21) \\ (31) \\ (41) \end{bmatrix}, \quad \begin{bmatrix} (12) \\ (13) \\ (14) \end{bmatrix}, \quad \begin{bmatrix} (22) \\ (33) \\ (44) \end{bmatrix}, \quad \begin{bmatrix} (23) \\ (34) \\ (42) \end{bmatrix}, \quad \begin{bmatrix} (24) \\ (32) \\ (43) \end{bmatrix}, \quad (11)\,. \tag{3.6}$$

Except for (11), all fixed points are grouped into triplets such that one finds in total six orbits per sector, i.e. 3×6, where all but the invariant fixed point (11) have a twisted complex structure modulus assigned (cf. table 2), i.e. $h^{2,1}_{\mathrm{tw},\mathbb{Z}_2} = 5 + 5 + 5$. The complex structure moduli of these fixed points will play an important role in the next chapters and will be used for deformations of the respective orbifold singularities.

In the $\mathbb{Z}_3$ twisted sector with generator ω^2, there arise $3 \times 3 \times 3$ fixed points, which are labelled $(\alpha\beta\gamma) \in T^2_{(1)} \times T^2_{(2)} \times T^2_{(3)}$ with $\mathbb{Z}_3$ fixed points $\alpha, \beta, \gamma \in \{1, \tilde{2}, \tilde{3}\}$. Here, it is the $\mathbb{Z}_2 \times \mathbb{Z}_2$ symmetry of the orbifold that groups the fixed points into orbits since $\tilde{2} \overset{\mathbb{Z}_2}{\leftrightarrow} \tilde{3}$ are identified, while fixed point 1 stays invariant. These orbits support only twisted Kähler moduli and will therefore not be discussed in more detail. Also for the $\mathbb{Z}_6$ fixed points I find in table 2 just contributions for $h^{1,1}_{\mathrm{tw},\mathbb{Z}_6}$, hence I will not carry out a further investigation on these.

Orbifold group $\mathbb{Z}_2 \times \mathbb{Z}_6$:   This orbifold has a similar construction as $\mathbb{Z}_2 \times \mathbb{Z}_6'$, but it is less symmetric due to the fact that it does not consist of three hexagonal tori, but of one rectangular (or tilted) and two hexagonal ones. In addition, the $\mathbb{Z}_3$ action has different effects on the two hexagonal tori, namely the two different fixed point orbits look like

$$\mathbb{Z}_2 \times \mathbb{Z}_6: \qquad \begin{aligned} T^2_{(2)}: &\qquad 1 \overset{\mathbb{Z}_3}{\longmapsto} 1\,, &\qquad 3 \overset{\mathbb{Z}_3}{\longmapsto} 2 \overset{\mathbb{Z}_3}{\longmapsto} 4 \overset{\mathbb{Z}_3}{\longmapsto} 3\,, \\ T^2_{(3)}: &\qquad 1 \overset{\mathbb{Z}_3}{\longmapsto} 1\,, &\qquad 3 \overset{\mathbb{Z}_3}{\longmapsto} 4 \overset{\mathbb{Z}_3}{\longmapsto} 2 \overset{\mathbb{Z}_3}{\longmapsto} 3\,, \end{aligned} \tag{3.7}$$

and one easily sees that the transformation on $T^2_{(3)}$ is "backwards" compared to the one on $T^2_{(2)}$. Thus, one obtains the following fixed point orbits in the different sectors $\mathbb{Z}_2^{(i)}$, where

in the first sector $\mathbb{Z}_2^{(1)}$ the invariant torus is the rectangular one:

$\mathbb{Z}_2 \times \mathbb{Z}_6$:

$$
\text{Sector 1:} \quad
\begin{bmatrix} (21) \\ (31) \\ (41) \end{bmatrix}, \quad
\begin{bmatrix} (12) \\ (13) \\ (14) \end{bmatrix}, \quad
\begin{bmatrix} (33) \\ (42) \\ (24) \end{bmatrix}, \quad
\begin{bmatrix} (22) \\ (34) \\ (43) \end{bmatrix}, \quad
\begin{bmatrix} (44) \\ (23) \\ (32) \end{bmatrix}, \quad (11),
$$

(3.8)

$$
\text{Sector 2:} \quad
\begin{bmatrix} (21) \\ (31) \\ (41) \end{bmatrix}, \quad
\begin{bmatrix} (22) \\ (32) \\ (42) \end{bmatrix}, \quad
\begin{bmatrix} (23) \\ (33) \\ (43) \end{bmatrix}, \quad
\begin{bmatrix} (24) \\ (34) \\ (44) \end{bmatrix}, \quad (11), (12), (13), (14),
$$

For sector two, the labels for fixed point $(\alpha\beta)$ are assigned such that $\alpha \in T_{(3)}^2$, $\beta \in T_{(1)}^2$, and sector 3 is the same as sector 2 with interchanged fixed point labels, i.e. $(\alpha\beta) \leftrightarrow (\beta\alpha)$. For each orbit in sector 1, there exists a twisted complex structure modulus, but for sector 2 (and 3, respectively) only the orbits $(2\rho), (3\rho), (4\rho)$ ($\rho = 1, 2, 3, 4$) support twisted complex structure moduli and can be deformed. Hence, I find $h_{\text{tw},\mathbb{Z}_2}^{2,1} = 6 + 4 + 4$, as displayed in table 2.

It will turn out in the following chapter that it is often sufficient to study deformations in the simpler $T^4/\mathbb{Z}_2$ orbifold, where only one generator

$$
\theta^p : z_i \longmapsto e^{2\pi i \cdot p v^i} z_i \qquad \text{with } \vec{v} = \frac{1}{2}(1, -1)
$$

(3.9)

remains. The results can then be easily generalized to either $T^6/(\mathbb{Z}_2 \times \mathbb{Z}_2)$ with discrete torsion or to the orbifolds $T^6/(\mathbb{Z}_2 \times \mathbb{Z}_6^{(\prime)})$ (also with $\eta = -1$).

3.1.2 Introducing yet another symmetry: orientifolds

If one divides the previously introduced orbifolds furthermore by the action of $\Omega\mathcal{R}$, one obtains so-called *orientifolds*. The worldsheet parity Ω, which is not to be confused with the holomorphic volume form Ω_n, will be introduced later for physical reasons in the context of (a priori oriented) string worldsheets. On the other hand, the antiholomorphic involution $\mathcal{R}$ is an additional symmetry of the underlying target space, i.e. of type II string theory on the orbifold. The antiholomorphic involution obeys the conditions

$$
\mathcal{R}(J_{1,1}^{\text{Kähler}}) = -J_{1,1}^{\text{Kähler}}, \qquad \mathcal{R}(\Omega_n) = e^{2i\varphi_a}\overline{\Omega_n},
$$

(3.10)

on the Kähler form $J_{1,1}^{\text{Kähler}}$ and on the holomorphic n-form Ω_n for complex n-dimensional manifolds. In the following discussions, the phase φ_a is mostly $\varphi_a = 0$ and thus the action of $\mathcal{R}$ is simply complex conjugation, $\mathcal{R} : z_i \mapsto \overline{z_i}$, on the underlying torus.

It is clear that the torus lattice has to stay invariant when I divide the orbifold by the action of $\mathcal{R}$, which means that $\mathcal{R}$ has to be a lattice automorphism. This severely restricts the possible shapes of the lattice and there remain only two different choices, namely untilted (**a**-type) or tilted (**b**-type) lattices. The two classes can be distinguished by the Klein invariant $j(\tau)$ that was introduced in equation (2.35). $j(\tau) \geq 1$ denotes *untilted* **a**-type lattices with a rectangular shape and $j(\tau) \leq 1$ refers to *tilted* or **b**-type lattices with a fundamental domain in form of a parallelogram.

The value $j(\tau) = 1$ is special because it describes both *untilted* and *tilted* lattices and has the form of a square, which exhibits an additional $\mathbb{Z}_4$ symmetry. The two pictures are only by $e^{\pi i/4}$ rotated versions of each other, see figure 1. Also $j(\tau) = 0$ gives rise to an additional symmetry, which is $\mathbb{Z}_3$. This implies that the lattice has a hexagonal shape. In the next section, I will see that the square torus is for models of **a**-type lattices the preferred choice because it simplifies the following calculations a lot. In addition, I will make extensive use of the hexagonal lattice, which proved to be quite useful in semi-realistic model building due to its $\mathbb{Z}_3$ symmetry.

3.1.3   Subspaces with special properties: cycles

To see how many independent three-cycles one can construct on a certain orbifold, one has to compute the Betti number b_3, which reads for $T^6/(\mathbb{Z}_2 \times \mathbb{Z}_{2M})$ orbifolds

$$b_3(T^6/(\mathbb{Z}_2 \times \mathbb{Z}_{2M})) = (2 + 2h_{\text{unt}}^{2,1}) + 2h_{\text{tw}}^{2,1}. \tag{3.11}$$

The number of bulk cycles is given by the first part $2 + 2h_{\text{unt}}^{2,1}$, and the counting of untwisted and twisted complex structure moduli $h_{\text{unt}}^{2,1}$ and $h_{\text{tw}}^{2,1}$ can be found in table 2. As results for the Betti numbers I find

$$
\begin{aligned}
\mathbb{Z}_2 \times \mathbb{Z}_2, \eta = +1: \quad & b_3 = 8_{\text{bulk}}, \\
\mathbb{Z}_2 \times \mathbb{Z}_2, \eta = -1: \quad & b_3 = 8_{\text{bulk}} + 96_{\text{tw}, \mathbb{Z}_2}, \\
\mathbb{Z}_2 \times \mathbb{Z}_6, \eta = -1: \quad & b_3 = 4_{\text{bulk}} + 28_{\text{tw}, \mathbb{Z}_2} + 8_{\text{tw}, \mathbb{Z}_3 + \mathbb{Z}_6}, \\
\mathbb{Z}_2 \times \mathbb{Z}_6', \eta = -1: \quad & b_3 = 2_{\text{bulk}} + 30_{\text{tw}, \mathbb{Z}_2}.
\end{aligned}
\tag{3.12}
$$

For the orbifold group $\mathbb{Z}_2 \times \mathbb{Z}_2$ without discrete torsion ($\eta = +1$), there are no twisted complex structure moduli, and therefore no exceptional three-cycles on this orbifold, as already mentioned in section 3.1.1.

For the $T^6/(\mathbb{Z}_2 \times \mathbb{Z}_{2M})$ orbifolds with discrete torsion I will now define different kinds of p-cycles on the six-torus or its orbifold, which are p-dimensional closed submanifolds without a boundary. For the definitions I closely follow [66]. To improve the readability, I will label all kinds of three-cycles with capital letters, while two- or one-cycles are named with lower-case letters, where it is always clear from the context which kind of cycle is used.

An arbitrary torus three-cycle is simply described by the tensor product of the basis one-cycles π_{2i-1} and π_{2i} on the torus $T^2_{(i)}$, cf. figure 1, weighted with the wrapping numbers $n_i, m_i \in \mathbb{Z}$,

$$\Pi^{\text{torus}} := \bigotimes_{i=1}^{3} \left(n_i \pi_{2i-1} + m_i \pi_{2i} \right) . \tag{3.13}$$

One can also define basis three-cycles on the six-torus by

$$\Pi_{IJK} := \pi_I \otimes \pi_J \otimes \pi_K , \tag{3.14}$$

where $I \in \{2i-1, 2i\}$, $J \in \{2j-1, 2j\}$, $K \in \{2k-1, 2k\}$. Taking into account that the cycles do not live on the torus, but on an orbifold thereof, one has to apply the specific orbifold generators $\theta^p \omega^q$ (cf. equations (3.1) and (3.2)) on the torus cycles and take the sum over all orbifold images. The resulting objects are called bulk cycles and have the form

$$\Pi^{\text{bulk}} := \sum_{p=0}^{1} \sum_{q=0}^{2M-1} \theta^p \omega^q \Pi^{\text{torus}} . \tag{3.15}$$

For all bulk cycles, this definition can be simplified by the observation that these cycles are mapped onto themselves under the $\mathbb{Z}_2 \times \mathbb{Z}_2$ action and therefore

$$\Pi^{\text{bulk}} := 4 \sum_{q=0}^{M-1} \omega^q \Pi^{\text{torus}} , \tag{3.16}$$

where the labelling with index O6 will become clear in the next section when physical objects are introduced. To these three-cycles I assign the parameters $\sigma^i \in \{0, 1\}$ which determine if the basis one-cycle π_{2i-1} or π_{2i} runs through the origin, described by $\sigma^i = 0$, or is displaced by a half lattice vector and has thus parameter $\sigma^i = 1$.

On the positions of the $\mathbb{Z}_2 \times \mathbb{Z}_2$ orbifold fixed points $(\alpha\beta) \in T^2_{(i)} \times T^2_{(j)} \equiv T^4_{(k)}$ with the labels $\alpha, \beta \in \{1, 2, 3, 4\}$, see figure 1, and $(ijk) = (123 \text{ cyclic})$, which arise due to the orbifold action $\mathbb{Z}_2^{(k)}$, there exist so-called exceptional two-cycles $e_{\alpha\beta}^{(k)}$. These come from the resolution of the complex codimension two orbifold singularities and obtain a non-vanishing volume upon deformations away from the orbifold point. More details on that will be given in the next
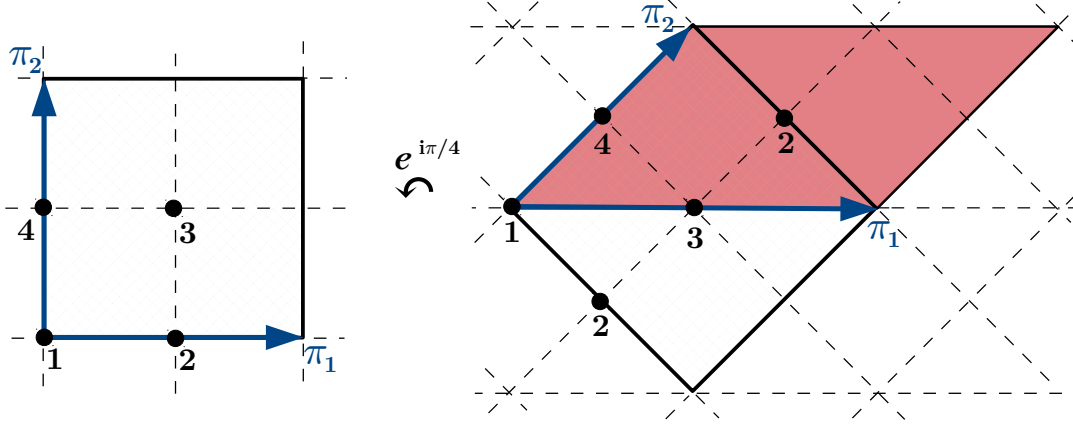
36

Figure 1: Square torus with underlying untilted (**a**-type) or tilted (**b**-type) lattice where both descriptions are related by a rotation of the coordinate $z_i \leftrightarrow e^{\pm i\pi/4} z_i$ (figure taken from [110]). The $\mathbb{Z}_2$ fixed point with label 1 is always located at the origin of the fundamental domain. The other fixed points 2,3,4 are assigned counter-clockwise in the left figure, and the same labels are given to the rotated image on the right hand side. The basis one-cycle π_1 in $T^2_{(1)}$ is throughout my thesis chosen to lie along the real axis (this setup is also known as **A**-type lattice, cf. e.g. [66]), and analogously for the other two-tori, where the basis one-cycles are called π_3, π_4, and π_5, π_6, respectively. It is clear that I use for other untilted (left) or tilted (right) lattices the same labelling, especially for the hexagonal lattice.

chapter. When the $\mathbb{Z}_2$ part of the second orbifold group, i.e. $\mathbb{Z}_2^{(i)}$ or $\mathbb{Z}_2^{(j)}$, acts on these exceptional cycles, they receive a sign factor $\eta = \pm 1$

$$e_{\alpha\beta}^{(k)} \xrightarrow{\mathbb{Z}_2^{(i)}} \eta \, e_{\alpha\beta}^{(k)} \,, \tag{3.17}$$

where η is the discrete torsion between the two orbifold actions, as explained around table 2. Since I will always work with orbifolds of $\eta = -1$, the exceptional cycles obtain a negative sign. Also the torus one-cycles are affected by the second $\mathbb{Z}_2$ orbifold group and change as well their sign,

$$\pi_{2k-1} \xrightarrow{\mathbb{Z}_2^{(i)}} -\pi_{2k-1} \,, \qquad \pi_{2k} \xrightarrow{\mathbb{Z}_2^{(i)}} -\pi_{2k} \,. \tag{3.18}$$

Hence, the combination of an exceptional two-cycle $e_{\alpha\beta}^{(k)}$ with a torus one-cycle π_{2k-1} or π_{2k} makes it possible to construct an exceptional three-cycle that is invariant under the orbifold,

$$E_{\alpha\beta}^{(k)} := 2 \sum_{q=0}^{M-1} \omega^q \left(e_{\alpha\beta}^{(k)} \otimes \pi_{2k-1} \right) \,, \qquad \tilde{E}_{\alpha\beta}^{(k)} := 2 \sum_{q=0}^{M-1} \omega^q \left(e_{\alpha\beta}^{(k)} \otimes \pi_{2k} \right) \,. \tag{3.19}$$

The reason for the factor two is that the group $\mathbb{Z}_2^{(i)}$ produces a second image of the basis one-cycle π_{2k-1} or π_{2k}. One should note that all exceptional cycles have vanishing volume unless they are subject to a deformation away from the singular orbifold point.

As explained around equation (3.16), torus cycles that run through the orbifold fixed points get mapped onto themselves under the orbifold action, and one finds that a bulk cycle consists of four images of the same torus cycle. A more general cycle is thus obtained by taking only one such image into account, i.e. one uses a fraction of one quarter, but in order to close such a bulk cycle one needs to add a suitable choice of exceptional cycles. These considerations lead for orbifolds $\mathbb{Z}_2 \times \mathbb{Z}_{2M}$ with $2M = 2, 6, 6'$ and discrete torsion $\eta = -1$ to the following definition of a fractional cycle,

$$\Pi^{\text{frac}} := \frac{1}{4} \left(\Pi^{\text{bulk}} + \sum_{k=1}^{3} \Pi^{\mathbb{Z}_2^{(k)}} \right) , \tag{3.20}$$

where Π^{bulk} is given by equation (3.16) and the combination of exceptional three-cycles $\Pi^{\mathbb{Z}_2^{(k)}}$ works as follows. These cycles are defined on two different fixed points with the labels $\alpha_0, \alpha_1 \in \{1, 2, 3, 4\}$ that live on $T_{(i)}^2$ and similarly for the torus $T_{(j)}^2$ with fixed points β_0, β_1. The exceptional three-cycles $E_{\alpha\beta}^{(k)}$, $\tilde{E}_{\alpha\beta}^{(k)}$ on these fixed points are weighted with the exceptional wrapping numbers $(\hat{x}_{\alpha\beta}^{(k)}, \hat{y}_{\alpha\beta}^{(k)})$,

$$\Pi^{\mathbb{Z}_2^{(k)}} := \sum_{\alpha = \alpha_0, \alpha_1} \sum_{\beta = \beta_0, \beta_1} \left(\hat{x}_{\alpha\beta}^{(k)} E_{\alpha\beta}^{(k)} + \hat{y}_{\alpha\beta}^{(k)} \tilde{E}_{\alpha\beta}^{(k)} \right) , \tag{3.21}$$

where $\hat{x}_{\alpha\beta}^{(k)}$ and $\hat{y}_{\alpha\beta}^{(k)}$ are composed of the torus wrapping numbers (n_k, m_k) with additional sign factors, i.e. for $\mathbb{Z}_2 \times \mathbb{Z}_2$

$$\begin{aligned}
\hat{x}_{\alpha_0\beta_0}^{(k)} &= \pm n_k , & \hat{y}_{\alpha_0\beta_0}^{(k)} &= \pm m_k , \\
\hat{x}_{\alpha_1\beta_0}^{(k)} &= \pm(-1)^{\tau^i} n_k , & \hat{y}_{\alpha_1\beta_0}^{(k)} &= \pm(-1)^{\tau^i} m_k , \\
\hat{x}_{\alpha_0\beta_1}^{(k)} &= \pm(-1)^{\tau^j} n_k , & \hat{y}_{\alpha_0\beta_1}^{(k)} &= \pm(-1)^{\tau^j} m_k , \\
\hat{x}_{\alpha_1\beta_1}^{(k)} &= \pm(-1)^{\tau^i+\tau^j} n_k , & \hat{y}_{\alpha_1\beta_1}^{(k)} &= \pm(-1)^{\tau^i+\tau^j} m_k .
\end{aligned} \tag{3.22}$$

The signs arise from the $\mathbb{Z}_2^{(k)}$ eigenvalue $(-1)^{\tau_0^{(k)}} = \pm 1$ (i.e. $\tau_0^{(k)} \in \{0, 1\}$), which describes roughly speaking the orientation with which the reference fixed point $(\alpha_0\beta_0)$ is encircled, and from the choice of discrete Wilson lines $\tau^k \in \{0, 1\}$, which fix the orientation of all other fixed points with respect to the reference point. Together with the discrete displacements $\sigma^k \in \{0, 1\}$ as introduced under equation (3.16), these parameters will play an important role in the discussion of concrete models. It is clear that bulk and exceptional contributions of a fractional cycle have to be defined on the same set of fixed points.

In the simpler picture of a $T^4/\mathbb{Z}_2$ orbifold, the above formulas have to be slightly modified. An obvious change is that the sums and products run only from one to two and there exists just one generator θ for the orbifold group $\mathbb{Z}_2$. In addition, the exceptional cycle consist only of the exceptional two-cycle, whereas the tensor product with the torus one-cycle does not appear. In all formulas, the factors of four and 1/4 are replaced by two and 1/2 because there exist only two orbifold images. To make a clear distinction between two- and one-cycles, the two-cycles have here names with capital letters, for example the cycles Π, and the one-cycles are again written in lower-case.

When I introduce orientifolds as in section 3.1.2, I also have to consider the effect of the antiholomorphic involution $\mathcal{R}$ on the cycles, with transformation properties given in equation (3.10). For model building I will consider cycles Π_a that are called *special Lagrangian (sLag)*, as defined in [47]. These have the following properties in terms of the Kähler form $J_{1,1}^{\text{Kähler}}$ and the holomorphic n-form Ω_n,

$$J_{1,1}^{\text{Kähler}}\big|_{\Pi_a} = 0\,, \tag{3.23}$$

$$\text{Im}\left(e^{i\varphi_a}\Omega_n\right)\big|_{\Pi_a} = 0\,, \quad \text{Re}\left(e^{i\varphi_a}\Omega_n\right)\big|_{\Pi_a} > 0\,, \tag{3.24}$$

with calibration phase φ_a and where the cycles are restricted to the subspaces Π_a. All previously constructed cycles automatically satisfy equation (3.23), which is called *Lagrangian* condition. Equation (3.24) puts further constraints on these cycles in terms of wrapping numbers and complex structure moduli and is named *special Lagrangian* condition. It also determines the calibration of a *sLag* cycle in terms of the phase φ_a, where the cycle is said to have calibration $\text{Re}\,(\Omega_n)$ if $\varphi_a = 0$ and is called calibrated with respect to $\text{Im}\,(\Omega_n)$ in the case $\varphi_a = \pi/2$.

One can show that in order to obtain $\mathcal{N} = 1$ supersymmetric models, dynamical physical objects called D6-branes, which are wrapped on the *sLag* cycles Π_a, must be calibrated with the same phase φ_a as non-dynamical physical objects called O6-planes. More details on D6-branes and O6-planes will be given in the following section 3.2. Choosing $\varphi_a = 0$, the *sLag* conditions of equation (3.24) simplify to

$$\text{Im}\,(\Omega_n)\big|_{\Pi_a} = 0\,, \quad \text{Re}\,(\Omega_n)\big|_{\Pi_a} > 0\,. \tag{3.25}$$

This can also be expressed in terms of the three angles between a D6_a-brane and the respective real axis in the three tori $T_{(1)}^2 \times T_{(2)}^2 \times T_{(3)}^2$, which have to satisfy

$$\phi_a^1 + \phi_a^2 + \phi_a^3 = 0 \bmod 2\pi \quad \forall a\,. \tag{3.26}$$

From the characteristics given in equation (3.24), one can deduce the volume of the *sLag* cycle Π_a with real calibration, which reads

$$\text{Vol}(\Pi_a) = \left|\int_{\Pi_a} \text{Re}\left(e^{i\varphi_a}\Omega_n\right)\right|\,. \tag{3.27}$$

For a *sLag* cycles with imaginary calibration, one would have to replace the real with the imaginary part of the term $e^{i\varphi_a}\Omega_n$. In chapter 4, equation (3.27) will play a crucial role, and I will derive the volumes of many different configurations.

It will turn out in the next section that the fixed sets of the antiholomorphic involution $\mathcal{R}$, which are always *sLag* cycles, are very important for model building. By a proper definition of the torus coordinates z_i ($i = 1, 2, 3$) I can always choose the antiholomorphic involution to act as complex conjugation $\mathcal{R} : z_i \mapsto \overline{z_i}$. This implies $\mathcal{R}(\Omega_n) = \overline{\Omega_n}$ and therefore the phase in equations (3.24) and (3.27) is fixed as $\varphi_a = 0$, cf. equation (3.10). Cycles of this type are special in the sense that they can be wrapped by orientifold-planes, which only consist of a bulk part, but also by cycles which are either pointwise invariant under $\mathcal{R}$ or when taken as a whole, see chapter 5 for concrete examples. On the other hand, *sLag* cycles Π_a that are not invariant under $\mathcal{R}$ have a so-called orientifold image $\Pi_{a'} = \mathcal{R}(\Pi_a)$. This also has to be taken into account for the description in homogeneous coordinates x, v, y in chapter 4 and will lead to certain restrictions on the cycles and their deformations.

3.2   String phenomenology of type IIA orientifolds

The basic idea of string theory is that, when going to a much higher spacial resolution (i.e. to much higher energies), the elementary particles appear not as point-like anymore, but as closed and/or open oscillating strings. This implies that quantum field theory is only an effective field theory of an underlying more fundamental theory. Strings have the size $l_s = 1/M_s$ with string scale M_s, where l_s is in most models considered to be tiny with M_s close to the Planck scale ($\sim 10^{19}$ GeV), but there exist also constructions of much lower energies, even at the TeV scale.

The oscillation modes of closed and open strings have different characteristics, and each mode corresponds to a specific particle. The more oscillators of the string are excited, the heavier the corresponding particle, which implies that there exist in fact infinitely many particles, known as tower of particles. However, at scales much below the string scale M_s, only the massless modes are visible, and these are the states that string phenomenologists are usually interested in. I will explain in the following sections their concrete construction. One will also see that one of the many nice features of string theory is that gravity is very naturally included, because all kinds of string theories include in the closed string massless sector a field with the properties of the graviton. Hence, it is not hard to reduce string theory to general relativity theory.

One of the most important characteristics of string theory is that it has to be supersymmetric in order to provide a stable vacuum, i.e. tachyonic fields have to be absent. There

exist in fact five related classes of supersymmetric string theories, called superstring theories, which all require ten space-time dimensions for being consistent, cf. e.g. [7]. I will consider here the branch called type IIA string theory, which has a very similar geometrical structure as the type IIB string theory. This means that both incorporate dynamical physical objects of higher dimensions called D-branes, which I will explain in section 3.2.2. The use of D-branes makes it possible to construct concrete models of particle physics in an easy way, the intersecting brane models. More concretely, the geometry works such that gauge symmetries are obtained by stacks of several identical D-branes, while charged chiral fermions appear at the intersections of different stacks of D-branes.

As references I used the following recently published introductory textbooks about string theory, namely the textbooks [9], [8], and [7], as well as the review article [48], unless differently stated.

3.2.1 Massless closed string particle spectrum

In the following, I will derive the massless field content of closed strings in type IIA/$\Omega\mathcal{R}$ orientifolds. Especially the bosonic fields have important relations to the geometry of orientifold models, and therefore their understanding gives not only a motivation for the study of specific string backgrounds, but gives also a reference on how my work is related to (semi-)realistic particle physics models.

Supersymmetric closed strings: A one-dimensional string has a spatial extension that is parametrised by a parameter σ. Furthermore, the combination (τ, σ) with τ being the time coordinate gives rise to a two-dimensional string worldsheet, which is mathematically a Riemann surface, cf. section 2.2.1 with a metric $g_{ab}(\tau, \sigma)$, where $a, b = 0, 1$. These worldsheets are now embedded into the flat ten-dimensional Minkowski space-time by the functions $X^M(\tau, \sigma)$, $M = 0, \ldots, 9$, and therefore it is clear that the concrete structures imposed on the worldsheet determine the physics in the ten-dimensional space-time. To get rid of unphysical degrees of freedom, one uses often the so-called light-cone gauge, which is not manifestly Lorentz-invariant, on the fields $X^0(\tau, \sigma)$, $X^1(\tau, \sigma)$, which leaves eight free massless scalar fields $X^i(\tau, \sigma)$ with $i = 2, \ldots, 9$.

The fields $X^i(\tau, \sigma)$ can be considered as bosonic fields living on the worldsheet and, if supersymmetry is assumed, there exists for each free bosonic field $X^i(\tau, \sigma)$ a free fermionic partner $\psi^i(\tau, \sigma)$. The collection of fields $\psi^i(\tau, \sigma)$ is a spinor on the worldsheet, but behaves as a vector under the Lorentz group of the ten-dimensional space-time. Let me emphasize here that supersymmetry on the worldsheet and supersymmetry in the ten-dimensional

space-time are two different aspects of the theory that are not necessarily related (but which is the case for all five superstring theories). To make a clear distinction, the amount of supersymmetry on the worldsheet is usually denoted by N, while for space-time super-symmetry one uses generally the letter $\mathcal{N}$.

Both $X^i(\tau, \sigma)$ and $\psi^i(\tau, \sigma)$ can be expressed in terms of decoupled left- and right-moving sectors, $X_L^i(\tau + \sigma)$, $\psi_L^i(\tau + \sigma)$, $X_R^i(\tau - \sigma)$, $\psi_R^i(\tau - \sigma)$, and for closed strings of length l one requires periodic boundary conditions for each sector,

$$
\begin{aligned}
& X_{L/R}^i(\tau \pm (\sigma + l)) = X_{L/R}^i(\tau \pm \sigma) \\
\text{NS:} \quad & \psi_{L/R}^i(\tau \pm (\sigma + l)) = -\psi_{L/R}^i(\tau \pm \sigma), \\
\text{R:} \quad & \psi_{L/R}^i(\tau \pm (\sigma + l)) = \psi_{L/R}^i(\tau \pm \sigma).
\end{aligned}
\tag{3.28}
$$

For the fermionic fields, there exist two possible boundary conditions because the $\psi_{L/R}^i$ are worldsheet spinors and observables in $\psi_{L/R}^i$ appear only quadratically, hence one groups the left- or right-moving fields either into the Neveu-Schwarz (NS) or the Ramond (R) sector.

In a next step one writes $X^i(\tau, \sigma)$ and $\psi^i(\tau, \sigma)$ in terms of oscillator expansions with commutation or anticommutation relations for the bosonic or fermionic oscillator modes, respectively. The oscillator modes can be separated into creation and annihilation operators which act on the vacuum, similarly to the quantum harmonic oscillator. As usual, annihilation operators are defined to annihilate the vacuum, while physical states can be constructed by application of a certain number of creation operators. The masses of the resulting particles are determined by the number and type of the creation operators needed to produce the state.

The construction of physical massless states in the ten-dimensional Minkowski space-time, which are representations of the little group $SO(8)$, leads then to an $\mathbf{8}_V$ vector representa-tion for the NS sector and a 16-component spinor under $SO(8)$ for the R sector, which can be reduced to two chiral representations $\mathbf{8}_C$, $\mathbf{8}_S$ of opposite chirality. Furthermore, at this stage there exist tachyons, which are projected out when physical states are constructed. The infinite tower of massive states, which arises from the application of oscillators on the vacuum, can be neglected if one assumes that the energy scale under consideration is much below the string scale $M_s = 1/l_s$, where l_s is the length of a string. Typically, one chooses l_s at the order of (or slightly bigger than) the Planck length $l_P \approx 10^{-35}$m. Note that the string length l_s, which has a dimension, is considered as a length scale, and may thus not be confused with the dimensionless parameter l of equation (3.28), which is usually $l = \pi, 2\pi$ (for open or closed strings, respectively).

Physical states in flat ten-dimensional space-time: To obtain physical states, one has to combine one left- and one right-moving sector, where each can be either of NS- or of R-type, cf. equation (3.28). This gives rise to four sectors: NS-NS, R-R, R-NS and NS-R. On the gluing of these sectors one has to impose further conditions, which are the level matching $M_L^2 = M_R^2$ (being automatically fulfilled for massless states) and the so-called GSO projection that has the nice effect of projecting out the tachyons. In the massless R sector, one possibility for the GSO projection is to project out $\mathbf{8}_S$ in the left and $\mathbf{8}_C$ in the right sector, which is called type IIA string theory. On the other hand, $\mathbf{8}_S$ can be removed in both sectors, which is known as type IIB string theory. Finally, one can write down the massless closed string spectrum for type IIA string theory, as presented in table 3. The type IIB spectrum is here of no further importance, but can be found in all introductory textbooks listed at the beginning of this chapter.

10d $\mathcal{N} = 2$ massless spectrum of the closed string (type IIA)			
Sector	$\lvert\rangle_L \times \lvert\rangle_R$	$SO(8)$	10d field
NS-NS	$\mathbf{8}_V \otimes \mathbf{8}_V$	$\mathbf{1} + \mathbf{28}_V + \mathbf{35}_V$	$\phi, (B_2)_{MN}, G_{MN}$
R-R	$\mathbf{8}_C \otimes \mathbf{8}_S$	$\mathbf{8}_V + \mathbf{56}_V$	$(C_1)_M, (C_3)_{MNP}$
R-NS	$\mathbf{8}_C \otimes \mathbf{8}_V$	$\mathbf{8}_S + \mathbf{56}_S$	$\lambda^{(+)}, \psi_M^{(+)}$
NS-R	$\mathbf{8}_V \otimes \mathbf{8}_S$	$\mathbf{8}_C + \mathbf{56}_C$	$\tilde{\lambda}^{(-)}, \tilde{\psi}_M^{(-)}$

Table 3: The table summarises the massless field content in ten-dimensional Minkowski space-time, obtained from the closed string of type IIA string theory. The first two rows show the bosonic fields, namely the graviton G_{MN}, the NS-NS two-form $(B_2)_{MN}$, the dilaton ϕ, the R-R one-form $(C_1)_M$ and the R-R three-form $(C_3)_{MNP}$. Furthermore, row three and four contain the space-time fermions, which are the gravitinos $\psi_M^{(+)}$, $\tilde{\psi}_M^{(-)}$, and the dilatinos $\lambda^{(+)}$, $\tilde{\lambda}^{(-)}$. One can arrange all depicted ten-dimenional fields into one supermultiplet, called gravity multiplet for obvious reasons, and speaks of $\mathcal{N} = 2$ space-time supersymmetry due to the appearance of two gravitini.

It is possible to interpret the symmetric traceless tensor field G_{MN} of table 3 as graviton, or equivalently as space-time metric of a curved background. As will become clear in the next paragraphs, this field is crucial for my discussion in the following chapters. The three q-forms can be considered as q-form gauge potentials, under which strings or higher-dimensional objects (i.e. the D6-branes and O6-planes as introduced in section 3.2.2) are charged. Especially the R-R q-forms C_1 and C_3 are of major importance for the construction of concrete particle physics models because in the sense of generalised gauge potentials, they give rise to a very important consistency requirement on the D6-branes and O6-planes, called R-R tadpole cancellation condition.

The vacuum expectation value (*vev*) of the dilaton encodes the information about the string coupling constant $g_s = e^\phi$. This is an important quantity in perturbative string theory, where one can describe scattering amplitudes by integrating over different topologies of worldsheets (cf. section 2.2.1), leading to well-known Feynman diagrams when going to the low-energy regime. Since scattering amplitudes are not directly related to my work, I will not go into more detail, but the interested reader will find a lot of information on this subject for instance in the text books [9, 24, 25, 39, 40]. The fermions do not play a significant role here, hence they are mostly omitted in the subsequent considerations.

Compactification of the six-dimensional internal space: In the next step, I subdivide the ten-dimensional space-time into four-dimensional Minkoski space-time $\mathbb{R}^{1,3}$ and an internal compactified space $\mathcal{M}_6$ of "curled up" dimensions, generally assumed to be of tiny size, where the compactified space is mathematically a Calabi-Yau manifold, cf. section 2.1. This separation is done in order to obtain the four-dimensional field content and directly translates to the ten-dimensional massless spectrum of the closed string. An important new feature due to the compactification is the fact that one obtains Kähler and complex structure moduli from the ten-dimensional graviton G_{MN}, which are scalar fields that give rise to the moduli space as presented in section 2.6.

4d $\mathcal{N} = 2$ bosonic massless spectrum of the closed string (type IIA)					
		Gravity mult.	$h^{1,1}$ vector mult.'s	$h^{2,1}$ hypermult.'s	Hypermult.
G_{MN}	$\rightarrow$	$G_{\mu\nu}$	$G_{m\bar{n}}$	$\boldsymbol{G_{mn}}$	
$(B_2)_{MN}$	$\rightarrow$		$(B_2)_{m\bar{n}}$		$(B_2)_{\mu\nu}$
ϕ	$\rightarrow$				ϕ
$(C_1)_M$	$\rightarrow$	$(C_1)_\mu$			
$(C_3)_{MNK}$	$\rightarrow$		$(C_3)_{\mu m\bar{n}}$	$\boldsymbol{(C_3)_{mn\bar{k}}}$	$\boldsymbol{(C_3)_{mnk}}$

Table 4: The first column shows the bosonic fields of the ten-dimensional type IIA string theory as derived in table 3 with indices $M, N, K = 0, \ldots, 9$. The fields are called graviton G, NS-NS two-form B_2, dilaton ϕ, R-R one-form C_1, and R-R three-form C_3. In the other four columns one finds the decomposition of these fields into the four-dimensional $\mathcal{N} = 2$ supermultiplets with complex fields depicted in bold face. An index M is decomposed into the components $\mu = 0, 1, 2, 3$ of four-dimensional Minkowski space-time $\mathbb{R}^{1,3}$, and into holomorphic and antiholomorphic indices $m, \bar{m} = 1, 2, 3$ of the internal six-dimensional space, which is mathematically a Calabi-Yau manifold $\mathcal{M}_6$.

The field content for type IIA string theory with four-dimensional $\mathcal{N} = 2$ supersymmetry can be grouped into supermultiplets, where each multiplet contains four bosonic and four

44

fermionic degrees of freedom. I will not go into much details for the fermions, as already mentioned in the last paragraph (for more details consult e.g. [66] or [9]). The derivation of the four-dimensional bosonic fields from the ten-dimensional ones as well as their combination into supermultiplets is presented in table 4. The number of zero, one or two greek indices determines if one finds in four-dimensional Minkowski space-time a scalar, a vector, or a two-tensor, respectively. On the other hand, the latin indices belong to the internal six-dimensional manifold, as explained below. To summarise, the supermultiplets read as follows, with complex fields depicted in bold face to facilitate the counting of degrees of freedom, and with the helicities given in brackets, where ± implies that also the reversed helicities are added:

- Gravity multiplet $(G_{\mu\nu}, \psi_\mu, \tilde{\psi}_\mu, (C_1)_\mu)$ with $(2, \frac{3}{2}, \frac{3}{2}, 1)_\pm$:
  This multiplet contains one graviton, two gravitinos of opposite chirality, and one graviphoton (i.e. a gauge boson).

- $h^{1,1}$ vector multiplets $((C_3)_{\mu m\bar{n}}, 2 \times \text{fermion}, G_{m\bar{n}}, B_{m\bar{n}})$ with $(1, \frac{1}{2}, \frac{1}{2}, 0)_\pm$:
  In each vector multiplet, there exist one gauge boson, two gauginos, which are Majorana fermions, and one complex scalar, which is composed of two real scalars. The field $G_{m\bar{n}}$ is a Kähler modulus and $B_{m\bar{n}}$ is its axionic partner.

- $h^{2,1}$ hypermultiplets $(\text{fermion}, \boldsymbol{G}_{mn}, (\boldsymbol{C_3})_{mn\bar{k}}, \text{fermion})$ with $(\frac{1}{2}, 0, 0, -\frac{1}{2}) + \text{h.c.}$:
  Each one of these multiplets contains two complex scalars and two Weyl fermions of the same chirality. The field $\boldsymbol{G}_{mn}$ can be interpreted as complex structure modulus with $(\boldsymbol{C_3})_{mn\bar{k}}$ being its axionic partner.

- Universal hypermultiplet $(\text{fermion}, B_{\mu\nu}, \phi, (\boldsymbol{C_3})_{mnk}, \text{fermion})$ with $(\frac{1}{2}, 0, 0, -\frac{1}{2}) + \text{h.c.}$:
  Since the field $B_{\mu\nu}$ is dual to a scalar field, one finds two real (pseudo)scalars, which can be combined into a complex scalar, and a second complex scalar. In addition, there are two spin 1/2 fields.

For the bosonic q-form fields and the spinors, one can show that both the ten-dimensional d'Alembertian and the Dirac operator factorise as $\Box_{10d} = \Box_{4d} + \Delta_{\mathcal{M}_6}$ and $\slashed{D}_{10d} = \slashed{D}_{4d} + \slashed{D}_{\mathcal{M}_6}$, respectively [8]. In the internal Calabi-Yau manifold, the zero-modes of the Laplacian operator $\Delta_{\mathcal{M}_6}\omega = 0$, named harmonic forms, correspond to the massless q-form fields. Due to the Hodge decomposition theorem for a Calabi-Yau manifold [115], a harmonic form is unique in its equivalence class. Hence, the number of harmonic forms is determined by the Betti number $\mathbf{b}_q$, as given in equation (2.52), which encodes the dimensions of the cohomology classes $H^q(\mathcal{M}_6, \mathbb{C})$.

The Betti numbers of a Calabi-Yau manifold with $\dim_{\mathbb{R}} = 6$ can be looked up in table 1, and for convenience, I rewrite here the relevant ones,

$$b_2(\mathcal{M}_6) = h^{1,1}\,, \qquad b_3(\mathcal{M}_6) = h^{3,0} + h^{2,1} + h^{1,2} + h^{0,3} = 2h^{2,1} + 2\,. \qquad (3.29)$$

Therefore, I construct a basis of $(1,1)$-forms $\{\omega_P\}_{P=1,\ldots,h^{1,1}}$ and a basis of three-forms $\{\alpha_Q, \beta^Q\}_{Q=0,1,\ldots,h^{2,1}}$, with the property

$$\int_{\mathcal{M}_6} \alpha_Q \wedge \beta^R = \delta_Q^R\,. \qquad (3.30)$$

Note that α_0 and β^0 are $(3,0)$- and $(0,3)$-forms, respectively, while all other forms α_K, β^K are $(2,1)$- and $(1,2)$-forms, respectively ($K = 1,\ldots,h^{2,1}$). I now relabel the fields of table 4 to obtain a more convenient notation for the next step, where I also use the fact that via the holomorphic three-form Ω_3 of the Calabi-Yau manifold, I can express the complex structure of the manifold as a $(2,1)$-form, which can be expanded in a basis of $(2,1)$-forms $\{\alpha_K\}_{K=1,\ldots,h^{2,1}}$. In addition, greek indices are omitted. Therefore, the bosonic parts of the above multiplets read

- Gravity multiplet $(G_{\mu\nu}, C_1)$,

- $h^{1,1}$ vector multiplets (A_1^P, v^P, b^P) ,

- $h^{2,1}$ hypermultiplets $(z^K, C^K, \tilde{C}_K)$,

- Universal hypermultiplet $(a, \phi, C^0, \tilde{C}_0)$,

where one should note that the Kähler moduli v^P are real scalars, while the complex structure moduli z^K are complex scalars. The concrete decompositions of the fields as q-forms (now understood with respect to the internal manifold, i.e. all q indices belong to the Calabi-Yau manifold) are given by

$$
\begin{aligned}
J_{1,1}^{\text{Kähler}} &\equiv \sum_{P=1}^{h^{1,1}} v^P \omega_P\,, \\
\tilde{\Omega}_{2,1} &\equiv \sum_{K=0}^{h^{2,1}} z^K \alpha_K\,, \\
B_2 &\equiv b_2(x) + \sum_{P=1}^{h^{1,1}} b^P \omega_P\,, \\
C_3 &\equiv \sum_{P=1}^{h^{1,1}} A_1^P(x) \wedge \omega_P + \sum_{Q=0}^{h^{2,1}} C^Q(x)\alpha_Q - \sum_{Q=0}^{h^{2,1}} \tilde{C}_Q(x)\beta^Q\,,
\end{aligned} \qquad (3.31)
$$

where the first two rows (that stem from the parts $G_{m\bar{n}}$ and $\boldsymbol{G}_{mn}$ of the metric) are the important parts for my own work.

Orientifolding the internal space: The last step is the subdivision of type IIA string theory by the orientifold action $\Omega\mathcal{R}$, which reduces the amount of supersymmetry from four-dimensional $\mathcal{N} = 2$ to four-dimensional $\mathcal{N} = 1$. The worldsheet parity Ω exchanges the left- and right-moving sectors of the string, and therefore the division by Ω gives rise to unoriented strings. This implies that only states invariant under Ω survive. The action of the antiholomorphic involution $\mathcal{R}$ was already explained in more detail in section 3.1.2 since it is purely geometrical. It satisfies $\mathcal{R}(J_{1,1}^{\text{Kähler}}) = -J_{1,1}^{\text{Kähler}}$ and $\mathcal{R}(\Omega_3) = \overline{\Omega_3}$ on the Kähler form $J_{1,1}^{\text{Kähler}}$ and on the holomorphic volume form Ω_3, cf. equation (3.10). The effect of $\mathcal{R}$ on the cohomology groups is $H^{r,s}(\mathcal{M}_6, \mathbb{C}) \leftrightarrow H^{s,r}(\mathcal{M}_6, \mathbb{C})$, and therefore one can split $H^{1,1}(\mathcal{M}_6, \mathbb{C})$ into subspaces $H_+^{1,1}(\mathcal{M}_6, \mathbb{C})$ and $H_-^{1,1}(\mathcal{M}_6, \mathbb{C})$ with eigenvalues ± 1 and dimensions $h_\pm^{1,1}$.

Depending on how harmonic forms react to the orientifold action, one can define a basis of odd or even $(1,1)$-forms ω_a and ω_α, respectively, with $a = 1, \ldots, h_-^{1,1}$, $\alpha = 1, \ldots, h_+^{1,1}$, and their dual $(2,2)$-forms $\tilde{\omega}_a$ and $\tilde{\omega}_\alpha$ by

$$\int \omega_a \wedge \tilde{\omega}^b = \delta_a^b, \qquad \int \omega_\alpha \wedge \tilde{\omega}^\beta = \delta_\alpha^\beta. \tag{3.32}$$

One can show that in type IIA string theory the basis of three-forms can be chosen such that the basis vectors α_K are even under the action of $\mathcal{R}$, while the β^K are odd. By finding suitable linear combinations, one can see that the number of complex structure moduli is reduced by half, leaving $h^{2,1}$ *real* scalars. By explicitly applying the action of $\Omega\mathcal{R}$, the q-forms of equation (3.31) reduce to

$$
\begin{aligned}
J_{1,1}^{\text{Kähler}} &= \sum_{a=1}^{h_-^{1,1}} v^a \omega_a \,, \\
\tilde{\Omega}_{2,1} &= \sum_{K=1}^{h^{2,1}} z^K \alpha_K \,, \\
B_2 &= \sum_{a=1}^{h_-^{1,1}} b^a \omega_a \,, \\
C_3 &= \sum_{\alpha=1}^{h_+^{1,1}} A_1^\alpha(x) \wedge \omega_\alpha + \sum_{Q=0}^{h^{2,1}} C^Q(x) \alpha_Q \,,
\end{aligned}
\tag{3.33}
$$

and the remaining fields can be grouped into new supermultiplets, as presented in table 5.

To summarise, closed strings propagate in all directions of the ten-dimensional space-time and contribute to the four-dimensional effective field theory of the $T^6/(\mathbb{Z}_2 \times \mathbb{Z}_{2M} \times \Omega\mathcal{R})$ orientifolds with $2M = 2, 6, 6'$ and $\eta = -1$ (see table 2) the following bosonic fields (omitting the fermionic superpartners in the enumeration): There are from the untwisted closed string

4d $\mathcal{N} = 1$ bosonic massless spectrum of the closed string (type IIA/$\Omega\mathcal{R}$)				
Gravity mult.	$h^{1,1}_+$ vector mult.	$h^{1,1}_-$ chiral mult.	$h^{2,1}$ chiral mult.	Chiral mult.
$G_{\mu\nu}$	A_1^α	v^a b^a	z^K C^K	ϕ C^0

Table 5: In type IIA /$\Omega\mathcal{R}$ orientifolds, the space-time supersymmetry is reduced to $\mathcal{N} = 1$, and one finds the depicted bosonic components of supermultiplets with the fermionic parts omitted. In the gravity multiplet one finds the four-dimensional graviton, in each vector multiplet one four-dimensional $U(1)$ gauge boson, and in the universal chiral multiplet the dilaton together with its axionic partner. The other chiral multiplets are here the important parts because they contain the Kähler moduli v^P and the complex structure moduli z^K (and their respective axionic and superpartners).

sector one graviton $G_{\mu\nu}$, one dilaton ϕ, which determines the string coupling constant g_s, and zero $U(1)$ gauge bosons A_1^α (cf. appendix D of [66], where the Hodge numbers $h^{1,1}_+$ and $h^{1,1}_-$ for the $T^6/(\mathbb{Z}_2 \times \mathbb{Z}_{2M} \times \Omega\mathcal{R})$ orientifolds without and with discrete torsion are summarised). Furthermore, one finds three real Kähler moduli v^a encoding the size of the three two-tori $(T^2)^3 = T^6$, and three, one, or zero (untwisted) complex structure moduli z^K for the orbifolds with $2M = 2, 6, 6'$, respectively, which are (on the orientifold) real scalar fields that correspond to the undetermined shape of some of the two-tori. Note that each field ϕ, v^a, and z^K has an axionic partner which complexifies the field, and which is a pseudoscalar.

Though $h^{1,1}_+ = 0$ implies that no dynamical fields A_1^α exist, a peculiarity on orbifolds is the fact that a remainder of the $U(1)$ gauge bosons A_1^α can appear as a constant background in terms of discrete Wilson lines $W_\alpha = \exp(i \oint_{\gamma_\alpha} A_1^\alpha)$, where γ_α are non-contractible closed loops around the orbifold fixed points. These discrete Wilson lines appear as factors $(-1)^{\tau^k}$ with $\tau^k \in \{0, 1\}$ in the fractional cycles, cf. equation (3.22) and the discussion around equation (3.34). Roughly speaking, the discrete Wilson lines determine the direction with which orbifold singularities are surrounded by the exceptional cycle, and from the four Wilson lines on a fractional three-cycle, only two are independent.

3.2.2 Massless open string particle spectrum

When considering open strings, one finds that these have to end on higher-dimensional dynamical objects, the Dp-branes with one time and p space dimensions, and for reasons of consistency these come with the non-dynamical Op-planes, as I will explain below.

Hence, a Dp-brane is defined by the fact that open strings can end on it. At first, I will introduce the massless field content of the open string in flat ten-dimensional space-time, before I come to the special properties of compactified orientifold models in type IIA string theory, especially to the $T^6/(\mathbb{Z}_2 \times \mathbb{Z}_{2M} \times \Omega\mathcal{R})$ orientifolds introduced in section 3.1, where I will wrap D6-branes and O6-planes around three-cycles.

Supersymmetric open strings and Dp-branes: For the supersymmetric open string, the first steps are similar to the ones presented for the closed string because both have the same local structure. This means that also an open string is considered as a worldsheet with bosonic and fermionic fields $X^i(\tau, \sigma)$ and $\psi^i(\tau, \sigma)$ propagating on it, where the fields can be split into left- and right-moving sectors. The fermions can be further separated into either NS- or R-type, cf. equation (3.28). Nevertheless, one should note that while a closed string has length $l = 2\pi$, for an open string this is $l = \pi$. Performing an expansion into oscillator modes, one can construct physical states by applying creation operators on the vacuum and then suitably gluing left- and right-moving sectors at the string end points, while taking the GSO projection for open strings into account. Again, only the resulting massless fields are of interest at low energies, and one finds one $U(1)$ gauge boson together with a spin 1/2 fermion, which combine into a vector supermultiplet if both end points are located on the same Dp-brane. As for the closed strings, the fermionic fields will be omitted in the subsequent discussion.

To be somewhat more precise, in the above derivation one has to take into account that closed and open strings satisfy different boundary conditions. While a closed string has to obey a periodicity condition, an open string has two end points at $\sigma = 0, l$, which are restricted by either Dirichlet (D) or Neumann (N) boundary conditions. The Dirichlet condition at an end point a means that the respective coordinate has a constant value and a cannot move in this direction. Therefore, open strings are confined to lower-dimensional subspaces of ten-dimensional space-time (the Dirichlet directions), which will prove to be dynamical objects themselves, the so-called Dp-branes (more details on them will be given in the next paragraph). On the other hand, the p space and one time dimensions of a Dp-brane form the $p+1$ Neumann directions, along which the end point a can move freely. With respect to a given Dp-brane, one can therefore split the fields $X^i(\tau, \sigma)$ into parallel and transverse directions with

$$
\begin{aligned}
&\text{NN:} \qquad \partial_\sigma X^j|_{\sigma=0,l} = 0 \qquad \text{with } j = 2, \dots, p\,, \\
&\text{DD:} \qquad X^k|_{\sigma=0,l} = 0 \qquad \text{with } k = p+1, \dots, 9\,,
\end{aligned}
\tag{3.34}
$$

respectively. Note that the fields are given in light-cone gauge (cf. section 3.2.1), and therefore the fields with indices $j = 0, 1$ do not contribute. The translational symmetry

of the vacuum is broken by the presence of a Dp-brane, and therefore the scalars X^k are Goldstone bosons, which parametrise the position of the Dp-brane by their vacuum expectation values (*vev*s). Interestingly, the GSO projection has the effect that in type IIA string theory only Dp-branes with even p are allowed, while type IIB string theory contains only odd numbers p. To summarise, the bosonic open field content for a single Dp-brane consists of a $U(1)$ gauge boson A_μ, propagating in the $(p+1)$-dimensional volume of the Dp-brane, and (in the absence of non-trivial compactifications) $9 - p$ real scalars. Note that it is also possible that open strings end on two different Dp-branes, which will be discussed further down. In this case, the boundary conditions N and D can be mixed.

Model building on type IIA orientifolds: From now on, I will assume that the ten-dimensional space-time splits into $\mathbb{R}^{1,3} \times \mathcal{M}_6$, i.e. four-dimensional Minkowski space-time times a six-dimensional (compact) Calabi-Yau manifold, which is assumed to have tiny size, as discussed for the closed string in the previous section. In such a setup, one uses Dp-branes which completely fill $\mathbb{R}^{1,3}$ (where therefore only NN boundary conditions appear) and which have $p-3$ dimensions in the internal space $\mathcal{M}_6$, wrapping $(p-3)$-cycles, in order to construct four-dimensional effective field theories. I consider here $T^6/(\mathbb{Z}_2 \times \mathbb{Z}_{2M} \times \Omega\mathcal{R})$ orientifolds of type IIA string theory (with $2M = 2, 6, 6'$, cf. section 3.1.1), which are singular limits of some Calabi-Yau manifold $\mathcal{M}_6$. In concrete models, I will only use D6-branes wrapping three-cycles.

General Dp-branes are not only related to the dynamics of open strings, but also couple to the massless closed string fields of table 3. In particular, the effective action includes the Dirac-Born-Infeld (DBI) and the Chern-Simons (CS) terms,

$$S_{\text{eff}} = S_{\text{DBI}}[\phi, g, B] + S_{\text{CS}}[C_q]. \tag{3.35}$$

S_{DBI} describes the couplings to the closed string NS-NS fields, i.e. the dilaton, the metric, and the two-form. In particular, the coupling to the metric assigns a positive tension to a Dp-brane, and also to the open strings [9], which therefore both tend to minimise their spatial extension. The term S_{CS} contains the couplings to the closed string R-R forms C_q and thus determines the R-R charge that is assigned to the Dp-brane. This charge can be obtained in a similar way as in electrodynamics by integrating the part of the volume of the Dp-brane which is contained in the internal space over the q-form field C_q, which can be interpreted as generalised gauge potential. For a D6$_a$-brane wrapped on a *sLag* three-cycle Π_a, one obtains in this way the generalised electric coupling $S_{\text{el}} = Q_6 \int_{\Pi_a} C_3$. Since D6-branes have a positive tension and therefore a positive contribution to the vacuum energy, one chooses also the electric charge Q_6 to be positive by convention.

On a compactified internal space, the cancellation of the positive R-R charges of all D6-branes is necessary in order to satisfy Gauss' law (since the fluxes cannot "escape" the space), and also the overall tension has to vanish to preserve supersymmetry. This can be achieved by introducing O6-planes, which are the fixed sets under the antiholomorphic involution $\mathcal{R}$, cf. the discussion in section 3.1.3. These O6-planes are objects of negative R-R charge, and also have negative tension. In fact, the requirement of cancelling all R-R charges gives rise to the most important consistency condition for the construction of concrete intersecting D-brane models, which is the so-called R-R tadpole cancellation condition. The term R-R tadpole is used in analogy to quantum field theory and stands for uncancelled R-R charges. For type IIA/$\Omega\mathcal{R}$ orientifolds, which I use as setup in my thesis, the R-R tadpole cancellation condition reads

$$\sum_a N_a \left([\Pi_a] + [\Pi_{a'}]\right) - 4 \left[\Pi_{O6}\right] = 0 \,, \tag{3.36}$$

and will indeed be applied in chapter 5, where I present concrete models. The square brackets stand for the homology classes of the three-cycles which are wrapped by the D6$_a$-branes, by their images D6$_{a'}$ under the antiholomorphic involution $\mathcal{R}$, and by the O6-planes, for which one can show that their charges contribute with a factor of four [48]. The number N_a stands for the number of identical D6$_a$ that can be piled up on a cycle Π_a.

To be more precise, one finds four O6-planes on the $T^6/(\mathbb{Z}_2 \times \mathbb{Z}_2 \times \Omega\mathcal{R})$ orientifolds that are simply the fixed sets under

$$\Omega\mathcal{R}, \quad \Omega\mathcal{R}\mathbb{Z}_2^{(1)}, \quad \Omega\mathcal{R}\mathbb{Z}_2^{(2)}, \quad \Omega\mathcal{R}\mathbb{Z}_2^{(3)}, \tag{3.37}$$

with the antiholomorphic involution $\mathcal{R}$ as defined in equation (3.10) and with the $\mathbb{Z}_2 \times \mathbb{Z}_2$ generators as given in equation (3.3). As already discussed in the last section for the closed string, the worldsheet parity operator Ω reverses the orientation of the string, which implies for the open string that the two end points are exchanged. Since the orientifolds with $2M = 6, 6'$ have an additional rotational symmetry corresponding to the action of $\mathbb{Z}_3$, there one has to consider also the $\mathbb{Z}_3$ orbits of the four O6-planes.

As mentioned above, usually the orientifold planes are assumed to have negative R-R charge and also negative tension (with contrary assignment $\eta_{\Omega\mathcal{R}g} = +1$, and where the index $g = \mathbb{1}, \mathbb{Z}_2^{(1)}, \mathbb{Z}_2^{(2)}, \mathbb{Z}_2^{(3)}$ denotes the respective $\Omega\mathcal{R}(\mathbb{Z}_2^{(i)})$ invariance). On the other hand, the choice of discrete torsion $\eta = -1$ and the requirement of worldsheet consistency imply that I have to choose one of the four O6-plane orbits to be exotic ([71, 66]), i.e. having positive R-R charge and tension with assignment $\eta_{\Omega\mathcal{R}g} = -1$. This can be written as

$$\left(\eta_{\Omega\mathcal{R}}, \eta_{\Omega\mathcal{R}\mathbb{Z}_2^{(1)}}, \eta_{\Omega\mathcal{R}\mathbb{Z}_2^{(2)}}, \eta_{\Omega\mathcal{R}\mathbb{Z}_2^{(3)}}\right) = \left(\underline{-1}, 1, 1, 1\right) \tag{3.38}$$

with the underline denoting all possible permutations. To construct the underlying cycle of the O6-plane one has to take into account that the O6-plane is a non-dynamical object. Hence, cycles that are identical under the orbifold action are counted only once [66], and the cycles can be expressed as

$$\Pi_{O6} := \frac{1}{4}\Pi^{\text{bulk}}, \tag{3.39}$$

with Π^{bulk} defined in equation (3.16).

The massless open string spectrum: For model building purposes, the D6-branes usually come in stacks of N coincident branes and are wrapped on three-cycles. For an open string attached to such a stack, the degeneracy for one of the end points is N. This is the dimension of the fundamental irreducible representation of the gauge group $U(N) = SU(N) \times U(1)$ and is denoted by $\mathbf{N}_{+1}$, where the index for the (here positive) $U(1)$ charge will be mostly omitted. One can show that a string coming out of a D6-brane is related by a CPT transformation (i.e. Charge, Parity, and Time reversal) to the part of the string which goes into the brane, and therefore the conjugate, so-called anti-fundamental, representation $\overline{\mathbf{N}}_{-1}$ is applied. Furthermore, assuming that the open string interactions happen at its end points, one can directly allocate the gauge quantum numbers to the end points. Hence, an open string with both end points attached to the same D6-brane stack is described by the tensor product $\mathbf{N} \times \overline{\mathbf{N}}$, i.e. the adjoint of $U(N)$.

For an orbifold with $\mathbb{Z}_2 \times \mathbb{Z}_2$ group, the underlying cycle structure for a stack of N D6-branes is somewhat more complicated, as discussed in section 3.1.3. One can show that a D6-brane stack wrapped on a fractional cycle Π^{frac}, as defined in equation (3.20), has gauge group $U(N)$. In the case of discrete torsion (i.e. $\eta = -1$), which I consider in my thesis, a bulk cycle consists of four fractional cycles (cf. equation (3.20)) and therefore has the gauge group $U(N)^4$, cf. [71]. However, the four gauge groups $U(N)^4$ can be identified into only one $U(N)$ gauge group, also referred to as $U(N)_{\text{diag}}$, in the following way. If the four fractional cycles have $\mathbb{Z}_2^{(i)}$ eigenvalues $(+++)$, $(+--)$, $(--+)$, and $(-+-)$, the sum of the first two fractional cycles gives $\frac{1}{2}\left(\Pi^{\text{bulk}} + \Pi^{\mathbb{Z}_2^{(1)}}\right)$, and two $U(N)$'s are identified by switching on a *vev* of the scalar field in the bifundamental representation, which appears in the spectrum for this specific pair of fractional cycles. One can proceed similarly for the fractional cycles with $\mathbb{Z}_2^{(i)}$ eigenvalues $(--+)$, and $(-+-)$, where $\Pi^{\mathbb{Z}_2^{(1)}}$ appears now with a negative sign, and where again two $U(N)$'s are identified. Summing these two remaining fractional cycles, the exceptional part $\Pi^{\mathbb{Z}_2^{(1)}}$ cancels and only the bulk part Π^{bulk} without a prefactor and a single $U(N)$ gauge group remain. The wrapped D6-brane cannot be shifted in the internal space because the exceptional cycles are stuck at the orbifold singularities, and if there are no real scalar fields transforming in the adjoint representation, the underlying fractional

three-cycles are so-called rigid cycles [71, 66]. Note that for $\mathbb{Z}_2 \times \mathbb{Z}_2$ orbifolds, all fractional cycles are automatically rigid. However, this is not always true when an additional $\mathbb{Z}_3$ group is apparent because in this case there exist self-interactions of the cycles.

All stacks N_a and N_b of D6-branes and their orientifold images D6$_{a'}$, D6$_{b'}$ can intersect in arbitrary combinations. This gives rise to charged chiral fermions, where the number of copies depends on the number of intersections in the six-dimensional compact space. This geometrical fact makes it possible to obtain several generations of particles. The topological intersection number $I_{ab} = [\Pi_a] \circ [\Pi_b]$ between two three-cycles Π_a and Π_b, wrapped by two stacks N_a and N_b of D6-branes, as generally defined in equation (2.46), is hence a very important ingredient for model building. The different representations that one obtains for open strings stretching between intersecting D6-brane stacks are summarised in table 6. Since I will not be concerned with the concrete open string particle spectrum in my later work, I will not give more details here, but the interested reader can consult for example [66, 71, 48].

4d $\mathcal{N} = 1$ massless chiral open string spectrum of $CY_3/\Omega\mathcal{R}$		
Sector	Representation	Multiplicity
ab	$(\mathbf{N}_a, \overline{\mathbf{N}}_b)$	$\Pi_a \circ \Pi_b$
ab'	$(\mathbf{N}_a, \mathbf{N}_b)$	$\Pi_a \circ \Pi_{b'}$
aa'	$\mathbf{Anti}_a$	$\frac{1}{2}\left(\Pi_a \circ \Pi_{a'} + \Pi_a \circ \Pi_{O6}\right)$
	$\mathbf{Sym}_a$	$\frac{1}{2}\left(\Pi_a \circ \Pi_{a'} - \Pi_a \circ \Pi_{O6}\right)$

Table 6: Massless chiral spectrum of open strings on a complex three-dimensional Calabi-Yau orientifold $CY_3/\Omega\mathcal{R}$. The open strings stretch between different kinds of D6-brane stacks of N_a, N_b coincident D6-branes with representations of the gauge groups $U(N_a)$, $U(N_b)$. The multiplicity refers to the topological intersection number between the D6-brane stacks and determines the number of copies and chirality of the respective particles.

In case that a stack of N_a D6$_a$-branes is invariant under $\Omega\mathcal{R}$, the gauge group $U(N_a)$ is enhanced to either $SO(2N_a)$ or to $USp(2N_a)$. The important point is here that these gauge groups do not contain a $U(1)$ factor, hence they do not contribute to moduli stabilisation via Fayet-Iliopoulos terms, which I will explain in the next section. Furthermore, one can write down the physical gauge coupling, which also depends on the respective gauge group,

$$\frac{4\pi}{g_{G_a}^2} = \frac{1}{2k_a c_a g_s} \frac{\mathrm{Vol}(\Pi_a) + \mathrm{Vol}(\Pi_{a'})}{l_s^3}, \quad k_a = \begin{cases} 1 & G_a = U(N_a) \\ 2 & G_a = USp(2N_a) \text{ or } SO(2N_a) \end{cases}, \quad (3.40)$$

where $g_s = e^\phi$ is the string coupling constant, which is determined by the dilaton ϕ, and l_s is the string length. The factor c_a is set to $c_a = 1$ for a pure bulk cycle and has the value

$c_a = 4$ when a fractional three-cycle in the presence of some underlying $\mathbb{Z}_2 \times \mathbb{Z}_2$ symmetry is used. Also the volumes of the three-cycles Π_a which are wrapped by the $D6_a$-branes and their orientifold images $\Pi_{a'}$ contribute, which I will compute explicitly in section 4 for some concrete configurations. At the orbifold point, for all models that were analysed so far, one finds $\text{Vol}(\Pi_a) = \text{Vol}(\Pi_{a'})$, but I will show that when I deform the three-cycle Π_a, this equality of the volumes will be violated. The reason for that violation is given in the next section 3.2.3.

3.2.3 Twisted closed strings and moduli stabilisation

For model building on toroidal orientifolds, here on $T^6/(\mathbb{Z}_2 \times \mathbb{Z}_{2M} \times \Omega\mathcal{R})$ with $2M = 2, 6, 6'$, there exists an additional mechanism which gives rise to massless fields. In the four-dimensional Minkowski space-time $\mathbb{R}^{1,3}$ only NN boundary conditions appear, as before, but in the six-dimensional internal space, it can happen that the orbifold action maps the open string end point $\sigma = l$ onto the other end point $\sigma = 0$. This simply means that the open string becomes a *twisted closed string* which forms a loop around one of the orbifold fixed points,

$$Z^m(\tau, \sigma + l) = \theta^p \omega^q \, Z^m(\tau, \sigma) \,, \tag{3.41}$$

where $Z^m(\tau, \sigma) = X^{2m+2}(\tau, \sigma) + iX^{2m+3}(\tau, \sigma)$ ($m = 1, 2, 3$) are the now complexified bosonic fields of the internal space. The orbifold generators θ and ω were already defined in equation (3.1). As mentioned before, an open string has tension and thus tends to minimise its volume, which has the effect that all twisted closed strings are shrunk to zero size and reside at the orbifold singularities.

Since the twisted strings are effectively closed strings, they contribute to the closed string spectrum for type IIA orientifolds of table 5. For the orientifolds $T^6/(\mathbb{Z}_2 \times \mathbb{Z}_{2M} \times \Omega\mathcal{R})$ with $2M = 2, 6, 6'$, the Hodge numbers are summarised in table 2, from which it is clear that only for the orbifolds with discrete torsion ($\eta = -1$) twisted Hodge numbers of type $h_{\text{tw}}^{2,1}$ are present. Hence, for $\eta = -1$ one finds at the orbifold singularities $h_{\text{tw}}^{2,1}$ twisted complex structure moduli. Naively, for massless fields the vacuum expectation values (*vev*s) can be varied continuously while the scalar potential, which provides the information about the ground state of the theory, still stays at its minimum. Hence, all these directions are said to be flat and one finds a continuous space of vacua, called moduli space (see section 2.6), which is not a desirable fact because in the real world the vacuum should be an isolated point. Hence, one has to stabilise these moduli in order the eliminate the flat directions.

As discussed in the previous section, if open strings end on the same stack of N_a $D6_a$-branes, this gives rise to a vector multiplet with gauge group $U(N_a) = SU(N_a) \times U(1)_a$.

When considering these supermultiplets (where I always omit the fermionic content) I did not mention that in fact, a vector multiplet contains off-shell an additional auxiliary field D, which is a real scalar field. When these fields are integrated out, they give contributions (called D-terms) to the scalar potential. The crucial part for my later analysis is the fact that all auxiliary fields D^a that appear in the scalar potential must be zero for unbroken supersymmetry in the vacuum. On the other hand, a D-term can be shifted by the Fayet-Iliopoulos parameter $D^a \to D^a + \xi$. This has the effect that the D-term scalar potential is modified as

$$V_D = \frac{1}{2} \sum_a |D^a|^2 = \sum_a \frac{1}{2g_a^2} \left| \sum_k q_a^k |\Phi_k|^2 + \xi_a \right|^2 \geq 0 \,, \tag{3.42}$$

and supersymmetry is spontaneously broken if the auxiliary field D^a obtains a *vev*, i.e. $\langle 0| D^a |0\rangle \neq 0$, which implies $V_D > 0$. The parameters q_a^k are $U(1)_a$ charges, and the Φ_k are all scalar fields of the theory. Considering the $T^6/(\mathbb{Z}_2 \times \mathbb{Z}_{2M} \times \Omega\mathcal{R})$ orientifolds with $2M = 2, 6, 6'$ and with discrete torsion, for a D6$_a$-brane that is wrapped on a fractional cycle, the usual open string gives rise to the $U(1)_a$ charge, to which the D6$_a$-brane couples. Furthermore, at the orbifold fixed points appear the $h_{\text{tw}}^{2,1}$ twisted complex structure moduli z_{tw}^K, which can obtain a *vev* resulting in the Fayet-Iliopoulos parameter ξ_a.

When D6-branes and O6-planes are wrapping *sLag* cycles and the R-R tadpole cancellation condition is satisfied, the configuration is supersymmetric and the scalar potential is zero. Therefore, in the concrete orientifold setups that I use, one can also write the scalar potential as

$$V \propto \left(\sum_a N_a [\text{Vol}(\text{D6}_a) + \text{Vol}(\text{D6}_{a'})] - \text{Vol}(\text{O6}) \right) \begin{cases} = 0 & \text{if all D6}_a \text{ are } sLag \\ > 0 & \text{else} \end{cases} \,. \tag{3.43}$$

with $\text{Vol}(\text{D6}_{a^{(\prime)}}) = \int_{\Pi_{a^{(\prime)}}} \text{Re}\,(\Omega_3)$ and $\text{Vol}(\text{O6}) = \int_{\Pi_{\text{O6}}} \text{Re}\,(\Omega_3)$. In addition, one can calculate [48] that here the Fayet-Iliopoulos parameter is given by the relation

$$\xi_a \propto \frac{\int_{\Pi_a} \text{Im}\,(\Omega_3)}{\int_{\Pi_a} \text{Re}\,(\Omega_3)} \,, \tag{3.44}$$

which coincides with the *sLag* property, see equation (3.24). Therefore, it is quite easy to determine if supersymmetry is broken, and a mechanism to do this is to change the volume of one or several exceptional cycles via a complex structure deformation, cf. section 2.6. In the next chapter 4, I will explicitly perform such complex structure deformations and test how the volumes of the exceptional cycles change, and in particular if the *sLag* condition is preserved or not. In chapter 5, this method will be applied to concrete models, where it will turn out that indeed, several or (nearly) all twisted complex structure moduli can be stabilised by Fayet-Iliopoulos terms.

Before I start with concrete deformations, let me point at the differences between orbifolds and the deformed versions thereof. At the orbifold point, only (fractions of) bulk cycles appear, which have the same volume for three-cycles Π_a and their orbifold images $\Pi_{a'}$. If a deformation is switched on, also exceptional cycles contribute with positive or negative sign, and therefore it is possible to find $\text{Vol}(\Pi_a) \neq \text{Vol}(\Pi_{a'})$. The big advantage of an orbifold is the fact that one can apply the powerful tools of conformal field theory (CFT), see e.g. [122–126] for an introduction, or the more specific article [127] about CFT on orbifolds. This makes it possible to compute not only the massless particle spectrum, but the whole tower of modes. In addition, CFT techniques can be used to calculate for example string scattering amplitudes or gauge thresholds. In fact, one can in principle also apply CFT to the deformed orbifolds, where the physical quantities now obtain non-vanishing expectation values. Since the gauge thresholds are directly related to the one-loop corrections to gauge couplings at the orbifold point, which depend on the volumes of the cycles, it will be interesting to analyse in the future how these quantities feel the deformation.

4 Lagrangian Cycles and Deformations

In this chapter I will describe the orbifolds and orientifolds that were introduced in sections 3.1.1 and 3.1.2 as hypersurfaces in a projective space, see section 2.3.2 for the mathematical basics, and translate also the cycles that were constructed in section 3.1.3 into this language. I start with one-dimensional cycles on the elliptic curve which have the *Lagrangian* property, cf. equation (3.23), and combine them to two- or three-dimensional cycles on T^4 or T^6, respectively. For these cycles I will analyse the effects of deformations of the orbifold singularities and study the changes in their volumes. In fact, the general idea of using hypersurfaces to perform blow-ups (deformations) in this description is widely known in the mathematical literature, see e.g. [36]. However, the sketch of Vafa and Witten [108] on how to apply this idea to orientifolds in the context of string theory was completely new and has, besides by me and my collaborators [109, 110], to my best knowledge not been worked out for the models that I consider here.

4.1 Lagrangian one-cycles on the torus in hypersurface language

In a first step I study how the torus lattice behaves under the map from the complex coordinate z to the homogeneous coordinates $x, v, y \in \mathbb{C}$ on the elliptic curve. As discussed in section 2.3, this map is provided by the Weierstrass function $\wp(z)$, cf. figures 2 and 3, with the identifications $\wp(z) = x/v$ and $\wp'(z) = y/v^2$.

In section 3.1.2 I pointed out that there remain two possible choices of orientation for the torus lattice when the antiholomorphic involution $\mathcal{R}$ is taken into account. The fixed points in such a torus lattice were labelled $\alpha = 1, 2, 3, 4$ and via $\wp(z) = \frac{x}{v}$ I assign to each fixed point a complex value $\frac{x}{v} = \epsilon_\alpha$, where always $\epsilon_1 = \infty$ and which have to satisfy the condition $\epsilon_2 + \epsilon_3 + \epsilon_4 = 0$, see section 2.3 for details. For the different types of lattices I find the following restrictions on the ϵ_α:

(a) $j(\tau) \geq 1$: For these *untilted* or **a**-type lattices the parameters ϵ_α are real numbers, which I order as $\epsilon_4 < \epsilon_3 < \epsilon_2$.

(b) $j(\tau) \leq 1$: The *tilted* or **b**-type lattices have two complex and one real parameter ϵ_α, which I label $\epsilon_2 = \overline{\epsilon_4} =: \epsilon \equiv \epsilon_R + i\epsilon_I$ and $\epsilon_3 = -2\epsilon_R$.

The case $j(\tau) = 1$ is special because it can describe both types of lattices, and also $j(\tau) = 0$ has additional features. For these particular configurations the complex structure is fixed and thus only one of the parameters ϵ_α can be chosen freely:
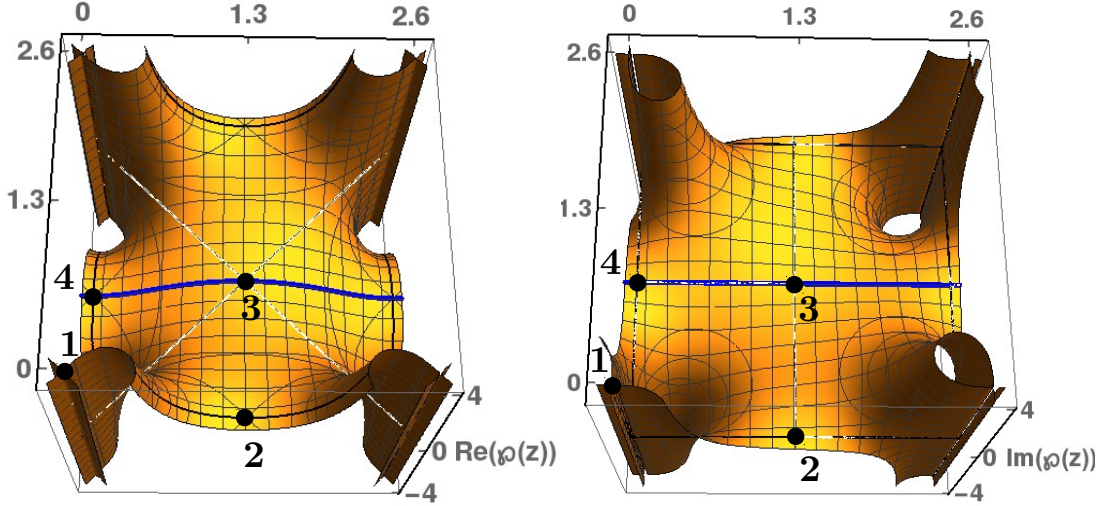
Figure 2: Real and imaginary part of the Weierstrass function $\wp(z)$ on the square *torus* lattice of **a**-type, where the *(s)Lag* line **aIII** (depicted in blue) is specified in table 7a. Moreover, the $\mathbb{Z}_2$ fixed points that one would find on a $T^2/\mathbb{Z}_2$ *orbifold* are indicated. This figure gives the translation $z \leftrightarrow (x,v,y)$ for the identifications $\wp(z) = x/v$ and $\wp'(z) = y/v^2$. The lines with $\mathrm{Re}\left(\wp(z)\right) = 0$ are the diagonal lines (left image), while one finds for $\mathrm{Im}\left(\wp(z)\right) = 0$ the horizontal and vertical lines through the origin and the ones shifted by half lattice vectors (right image), i.e. the cycles **aX** with **X** = **I**, **II**, **III**, **IV** of table 7a take only real values.

- $j(\tau) = 1$: This choice represents a *square* torus and can be seen either as **a**- or **b**-type, depending on the description. Here one finds $\epsilon_3 = 0$, $-\epsilon_4 = \epsilon_2$, and I will always work with $\epsilon_4 = -1$, $\epsilon_3 = 0$, $\epsilon_2 = 1$. For a pictorial view see figure 2.

- $j(\tau) = 0$: In this case one obtains a *hexagonal* lattice as depicted in figure 3 and the parameters ϵ_α obey the $\mathbb{Z}_3$ symmetry, thus I will choose $\epsilon_3 = \xi^0$, $\epsilon_2 = \xi^1$, $\epsilon_4 = \xi^2$ with $\xi \equiv e^{2\pi i/3}$.

Similar to the *(s)Lag* cycles defined in equation (3.23), which come into play with the antiholomorphic involution $\mathcal{R}$ of the orientifold, I want to find *(s)Lag* lines on the elliptic curve in coordinates x, v, y. Unfortunately, the translation turns out to be complicated for general cases and therefore I consider only the small number of *(s)Lag* lines that can be described by an antilinear, meaning antiholomorphic and linear, map σ (not to be confused with the discrete displacements $\sigma^k \in \{0, 1\}$ of section 3.1.3) as

$$\sigma : \begin{pmatrix} x \\ v \end{pmatrix} \longmapsto A \begin{pmatrix} \overline{x} \\ \overline{v} \end{pmatrix}, \quad y \longmapsto \pm e^{i\beta}\overline{y}. \tag{4.1}$$
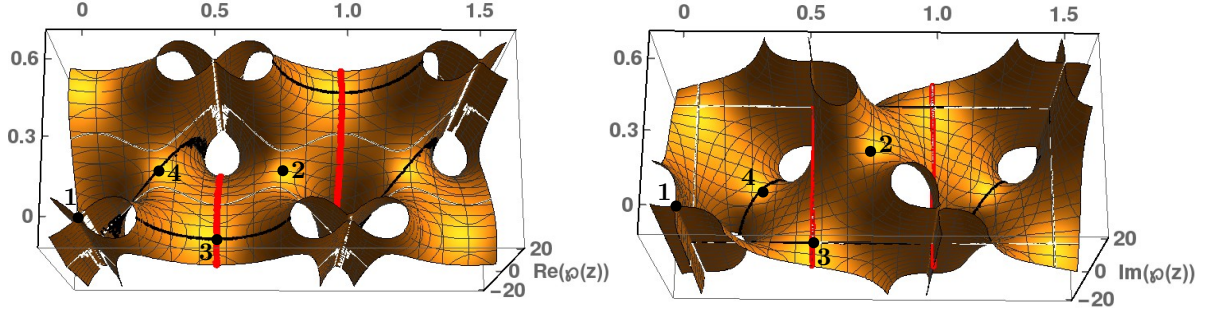
58

Figure 3: Real and imaginary part of the Weierstrass function $\wp(z)$ imposed on the hexagonal lattice with the border of the fundamental domain indicated by bold black lines, where the $\mathbb{Z}_2$ fixed points and the *(s)Lag* line **bII** (bold red vertical lines) are illustrated. One can see in the right figure the lines of $\mathrm{Im}\,(\wp(z)) = 0$ that are the horizontal and vertical white lines (the ones through the origin and the vertical line shifted by the half lattice vector ζ_1), which coincide with the *(s)Lag* lines **bI** and **bII** (bold, red), respectively. The lines with property $\mathrm{Re}\,(\wp(z)) = 0$ are not straight lines on the torus (left figure).

The matrix A is an element of $GL_2(\mathbb{C})$ and may contain an additional complex phase. The meaning of the two signs for the coordinate y is that each cycle consists actually of two components, which will be explained in more detail further down. For the phase one finds normally $\beta = 0$, except for square and hexagonal lattices where different values appear due to the enhanced rotational symmetry. When I impose on σ the following further restrictions, I can turn it into an antiholomorphic involution which I call $\sigma_{\mathcal{R}}$,

$$
\begin{aligned}
\overline{A}A &= \mathbb{1}, \\
\sigma_{\mathcal{R}}(F(x,v)) &= e^{-2i\beta}F(\overline{x},\overline{v}).
\end{aligned}
\tag{4.2}
$$

On the elliptic curve, the action of $\sigma_{\mathcal{R}}$ plays a similar role to $\mathcal{R}$ on the orientifold lattice.

The *(s)Lag* lines that can be realised in this way are listed in table 7 for the untilted lattice and in table 8 for the tilted one. The cycles **aX** and **bX** ($\mathbf{X} = \mathbf{I}, \mathbf{II}, \mathbf{III}, \mathbf{IV}$) are fractional cycles, as defined in equation (3.20) on the torus, and cannot be moved away from their position. Nevertheless, when the bulk part is considered separately, it can be shifted away from the fixed points and be expressed by another bulk cycle of the same homology class, see section 2.5. The cycles **cX** ($\mathbf{X} = \mathbf{I}, \mathbf{II}$) do not run through the fixed points and are thus pure bulk cycles, cf. equation (3.15) for the description on the torus. They can be always moved in their position as long as they stay in the same homology class.

The labelling of all cycles **aX**, **bX**, **cX** is chosen in such a way that the number **X** directly

(s)*Lag* lines on the a-type lattice		
Label	View on T^2	Map $\wp(z) \equiv \frac{x}{v}$
aI		$\epsilon_2 \leq \left(\frac{x}{v}\right) \leq +\infty$
aII		$-\infty \leq \left(\frac{x}{v}\right) \leq \epsilon_4$
aIII		$\epsilon_4 \leq \left(\frac{x}{v}\right) \leq \epsilon_3$
aIV		$\epsilon_3 \leq \left(\frac{x}{v}\right) \leq \epsilon_2$

(a) *(s)Lag* lines crossing two $\mathbb{Z}_2$ fixed points.

(s)*Lag* lines on the a-type lattice		
Label	View on T^2	Map $\wp(z) \equiv \frac{x}{v}$
cI		$\left|\frac{x}{v} - \epsilon_4\right|^2 = 2\epsilon_4^2 + \epsilon_2\epsilon_3$
cII		$\left|\frac{x}{v} - \epsilon_2\right|^2 = 2\epsilon_2^2 + \epsilon_4\epsilon_3$

(b) *(s)Lag* lines which do not intersect any of the $\mathbb{Z}_2$ fixed points.

Table 7: Linearly realised *Lag* lines on the *untilted* elliptic curve as defined in equations (4.1) and (4.2). The column in the middle indicates the position on the torus lattice T^2, cf. figure 2 for the square lattice. On the right hand side I list the equations that are obtained by the Weierstrass map $\wp(z) \equiv \frac{x}{v}$, and the resulting lines are depicted in figures 4(a) and 5(a) for the chart $v \equiv 1$.

shows the calibration, see the discussion under equation (3.24), which means that the

$$\text{cycle is } sLag \text{ with calibration} \begin{cases} \mathrm{Re}\,(\Omega_1) & \text{if } \mathbf{X} = \text{odd} \\ \mathrm{Im}\,(\Omega_1) & \text{if } \mathbf{X} = \text{even} \end{cases} \quad (\text{for } \mathbf{aX}, \mathbf{bX}, \mathbf{cX}). \quad (4.3)$$

More concretely, 'real calibration' simply means that the holomorphic one-form defined as

$$\Omega_1 := \mathrm{d}z = \frac{\mathrm{d}\wp}{\wp'} = \frac{v \cdot \mathrm{d}x - x \cdot \mathrm{d}v}{y} \overset{v \equiv 1}{=} \frac{\mathrm{d}x}{y} \quad (4.4)$$

has real values, while for calibration $\mathrm{Im}\,(\Omega_1)$ it has purely imaginary values. For the cycles $\mathbf{aX}$ and $\mathbf{bX}$ the labels indicate furthermore the discrete displacements $\sigma \in \{0, 1\}$, cf. section 3.1.3,

$$\sigma = \begin{cases} 0 & \text{if } \mathbf{X} = \mathbf{I}, \mathbf{II} \\ 1 & \text{if } \mathbf{X} = \mathbf{III}, \mathbf{IV} \end{cases} \quad (\text{for } \mathbf{aX}, \mathbf{bX}), \quad (4.5)$$

where $\sigma = 0$ denotes undisplaced and $\sigma = 1$ displaced from the origin.

For a square torus, figures 5(a) and 6 depict not only the universally existent cycles for any rectangular torus, but also the additional *(s)Lag* lines and the enhanced symmetry. Figure 6 shows that the square torus can be described either in the **a**- or **b**-type picture, which differ only by a rotation of $\frac{x}{v} \mapsto e^{-i\beta}\frac{x}{v}$ with $\beta = \pm\pi/2$. According to equation (4.1), this leaves the two components $y \mapsto \pm i\overline{y}$. On the **a**-type lattice, one finds not only the
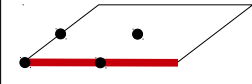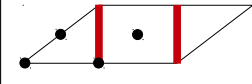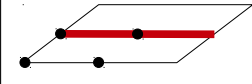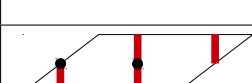
(s)*Lag* lines of b-type lattice		
Label	View in T^2	Map $\wp(z) \equiv \frac{x}{v}$
bI		$\epsilon_3 \leq \left(\frac{x}{v}\right) \leq +\infty$
bII		$-\infty \leq \left(\frac{x}{v}\right) \leq \epsilon_3$
bIII		$\left|\frac{x}{v} - \epsilon_3\right|^2 = 2\epsilon_3^2 + \epsilon_2\epsilon_4$ $\text{Re}\left(\frac{x}{v}\right) \geq \epsilon_R$
bIV		$\left|\frac{x}{v} - \epsilon_3\right|^2 = 2\epsilon_3^2 + \epsilon_2\epsilon_4$ $\text{Re}\left(\frac{x}{v}\right) \leq \epsilon_R$

Table 8: The linearly realised *Lag* lines on the *tilted* elliptic curve are labelled **bX** referring to the **b**-type lattice, and no cycles **cX** arise. The table is structured in the same way as table 7, and the Weierstrass function on the hexagonal lattice can be found in figure 3. The pictorial view for the equations in column three is given in figures 4(b) and 5(b) for the chart $v \equiv 1$, where figures 4(b) is tilted in general, while figure 5(b) is the special hexagonal case.

(s)*Lag* lines of the square and hexagonal lattice			
	Square **a**-type	Square **b**-type	Hexagonal
	aX	**aX***	**bX**$^0 \equiv$ **bX**
Cycles	**cX**	**cX***	**bX**$^+$
	bX*	**bX**	**bX**$^-$
$\frac{x}{v} \mapsto e^{-i\beta}\frac{x}{v}$	**bX*** : $\beta = +\frac{\pi}{2}$	**aX***, **cX*** : $\beta = -\frac{\pi}{2}$	**bX**$^\pm$: $\beta = \pm\frac{2\pi}{3}$

Table 9: All linearly realised *(s)Lag* lines for square and hexagonal tori, which are a combination of the *(s)Lag* lines given in tables 7 and 8. For all cycles with an upper index, I have to multiply the coordinates $\frac{x}{v}$ of the original cycles with an additional phase as indicated in the last row.

(s)Lag cycles **aX** and **cX**, but also the additional lines **bX***, which are constructed as in the **b**-type lattice, but with an additional phase. In the **b**-type description the approach is similar, but now the cycles **aX*** and **cX*** appear, which come with a phase. The details of the cycles and their replacements are summarised in table 9. There can be found also the *(s)Lag* lines **bX**^{0}, **bX**$^+$, **bX**$^-$ for the hexagonal torus, where the lines **bX**^{0} are the cycles **bX** of table 8, and **bX**$^+$, **bX**$^-$ are by $\xi^{\pm 1}\frac{x}{v}$ rotated versions thereof, see also figure 5(b) for the illustration.
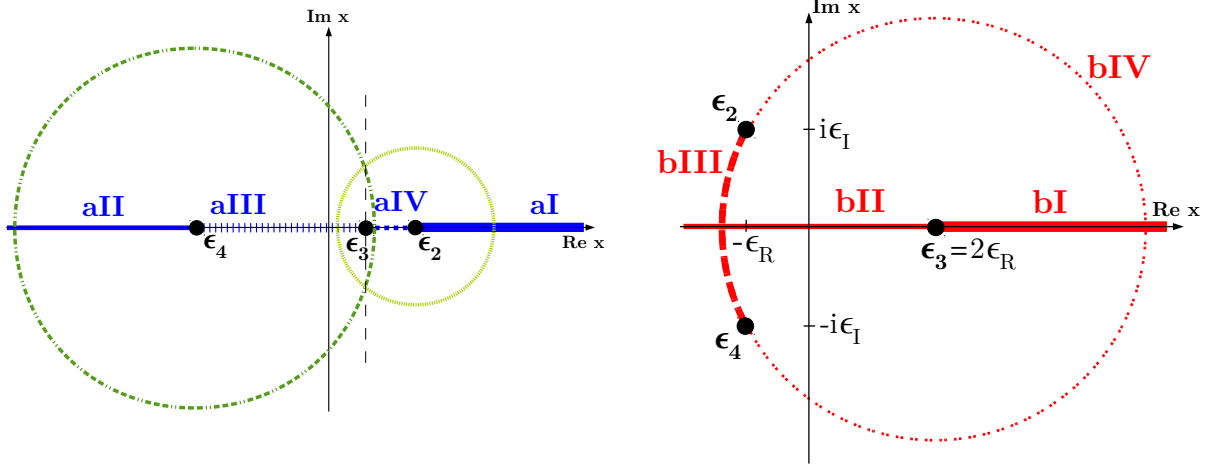
(a) For the untilted torus the cycles **aX** lie on the real x-axis, starting and ending at the fixed points ϵ_α. The line **cI** is a circle around ϵ_4 and ϵ_3, centred in ϵ_4 (replace $4 \leftrightarrow 2$ for the description of **cII**). Furthermore, **cI** and **cII** intersect twice at $\mathrm{Re}\,(x) = \epsilon_3$.

(b) Tilted torus, where the *(s)Lag* lines **bX** are apparent. Only **bI** and **bII** lie on the real axis, while **bIII** and **bIV** form an arch of a circle around ϵ_3 with end points ϵ_2 and ϵ_4.

Figure 4: *(s)Lag* lines of tables 7 and 8, projected onto the complex x-plane and for the chart $v \equiv 1$.

As mentioned below equation (4.1), each cycle consists actually of two components with different sign $+y$ or $-y$, which are projected onto the same curve in figures 4 to 6 and are therefore indistinguishable in this representation. It is important to distinguish between fractional and pure bulk cycles because their components exhibit a remarkable difference.

Looking at the Weierstrass function on the torus lattice (figures 2 and 3), one can see that a fractional cycle runs from one fixed point to another one, and then back to the first fixed point, where all fixed points have the property $y = 0$. On the first segment of the path one finds $\pm y$, and opposite sign $\mp y$ on the second part. Therefore, in coordinates x, y (and chart $v \equiv 1$) the described curve is closed and has the topology of an S^1.

On the other hand, pure bulk cycles do not run through the fixed points with $y = 0$, which implies that they consist of two disconnected components $+y$ and $-y$. Following the path of a bulk cycle on the Weierstrass function (figures 2 and 3), e.g. for the cycle **cI** of table 7b, one finds that already the upper part of **cI** forms the left circle depicted in diagram 4(a), which has negative sign for y. For the lower component one obtains in figure 4(a) the same circle, but here with property $+y$.

Considering pure bulk cycles, it is useful to think in terms of homology. This will become important in later sections, where in some cases it will be too hard to integrate over the
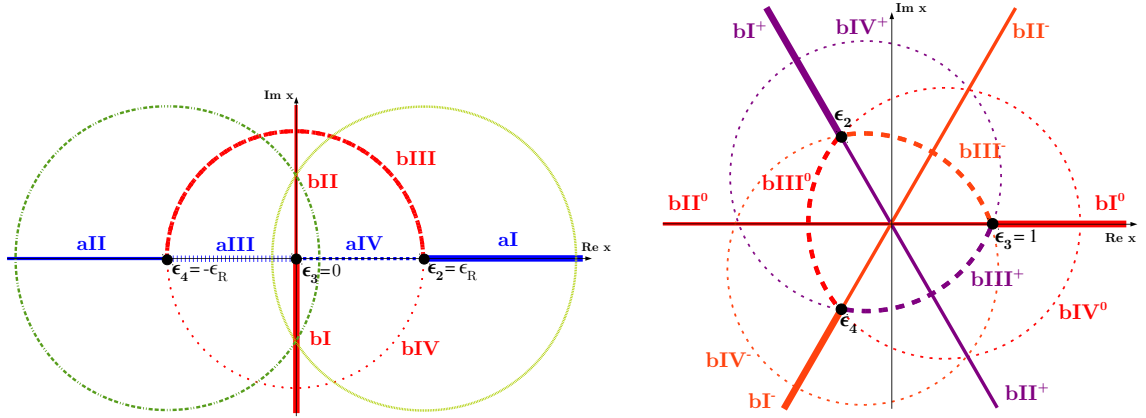
(a) One finds on the square **a**-type lattice all three types of cycles, namely **aX**, **bX**, **cX**, cf. figures 4(a) and 4(b), respectively, where the left and right circle correspond to the lines **cI** and **cII**, respectively. The lines that are inherited from the **b**-type lattice of figure 4(b) are by $-\pi/4$ rotated.

(b) On the hexagonal lattice, one easily sees the enhanced symmetry, which is $\mathbb{Z}_3$, compared to figure 4(b). Therefore the fixed points are at $\epsilon_3 = \xi^0$, $\epsilon_2 = \xi^1$ and $\epsilon_4 = \xi^{-1}$ (with $\xi \equiv e^{2\pi i/3}$), and besides $\mathbf{bX^0} \equiv \mathbf{bX}$ the additional *(s)Lag* lines $\mathbf{bX^+}$, $\mathbf{bX^-}$ appear.

Figure 5: All *(s)Lag* lines on the square **a**-type lattice (left figure) and on the hexagonal lattice (right figure), depicted in the complex x-plane (in the chart $v \equiv 1$).

desired fractional cycles directly. Therefore, I will, loosely speaking, move the bulk part away from the deformed fixed points and integrate over another bulk cycle of the same homology class, combined with an integration purely over the exceptional contributions. Since bulk cycles in the same homology class should ideally have identical volume, one has to analyse beforehand what a suitable choice for the bulk cycle is in order to keep unwanted effects of the deformation small upon integration.

Shifts by half lattice vectors   The symmetry of the torus lattice with respect to shifts by the half lattice vectors ζ_1, ζ_2, ζ_3 will become quite important in the chapter about concrete deformations. If an exceptional cycle at a certain fixed point of the orbifold is deformed and develops a non-vanishing volume, it is described by a relation in the homogeneous coordinates. Depending on the position on the torus lattice, the description of the exceptional cycle may be relatively easy (i.e. real-valued equations) or quite complicated. By shifting a fixed point in a proper way to another one it will be possible to find explicit expressions for most of the deformed exceptional cycles in the following sections.

I begin with recalling the addition theorem for the Weierstrass $\wp$-function on the torus

63

(a) Representation on the **a**-type lattice.

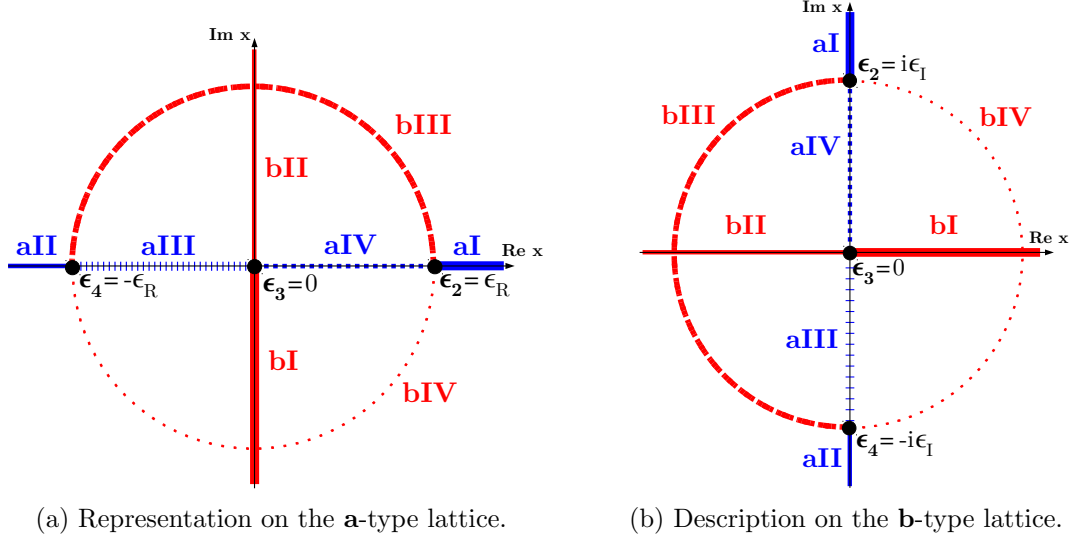(b) Description on the **b**-type lattice.

Figure 6: The *(s)Lag* lines of square tori can be described in the picture of either an untilted or a tilted torus, which are identical if the complex coordinates x (chart $v \equiv 1$) are rotated by $\pm\pi/2$. For reasons of readability, the cycles **cX** are omitted (cf. figure 4(a)).

lattice given in section 2.3.1,

$$\wp(z_1 + z_2) = \frac{1}{4}\left\{\frac{\wp'(z_1) - \wp'(z_2)}{\wp(z_1) - \wp(z_2)}\right\}^2 - \wp(z_1) - \wp(z_2), \tag{4.6}$$

which sums the coordinates z_1 and z_2 up. Inserting $z_i \in \{0, \zeta_1, \zeta_2, \zeta_3\}$, I can shift the fixed point at position z_1 to the fixed point at $z_1 + z_2$, cf. figure 7. With the known identifications $\wp(z) \equiv \frac{x}{v}$, $\wp'(z) \equiv \frac{y}{v^2}$, equation (4.6) translates to the shift transformations λ_α on the coordinates x, v, y,

$$\lambda_\alpha : \begin{pmatrix} x \\ v \end{pmatrix} \longmapsto \lambda_\alpha \cdot \begin{pmatrix} x \\ v \end{pmatrix} \equiv \frac{1}{\sqrt{2\epsilon_\alpha^2 + \epsilon_\beta\epsilon_\gamma}} \begin{pmatrix} \epsilon_\alpha & \epsilon_\alpha^2 + \epsilon_\beta\epsilon_\gamma \\ 1 & -\epsilon_\alpha \end{pmatrix} \begin{pmatrix} x \\ v \end{pmatrix}, \qquad y \longmapsto y. \tag{4.7}$$

If one inserts the fixed point $x = \epsilon_\alpha v$, it is shifted to the fixed point at the origin with $v = 0$, or vice versa, and fixed point $x = \epsilon_\beta v$ is moved to $x = \epsilon_\gamma v$, where $\alpha \neq \beta \neq \gamma$. These transformations have the following properties,

$$\lambda_\alpha\lambda_\alpha = \mathbb{1}, \qquad \lambda_\alpha\lambda_\beta\lambda_\gamma = \begin{cases} +i\mathbb{1} & \text{if } (\alpha\beta\gamma) = (234 \text{ cyclic}) \\ -i\mathbb{1} & \text{if } (\alpha\beta\gamma) = (234 \text{ anti-cyclic}) \end{cases}, \tag{4.8}$$

and under complex conjugation I find

$$\overline{\lambda_\alpha} = \lambda_\alpha \quad \text{(untilted)} \qquad \text{or} \qquad \overline{\lambda_4} = \lambda_2, \ \overline{\lambda_3} = \lambda_3 \quad \text{(tilted)}, \tag{4.9}$$

64

where it is important to distinguish between an untilted or tilted torus lattice.

Restricted to a square torus with $\epsilon_2 = 1$, $\epsilon_3 = 0$ and $\epsilon_4 = -1$, I obtain the following transformations,

$$\lambda_2 = \frac{1}{\sqrt{2}} \begin{pmatrix} 1 & 1 \\ 1 & -1 \end{pmatrix}, \qquad \lambda_3 = -i \begin{pmatrix} 0 & -1 \\ 1 & 0 \end{pmatrix}, \qquad \lambda_4 = \frac{1}{\sqrt{2}} \begin{pmatrix} -1 & 1 \\ 1 & 1 \end{pmatrix}, \tag{4.10}$$

and for a hexagonal lattice the shifts are

$$\lambda_2 = \frac{\xi^2}{\sqrt{3}} \begin{pmatrix} \xi & 2\xi^2 \\ 1 & -\xi \end{pmatrix}, \qquad \lambda_3 = \frac{1}{\sqrt{3}} \begin{pmatrix} 1 & 2 \\ 1 & -1 \end{pmatrix}, \qquad \lambda_4 = \frac{\xi}{\sqrt{3}} \begin{pmatrix} \xi^2 & 2\xi \\ 1 & -\xi^2 \end{pmatrix}, \tag{4.11}$$

where the fixed points have the values $\epsilon_2 = \xi$, $\epsilon_3 = 1$ and $\epsilon_4 = \xi^2$ with $\xi \equiv e^{2\pi i/3}$.
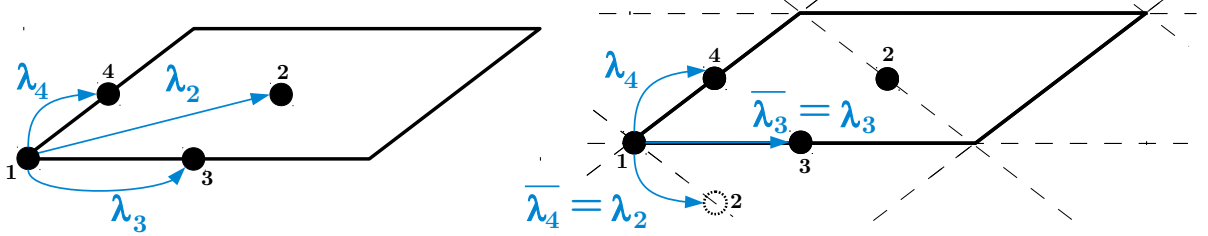

Figure 7: The figures show exemplarily on a tilted torus lattice how the shift transformations λ_α act on the four $\mathbb{Z}_2$ fixed points. The left image illustrates that the shift λ_α moves fixed point 1 to fixed point α, which works analogously for an untilted torus. In the right figure one can see the effect of complex conjugation on the transformations, which is $\overline{\lambda_4} = \lambda_2$, $\overline{\lambda_3} = \lambda_3$. In contrast, for untilted tori always $\overline{\lambda_\alpha} = \lambda_\alpha$ holds.

For later calculations, it is important to find out how the transformation λ_α acts on the polynomial $F(x, v)$, defined in equation (2.39). I observe that the polynomial has degree four, which means that I find in each term a contribution

$$x^a \cdot v^{4-a} = \left(\frac{x}{v}\right)^a \cdot v^4 \qquad \Rightarrow F(x, v) = F\left(\frac{x}{v}, 1\right) \cdot v^4. \tag{4.12}$$

To perform a shift $\lambda_\alpha(F(x, v))$, I write with a slight abuse of notation $\lambda_\alpha\left(\frac{x}{v}\right)$. This means that I use from equation (4.7) the projection onto the first component, which is x, and divide it by the projection on the second component v, hence

$$\lambda_\alpha\left(\frac{x}{v}\right) = \frac{\epsilon_\alpha x + \left(\epsilon_\alpha^2 + \epsilon_\beta \epsilon_\gamma\right) v}{x - \epsilon_\alpha v}, \tag{4.13}$$

where the indices $(\alpha\beta\gamma)$ are a permutation of (234). The shift of the function $F(x,v)$ can then be expressed as

$$\lambda_\alpha(F(x,v)) = F\left(\lambda_\alpha\left(\frac{x}{v}\right)\right) \cdot (\lambda_\alpha(v))^4 = F\left(\lambda_\alpha\left(\frac{x}{v}\right)\right) \cdot \frac{(x - \epsilon_\alpha v)^4}{(2\epsilon_\alpha^2 + \epsilon_\beta\epsilon_\gamma)^2}, \qquad (4.14)$$

which can be restricted to the chart $v \equiv 1$ very easily. This will be quite important in the following chapters since I will work most of the time in this chart.

For a torus lattice of square shape, equation (4.13) reads

$$\lambda_2\left(\frac{x}{v}\right) = \frac{x+v}{x-v}, \qquad \lambda_3\left(\frac{x}{v}\right) = \frac{-v}{x}, \qquad \lambda_4\left(\frac{x}{v}\right) = \frac{-x+v}{x+v}, \qquad (4.15)$$

and for a hexagonal one, I find

$$\lambda_\alpha\left(\frac{x}{v}\right) = \frac{\xi^{-\alpha}x + 2\xi^\alpha v}{x - \xi^{-\alpha}v}, \qquad \alpha = 2,3,4. \qquad (4.16)$$

To summarise, I will use the following specific shift transformations of equation (4.14) in the subsequent chapters, which are

$$\begin{aligned}
\lambda_2\left(F\left(\frac{x}{v}\right) \cdot v^4\right) &= F\left(\frac{x+v}{x-v}\right) \cdot \frac{(x-v)^4}{4}, \\
\lambda_3\left(F\left(\frac{x}{v}\right) \cdot v^4\right) &= F\left(\frac{-v}{x}\right) \cdot x^4, \\
\lambda_4\left(F\left(\frac{x}{v}\right) \cdot v^4\right) &= F\left(\frac{-x+v}{x+v}\right) \cdot \frac{(x+v)^4}{4}
\end{aligned} \qquad (4.17)$$

for the square torus and

$$\begin{aligned}
\lambda_2\left(F\left(\frac{x}{v}\right) \cdot v^4\right) &= F\left(\frac{\xi x + 2\xi^2 v}{x - \xi v}\right) \cdot \frac{(x - \xi v)^4}{9\xi}, \\
\lambda_3\left(F\left(\frac{x}{v}\right) \cdot v^4\right) &= F\left(\frac{x + 2v}{x - v}\right) \cdot \frac{(x - v)^4}{9}, \\
\lambda_4\left(F\left(\frac{x}{v}\right) \cdot v^4\right) &= F\left(\frac{\xi^2 x + 2\xi v}{x - \xi^2 v}\right) \cdot \frac{(x - \xi^2 v)^4}{9\xi^2},
\end{aligned} \qquad (4.18)$$

for the hexagonal torus lattice. Later, I will also insert modified polynomials $\delta F^\alpha\left(\frac{x}{v}\right)$ instead of $F\left(\frac{x}{v}\right)$ into these transformation functions. Since for all phenomenologically interesting cases I can consider horizontal branes, it is sufficient to consider only square tori instead of rectangular ones, for which the shifts could be easily generalised.

4.2 Lagrangians on local deformations: $\mathbb{C}^2/\mathbb{Z}_2$ and $\mathbb{C}^3/(\mathbb{Z}_2 \times \mathbb{Z}_2)$

As a first step to understand how deformations as sketched in [108] work, I will explain the procedure in the simpler setup of local deformations, which was also shortly discussed by the authors of this article. As examples, I consider here the deformation of a $\mathbb{C}^2/\mathbb{Z}_2$ singularity and then the case of $\mathbb{C}^3/(\mathbb{Z}_2 \times \mathbb{Z}_2)$, where it is important to note that these spaces are not compact. One should also keep in mind that in string theory one only finds deformation moduli that are associated to codimension two singularities. These completely restrict the parameters of codimension three singularities that can show up as conifold singularities. These characteristics will govern the following discussion about deformations.

4.2.1 Deformation of a $\mathbb{C}^2/\mathbb{Z}_2$ singularity

Take z_1, z_2 as coordinates of the complex space $\mathbb{C}^2$ and let $\mathbb{Z}_2$ act as $(z_1, z_2) \mapsto (-z_1, -z_2)$, where the $\mathbb{Z}_2$ generator reads $\vec{v} = \frac{1}{2}(1, -1)$. A basis of invariant polynomials is then given by the equations $y := z_1 z_2$ and $x_i := z_i^2$ with $i = 1, 2$. Their composition into one relation provides the hypersurface description of the quotient space $\mathbb{C}^2/\mathbb{Z}_2$, i.e.

$$\mathbb{C}^2/\mathbb{Z}_2 = \{f \equiv -y^2 + x_1 x_2 = 0\} \subset \mathbb{C}^3 . \tag{4.19}$$

The solutions of $f = \mathrm{d}f = 0$ reveal the singularities of the hypersurface, and a short look at the total derivative

$$\mathrm{d}f = -2y\,\mathrm{d}y + x_2\,\mathrm{d}x_1 + x_1\,\mathrm{d}x_2 \tag{4.20}$$

makes clear that $\mathrm{d}f = 0$ is only fulfilled if $y = 0$ and $x_1 = x_2 = 0$, which implies that there is one singularity at the origin $(z_1, z_2) = (0, 0)$. To deform the singularity, I add a complex deformation parameter ε to the hypersurface equation,

$$\mathrm{Def}(\mathbb{C}^2/\mathbb{Z}_2) = \{f \equiv -y^2 + x_1 x_2 - \varepsilon = 0\} \subset \mathbb{C}^3 . \tag{4.21}$$

For $\varepsilon \neq 0$, I obtain in this way a smooth space since $f = \mathrm{d}f = 0$ has no longer a solution. Note that deformation terms linear in y and x do not contribute because they disappear if one redefines the coordinates in a suitable way.

The framework of a local patch makes it possible to rotate the coordinates such that I can always choose a *real* deformation parameter, which implies that there are two possible scenarios for either positive or negative ε. Only the following restrictions give rise to the hypersurface equation of a sphere,

$$\varepsilon > 0 : \qquad \mathbf{e}^+ = \{y \in i\mathbb{R}, \, x_1 = \overline{x_2}\} \qquad \Rightarrow \quad \mathrm{Im}\,(y)^2 + |x_1|^2 = \varepsilon , \tag{4.22}$$

Exceptional *sLag* cycles of $\mathbb{C}^2/\mathbb{Z}_2$					
Cycle	Position	ε	Conditions on f	Calibration	$\Omega\mathcal{R}$ transf.
$\mathbf{e}^+$	(0,0)	+	$y^2 \le 0,\ x_1 = \overline{x_2}$	$\mathrm{Re}\,(\Omega_2)$	even
$\mathbf{e}^-$	(0,0)	$-$	$y^2 \ge 0,\ x_1 = -\overline{x_2}$	$\mathrm{Im}\,(\Omega_2)$	odd

Table 10: Specifications of the exceptional *sLag* cycles of $\mathbb{C}^2/\mathbb{Z}_2$ which appear due to a deformation of the singularity at the origin. The last column states if the respective cycle is even or odd under the orientifold involution $\Omega\mathcal{R}$.

$$\varepsilon < 0: \qquad \mathbf{e}^- = \{y \in \mathbb{R},\ x_1 = -\overline{x_2}\} \qquad \Rightarrow\ \mathrm{Re}\,(y)^2 + |x_1|^2 = -\varepsilon\,, \qquad (4.23)$$

while all other solutions that satisfy the condition $\sigma_\mathcal{R}(f) = f$ of the antiholomorphic involution describe hyperboloids or cones, which are not compact surfaces and therefore uninteresting for the following analysis of compact manifolds. For $y = 0$, the spheres $\mathbf{e}^\pm$ shrink to zero size, and one recovers the singular orbifold limit. A short computation, where I insert the condition $x_1 = \pm\overline{x_2}$ into the Kähler form, shows that $\mathbf{e}^\pm$ are *Lag* cycles because the Kähler form vanishes on them,

$$J_{1,1}^{\text{Kähler}}\Big|_{\mathbf{e}^\pm} = 0\,. \qquad (4.24)$$

I define the holomorphic two-form with a reasonable similarity to the holomorphic one-form of the elliptic curve, equation (2.40), as

$$\Omega_2 = \frac{\mathrm{d}x_1 \wedge \mathrm{d}x_2}{4y(x_1, x_2, \varepsilon)} \xrightarrow{\varepsilon \to 0} \mathrm{d}z_1 \wedge \mathrm{d}z_2\,, \qquad (4.25)$$

where I insert for y equation (4.21) solved for $y(x_1, x_2, \varepsilon)$. Thus, Ω_2 can only be traced back to the usual definition at the right side if no deformation is switched on, i.e. $\varepsilon = 0$. An explicit computation shows that $\mathrm{Im}\,(\Omega_2)|_{\mathbf{e}^+} = 0$, i.e. $\mathbf{e}^+$ is *sLag* with calibration $\mathrm{Re}\,(\Omega_2)$, while $\mathrm{Re}\,(\Omega_2)|_{\mathbf{e}^-} = 0$ and thus $\mathbf{e}^-$ is calibrated with respect to $\mathrm{Im}\,(\Omega_2)$. The specifications of the cycles $\mathbf{e}^\pm$ are summarised in table 10.

Integrating $\mathrm{Re}\,(\Omega_2)$ over the exceptional cycle $\mathbf{e}^+$,

$$\mathrm{Vol}(\mathbf{e}^+) = \int_{\mathbf{e}^\pm} \mathrm{Re}\,(\Omega_2)\,, \qquad (4.26)$$

reveals that the volume of $\mathbf{e}^+$ is $2\pi\sqrt{\varepsilon}$, as depicted in figure 8. Similarly, one can insert the relation $x_1 = -\overline{x_2}$ into the hypersurface equation (4.21) and study the exceptional cycle $\mathbf{e}^-$. As expected, in this case the plots in figure 8 have reversed sign for the deformation parameter and hence, on finds the same images, but in the reversed ε-direction.
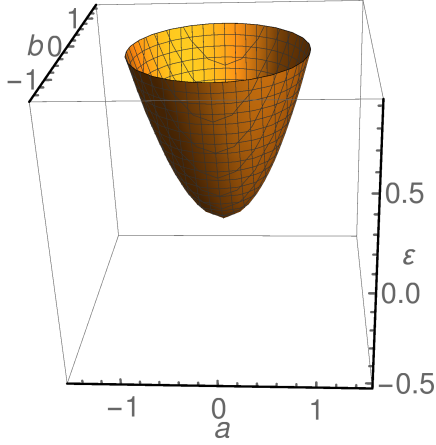
(a) The surface of the singular locus, i.e. equation (4.21) with $y^2 = 0$, shows that only for a positive deformation parameter $\varepsilon > 0$ an exceptional contribution of non-vanishing volume arises.
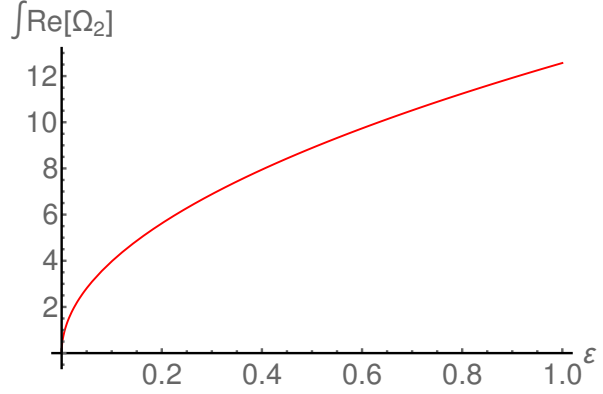
(b) The volume of the exceptional cycle $\mathbf{e}^+$ shows a square-root like behaviour, which will be the characteristic shape to determine in later scenarios if a deformed cycle has an exceptional contribution.

Figure 8: On the exceptional cycle $\mathbf{e}^+$, i.e. if the condition $x_1 = \overline{x_2}$ with $x_1 = a + ib$ is inserted into the hypersurface equation (4.21), one can study explicitly the behaviour under deformations.

4.2.2 Deformation of a $\mathbb{C}^3/(\mathbb{Z}_2 \times \mathbb{Z}_2)$ singularity

The hypersurface equation for $\mathbb{C}^3/(\mathbb{Z}_2 \times \mathbb{Z}_2)$, which has the $\mathbb{Z}_2 \times \mathbb{Z}_2$ generators $\vec{v} = \frac{1}{2}(1, -1, 0)$ and $\vec{w} = \frac{1}{2}(0, 1, -1)$, can be constructed with a similar course of action as for $\mathbb{C}^2/\mathbb{Z}_2$. The coordinates z_1, z_2, z_3 of $\mathbb{C}^3$ obey the relations $x_i = z_i^2$ with $i = 1, 2, 3$ and $y = z_1 z_2 z_3$, which are, as above, a basis of $\mathbb{Z}_2 \times \mathbb{Z}_2$ invariant polynomials. Their combination leads to

$$\mathbb{C}^3/(\mathbb{Z}_2 \times \mathbb{Z}_2) = \{f \equiv -y^2 + x_1 x_2 x_3 = 0\} \subset \mathbb{C}^4 \tag{4.27}$$

with

$$\mathrm{d}f = -2y\,\mathrm{d}y + x_2 x_3\,\mathrm{d}x_1 + x_1 x_3\,\mathrm{d}x_2 + x_1 x_2\,\mathrm{d}x_3\,, \tag{4.28}$$

and one easily sees that the three lines $\{y = 0, x_i = x_j = 0 \,|\, i \neq j\}$ form the singular locus thus satisfying $f = \mathrm{d}f = 0$, cf. figure 9(a). The deformed hypersurface can be obtained by including lower order terms with parameters $\varepsilon_1, \varepsilon_2, \varepsilon_3$,

$$\mathrm{Def}(\mathbb{C}^3/(\mathbb{Z}_2 \times \mathbb{Z}_2)) = \{f \equiv -y^2 + x_1 x_2 x_3 - \varepsilon_1 x_1 - \varepsilon_2 x_2 - \varepsilon_3 x_3 + 2\sqrt{\varepsilon_1 \varepsilon_2 \varepsilon_3} = 0\} \subset \mathbb{C}^4\,, \tag{4.29}$$

where, similar to the deformation of $\mathbb{C}^2/\mathbb{Z}_2$, no deformation terms linear in y or $x_i x_j$ appear due to a proper choice of coordinates. Following the reasoning in [108], I chose

69

the constant term as $2\sqrt{\varepsilon_1\varepsilon_2\varepsilon_3}$ because in string theory one finds only three deformation parameters, and all deformations leave a conifold singularity of codimension three. The conifold of equation (4.29) resides at the coordinates $x_i = \sqrt{\varepsilon_1\varepsilon_2\varepsilon_3}/\varepsilon_i$. The total derivative of equation (4.29) is

$$\mathrm{d}f = -2y\,\mathrm{d}y + (x_2 x_3 - \varepsilon_1)\,\mathrm{d}x_1 + (x_1 x_3 - \varepsilon_2)\,\mathrm{d}x_2 + (x_1 x_2 - \varepsilon_3)\,\mathrm{d}x_3\,, \qquad (4.30)$$

and there exist several possibilities to deform the singular loci.
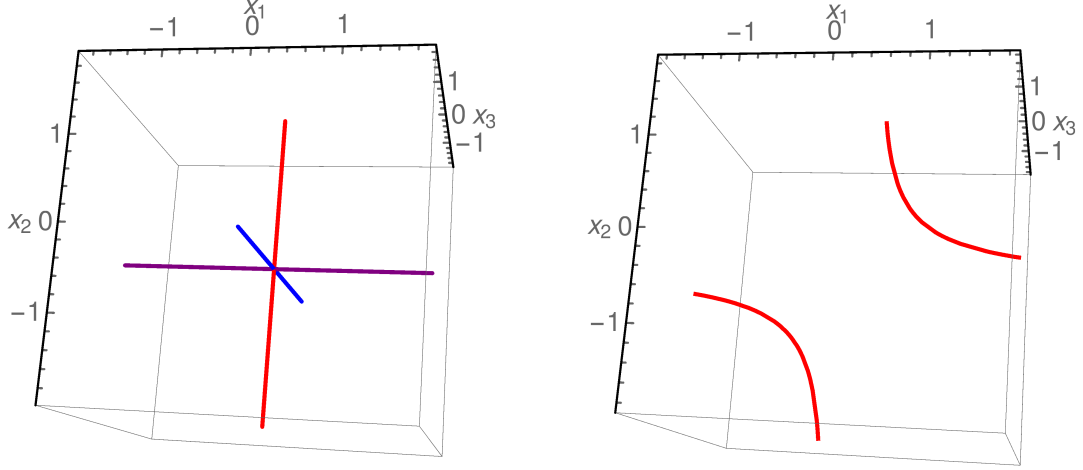
(a) Undeformed hypersurface with $\varepsilon_i = 0$, where three singular lines that run through the origin are apparent.

(b) Deformation with $\varepsilon_1 = \varepsilon_2 = 0$, $\varepsilon_3 = 0.5$. The singular line $\{y = 0, x_1 = x_2 = 0\}$ vanishes, and the other two singular lines merge to form a hyperbola, described by $x_1 x_2 = \varepsilon_3$ at $x_3 = 0$.

Figure 9: Solutions of $y^2(x_1, x_2, x_3) = 0$ of the space $\mathbb{C}^3/(\mathbb{Z}_2 \times \mathbb{Z}_2)$, which form singular lines, projected on the real values of the coordinates x_1, x_2, x_3.

For only one deformation, e.g. $\varepsilon_1 = \varepsilon_2 = 0$, $\varepsilon_3 \neq 0$, the hypersurface equation (4.29) becomes very simple and factorises with respect to x_3,

$$f \equiv -y^2 + (x_1 x_2 - \varepsilon_3)x_3 = 0\,. \qquad (4.31)$$

The relation $\mathrm{d}f = 0$ is solved in two different ways both demanding $y = 0$. If $x_3 = 0$, there remains only one line with a form of a hyperbola, $x_1 x_2 = \varepsilon_3$, cf. also equation (4.31). This solution is presented in figure 9(b), where the singular line $\{y = 0, x_1 = x_2 = 0\}$ of figure 9(a) disappears and only the depicted hyperbolic line remains. On the other hand, for $x_3 \neq 0$ the condition $x_1 x_2 - \varepsilon_3 = 0$ has to be satisfied, and I find at the origin a deformed $\mathbb{C}^2/\mathbb{Z}_2$ singularity as in the previous section.

70

The case of a generic deformation, where several or all deformation parameters ε_i are deformed, is more difficult and was presented in the publication [109] of me and my collaborators. Since a further discussion is here of no importance, I refer the reader to our article.

4.3 Deformations of $T^4/\mathbb{Z}_2$ orbifolds

The main difference between the analysis of the local deformations and the discussion of $T^4/\mathbb{Z}_2$ orbifolds is that for the latter there exist bulk cycles, exceptional cycles, and fractional cycles. In the following sections I will search for suitable descriptions of them and analyse how these cycles are influenced by deformations of the singularities at the orbifold fixed points. I consider the $T^4/\mathbb{Z}_2$ orbifold on underlying untilted tori, which I will restrict to the square torus because this remarkably simplifies the calculations and is absolutely sufficient for my discussion.

4.3.1 Hypersurface description of the $T^4/\mathbb{Z}_2$ orbifold on square tori

For the hypersurface description of a $T^4/\mathbb{Z}_2$ orbifold, I use two elliptic curves with the $\mathbb{Z}_2$ action on the homogeneous coordinates given by $(x_i, v_i, y_i) \mapsto (x_i, v_i, -y_i)$, where $i = 1, 2$. The invariant polynomials $y_i^2 = F_{(i)}(x_i, v_i)$ describe the tori $T_{(1)}^2$ and $T_{(2)}^2$, while the third monomial $y := y_1 y_2$ is a definition that I will additionally insert into the following equation in order to obtain an orbifold,

$$T^4/\mathbb{Z}_2 = \left\{ f \equiv -y^2 + F_{(1)}(x_1, v_1) \cdot F_{(2)}(x_2, v_2) = 0 \right\}. \tag{4.32}$$

By the same procedure as in the local examples, I find $4 \times 4 = 16$ isolated singularities on the $T^4/\mathbb{Z}_2$ orbifold, which are at the positions of the fixed points $\alpha \in T_{(1)}^2$, $\beta \in T_{(2)}^2$ $(\alpha, \beta = 1, 2, 3, 4)$, cf. figure 2, and which I label $(\alpha\beta)$ in the following discussion. To deform these fixed points I choose the following basis of polynomials of degree four:

$$\begin{aligned}
F_{(i)}(x_i, v_i) &= 4v_i \left(x_i - \epsilon_2 v_i \right) \left(x_i - \epsilon_3 v_i \right) \left(x_i - \epsilon_4 v_i \right), \\
\delta F_{(i)}^1(x_i, v_i) &= -4 \left(x_i - \epsilon_2 v_i \right) \left(x_i - \epsilon_3 v_i \right)^2 \left(x_i - \epsilon_4 v_i \right), \\
\delta F_{(i)}^2(x_i, v_i) &= -4v_i \left(x_i - \epsilon_3 v_i \right) \left(x_i - \epsilon_4 v_i \right)^2, \\
\delta F_{(i)}^3(x_i, v_i) &= 4v_i^2 \left(x_i - \epsilon_2 v_i \right) \left(x_i - \epsilon_4 v_i \right), \\
\delta F_{(i)}^4(x_i, v_i) &= 4v_i \left(x_i - \epsilon_2 v_i \right)^2 \left(x_i - \epsilon_3 v_i \right).
\end{aligned} \tag{4.33}$$

The first equation is the same as the one that already appeared in the definition of the elliptic curve, equation (2.39), while the others are chosen in such a way that the term

with the singularity α, having the fixed point value ϵ_α, is replaced by the term of a different singularity. Therefore, the polynomials $\delta F^\alpha_{(i)}(x_i, v_i)$ can be used to deform a certain singularity α, and in combination with 16 deformation parameters $\varepsilon_{\alpha\beta}$ one can construct the hypersurface equation of the deformed orbifold as

$$\mathrm{Def}(T^4/\mathbb{Z}_2) = \left\{ f \equiv -y^2 + F_{(1)} \cdot F_{(2)} - \sum_{\alpha,\beta=1}^{4} \varepsilon_{\alpha\beta}\, \delta F^\alpha_{(1)} \cdot \delta F^\beta_{(2)} = 0 \right\}. \tag{4.34}$$

The polynomials of equation (4.33) simplify to

$$
\begin{aligned}
F_{(i)}(x_i, v_i) &= 4x_i v_i \left(x_i^2 - v_i^2 \right), \\
\delta F^1_{(i)}(x_i, v_i) &= -4x_i^2 \left(x_i^2 - v_i \right), \\
\delta F^2_{(i)}(x_i, v_i) &= -4x_i v_i \left(x_i + v_i \right)^2, \\
\delta F^3_{(i)}(x_i, v_i) &= 4v_i^2 \left(x_i^2 - v_i^2 \right), \\
\delta F^4_{(i)}(x_i, v_i) &= 4x_i v_i \left(x_i - v_i \right)^2,
\end{aligned}
\tag{4.35}
$$

when I restrict the underlying torus lattice to square shape with fixed points $\epsilon_4 = -1$, $\epsilon_3 = 0$, $\epsilon_2 = +1$.

It is important to note that for a square torus, the four deformation polynomials obey the shift symmetry of half lattice vectors such that shifting a fixed point α with equation (4.7) to fixed point β is reflected in the transformations of equation (4.17), which map the polynomials $\delta F^\alpha_{(i)}(x_i, v_i)$ of equation (4.35) in the following way onto each other,

$$
\lambda_2 : \begin{array}{c} \delta F^1_{(i)} \leftrightarrow \delta F^2_{(i)}, \\ \delta F^3_{(i)} \leftrightarrow \delta F^4_{(i)} \end{array} \qquad
\lambda_3 : \begin{array}{c} \delta F^1_{(i)} \leftrightarrow \delta F^3_{(i)}, \\ \delta F^2_{(i)} \leftrightarrow \delta F^4_{(i)} \end{array} \qquad
\lambda_4 : \begin{array}{c} \delta F^1_{(i)} \leftrightarrow \delta F^4_{(i)}, \\ \delta F^2_{(i)} \leftrightarrow \delta F^3_{(i)} \end{array}
\tag{4.36}
$$

and the undeformed polynomials $F_{(i)}(x_i, v_i)$ stay invariant. Therefore, a shift transformation on the square torus lattice is basically a relabelling of the fixed points in a suitable way.

The Holomorphic two-form on the orbifold is for the homogeneous coordinates defined as

$$\Omega_2 = \frac{(v_1 \cdot dx_1 - x_1 \cdot dv_1) \wedge (v_2 \cdot dx_2 - x_2 \cdot dv_2)}{y} \overset{v_i \equiv 1}{=} \frac{dx_1 \wedge dx_2}{y}, \tag{4.37}$$

where $y := y_1 \cdot y_2$ was inserted to account for the orbifold action. For the complex values $x_i \equiv |x_i| e^{i\phi_i}$ on the *Lag* cycles only combinations of the phases with $e^{i(\phi_1+\phi_2)} = \pm 1$, called real calibrations, are allowed to obtain supersymmetric cycles, cf. section 3.1.3. Contrary, phases that result in $e^{i(\phi_1+\phi_2)} = \pm i$ are called calibrations with respect to $\mathrm{Im}(\Omega_2)$.

4.3.2 Bulk cycles: structure and integrals

When dealing with bulk cycles one has to keep in mind that I use as ansatz only factorised two-tori $T^4 \equiv T^2_{(1)} \times T^2_{(2)}$, where the factorisation also translates to the two-cycles. Hence, these can be decomposed into the product $\mathbf{N_1} \otimes \mathbf{N_2}$. According to tables 7 and 8, for **a**-type lattices there exist simple descriptions of the *Lag* lines $\mathbf{N_i} = \mathbf{aX_i}$, running through the fixed points, and for the lines with label $\mathbf{N_i} = \mathbf{cX_i}$, which do not intersect the fixed points of the orbifold. For the tilted **b**-type tori I find the cycles named $\mathbf{N_i} = \mathbf{bX_i}$, which also cross the fixed points. Remember that the additional cycles for square and hexagonal tori are listed in table 9.

As on the elliptic curve, one can directly read off the calibration of the cycles from their labelling, and a

$$
\text{cycle is } sLag \text{ with calibration } \begin{cases} \text{Re}\,(\Omega_2) & \text{if } \mathbf{X_1} + \mathbf{X_2} = \text{even} \\ \text{Im}\,(\Omega_2) & \text{if } \mathbf{X_1} + \mathbf{X_2} = \text{odd} \end{cases}. \tag{4.38}
$$

In this relation, $\mathbf{X_i}$ ($i = 1, 2$) does not refer to the cycle itself, but denotes the number of the label, i.e. $\mathbf{X_i} \in \{1, 2, 3, 4\}$ for the cycles $\mathbf{aX_i}$ and $\mathbf{bX_i}$, and $\mathbf{X_i} \in \{1, 2\}$ if a cycle of type $\mathbf{cX_i}$ is considered. To understand the topology of the combined two-cycles, one has to distinguish again between fractional and pure bulk cycles, as worked out in section 4.1 for the one-cycles. I will address here only the topology of the bulk cycles on the untilted lattice and discuss bulk cycles on tilted tori in the context of the orbifold $T^6/(\mathbb{Z}_2 \times \mathbb{Z}'_6)$ (on hexagonal tori) in section 4.5. One should note that on the orbifold one has defined $y := y_1 y_2$, and thus the combination of the y_i forms again two components $\pm y$ with $y = 0$ at the fixed points, cf. also the discussion in section 4.1, which causes specific topologies of the combined two-cycles.

Fractional cycles of type $\mathbf{aX_1} \otimes \mathbf{aX_2}$ give rise to a $T^2/\mathbb{Z}_2$ orbifold that has the shape of a pillow, which is isomorphic to a sphere S^2 with punctures. In detail, the borders of the square base area have values $y = 0$, inside of which the area curves up- and downwards with $+y$ or $-y$, respectively. On the contrary, cycles of type $\mathbf{aX_1} \otimes \mathbf{cX_2}$ or $\mathbf{cX_1} \otimes \mathbf{cX_2}$ exhibit the topology of a T^2. This is simply because there is no identification of fixed points at $y = 0$, which leaves in all cases the combination of two separate circles (with signs merged according to $y := y_1 y_2$).

There exist two different ways to perform the integration over a bulk cycle. Either one defines the cycle on the torus lattice and translates it via the Weierstrass function to the homogeneous coordinates, or one constructs the path of integration directly in the x_i-plane (when working in the chart $v_i \equiv 1$). Both methods can be useful, so I will explain them

73
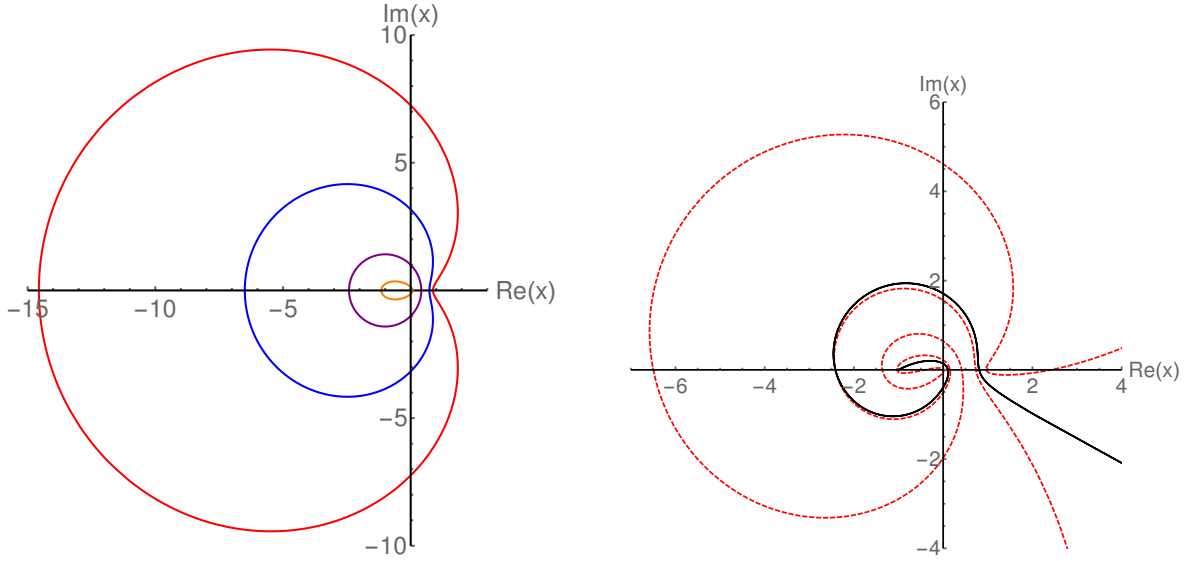
(a) The parameters are $(n, m) = (1, 0)$, $c = 0$, and from outside to inside $d = 0.2$, $d = 0.3$, $d = 0.5$, $d = 0.8$, where $d = 0.5$ equals cycle **cI**.

(b) The solid black curve has winding numbers $(n, m) = (4, 1)$ and shifts $c = 0$, $d = 0$, while the dashed red curve has properties $(n, m) = (5, 1)$, $c = 0$, $d = 0.3$.

Figure 10: Bulk cycles in hypersurface language in the complex x-plane and chart $v \equiv 1$, obtained with a parametric plot as indicated in equation (B.3) in appendix B. While horizontal (or vertical) bulk cycles have relatively simple shapes in the x-plane (left diagram), bulk cycles with higher winding numbers look quite complicated (right figure). The parameters n, m, c, d of the curves are given in equation (4.40).

in more detail. The integration over a bulk two-cycle on $\mathbb{C}^2$, where the coordinates are (x_1, x_2), looks like

$$\int_0^1 \mathrm{d}t_1 \int_0^1 \mathrm{d}t_2 \left[\left| \mathrm{Re} \left(\frac{\frac{\partial x_1}{\partial t_1} \cdot \frac{\partial x_2}{\partial t_2}}{\sqrt{y^2(x_1(t_1), x_2(t_2), \varepsilon)}} \right) \right| + i \, \mathrm{Im} \left(\frac{\frac{\partial x_1}{\partial t_1} \cdot \frac{\partial x_2}{\partial t_2}}{\sqrt{y^2(x_1(t_1), x_2(t_2), \varepsilon)}} \right) \right] \quad (4.39)$$

with parameter t_i for each bulk one-cycle and deformation parameter ε that stands for $\varepsilon := \varepsilon_{\alpha\beta} \neq 0$ if only one singularity is deformed. Note that due to equation (3.27), one has to take the absolute value for the real part of the integrand, while, for a *sLag* cycle, the imaginary part should be zero (up to very small numerical fluctuations) and taking the absolute value is therefore of no importance.

The first way to introduce the paths of integration is to choose a curve $z_i(t_i)$ with parameter $t_i \in \mathbb{R}$ on the torus, e.g. a cycle **cX**, and to map it via

$$x_i(t_i) = \wp \big(2t_i (n_i \, \zeta_1 + m_i \, \zeta_2) + c_i \, \zeta_1 + d_i \, \zeta_2 \big) \quad (4.40)$$

to the complex x_i-plane. (n_i, m_i) are the integer wrapping numbers on the torus, ζ_1 and ζ_2 are basis half-lattice vectors, and the parameters $c_i, d_i \in [0, 1)$ encode continuous shifts.

The second approach is to directly parametrise a curve on the complex planes x_i, for example an ellipse around the fixed points $\epsilon_4 = -1$ and $\epsilon_3 = 0$ centred at $x_i = \left(\frac{3}{4} - a_i\right)$,

$$x_i(t_i) = (3/4 - a_i) + a_i \cos(t_i) + i\, b_i \sin(t_i)\,, \tag{4.41}$$

where the parameters have ranges $t_i \in [0, 2\pi)$ and $a_i, b_i \in \mathbb{R}^+$. Based on the study of several examples I assume that the choice of the zero-crossing between $\epsilon_3 = 0$ and $\epsilon_2 = +1$, here at $x_i = \frac{3}{4}$, is of minor importance as long as it is not too close to one of these fixed points (especially if they are deformed). Furthermore, for different values of a_i, b_i the integrals show very small differences as long as a_i, b_i are large (e.g. $\mathcal{O} = 100, 1000$).

As an example I will deform the fixed point (33) at $x_1 = x_2 = 0$ and observe the effect of the deformation on some bulk cycles that are constructed by the above methods. For the (33) deformation, the hypersurface equation (4.34) reads

$$\begin{aligned}
y^2 &= F_{(1)}(x_1, v_1) \cdot F_{(2)}(x_2, v_2) - \varepsilon_{33} \cdot \delta F_{(1)}^3(x_1, v_1) \cdot \delta F_{(2)}^3(x_2, v_2) \\
&= v_1 v_2 \left(x_1^2 - v_1^2\right)\left(x_2^2 - v_2^2\right)(x_1 x_2 - \varepsilon_{33}\, v_1 v_2) \\
&\stackrel{v_i \equiv 1}{=} \left(x_1^2 - 1\right)\left(x_2^2 - 1\right)(x_1 x_2 - \varepsilon_{33})\,,
\end{aligned} \tag{4.42}$$

and I find that the ellipses seem to be much less affected upon deformations $\varepsilon_{33} \in (-1, 1)$ than the curves defined via the Weierstrass map, e.g. the curves presented in figure 10(a). The reason why the second method seems to be more "robust" is probably the fact that the path of integration is here relatively simple and hence unwanted effects of deformations can be better avoided.

4.3.3 Exceptional cycles: description and integrals

On the basis of the local deformations, it makes sense to describe an exceptional cycle in a similar way as in equations (4.22) and (4.23). The fixed set of equation (4.42) under the involution $\sigma_{\mathcal{R}} : x_1 \leftrightarrow \overline{x_2}, v_1 \leftrightarrow \overline{v_2}, y \mapsto \pm\overline{y}$ is given by

$$\left(\frac{\mathrm{Im}\,(y)}{\sqrt{(x_1^2 - 1) \cdot \left(\overline{x_1}^2 - 1\right)}}\right)^2 + |x_1|^2 = \varepsilon \tag{4.43}$$

for the choice $y \mapsto -\overline{y}$, which means calibration $\mathrm{Re}\,(\Omega_2)$ for the *sLag* exceptional cycle. To describe an S^2, the requirement $|x_1| < 1$ has to be fulfilled, which implies $0 < \varepsilon < 1$. For a

deformation in opposite direction, $-1 < \varepsilon < 0$, on has to use $x_1 = -\overline{x_2}$ to find the equation of a two-sphere and the appropriate branch is $y \mapsto +\overline{y}$ with calibration $\mathrm{Im}\,(\Omega_2)$.

To obtain the volume of the exceptional cycle, I introduce the condition $x_1 = \pm\overline{x_2}$ into equation (4.42), or a similar equation for the deformation of another singularity. Differently written, I insert $x_1 = a + ib$, $x_2 = \pm(a - ib)$ to get

$$y_\pm^2(a,b) = \pm\big(a^4 + 2a^2(b^2 - 1) + (b^2 + 1)^2\big)\big(a^2 + b^2 \mp \varepsilon_{33}\big). \tag{4.44}$$

It is instructive to look at the plots of $y_+^2(a,b)$ in figure 11 that make clear which singularities are included in the equation $x_1 = \pm\overline{x_2}$ and what happens if a deformation ε_{33} is switched on.
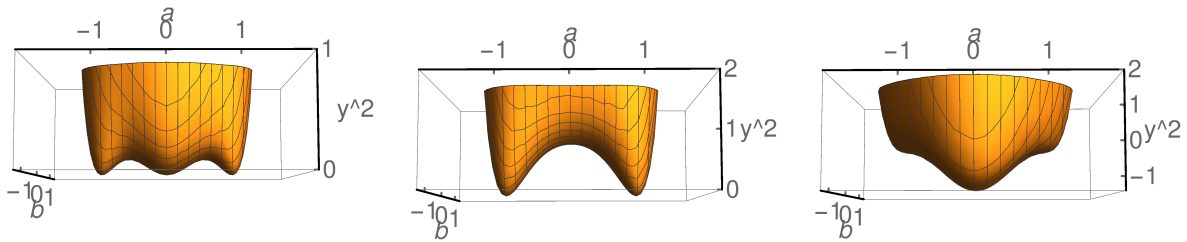
(a) Undeformed: $y_+^2(a,b) \geq 0$, and for $y_+^2 = 0$ one finds the singularities (44), (33), and (22) at $(a,b) = (-1,0),(0,0),(1,0)$, respectively.

(b) $\varepsilon_{33} < 0$: The singularity (33) vanishes, i.e. $y_+^2(0,0) \neq 0$, but no exceptional cycle arises. The singularities (44) and (22) remain unchanged.

(c) $\varepsilon_{33} > 0$: An exceptional cycle with calibration $\mathrm{Re}\,(\Omega_2)$ grows out of the singularity (33), for which $y_+^2 < 0$. (44) and (22) are still singular points at $y_+^2(\pm1,0) = 0$.

Figure 11: Three-dimensional plots of the function $y_+^2(a,b)$ of equation (4.44), which shows all exceptional cycles that are described by $x_1 = +\overline{x_2} = a + ib$, and where the singular points at $y_+^2 = 0$ are visible.

Figure 11(a) implies that the description $x_1 = \pm\overline{x_2}$ holds for all singularities $(\alpha\alpha)$, where (11) lies at infinity and is thus not apparent in this picture. Figures 11(b) and 11(c) illustrate that for a certain sign choice of $x_1 = \pm\overline{x_2}$, the sign of the deformation parameter is already determined in order to let an exceptional cycle grow out of the deformed singularity. This is also confirmed by the plot in figure 12(a), where obviously only for deformations in positive direction an exceptional cycle of non-vanishing volume develops. Looking at equation (4.44), it is clear that for $x_1 = -\overline{x_2}$ one finds figures 11 and 12(a) with reversed sign of the vertical axis, and ε_{33} has to be deformed in negative direction in order to find an exceptional cycle.

In table 11 all specifications of the exceptional cycles are summarised. The calibration can be easily computed if one inserts the condition $x_1 = a + ib$, $x_2 = \pm(a - ib)$ into the
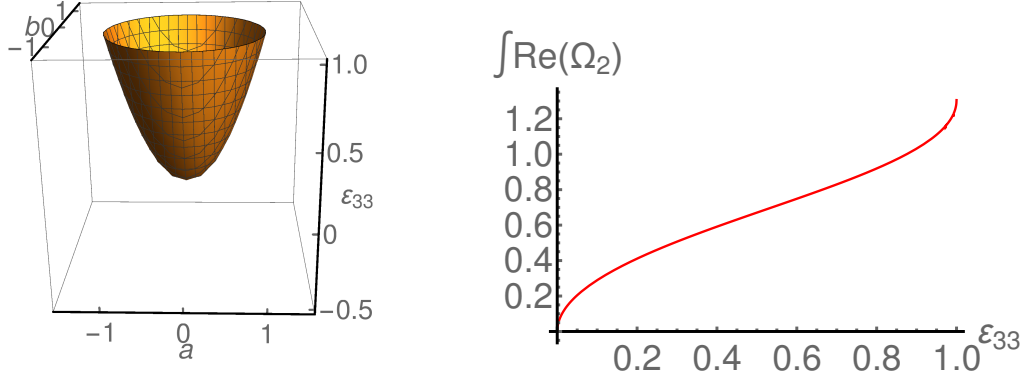
(a) The plot of $y_+^2(a, b, \varepsilon_{33}) = 0$ shows that only deformations with $\varepsilon_{33} > 0$ give rise to an exceptional cycle of calibration $\mathrm{Re}\,(\Omega_2)$, i.e. $\mathbf{e}_{33}^+$, and that no other exceptional cycle appears.

(b) Direct integration of $\mathbf{e}_{33}^+$, as done in equation (4.47), where $\mathbf{e}_{33}^+$ obtains a non-zero volume upon deformation with $\varepsilon_{33} > 0$. The volume is normalised with respect to the volume of a bulk cycle in the undeformed case.

Figure 12: Properties of the exceptional cycle $\mathbf{e}_{33}^+$ upon deformation by the parameter ε_{33}.

holomorphic two-form,

$$\Omega_2 = \frac{\mathrm{d}x_1 \wedge \mathrm{d}x_2}{y} = \ldots = \mp i \cdot \frac{2\,\mathrm{d}a \wedge \mathrm{d}b}{\sqrt{y^2}} = \begin{cases} \mp \mathrm{Re}\,(\Omega_2) & \text{if } y^2 < 0 \\ \pm \mathrm{Im}\,(\Omega_2) & \text{if } y^2 > 0 \end{cases}. \tag{4.45}$$

With these considerations, it is easy to compute the volume of the exceptional cycle $\mathbf{e}_{33}^+$ (and similarly for any other exceptional cycle $\mathbf{e}_{\alpha\beta}^\pm$). According to figure 12(a) it is sufficient to integrate over the intervals $a, b \in (-1, 1)$, and including the Heaviside step function

$$H[n] = \begin{cases} 0 & \text{if } n < 0 \\ 1 & \text{if } n \geq 0 \end{cases} \tag{4.46}$$

in a suitable form into the integration ensures that only the exceptional contributions with $y_+^2(a, b) < 0$ are included. Hence, the complete integral over the exceptional cycle $\mathbf{e}_{33}^+$ has the form

$$\int_{\mathbf{e}_{33}^+} \Omega_2 = -2i \int_{-1}^{1} \mathrm{d}a \int_{-1}^{1} \mathrm{d}b \, \frac{H[-y_+^2(a, b)]}{\sqrt{y_+^2(a, b)}}, \tag{4.47}$$

where the imaginary factor is cancelled by the purely imaginary denominator with the restriction $y_+^2(a, b) < 0$. The result is depicted in figure 12(b), but the graph is normalised in terms of the volume of any bulk cycle at zero deformation, as I will do it for all following graphs of the integrations. The reason is that here I am only interested in the behaviour of the cycles, but not in their concrete values. Remark also that an integration over $\mathbf{e}_{33}^-$ gives the same graph, but mirrored on the y-axis, i.e. the values of ε_{33} are negative.

77

Exceptional *sLag* cycles of $T^4/\mathbb{Z}_2$						
Cycle	Condition	Position	$\varepsilon_{\alpha\beta}$	Conditions on f	Calibration	$\Omega\mathcal{R}$ transf.
$\mathbf{e}^+_{\alpha\beta}$	$\alpha + \beta$ = even	$(\epsilon_\alpha, \epsilon_\beta)$	$+$	$y^2 < 0,\ x_1 = \overline{x_2}$	$\mathrm{Re}\,(\Omega_2)$	even
$\mathbf{e}^-_{\alpha\beta}$	$\alpha + \beta$ = odd	$(\epsilon_\alpha, \epsilon_\beta)$	$-$	$y^2 > 0,\ x_1 = -\overline{x_2}$	$\mathrm{Im}\,(\Omega_2)$	odd

Table 11: Properties of all exceptional *sLag* cycles of $T^4/\mathbb{Z}_2$, which develop a non-vanishing volume upon deformation of $\varepsilon_{\alpha\beta}$. The cycles can be separated into two classes, where the condition is already encoded in the fixed point labels $\alpha, \beta \in \{1, 2, 3, 4\}$, cf. the second column. The classes $\mathbf{e}^\pm_{\alpha\beta}$ allow for either positive or negative deformations, $\varepsilon_{\alpha\beta} \in [0, 1]$ or $\varepsilon_{\alpha\beta} \in [-1, 0]$, respectively.

4.3.4 Fractional cycles: integrals

The integration of the holomorphic two-form Ω_2 over the deformed *Lag* cycles, depending on the deformation parameter ε, gives information about the exceptional part of a fractional cycle and shows the homology class. To start with, I will show how to compute the integrals over undeformed fractional two-cycles for untilted tori, and then I will go over to the deformed cycles. Since the integration over cycles on tilted tori has some technical issues, I will discuss these later.

The fractional cycles with the labels $\mathbf{N_i} \in \{\mathbf{aI}, \mathbf{aII}, \mathbf{aIII}, \mathbf{aIV}, \mathbf{bI}, \mathbf{bII}\}$ ($i = 1, 2$) satisfy the condition $\mathrm{Im}\,\left(\frac{x}{v}\right) = 0$, which allows to display products $\mathbf{N_1} \otimes \mathbf{N_2}$ of them in the real plane with coordinates (x_1, x_2) (chart $v \equiv 1$). For the untilted torus with cycles $\mathbf{aX_i}$, the singularities of the hypersurface equation are then the vertical and horizontal lines $x_1, x_2 = \epsilon_\alpha$ with fixed point values $\epsilon_1 = \infty$, $\epsilon_4 < \epsilon_3 < \epsilon_2 \in \mathbb{R}$, and these form the boundaries of the *Lag* cycles $\mathbf{aX_1} \otimes \mathbf{aX_2}$. Figure 13(a) illustrates this for the square torus, where $\epsilon_4 = -1$, $\epsilon_3 = 0$, $\epsilon_2 = 1$.

The diagram of equation (4.42) in figure 13(b) illustrates the deformation. As for the local deformations, there is a remarkable difference between deformations in positive and negative direction of ε_{33}. Diagram 13(b) depicts the case of $\varepsilon_{33} > 0$, where the deformation causes the cycles $\mathbf{aIII} \otimes \mathbf{aIII}$ and $\mathbf{aIV} \otimes \mathbf{aIV}$ to shrink until they vanish at $\varepsilon_{33} = 1$, while the formerly separated cycles $\mathbf{aIII} \otimes \mathbf{aIV}$ and $\mathbf{aIV} \otimes \mathbf{aIII}$ merge. The exceptional cycle $\mathbf{e}^+_{33}$ of real calibration, which has zero volume in the undeformed scenario ($\varepsilon_{33} = 0$), starts growing out of the former singularity at $(x_1, x_2) = (0, 0)$. For a deformation $\varepsilon_{33} < 0$ the cycles $\mathbf{aIII} \otimes \mathbf{aIII}$ and $\mathbf{aIV} \otimes \mathbf{aIV}$ switch the roles with $\mathbf{aIII} \otimes \mathbf{aIV}$ and $\mathbf{aIV} \otimes \mathbf{aIII}$.

From these observations I already reason that the $\mathbb{Z}_2$ eigenvalue is $(-1)^{\tau_{\mathbb{Z}_2}} = -1$ in front of $\mathbf{e}^+_{33}$ because the volume of the *sLag* cycles $\mathbf{aIII} \otimes \mathbf{aIII}$ and $\mathbf{aIV} \otimes \mathbf{aIV}$ decreases with growing ε_{33}. Therefore, the exceptional cycle must have the same calibration as these *sLag*
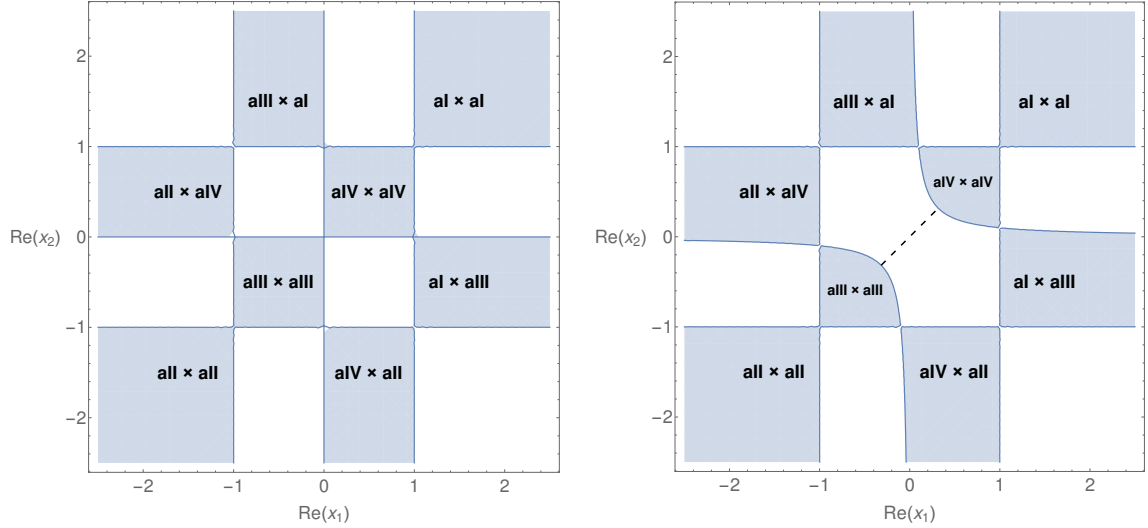
(a) All singularities, represented by the intersections of the horizontal and vertical lines, are undeformed and thus $\varepsilon_{\alpha\beta} = 0$ for all $(\alpha\beta)$.

(b) The singularity at $x_1 = x_2 = 0$ is deformed with $\varepsilon_{33} = 0.1$, i.e. the former intersection point is replaced by the curve $\varepsilon_{33} = x_1 x_2$. The exceptional cycle $\mathbf{e}_{33}^+$, which grows out of the former singularity, is illustrated by the dashed line.

Figure 13: The above diagrams illustrate the cycles $\mathbf{aX_1} \otimes \mathbf{aX_2}$ on a square torus in the real (x_1, x_2)-plane, where areas with the property $y^2(x_1, x_2) > 0$ (cf. equation (4.42)) are highlighted in blue. The fixed points with values $\epsilon_4 = -1$, $\epsilon_3 = 0$, $\epsilon_2 = 1$ (and $\epsilon_1 = \infty$) are indicated by the vertical and horizontal lines. Their intersection points are the zeros of the hypersurface equation, which become the deformable singularities of the holomorphic two-form. The cycles $\mathbf{aX_1} \otimes \mathbf{aX_2}$ are represented by the areas between these lines, which have actually the shape of a pillow as explained in section 4.3.2, and where the colouring indicates real calibration.

cycles with bulk parts Π_{13} and $-\Pi_{24}$ in the standard $T^4/\mathbb{Z}_2$ language, respectively. This implies that it has a different calibration from the merged *Lag* cycle, so the unification of $\mathbf{aIII} \otimes \mathbf{aIV}$ and $\mathbf{aIV} \otimes \mathbf{aIII}$ was also necessary in order to cancel the exceptional part of the cycle $\Pi_{14} + \Pi_{23}$.

The deformation of the singularity (33) can be easily translated to the deformation of any other singularity. It is also possible to deform all singularities at the same time with the same deformation parameter ε, where all *sLag* cycles of calibration $\mathrm{Im}\,(\Omega_2)$ merge and the *sLag* cycles of calibration $\mathrm{Re}\,(\Omega_2)$ decrease with growing deformation parameter, see figure 14. This case was discussed in more detail in our article [109].

When switching on deformations, I insert equation (4.34) for $y^2(x_1, x_2)$. Deforming for instance fixed point (33), I use equation (4.42). This implies that some other fixed points change their position depending on ε_{33} as well, which one can already suppose when looking
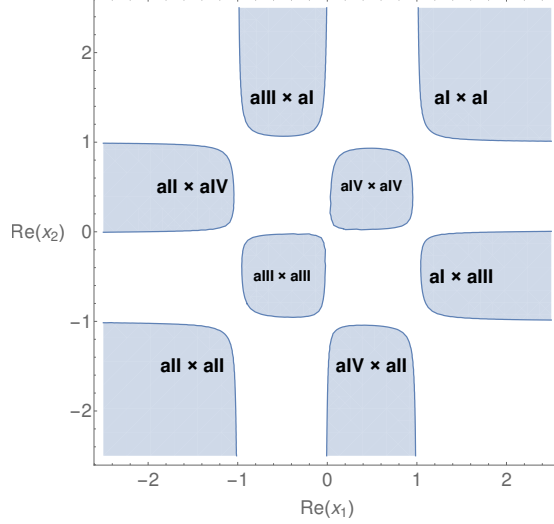
Figure 14: All singularities deformed with either $+\varepsilon$ or $-\varepsilon$ in such a way that the *sLag* cycles with real calibration (shaded areas) do not merge with other cycles. On the other hand, all *sLag* cycles with imaginary calibration merge to one big cycle (white regions).

carefully at the diagram in figure 13(b), e.g. examine the fixed point at $(x_1, x_2) = (1, 0)$. Therefore, one has to take care of the integration boundaries when leaving the orbifold point. Since explicitly adjusting the boundaries by some function can be difficult for more involved integrations, I use again the Heaviside step function as defined in equation (4.46).

Integrals over one-cycles $\mathbf{aX}$ are especially simply because they run only over real values x (in chart $v \equiv 1$), cf. table 7, starting at the initial fixed point value ϵ_{k_i} and ending at the final fixed point value ϵ_{k_f}. In the chart $v_i \equiv 1$, the integrals can be constructed as

$$\int_{\mathbf{aX}} \Omega_1 = 2 \int_{\epsilon_{k_i}}^{\epsilon_{k_f}} \frac{\mathrm{d}x_1}{\sqrt{y^2(x_1)}} \approx i^{\mathbf{X}-1} \cdot 5.24\dots, \tag{4.48}$$

where I set all results to positive values since volumes are always positive, but here the volumes may have a different calibration, i.e. an imaginary factor. The holomorphic one-form is defined in equation (2.40), and I also take a factor of two since the integral runs only over half a cycle. At the orbifold point, the formula for $y^2(x_1)$ is simply the equation of the elliptic curve, i.e. $y^2(x_1) = x_1^3 - x_1$. The evaluation of this integral for an arbitrary cycle $\mathbf{aX}$ gives always the same result and changes only in the calibration, which can be real or imaginary depending on the label $\mathbf{X} = \mathbf{1}, \mathbf{2}, \mathbf{3}, \mathbf{4}$. For example, on a square torus lattice with $\epsilon_1 = \pm\infty$, $\epsilon_2 = 1$, $\epsilon_3 = 0$, $\epsilon_4 = -1$, the integral over the cycle $\mathbf{aI}$ has the simple form

$$\int_{\mathbf{aI}} \Omega_1 = 2 \int_1^\infty \frac{\mathrm{d}x_1}{\sqrt{x^3 - x}} \approx 5.24\dots \tag{4.49}$$

80

with real calibration.

If the orbifold is undeformed, the integral over a two-cycle is then simply the product of integrals over one-cycles (where again I set the result to a positive value),

$$\int_{\mathbf{aX_1} \otimes \mathbf{aX_2}} \Omega_2 = 2 \int_{\epsilon_{j_i}}^{\epsilon_{j_f}} \int_{\epsilon_{k_i}}^{\epsilon_{k_f}} \frac{\mathrm{d}x_1 \mathrm{d}x_2}{\sqrt{y^2(x_1, x_2)}} \approx i^{\mathbf{X}-1} \cdot 13.75 \ldots , \tag{4.50}$$

and $y^2(x_1, x_2) = (x_1^3 - x_1)(x_2^3 - x_2)$, namely the combination of two elliptic curves, cf. equation (4.32). Since all integrals over the cycles $\mathbf{aX_1} \otimes \mathbf{aX_2}$ have an equal value, I will normalise the subsequent plots to one for $\varepsilon \equiv 0$.
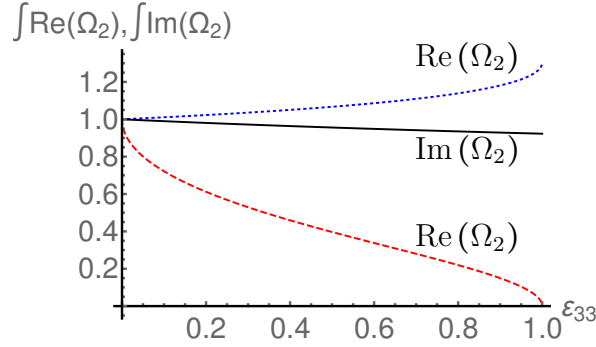

Figure 15: Normalised integrals over $\mathrm{Re}\,(\Omega_2)$ or $\mathrm{Im}\,(\Omega_2)$ depending on the deformation parameter ε_{33}. The red dashed curve shows the integral over the cycles $\mathbf{aIII} \otimes \mathbf{aIII}$ or $\mathbf{aIV} \otimes \mathbf{aIV}$, running through the deformed singularity, and the blue dotted curve is the result for all other cycles with real calibration. All integrals over cycles calibrated with $\mathrm{Im}\,(\Omega_2)$ (i.e. white regions in figure 13) show the behaviour of the black solid curve.

When deformations are taken into account, it can be hard to find the correct bounds of integration. I solve this difficulty by integrating over a larger area where the extra parts need to have opposite calibration, i.e. areas of different colour in figure 13, and which are modded out upon integration by the Heaviside step function as defined in equation (4.46). For instance, the integral over the cycle $\mathbf{aI} \otimes \mathbf{aIII}$ looks like

$$\int_{\mathbf{aI} \otimes \mathbf{aIII}} \mathrm{Re}\,(\Omega_2) = 2 \int_1^{\infty} \mathrm{d}x_1 \int_{-1}^{1} \mathrm{d}x_2 \frac{H[(x_1^2 - 1)(x_2^2 - 1)(x_1 x_2 - \varepsilon_{33})]}{\sqrt{(x_1^2 - 1)(x_2^2 - 1)(x_1 x_2 - \varepsilon_{33})}} , \tag{4.51}$$

where I integrate x_2 from -1 to 1 thus including the cycle $\mathbf{aI} \otimes \mathbf{aIV}$ of calibration $\mathrm{Im}\,(\Omega_2)$ into the evaluation, cf. figure 13. This extra cycle does not contribute to the integral due to $H[y^2(x_1, x_2)]$, which includes only regions of real calibration (grey areas in figure 13).

In this way I obtain the plots depicted in figure 15. One can easily see the square-root like behaviour of the red dashed curve, which shows that the corresponding fractional cycles

81

with bulk part of either **aIII** $\otimes$ **aIII** or **aIV** $\otimes$ **aIV** incorporate the exceptional cycle $\mathbf{e}_{33}^+$, cf. also figure 13(b), which has the same calibration as the bulk cycles. Due to this curve, one can conclude that the deformation is only valid up to $\varepsilon = 1$, where the volume of these fractional cycles vanishes, and that the exceptional cycle comes with a negative sign. All other fractional cycle have only a bulk part and therefore one observes only some slight changes in the volume that are linear (for small deformations). One should note that the volume for the merged cycle **aIII** $\otimes$ **aIV** + **aIV** $\otimes$ **aIII** is actually by a factor of two larger because two cycles contribute to the volume, see also figure 13(b), but due to the normalisation this cannot be seen in figure 15. Summing up the two merged fractional cycles, one finds that the exceptional contributions exactly cancel and that only a bulk part remains.

Remark that I will not discuss the cycles of type **bX** on the tilted square lattice in more detail because the whole discussion can be easily generalised to them. Hence, I directly move on to deformations of $\boldsymbol{T^6/(\mathbb{Z}_2 \times \mathbb{Z}_2)}$ on square tori in the next section, before I introduce cycles of type **bX** in the context of the $\boldsymbol{T^6/(\mathbb{Z}_2 \times \mathbb{Z}_6')}$ orbifold in section 4.5, where for these cycles new issues arise.

4.4 Deformations of $\boldsymbol{T^6/(\mathbb{Z}_2 \times \mathbb{Z}_2)}$ on square tori

Many properties of the $T^6/(\mathbb{Z}_2 \times \mathbb{Z}_2)$ orbifold on square tori can be deduced from the discussion of $T^4/\mathbb{Z}_2$ in section 4.3. Especially the deformation of only one singularity directly translates to $T^6/(\mathbb{Z}_2 \times \mathbb{Z}_2)$, where only an additional one-cycle has to be added. Nevertheless, in this orbifold exist further possibilities to deform singularities which include in particular simultaneous deformations in several $\mathbb{Z}_2^{(i)}$-twisted sectors.

4.4.1 Hypersurface description of the $\boldsymbol{T^6/(\mathbb{Z}_2 \times \mathbb{Z}_2)}$ orbifold

The undeformed hypersurface equation for $T^6/(\mathbb{Z}_2 \times \mathbb{Z}_2)$ is a straightforward generalisation of the $T^4/\mathbb{Z}_2$ orbifold with three instead of two elliptic curves,

$$T^6/(\mathbb{Z}_2 \times \mathbb{Z}_2) = \left\{ f \equiv -y^2 + F_{(1)}(x_1, v_1) \cdot F_{(2)}(x_2, v_2) \cdot F_{(3)}(x_3, v_3) = 0 \right\}, \qquad (4.52)$$

and the invariant polynomial y is now defined as $y := y_1 y_2 y_3$. A closer look on this equation reveals that there are 48 codimension two singularities and 64 codimension three singularities. The former are fixed lines of $\mathbb{Z}_2 \times \mathbb{Z}_2$, where $F_i = F_j = 0$ and with unrestricted coordinates (x_k, v_k) in the remaining torus ((ijk) are here cyclic permutations of $(1, 2, 3)$). Comparing to equation (4.33) shows that $F_i = 0$ is fulfilled in four points and

taking into account the possible permutation of the tori gives rise to a factor of three. Therefore, the counting is $3 \times 4 \times 4 = 48$. The codimension three singularities arise if one sets $F_i = F_j = F_k = 0$, and they lie thus at the intersection points of the codimension two singularities.

However, the description of the deformation is more involved for the $T^6/(\mathbb{Z}_2 \times \mathbb{Z}_2)$ orbifold and needs further explanation. The hypersurface equation is given by

$$
\begin{aligned}
\mathrm{Def}(T^6/(\mathbb{Z}_2 \times \mathbb{Z}_2)) = \{ f \equiv & -y^2 + F_{(1)}(x_1, v_1) F_{(2)}(x_2, v_2) F_{(3)}(x_3, v_3) \\
& - \sum_{\substack{(i,j,k)=(1,2,3) \\ \text{cyclic}}} \sum_{\alpha,\beta=1}^{4} \varepsilon_{\alpha\beta}^{(i)} F_{(i)}(x_i, v_i) \delta F_{(j)}^{\alpha}(x_j, v_j) \delta F_{(k)}^{\beta}(x_k, v_k) \\
& + \sum_{\alpha,\beta,\gamma=1}^{4} \varepsilon_{\alpha\beta\gamma} \delta F_{(1)}^{\alpha}(x_1, v_1) \delta F_{(2)}^{\beta}(x_2, v_2) \delta F_{(3)}^{\gamma}(x_3, v_3) = 0 \},
\end{aligned}
\tag{4.53}
$$

where the different components have the following meaning. The expression in the first line is the same as equation (4.52), which is the undeformed orbifold. The next $3 \times 4 \times 4$ terms are the most important ones because they control the deformations and give rise to exceptional three-cycles with non-vanishing volume, similar to deformations of the $T^4/\mathbb{Z}_2$ orbifold. The structure is here such that one deformation parameter $\varepsilon_{\alpha\beta}^{(i)}$ deforms exactly one singularity $(\alpha\beta)$ of codimension two, which is a fixed line when tensored with a one-cycle in the invariant torus. Here, $(\alpha\beta)$ is a fixed point in the four-torus $T_{(i)}^4 \equiv T_{(j)}^2 \times T_{(k)}^2$ and the index (i) stands for the torus that stays invariant under the $\mathbb{Z}_2^{(i)}$ action. The deformed singularity is described by the deformation terms $\delta F_{(j)}^{\alpha} \delta F_{(k)}^{\beta}$ and by the term $F_{(i)}$, because in the invariant torus $T_{(i)}^2$ one has to add a one-cycle. In the last row of equation (4.53) one finds deformations of codimension three singularities, where the parameters $\varepsilon_{\alpha\beta\gamma}$ depend on the deformation parameters $\varepsilon_{\alpha\beta}^{(i)}$, i.e. $\varepsilon_{\alpha\beta\gamma}$ cannot be chosen freely. This coincides with the fact that string theory does not allow for such free parameters. To be somewhat more precise, the $\varepsilon_{\alpha\beta\gamma}$ encode 64 conifold singularities which reside at the places where the singular lines of the $\mathbb{Z}_2 \times \mathbb{Z}_2$ codimension two singularities intersect (or used to intersect if they are deformed), see [108] for more information on that.

The coefficients of the terms $F_{(i)} F_{(j)} \delta F_{(k)}^{\alpha}$, which are not part of equation (4.53), describe the three untwisted complex structure moduli with $PGL(2, \mathbb{C})$ transformations being absorbed in the coordinates (x_k, v_k). To perform concrete integrations , I need again the holomorphic three-form

$$
\Omega_3 = \frac{dx_1 \wedge dx_2 \wedge \mathrm{d}x_3}{y(x_i)},
\tag{4.54}
$$

which is here defined in a similar way as in the previous sections. Let me remark that the construction in this section is a good starting point for the hypersurface description of a

$T^6/(\mathbb{Z}_2 \times \mathbb{Z}_{2M})$ orbifold. Such a description can be obtained by first building the $T^6/(\mathbb{Z}_2 \times \mathbb{Z}_2)$ orbifold, and in a second step by modding out the additional $\mathbb{Z}_M$ symmetry by hand, i.e. by restricting the concrete form of $F_{(i)}(x_i, v_i)$ and of the deformation polynomials $\delta F_{(i)}^\alpha(x_i, v_i)$ in a suitable way.

4.4.2 Cycles: structure and integrals

Fractional three-cycles $\mathbf{N_1} \otimes \mathbf{N_2} \otimes \mathbf{N_3}$ are described by the coordinates (x_1, x_2, x_3) with only real values if the cycles of type $\mathbf{aX_i}$ are considered. Hence, they can be visualised as volumes in a three-dimensional diagram, where the boundaries of the cycles are the solutions to equation (4.53) with $y^2 = 0$. If no deformation is switched on, the boundaries are simply 3×4 planes at the coordinate values $x_i = \infty, -1, 0, 1$ ($i = 1, 2, 3$), i.e. one obtains a three-dimensional generalisation of figure 13(a). The calibration is here such that a

$$
\text{cycle is } sLag \text{ with calibration} \begin{cases} \text{Re}\,(\Omega_3) & \text{if } \mathbf{X_1} + \mathbf{X_2} + \mathbf{X_3} = \text{odd} \\ \text{Im}\,(\Omega_3) & \text{if } \mathbf{X_1} + \mathbf{X_2} + \mathbf{X_3} = \text{even} \end{cases}, \qquad (4.55)
$$

where again the expressions $\mathbf{X_i} \in \{1, 2, 3, 4\}$ only refer to the number of the label and not to the cycle itself.

For the deformation in only one sector i the description is still very simple. One takes a deformed two-cycle on $T_{(i)}^4/\mathbb{Z}_2$, completely analogously to the discussion in section 4.3, tensored with a one-cycle on the undeformed torus $T_{(i)}^2$, and includes the orbifold image of the second $\mathbb{Z}_2$ factor on this three-cycle. This factorisation holds also true for the holomorphic three-form $\Omega_3 = \Omega_2 \wedge \Omega_1$ and for the integrals, which can be computed as in section 4.3 for the part of Ω_2 multiplied with a constant factor for the integration over Ω_1, which is suppressed if one introduces a normalisation to one.

A more general deformation is difficult to compute because contrary to $T_{(i)}^4/\mathbb{Z}_2$, the parameters $\varepsilon_{\alpha\beta\gamma}$ have to be taken into account, which are restricted by the deformation parameters $\varepsilon_{\alpha\beta}^{(i)}$. Nevertheless, in [109] my collaborators and me pointed out two special cases for which we found a description, but which I will not reproduce here.

4.5 Deformations of $T^6/(\mathbb{Z}_2 \times \mathbb{Z}_6')$ on hexagonal tori

The $T^6/(\mathbb{Z}_2 \times \mathbb{Z}_6')$ orbifold on three hexagonal tori was worked out by me and my collaborators in the article [110]. Since in this setup special cases of tilted tori are used, one has to work with the *(s)Lag* cycles of type $\mathbf{bX}$ with $\mathbf{bX} = \mathbf{I, II, III, IV}$ (and with the additional

cycles that appear on hexagonal torus lattices). As one will see in section, this gives rise to some technical issues.

4.5.1 Hypersurface description of the $T^6/(\mathbb{Z}_2 \times \mathbb{Z}'_6)$ orbifold

The orbifold action for $T^6/(\mathbb{Z}_2 \times \mathbb{Z}'_6)$ is defined as

$$\theta^p \omega^q : z_i \longmapsto e^{2\pi i (pv^i + qw^i)} z_i \,, \qquad \vec{v} = \frac{1}{2}(1, -1, 0) \,, \quad \vec{w} = \frac{1}{6}(-2, 1, 1) \,, \tag{4.56}$$

with $i = 1, 2, 3$. This implies that the lattice vectors of T^6 form the root lattice of $SU(3)^3$, for which all two-tori have a hexagonal shape, and the three complex structure parameters are $\tau_i = e^{\pi i/3}$ for the two-tori $T^2_{(i)}$. The $\mathbb{Z}_3$ twisted sector ω^2 acts by the shift vector $\frac{1}{3}(1, 1, 1)$, which translates in homogeneous coordinates to $\omega^2 : (x_1, x_2, x_3) \mapsto \xi(x_1, x_2, x_3)$.

The action of ω^2 has the following effect on the deformation polynomials in equation (4.33), while the original polynomials F_i remain unchanged,

$$\delta F^1_{(i)} \xmapsto{\omega^2} \xi \delta F^1_{(i)} \,, \qquad \delta F^2_{(i)} \xmapsto{\omega^2} \delta F^3_{(i)} \xmapsto{\omega^2} \delta F^4_{(i)} \xmapsto{\omega^2} \delta F^2_{(i)} \,, \qquad i = 1, 2, 3 \,, \tag{4.57}$$

and therefore they have to be slightly modified,

$$\begin{aligned}
F_{(i)}(x_i, v_i) &= 4 \left(v_i x_i^3 - v_i^4 \right) \;=\; 4 v_i \left(x_i - v_i \right) \left(x_i - \xi v_i \right) \left(x_i - \xi^2 v_i \right) \,, \\
\delta F^1_{(i)}(x_i, v_i) &= 4 \left(x_i^4 - x_i v_i^3 \right) \,, \\
\delta F^2_{(i)}(x_i, v_i) &= 4 v_i^2 \left(v_i - x_i \right) \left(v_i - \xi x_i \right) \,, \\
\delta F^3_{(i)}(x_i, v_i) &= 4 v_i^2 \left(v_i - \xi x_i \right) \left(v_i - \xi^2 x_i \right) \,, \\
\delta F^4_{(i)}(x_i, v_i) &= 4 v_i^2 \left(v_i - \xi^2 x_i \right) \left(v_i - x_i \right) \,.
\end{aligned} \tag{4.58}$$

Here I defined $\xi \equiv e^{2\pi i/3}$ in order to represent the fixed points by $\epsilon_3 = \xi^0, \epsilon_2 = \xi^1, \epsilon_4 = \xi^2$ and $\epsilon_1 = \infty$. These restrictions directly affect the deformation parameters $\varepsilon^{(i)}_{\alpha\beta}$ in the hypersurface equation of the deformed orbifold,

$$\begin{aligned}
\mathrm{Def}(T^6/(\mathbb{Z}_2 \times \mathbb{Z}'_6)) = \{ f &\equiv -y^2 + F_{(1)}(x_1, v_1) F_{(2)}(x_2, v_2) F_{(3)}(x_3, v_3) \\
&- \sum_{\substack{(i,j,k) = (1,2,3) \\ \text{cyclic}}} \sum_{\alpha, \beta = 1}^{4} \varepsilon^{(i)}_{\alpha\beta} F_{(i)}(x_i, v_i) \delta F^\alpha_{(j)}(x_j, v_j) \delta F^\beta_{(k)}(x_k, v_k) = 0 \}
\end{aligned} \tag{4.59}$$

such that the $\varepsilon^{(i)}_{\alpha\beta}$ are identified as $\varepsilon^{(i)}_\rho$ with

$$
\begin{aligned}
\varepsilon^{(i)}_1 &:= \varepsilon^{(i)}_{31} = \xi\varepsilon^{(i)}_{21} = \xi^2\varepsilon^{(i)}_{41}\,, \\
\varepsilon^{(i)}_2 &:= \varepsilon^{(i)}_{13} = \xi\varepsilon^{(i)}_{12} = \xi^2\varepsilon^{(i)}_{14}\,, \\
\varepsilon^{(i)}_3 &:= \varepsilon^{(i)}_{22} = \varepsilon^{(i)}_{33} = \varepsilon^{(i)}_{44}\,, \\
\varepsilon^{(i)}_4 &:= \varepsilon^{(i)}_{23} = \varepsilon^{(i)}_{34} = \varepsilon^{(i)}_{42}\,, \\
\varepsilon^{(i)}_5 &:= \varepsilon^{(i)}_{24} = \varepsilon^{(i)}_{32} = \varepsilon^{(i)}_{43}\,.
\end{aligned}
\tag{4.60}
$$

The parameter $\varepsilon^{(i)}_{11}$ must be zero in accordance with the fact that the fixed point at the origin has no complex structure modulus and can therefore not be deformed.

Furthermore, the deformation parameters are subject to conditions under the orientifold action $\sigma_\mathcal{R} : (y, x_i, v_i) \mapsto (\overline{y}, \overline{x_i}, \overline{v_i})$, which has the effect

$$
\delta F^1_{(i)} \mapsto \overline{\delta F^1_{(i)}}\,, \quad \delta F^2_{(i)} \mapsto \overline{\delta F^4_{(i)}}\,, \quad \delta F^3_{(i)} \mapsto \overline{\delta F^3_{(i)}}\,, \quad \delta F^4_{(i)} \mapsto \overline{\delta F^2_{(i)}}\,,
\tag{4.61}
$$

i.e. $\delta F^2_{(i)}$ and $\delta F^4_{(i)}$ are exchanged. Inserting the deformation polynomials into equation (4.59) gives the result

$$
\begin{aligned}
0 = f \equiv &-y^2 + F_{(1)}F_{(2)}F_{(3)} - \sum_{\substack{(i,j,k)=(1,2,3) \\ \text{cyclic}}} F_{(i)}\cdot \\
&\cdot\Big[\varepsilon^{(i)}_1\big(\delta F^3_{(j)} + \xi^2\delta F^2_{(j)} + \xi\delta F^4_{(j)}\big)\delta F^1_{(k)} \\
&+ \varepsilon^{(i)}_2\delta F^1_{(j)}\big(\delta F^3_{(k)} + \xi^2\delta F^2_{(k)} + \xi\delta F^4_{(k)}\big) \\
&+ \varepsilon^{(i)}_3\big(\delta F^2_{(j)}\delta F^2_{(k)} + \delta F^3_{(j)}\delta F^3_{(k)} + \delta F^4_{(j)}\delta F^4_{(k)}\big) \\
&+ \varepsilon^{(i)}_4\big(\delta F^2_{(j)}\delta F^3_{(k)} + \delta F^3_{(j)}\delta F^4_{(k)} + \delta F^4_{(j)}\delta F^2_{(k)}\big) \\
&+\varepsilon^{(i)}_5\big(\delta F^2_{(j)}\delta F^4_{(k)} + \delta F^3_{(j)}\delta F^2_{(k)} + \delta F^4_{(j)}\delta F^3_{(k)}\big)\Big]\,,
\end{aligned}
\tag{4.62}
$$

where one directly sees that under the orientifold the terms with $\varepsilon^{(i)}_4$ and $\varepsilon^{(i)}_5$ are exchanged, i.e. $\varepsilon^{(i)}_4 = \overline{\varepsilon_5}^{(i)} \in \mathbb{C}$, while the other indices are preserved and thus $\varepsilon^{(i)}_1, \varepsilon^{(i)}_2, \varepsilon^{(i)}_3 \in \mathbb{R}$. For later calculations, it is convenient to define the complex parameters as

$$
\varepsilon^{(i)}_{4/5} = \frac{1}{2}\left(\varepsilon^{(i)}_{4+5} \pm i\varepsilon^{(i)}_{4-5}\right)
\tag{4.63}
$$

in order to have only real deformation paramters $\varepsilon^{(i)}_{4+5}$, $\varepsilon^{(i)}_{4-5}$. These facts are summarised in table 12, where also the associated exceptional wrapping numbers are stated.

Since all three sectors behave analogously under deformations, I will only describe the first sector $(i) = (1)$ in the subsequent discussion, thus setting $\varepsilon^{(2)}_\rho = \varepsilon^{(3)}_\rho = 0$ and omitting the

Restrictions on the deformation parameters of $T^6/(\mathbb{Z}_2 \times \mathbb{Z}_6')$			
ρ	Parameter identifications for $\varepsilon_\rho^{(i)}$	Parameter range	Exceptional wrapping numbers
1	$\xi\varepsilon_{21}^{(i)} = \varepsilon_{31}^{(i)} = \xi^2\varepsilon_{41}^{(i)}$	$\mathbb{R}$	$\hat{x}_1^{(i)}, \hat{y}_1^{(i)}$
2	$\xi\varepsilon_{12}^{(i)} = \varepsilon_{13}^{(i)} = \xi^2\varepsilon_{14}^{(i)}$	$\mathbb{R}$	$\hat{x}_2^{(i)}, \hat{y}_2^{(i)}$
3	$\varepsilon_{22}^{(i)} = \varepsilon_{33}^{(i)} = \varepsilon_{44}^{(i)}$	$\mathbb{R}$	$\hat{x}_3^{(i)}, \hat{y}_3^{(i)}$
$4, \bar{5}$	$\varepsilon_{23}^{(i)} = \varepsilon_{34}^{(i)} = \varepsilon_{42}^{(i)} = \bar{\varepsilon}_{24}^{(i)} = \bar{\varepsilon}_{32}^{(i)} = \bar{\varepsilon}_{43}^{(i)}$	$\mathbb{C}$	$\hat{x}_4^{(i)}, \hat{y}_4^{(i)}, \hat{x}_5^{(i)}, \hat{y}_5^{(i)}$

Table 12: $\mathbb{Z}_3$ and $\Omega\mathcal{R}$ restrictions on the deformation parameters together with the wrapping numbers for the associated exceptional three-cycles.

upper index $\varepsilon_\rho^{(1)} \equiv \varepsilon_\rho$. The equation of the deformed orbifold $T^6/(\mathbb{Z}_2 \times \mathbb{Z}_6')$ then reads

$$
\begin{aligned}
0 = f \equiv -y^2 &+ \left(v_1 x_1^3 - v_1^4\right) \cdot \Big\{ \left(v_2 x_2^3 - v_2^4\right)\left(v_3 x_3^3 - v_3^4\right) \\
&- \varepsilon_1 \, x_2^2 v_2^2 \left(x_3^4 - x_3 v_3^3\right) \\
&- \varepsilon_2 \left(x_2^4 - x_2 v_2^3\right) x_3^2 v_3^2 \\
&- \varepsilon_3 \left(v_2^4 v_3^4 + v_2^2 x_2^2 v_3^3 x_3 + v_2^3 x_2 v_3^2 x_3^2\right) \\
&- \varepsilon_{4+5} \left(2 v_2^4 v_3^4 - v_2^2 x_2^2 v_3^3 x_3 - v_2^3 x_2 v_3^2 x_3^2\right) \\
&- \varepsilon_{4-5} \left(v_2^2 x_2^2 v_3^3 x_3 - v_2^3 x_2 v_3^2 x_3^2\right) \Big\}.
\end{aligned}
\tag{4.64}
$$

One can easily analyse the position of the singularities by solving $f = \mathrm{d}f = 0$. From $\partial f/\partial y = 0$ follows $y = 0$, and considering only the second and third torus with chart $v_i \equiv 1$, the singularities are the solutions of the system

$$
f = 0 \quad \wedge \quad \frac{\partial f}{\partial x_2} = 0 \quad \wedge \quad \frac{\partial f}{\partial x_3} = 0,
\tag{4.65}
$$

where the equations can be divided by the term containing x_1. The singularities of the undeformed hypersurface f can be found as expected at the coordinates $x_i = \infty, 1, e^{\pm 2\pi i/3}$ ($i = 2, 3$). In the chart $x_i \equiv 1$, the course of action is completely analogous with $x_i \leftrightarrow v_i$ in the above equation, and the singularities have coordinates $v_i = 0, 1, e^{\mp 2\pi i/3}$. It is clear that this is much more convenient to search for the positions of the singularities and to see which ones are deformed.

4.5.2 Bulk cycles: structure and integrals

The integration for the displaced fractional cycle $\mathbf{bIII^0}$ can be separated into the integrals over the bulk and exceptional part. For the integral $\int_{\Pi_{\mathbf{bIII^0}}^{\text{bulk}}} \Omega_1$, I can choose as well any

other path of integration which is in the same homology class, for example the cycles $\mathcal{C}_1$ or $\mathcal{C}_2$ of figure 16, but one should note that these cycles are not *sLag* anymore. The cycle $\mathcal{C}_1$ is shifted such that it doesn't run through any fixed point, while $\mathcal{C}_2$ passes through the $\mathbb{Z}_3$ fixed points $\epsilon_1 = \infty$, $\epsilon_{\tilde{2}}, \epsilon_{\tilde{3}} = 0$ ($1, \tilde{2}, \tilde{3}$, respectively) of figure 16, which should not influence the integral due to their lack of deformation moduli, see table 2. The intuitive expectation is that this path $\mathcal{C}_2$ is least affected by the deformation of $\mathbb{Z}_2$ fixed points simply because it has the most separation from these.
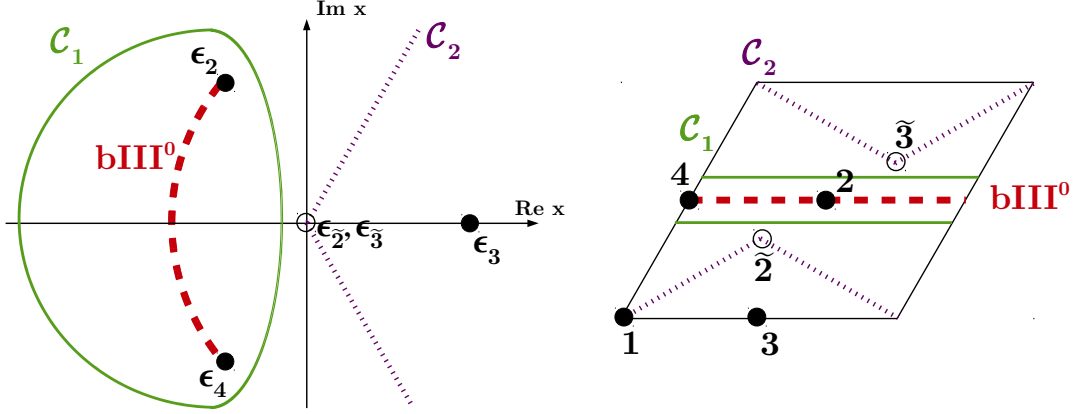

Figure 16: Different choices of the path of integration for the bulk part of the cycle $\mathbf{bIII^0}$ of the hexagonal torus, depicted in the complex plane of the homogeneous coordinate x (in the chart $v = 1$), left picture, and in the fundamental domain of the torus with coordinate $z \in \mathbb{C}$, right picture. The cycles $\Pi_{\mathbf{bIII^0}}^{\text{bulk}}$, $\mathcal{C}_1$ and $\mathcal{C}_2$ are in the same homology class and give thus the same result when integrated over Ω_3. Nevertheless, the choice of $\mathcal{C}_2$, which consists of straight lines with phase $e^{\pm i\pi/3}$, is especially useful due to technical reasons.

In order to integrate over $\mathcal{C}_2$, I parametrise the curve by

$$\mathcal{C}_2: \quad u_i \mapsto x_i(u_i) = |u_i| + i\sqrt{3}u_i \qquad \text{with } u_i \in \mathbb{R}, \tag{4.66}$$

which has the derivative

$$\frac{\partial x_i}{\partial u_i} = \begin{cases} 1 + i\sqrt{3} & \text{if } u_i \geq 0 \\ 1 - i\sqrt{3} & \text{if } u_i < 0 \end{cases}, \tag{4.67}$$

and therefore the Jacobi determinant reads for an integration over $\mathrm{d}x_i \mathrm{d}x_j$

$$\mathbf{J}(u_i, u_j) = \begin{cases} -2 + 2i\sqrt{3} & \text{if } u_i, u_j > 0 \\ -2 - 2i\sqrt{3} & \text{if } u_i, u_j < 0 \\ 4 & \text{if } u_i \geq 0, u_j \leq 0 \end{cases}. \tag{4.68}$$

This determines the integation, where $y^2 = \left(v_k x_k^3 - v_k^4\right) \cdot \tilde{y}^2(x_i, v_i, x_j, v_j)$ in its factorised form with definition

$$
\begin{aligned}
\tilde{y}^2 := & \left(v_2 x_2^3 - v_2^4\right)\left(v_3 x_3^3 - v_3^4\right) \\
& - \varepsilon_1\, x_2^2 v_2^2 \left(x_3^4 - x_3 v_3^3\right) - \varepsilon_2 \left(x_2^4 - x_2 v_2^3\right) x_3^2 v_3^2 \\
& - \varepsilon_3 \left(v_2^4 v_3^4 + v_2^2 x_2^2 v_3^3 x_3 + v_3^3 x_2 v_3^2 x_3^2\right) - \varepsilon_{4+5}\left(2 v_2^4 v_3^4 - v_2^2 x_2^2 v_3^3 x_3 - v_3^3 x_2 v_3^2 x_3^2\right) \\
& - \varepsilon_{4-5}\left(v_2^2 x_2^2 v_3^3 x_3 - v_3^3 x_2 v_3^2 x_3^2\right)
\end{aligned}
\tag{4.69}
$$

has to be included,

$$
\int_{\mathbf{bX}} \int_{\mathcal{C}_2} \int_{\mathcal{C}_2} \Omega_1 \wedge \Omega_2 = \int_{x_{k_i}}^{x_{k_f}} \frac{\mathrm{d}x_k}{\left(x_k^3 - 1\right)} \cdot \int_{-\infty}^{\infty} \int_{-\infty}^{\infty} \frac{\mathbf{J}\left(u_i, u_j\right)\mathrm{d}u_i \mathrm{d}u_j}{\tilde{y}\left(x_i(u_i), x_j(u_j)\right)} .
\tag{4.70}
$$

The first term gives a non-vanishing constant and does not play a role when I introduce a normalisation.

### 4.5.3 Exceptional cycles: description and correction terms

In the following, I will explain how to find descriptions of the exceptional three-cycles of the $T^6/(\mathbb{Z}_2 \times \mathbb{Z}_6')$ orbifold, where table 12 shows which deformation parameters correspond to the orbit of a certain exceptional cycle $\mathbf{e}_\rho^{(i)}$ of sector $\mathbb{Z}_2^{(i)}$. I will use only one sector $\mathbb{Z}_2^{(1)}$, cf. the hypersurface equation (4.64), while the other sectors work completely analogously.

Switching on one parameter ε_ρ after the other and solving the equations (4.65), I find that some orbits of singularities are invariant, others change their position in dependence of ε_ρ, and some singularities are undesirably also deformed, i.e. they do not appear anymore as solutions of (4.65). This last aspect is new compared to the deformations on square tori and requires an additional adjustment by hand. This means that in order to switch on deformations in a controlled way, I will calculate correction terms which cancel this unwanted effect.

Exceptional cycles $\mathbf{e}_4^{(1)}$ and $\mathbf{e}_5^{(1)}$: The first exceptional cycles to be studied are $\mathbf{e}_4^{(1)}$ and $\mathbf{e}_5^{(1)}$, which are treated together because they are complex conjugates of each other. Once their description is understood, it is easy to go over to the other exceptional cycles. The combination of $\mathbf{e}_4^{(1)}$ and $\mathbf{e}_5^{(1)}$ makes it possible to separate the deformation into the orientifold-even and -odd parts by using the two deformation parameters $\varepsilon_{4+5}^{(1)}$ and $\varepsilon_{4-5}^{(1)}$ defined in equation (4.63) by $\varepsilon_{4/5}^{(1)} := \frac{1}{2}\left(\varepsilon_{4+5}^{(1)} \pm i\varepsilon_{4-5}^{(1)}\right)$. For convenience, I give equation (4.69) with parameters $\varepsilon_1 = \varepsilon_2 = \varepsilon_{4-5} = 0$ and in the chart $v_i \equiv 1$,

$$
\tilde{y}^2 = \left(x_2^3 - 1\right)\left(x_3^3 - 1\right) - \varepsilon_3\left(1 + x_2 x_3^2 + x_2^2 x_3\right) - \varepsilon_{4+5}\left(2 - x_2 x_3^2 - x_2^2 x_3\right) ,
\tag{4.71}
$$

for which the symmetry $x_2 \leftrightarrow \overline{x_3}$ is obeyed (because $\tilde{y} = \overline{\tilde{y}}$ is fulfilled).
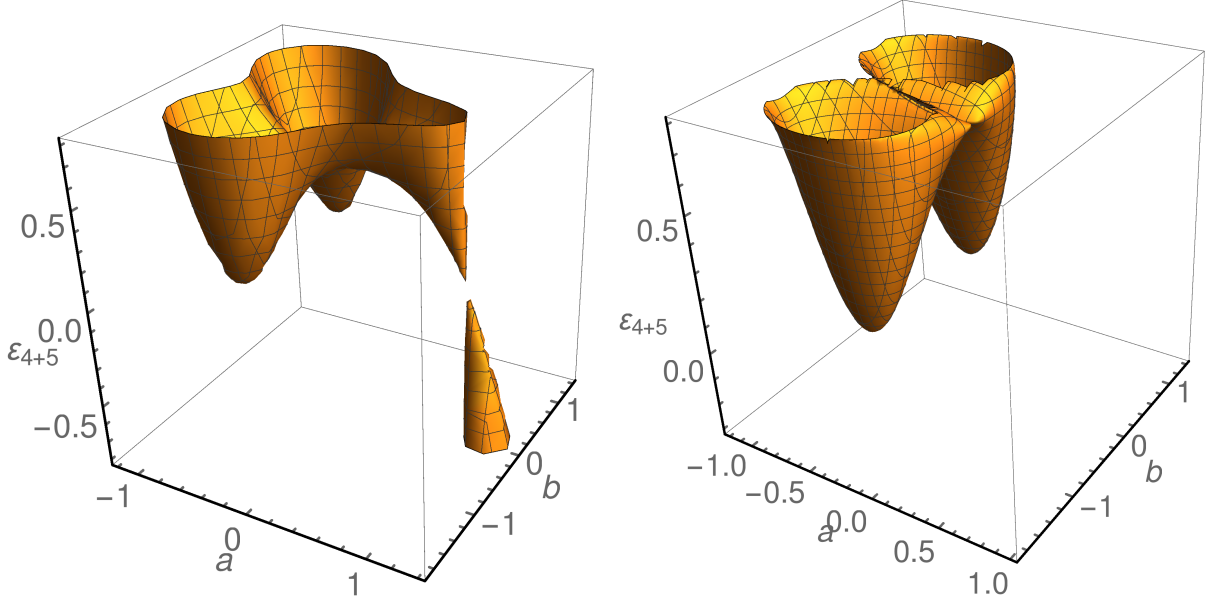

(a) If no correction term is included, i.e. $\varepsilon_3 = 0$, the singularities (24), (42) obtain as expected an exceptional contribution for $\varepsilon_{4+5} > 0$, but also (33) is deformed for $\varepsilon_{4+5} \neq 0$.

(b) With correction $\varepsilon_3(\varepsilon_{4+5})$, the singularity (33) is not deformed when ε_{4+5} is switched on and has therefore no exceptional contribution.

Figure 17: The plots show the surface of the relation $\tilde{y}^2(a, b, \varepsilon_3(\varepsilon_{4+5}), \varepsilon_{4+5}) = 0$, where the function is given by equation (4.71) with $x_2 = a + ib = \overline{x_3}$ inserted. The figures illustrate the effect of the correction term $\varepsilon_3(\varepsilon_{4+5})$, cf. equation (4.71). At $\varepsilon_{4+5} = 0$ on the vertical axis, one finds the undeformed singularities (33), (24), (42) at $(a, b) = (1, 0), (-\frac{1}{2}, \frac{\sqrt{3}}{2}), (-\frac{1}{2}, -\frac{\sqrt{3}}{2})$, respectively.

As a starting point, I analyse the equation $x_2 = \overline{x_3} = a + ib$ that was already used in the previous sections in order to describe the exceptional cycles. Inserting for x_2 the positions of the fixed points $\epsilon_1 = \infty$, $\epsilon_2 = \xi$, $\epsilon_3 = 1$, $\epsilon_4 = \xi^2$ with $\xi \equiv e^{2\pi i/3}$, I find that $x_2 = \overline{x_3}$ describes (11), (33), (42), (24). The fixed point (11) does not have a deformation parameter and can thus not develop an exceptional cycle. On the other hand, the fixed point (33) belongs to the orbit of the exceptional cycle $\mathbf{e}_3^{(1)}$, while (42) is part of $\mathbf{e}_4^{(1)}$ and (24) of $\mathbf{e}_5^{(1)}$, cf. table 12. Figure 17(a) illustrates all exceptional contributions in form of a surface, and one can see that for $\varepsilon_{4+5} \neq 0$ not only the singularities (42), (24) are deformed, but also (33). In addition, the plots show that (42) and (24) develop only for $\varepsilon_{4+5} > 0$ an exceptional cycle of non-vanishing volume, which means that this exceptional cycle is *sLag* (with real calibration) for $\varepsilon_{4+5} > 0$.

In order to keep (33) singular, I deform it with a suitable correction term $\varepsilon_3(\varepsilon_{4+5})$. This
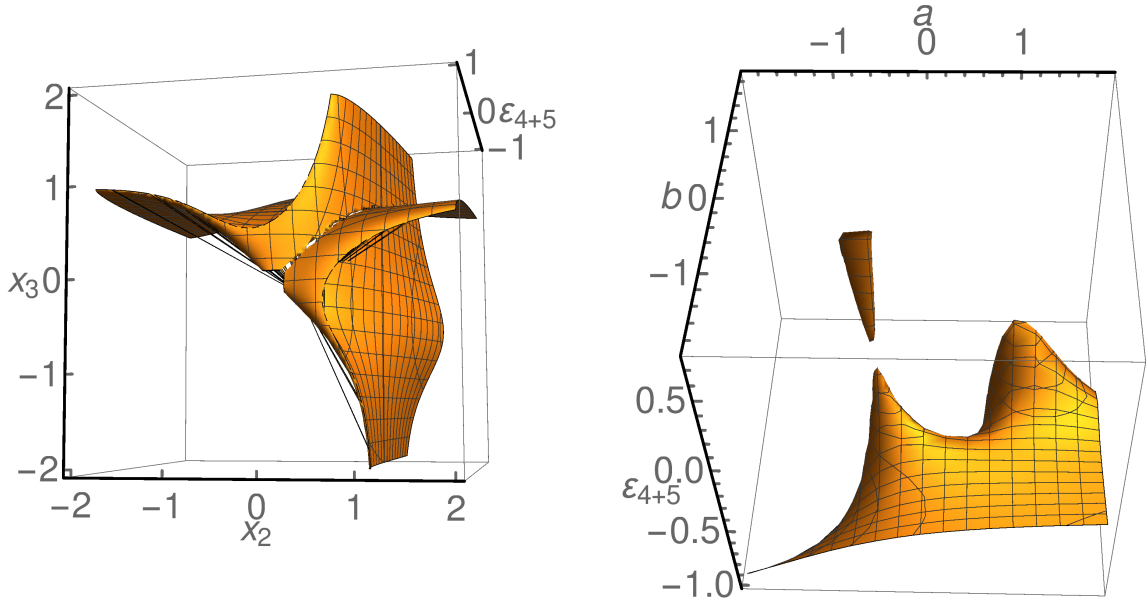
(a) The intersection point of two lines in the coordinates x_2, x_3 indicates the existence of a singularity. Upon deformation of ε_{4+5}, the singularity (33) is not deformed, but changes its position.

(b) The exceptional cycle (42), shifted to the coordinates $(a,b) = (1,0)$, grows under the deformation $\varepsilon_{4+5} < 0$, but since no correction term is included, also (33) that was moved to $(a,b) = (-\frac{1}{2}, -\frac{\sqrt{3}}{2})$ obtains a volume for $\varepsilon_{4+5} \neq 0$.

Figure 18: Plots of the relation $\tilde{y}^2(x_2, x_3, \varepsilon_3(\varepsilon_{4+5}), \varepsilon_{4+5}) = 0$, as defined in equation (4.71). In the left figure, which shows the projection onto the real x_2, x_3-plane, the correction term $\varepsilon_3(\varepsilon_{4+5})$ of equation (4.72) was inserted. To obtain the plot on the right hand side where $\varepsilon_3 = 0$, I first applied the shift λ_2 on x_2 and λ_4 on x_3 in order to map the singularities (42) $\leftrightarrow$ (33) and (24) $\leftrightarrow$ (11). After that I inserted $x_2 = a + ib = \overline{x_3}$ to go to the exceptional cycle.

function, whose explicit calculation is shown in appendix A.1, reads

$$
\begin{aligned}
\varepsilon_3(\varepsilon_{4+5}) &= -\frac{3}{2} + \varepsilon_{4+5} + \frac{1}{2}\sqrt{9 - 12\varepsilon_{4+5}} \\
&= -\frac{1}{3}\varepsilon_{4+5}^2 - \frac{2}{9}\varepsilon_{4+5}^3 + \mathcal{O}(\varepsilon_{4+5}^4)
\end{aligned}
\tag{4.72}
$$

with restriction $\varepsilon_{4+5} \leq \frac{3}{4}$ for the analytic expression. The plot in figure 17(b) confirms that the insertion of the correction $\varepsilon_3(\varepsilon_{4+5})$ into equation (4.71) causes the exceptional cycle at fixed point (33) to vanish. Furthermore, figure 18(a) reveals that though the singularity at (33) stays singular for arbitrary deformations of ε_{4+5}, i.e. there is always an intersection point of two lines, it changes its position in the coordinates x_2, x_3.

In order to describe the exceptional cycles $\mathbf{e}_4^{(1)}$ and $\mathbf{e}_5^{(1)}$ concretely, I use the shift λ_2 on x_2 and λ_4 on x_3, see equation (4.18). This interchanges (42) $\leftrightarrow$ (33) and (24) $\leftrightarrow$ (11),

or differently said, moving singularity $(x_2, x_3) = (e^{-2\pi i/3}, e^{+2\pi i/3})$ to $(x_2, x_3) = (1,1)$, as demonstrated in section 4.1. This ensures that the exceptional cycle is described by a real-valued expression when I introduce $\lambda_2(x_2) = \lambda_4(\overline{x_3})$ into the shifted equation (4.71). Due to the property $\lambda_2 = \overline{\lambda_4}$, the symmetry $x_2 \leftrightarrow \overline{x_3}$ of equation (4.71) remains unbroken.
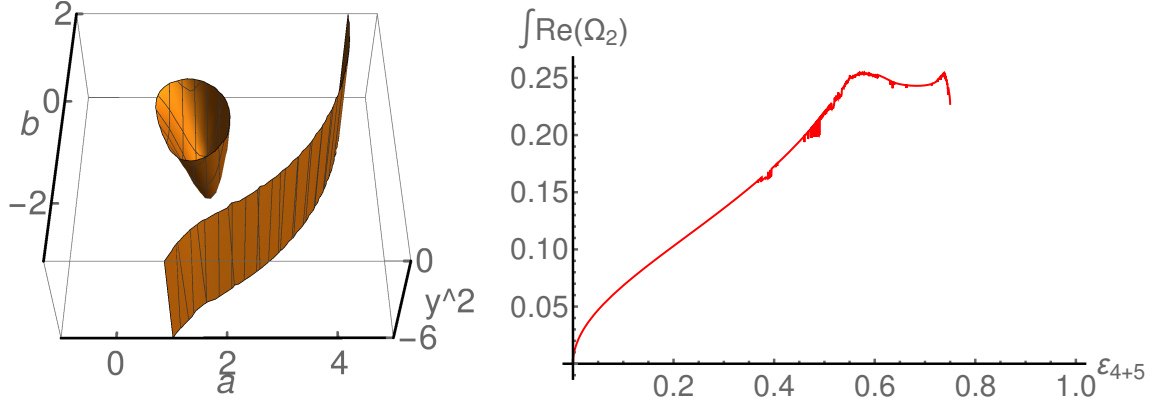
(a) Deformation at $\varepsilon_{4+5} = 0.6$. The depicted plane approaches the exceptional cycle for growing ε_{4+5} until they combine, and the extensions of the cycle seems to not exceed the values $a \in (0,2)$, $b \in (-1,1)$.

(b) Integration over $\mathbf{e}_4^{(1)}$, where $\varepsilon_{4+5} > 0$. The volume is zero when no deformation is switched on and shows in the first part the characteristic square-root like behaviour. After the limit $\varepsilon_{4+5} \leq \frac{3}{4}$, the curve breaks off.

Figure 19: The plot on the left hand side shows the function $\tilde{y}^2(a, b, \varepsilon_3(\varepsilon_{4+5}), \varepsilon_{4+5}) \leq 0$ with applied shift, as argued under equation (4.72), and exceptional cycle $x_2 = \overline{x_3}$ inserted, where $\varepsilon_{4+5} = 0.6$ is chosen. On the right hand side the result of the integration as in equation (4.73) is given.

To compute the volume of the exceptional cycles, I integrate the holomorphic two-form in a similar manner as for the $T^4/\mathbb{Z}_2$ manifold on a square torus lattice, cf. equation (4.47) in section 4.3.3, and obtain in this way the following new integral for $\mathbf{e}_4^+$:

$$\int_{\mathbf{e}_4^+} \Omega_2 = 2i \int_0^2 \mathrm{d}a \int_{-1}^1 \mathrm{d}b \, \frac{H[-y^2(a, b, \varepsilon_{4+5})]}{\sqrt{y^2(a, b, \varepsilon_{4+5})}} \,, \tag{4.73}$$

with the Heaviside step function as defined in equation (4.46).

Figure 19(a) clarifies that I use the correct integration boundaries upon deformation of ε_{4+5}. In addition, one can see that for larger values of ε_{4+5} it becomes difficult to choose a suitable lower boundary due to the approaching plane, depicted in figure 19(a), which recombines with the cycle. This also explains why the graph in figure 19(b), which depicts the result of the integration, seems to have numerical artefacts starting at about $\varepsilon_{4+5} = 0.4$.

Exceptional cycle $\mathbf{e}_3^{(1)}$: In a second step, I will present the properties of the exceptional cycle $\mathbf{e}_3^{(1)}$, where now ε_3 is the deformation parameter of interest. As already explained under equation (4.71), the singularity (33) is again given by the relation $x_2 = \overline{x_3}$. Hence, one finds a similar picture as in figure 17, where (42), (24) obtain an unwanted exceptional contribution for $\varepsilon_3 \neq 0$, while (33) grows as expected for $\varepsilon_3 > 0$. Unfortunately, one cannot write down an analytic expression for the correction term $\varepsilon_{4+5}(\varepsilon_3)$, but only the series expansion

$$\varepsilon_{4+5}(\varepsilon_3) = -\frac{1}{9}\varepsilon_3^2 - \frac{1}{81}\varepsilon_3^3 + \mathcal{O}(\varepsilon_3^5), \tag{4.74}$$

as derived in appendix A.2.

For $\tilde{y}^2(x_2, x_3, \varepsilon_3, \varepsilon_{4+5}(\varepsilon_3)) = 0$, cf. equation (4.71), it is not possible to illustrate the effect of the correction term $\varepsilon_{4+5}(\varepsilon_3)$ on the singularities (42) and (24) in the real x_2, x_3-plane, similar to figure 18(a), because these have complex values. On the contrary, I can perform a shift as for the exceptional cycles $\mathbf{e}_4^{(1)}$ and $\mathbf{e}_5^{(1)}$, which gives rise to a picture as in figure 18(b), but with switched roles for the exceptional contributions. Nonetheless, the deformation of $\mathbf{e}_3^{(1)}$ can be executed without any shift transformation.

The integration of the exceptional cycle $\mathbf{e}_3^{(1)}$ works completely analogous to the cycle $\mathbf{e}_4^{(1)}$ with the only difference that no shift transformation is necessary and that the parameter ε_3 has no restriction, which is due to the fact that I use a series expansion. Concretely, I use equation (4.73) with the same integration boundaries, as can be checked in figure 20(a), and obtain the result that is depicted in figure 20(b).
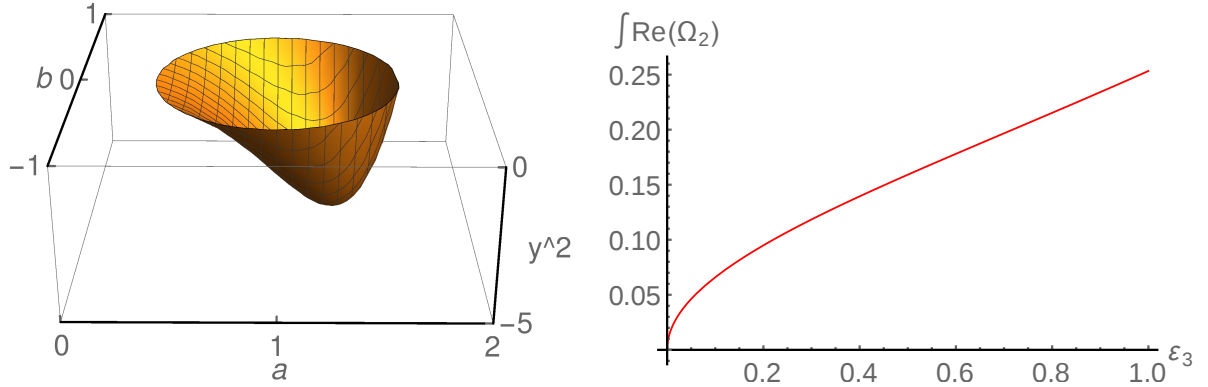
(a) For $\varepsilon_3 = 1$, the boundaries of the exceptional cycle lie in the intervals $a \in (0, 2)$, $b \in (-1, 1)$.

(b) The volume of $\mathbf{e}_3^{(1)}$ vanishes at $\varepsilon_3 = 0$ and grows for $\varepsilon_3 > 0$ with the shape of $\sqrt{\varepsilon_3}$.

Figure 20: The left image depicts the function $\tilde{y}^2(a, b, \varepsilon_3, \varepsilon_{4+5}(\varepsilon_3)) \leq 0$ with exceptional cycle $x_2 = a + ib = \overline{x_3}$ inserted and with maximal deformation $\varepsilon_3 = 1$. The graph on the right hand side shows the volume of the exceptional cycle $\mathbf{e}_3^{(1)}$, where the integration is given in equation (4.73).

Exceptional cycles $\mathbf{e}_1^{(1)}$ and $\mathbf{e}_2^{(1)}$: The exceptional cycles $\mathbf{e}_1^{(1)}$ and $\mathbf{e}_2^{(1)}$ show exactly the same behaviour upon deformation because only the order and labelling of the tori $T_{(2)}^2$ and $T_{(3)}^2$ is interchanged. Hence, I have to analyse only the single deformation of $\mathbf{e}_1^{(1)}$ and can omit the explicit discussion of $\mathbf{e}_2^{(1)}$. It turns out that for these exceptional cycles no explicit description as for the other exceptional cycles just discussed exists. The reason is that I would have to apply a shift $x_2 = \lambda_3(\overline{x_3})$, but this equation is not the fixed set of an antiholomorphic involution and therefore cannot be used here. However, when computing the volumes of fractional cycles in the next section, I will show that there exists an indirect way to not only describe the fractional cycle, but also to access the exceptional cycle.

One can also look at the case where both exceptional cycles are equally deformed with $\varepsilon := \varepsilon_1 = \varepsilon_2$, cf. [110], where one finds the symmetry $x_2 \leftrightarrow x_3$. By switching on $\varepsilon \neq 0$, the singularities of the other orbits $\mathbf{e}_3^{(1)}$, $\mathbf{e}_{4+5}^{(1)}$, and $\mathbf{e}_{4-5}^{(1)}$ are as well deformed. Hence, also in this case the calculation of correction terms $\varepsilon_3(\varepsilon)$ and $\varepsilon_{4+5}(\varepsilon)$ is necessary, which works similarly as for the exceptional cycles $\mathbf{e}_3^{(1)}$, $\mathbf{e}_4^{(1)}$ and $\mathbf{e}_5^{(1)}$, cf. appendix A. However, I do not consider it necessary to reproduce this result here once more and instead refer the interested reader to our article [110], where he/she will find the concrete equations for the correction terms $\varepsilon_3(\varepsilon)$ and $\varepsilon_{4+5}(\varepsilon)$.

4.5.4 Fractional cycles: description and integrals

For this orbifold we had to develop several ways to perform deformations of all kinds of fractional cycles. Roughly speaking, these different methods are:

1. Deform the fractional cycle directly,

2. Compute the bulk and exceptional contributions separately,

3. Access exceptional cycles indirectly by a suitable subtraction of bulk and fractional cycles.

I will discuss the fractional cycles in the same ordering as the exceptional cycles in the previous section, for which the concrete integrals are obtained in the following way. For simplicity, the invariant torus is factored out, and I use as bulk cycle a horizontal cycle. For the integrals over the fractional cycles

$$\Pi^{\text{frac}} = \frac{1}{2}(\Pi^{\text{bulk}} \pm \mathbf{e}_{4+5}^{(i)}), \qquad \Pi^{\text{frac}} = \frac{1}{2}(\Pi^{\text{bulk}} \pm \mathbf{e}_3^{(i)}), \tag{4.75}$$
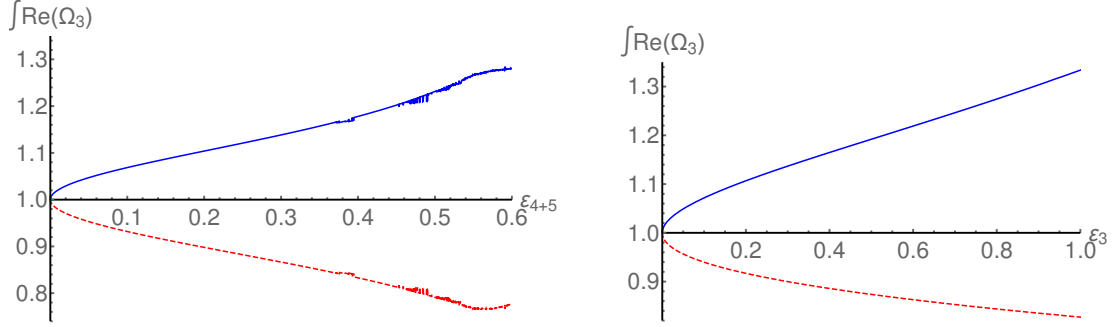
(a) Normalised volumes of the fractional cycles $\frac{1}{2}(\Pi^{\text{bulk}} \pm \mathbf{e}_{4+5}^{(i)})$ with positive (upper blue curve) or negative (lower red curve) exceptional part. The reason for the abnormal behaviour of the graph for large values of ε_{4+5} is clear when examining figure 19.

(b) Normalised volumes the fractional cycles $\frac{1}{2}(\Pi^{\text{bulk}} \pm \mathbf{e}_3^{(i)})$, in dependence of the deformation parameter ε_3, with positive (upper blue curve) or negative (lower red curve) exceptional part.

Figure 21: Normalised volumes of horizontal fractional $sLag$ cycles with exceptional contributions $\mathbf{e}_{4+5}^{(i)}$ (left figure) or $\mathbf{e}_3^{(i)}$ (right figure), cf. equation (4.75), which are the same for all three sectors $i = 1, 2, 3$. The volumes are obtained by the integrals as sketched in equation (4.76).

I integrate the bulk and exceptional part separately, see sections 4.5.2 and 4.5.3, respectively, which means that I apply the second method for the deformation. In a schematic way, this integration looks like

$$\text{Vol}\left(\Pi^{\text{frac}}(\varepsilon_{4+5})\right) = \left(\text{Vol}\left(\Pi^{\text{bulk}}(\varepsilon_{4+5})\right) \pm \text{Vol}\left(\mathbf{e}_{4+5}^{(i)}(\varepsilon_{4+5})\right)\right) / \text{Vol}\left(\Pi^{\text{bulk}}(0)\right), \qquad (4.76)$$

and analogously for $\mathbf{e}_3^{(i)}$. For the bulk part, I use the curve $\mathcal{C}_2$ of figure 16 and integrate as in equation (4.70) with deformation parameter ε_3 or ε_{4+5}, respectively. Since I normalise the integral over the fractional cycle by the value of the bulk integral with zero deformation, I can omit the first part of the integral in equation (4.70) that gives only rise to a constant factor. The integration over the exceptional cycle works as explained in the previous section 4.5.3, and the concrete integration of equation (4.73) is applied. This gives rise to the plots in figure 21, which shows the integrals over the respective fractional cycles.

The fractional $sLag$ cycle with exceptional part $\mathbf{e}_1^{(i)}$ (and analogously $\mathbf{e}_2^{(i)}$) has to be accessed by the third, indirect way of performing a deformation. This is due to the fact that this exceptional cycle cannot be accessed directly, as argued in the previous section. Therefore, I use a construction that incorporates the fractional cycle

$$\Pi_0^{\text{frac}} = \frac{1}{2}\left(\Pi_{13}^{\text{bulk}} \pm e_{13}^{(i)} \pm e_{31}^{(i)} \pm e_{33}^{(i)}\right), \qquad (4.77)$$

which can be easily computed by the first method for deformations since in the hypersurface description appear only real values of x_j, x_k. The basis two-cycle Π_{13}^{bulk} consists of the two

95

(a) Normalised volumes of the fractional cycles $\frac{1}{2}(\Pi^{\text{bulk}} \pm \mathbf{e}_1^{(i)})$ with positive (upper blue curve) or negative (lower red curve) exceptional part.

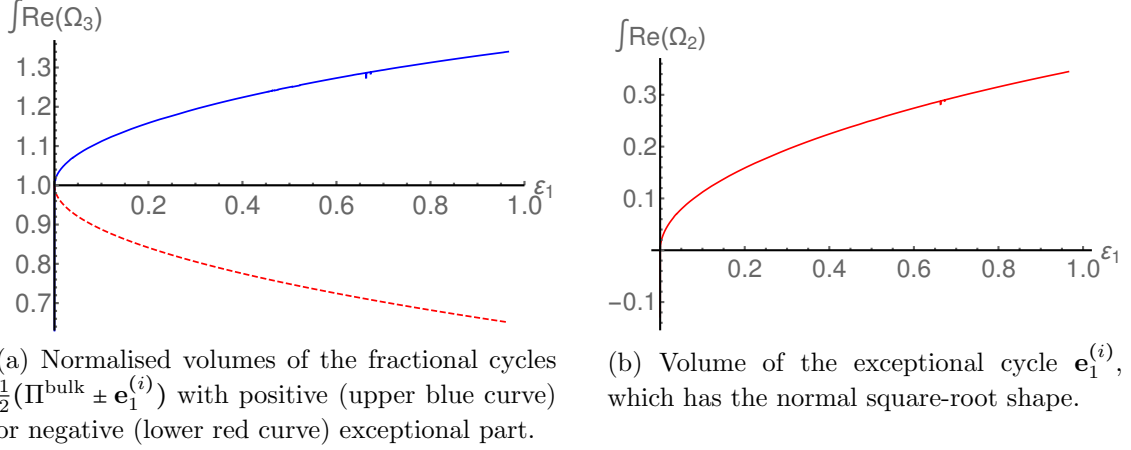(b) Volume of the exceptional cycle $\mathbf{e}_1^{(i)}$, which has the normal square-root shape.

Figure 22: Volumes of the fractional cycles which incorporate the exceptional cycle $\mathbf{e}_1^{(i)}$ (left), and of the exceptional cycle $\mathbf{e}_1^{(i)}$ itself (right). The volumes had to be computed by an indirect method, see equations (4.78) and (4.79), respectively.

horizontal basis one-cycles π_1 and π_2 on the torus, which can again be replaced by the curve $\mathcal{C}_2$. The exceptional two-cycles $e_{\alpha\beta}^{(i)}$, which are contained in the orbits $\mathbf{e}_\rho^{(i)}$, sit at the fixed points $(\alpha\beta)$ $(\alpha, \beta = 1, 2, 3, 4)$, where the upper index for the $\mathbb{Z}_2$ twisted sector is omitted. Note that $e_{13}^{(i)}$ does not appear because the singularity (11) does not have a deformation modulus. Hence, the volume of the fractional cycle can be obtained as

$$\text{Vol}\left(\Pi^{\text{frac}}(\varepsilon_1)\right) = \left[\text{Vol}\left(\Pi^{\text{bulk}}(\varepsilon_1)\right) \pm \left(2\text{Vol}\left(\Pi_0^{\text{frac}}(\varepsilon_1)\right) - \text{Vol}\left(\Pi_{13}^{\text{bulk}}(\varepsilon_1)\right)\right)\right] / \text{Vol}\left(\Pi^{\text{bulk}}(0)\right),$$

(4.78)

and is depicted in figure 22(a). In this way, I can also compute the volume of the exceptional cycle $\mathbf{e}_1^{(i)}$ by the relation

$$\text{Vol}\left(\mathbf{e}_1^{(i)}(\varepsilon_1)\right) = \left[2\text{Vol}\left(\Pi_0^{\text{frac}}(\varepsilon_1)\right) - \text{Vol}\left(\Pi_{13}^{\text{bulk}}(\varepsilon_1)\right)\right] / \text{Vol}\left(\Pi^{\text{bulk}}(0)\right).$$

(4.79)

The result can be found in figure 22, which shows no peculiarities.

4.6 Deformations of $T^6/(\mathbb{Z}_2 \times \mathbb{Z}_6)$ on one rectangular and two hexagonal tori

The definition of the orbifold action is the following,

$$\theta^k \omega^l : z_i \longmapsto e^{2\pi i(kv^i + lw^i)} z_i, \qquad \vec{v} = \frac{1}{2}(1, -1, 0), \qquad \vec{w} = \frac{1}{6}(0, 1, -1), \tag{4.80}$$

96

and the shift vector for the $\mathbb{Z}_3$ twisted sector ω^2 reads $\frac{1}{3}(0, 1, -1)$. Therefore, only the second and third torus are required to have hexagonal shape, while the complex structure parameter τ_1 is unrestricted. The $\mathbb{Z}_3$ action translates to $\omega^2 : (x_1, x_2, x_3) \mapsto (x_1, \xi x_2, \xi^2 x_3)$, and this has the following effect on the deformation polynomials,

$$
\begin{aligned}
\delta F^\alpha_{(1)} &\mapsto \delta F^\alpha_{(1)}, && (\alpha = 1, 2, 3, 4) \\
\delta F^1_{(2)} &\mapsto \xi \delta F^1_{(2)}, && \delta F^2_{(2)} \mapsto \delta F^3_{(2)} \mapsto \delta F^4_{(2)} \mapsto \delta F^2_{(2)}, \\
\delta F^1_{(3)} &\mapsto \xi^2 \delta F^1_{(3)}, && \delta F^4_{(3)} \mapsto \delta F^3_{(3)} \mapsto \delta F^2_{(3)} \mapsto \delta F^4_{(3)}.
\end{aligned}
\tag{4.81}
$$

The orientifold leads to the mappings

$$
\begin{aligned}
\delta F^\alpha_{(1)} &\mapsto \overline{\delta F^\alpha_{(1)}}, && (\alpha = 1, 2, 3, 4) \\
\delta F^1_{(k)} &\mapsto \overline{\delta F^1_{(k)}}, \quad \delta F^2_{(k)} \mapsto \overline{\delta F^4_{(k)}}, \quad \delta F^3_{(k)} \mapsto \overline{\delta F^3_{(k)}}, \quad \delta F^4_{(k)} \mapsto \overline{\delta F^2_{(k)}}, && (k = 2, 3)
\end{aligned}
\tag{4.82}
$$

and therefore one finds the deformation parameters for the $T^6/(\mathbb{Z}_2 \times \mathbb{Z}_6 \times \Omega\mathcal{R})$ orientifold as given in table 13.

Restrictions on the deformation parameters of $T^6/(\mathbb{Z}_2 \times \mathbb{Z}_6 \times \Omega\mathcal{R})$			
ρ	Parameter identifications for $\varepsilon^{(i)}_\rho$	Parameter range	Exceptional wrapping numbers
0	$\varepsilon^{(1)}_{11}$	$\mathbb{R}$	$\hat{x}^{(1)}_0, \hat{y}^{(1)}_0$
1	$\varepsilon^{(1)}_{31} = \xi^2 \varepsilon^{(1)}_{41} = \xi \varepsilon^{(1)}_{21}$	$\mathbb{R}$	$\hat{x}^{(1)}_1, \hat{y}^{(1)}_1$
2	$\varepsilon^{(1)}_{13} = \xi \varepsilon^{(1)}_{14} = \xi^2 \varepsilon^{(1)}_{12}$	$\mathbb{R}$	$\hat{x}^{(1)}_2, \hat{y}^{(1)}_2$
3	$\varepsilon^{(1)}_{33} = \varepsilon^{(1)}_{42} = \varepsilon^{(1)}_{24}$	$\mathbb{R}$	$\hat{x}^{(1)}_3, \hat{y}^{(1)}_3$
4,5	$\varepsilon^{(1)}_{34} = \varepsilon^{(1)}_{43} = \varepsilon^{(1)}_{22} = \bar{\varepsilon}^{(1)}_{32} = \bar{\varepsilon}^{(1)}_{44} = \bar{\varepsilon}^{(1)}_{23}$	$\mathbb{C}$	$\hat{x}^{(1)}_4, \hat{y}^{(1)}_4, \hat{x}^{(1)}_5, \hat{y}^{(1)}_5$
1,2,3,4	$\varepsilon^{(2)}_{2\rho} = \varepsilon^{(2)}_{3\rho} = \varepsilon^{(2)}_{4\rho}$	$\mathbb{R}$	$\hat{x}^{(2)}_\rho, \hat{y}^{(2)}_\rho$
1,2,3,4	$\varepsilon^{(3)}_{\rho 2} = \varepsilon^{(3)}_{\rho 3} = \varepsilon^{(3)}_{\rho 4}$	$\mathbb{R}$	$\hat{x}^{(3)}_\rho, \hat{y}^{(3)}_\rho$

Table 13: $\mathbb{Z}_3$ and $\Omega\mathcal{R}$ restrictions on deformation parameters and wrapping numbers for the associated exceptional three-cycles.

In addition, I can write down the hypersurface equation in the homogeneous coordinates, where due to the different torus lattices (i.e. rectangular and hexagonal), sector one resembles the previously considerd orbifold $T^6/(\mathbb{Z}_2 \times \mathbb{Z}'_6)$, and the sectors two and three have

a new structure:

$$
0 = f \equiv -y^2 + \big[v_1(x_1 - v_1\epsilon_2)(x_1 - v_1\epsilon_3)(x_1 - v_1\epsilon_4)\big] \cdot \Big\{ v_2(x_2^3 - v_2^3) \cdot v_3(x_3^3 - v_3^3)
$$

$$
- \varepsilon_0^{(1)} \cdot x_2(x_2^3 - v_2^3) \cdot x_3(x_3^3 - v_3^3)
$$
$$
- \varepsilon_1^{(1)} \cdot 3\, x_2^2 v_2^2 \cdot x_3(x_3^3 - v_3^3)
$$
$$
- \varepsilon_2^{(1)} \cdot 3\, x_2(x_2^3 - v_2^3) \cdot x_3 v_3^3
$$
$$
- \varepsilon_3^{(1)} \cdot 3\, v_2^2 v_3^2 (x_2^2 x_3^2 + x_2 v_2 \cdot x_3 v_3 + v_2^2 v_3^2)
$$
$$
- \varepsilon_{4+5}^{(1)} \cdot 3\, v_2^2 v_3^2 (-x_2^2 x_3^2 - x_2 v_2 \cdot x_3 v_3 + 2 v_2^2 v_3^2)
$$
$$
- \varepsilon_{4-5}^{(1)} \cdot 3\sqrt{3}\, x_2 v_2^2 \cdot x_3 v_3^2 (-x_2 x_3 + v_2 v_3) \Big\}
$$
$$
- \sum_{\substack{j \neq k = 2}}^{3} \Big[-\varepsilon_1^{(j)} \cdot (x_1 - v_1\epsilon_2)(x_1 - v_1\epsilon_3)^2(x_1 - v_1\epsilon_4)
$$
$$
+ \varepsilon_2^{(j)} \cdot v_1(x_1 - v_1\epsilon_3)(x_1 - v_1\epsilon_4)^2
$$
$$
+ \varepsilon_3^{(j)} \cdot v_1^2(x_1 - v_1\epsilon_2)(x_1 - v_1\epsilon_4)
$$
$$
- \varepsilon_4^{(j)} \cdot v_1(x_1 - v_1\epsilon_2)^2(x_1 - v_1\epsilon_3) \Big] \cdot 3\, v_j(x_j^3 - v_j^3) \cdot v_k^4 .
$$

$$(4.83)$$

By analysing concrete deformations, I will see that the asymmetry in the three sectors due to the different torus lattices has severe effects on the deformations, as I will explain in the following for sector one in section 4.6.1 and sectors two and three in section 4.6.2. Note that sectors two and only depend on the coordinate v_3^4 and v_2^4, respectively.

4.6.1   Sector one $(\mathbb{Z}_2^{(1)})$

At first sight, the exceptional cycles of sector one seem to be quite similar to the previously analysed orbifold $T^6/(\mathbb{Z}_2 \times \mathbb{Z}_6')$, cf. tables 12 and 13, and section 4.5.3. However, only the exceptional cycle $\mathbf{e}_1^{(1)}$ can be treated completely analogously, while all other exceptional cycles show surprisingly many characteristics that are different from the $\mathbb{Z}_2 \times \mathbb{Z}_6'$ orbifold. One of the unexpected findings is that the formerly used procedure to calculate the correction terms cannot be applied here. Therefore, so far one can only investigate local deformations and see for example how the individual exceptional cycles behave under a deformation, which I discuss now. For the bulk part of the fractional cycle under consideration, I used a horizontal bulk cycle that I shifted close to the *(s)Lag* cycle **bIII** in order to be not to close to the singularity at the origin, which can be deformed in the $T^6/(\mathbb{Z}_2 \times \mathbb{Z}_6')$ orbifold.

Exceptional cycles $\mathbf{e}_3^{(1)}$, $\mathbf{e}_4^{(1)}$ and $\mathbf{e}_5^{(1)}$:   A first important observation in sector one is the fact that by simply rotating both lattices of the tori $T_{(2)}^2$ and $T_{(3)}^2$ by $e^{2\pi i/6}$, I can
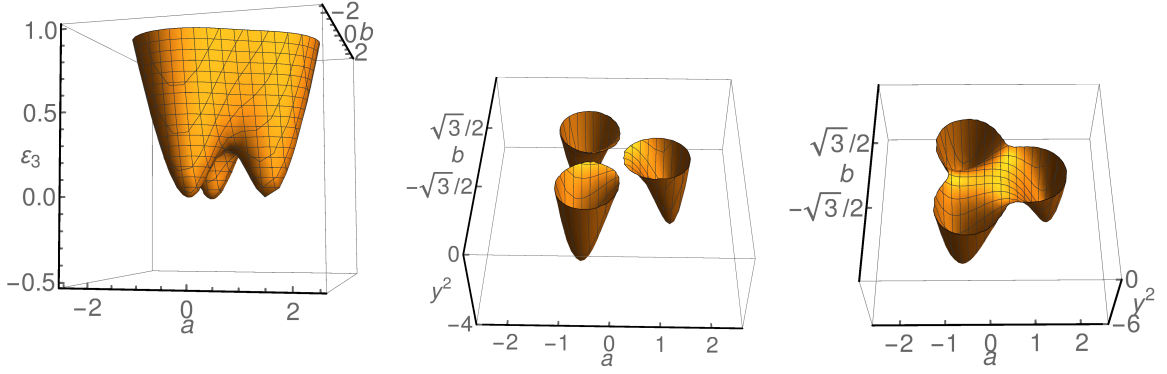
(a) Surface of the relation $y^2(a, b, \varepsilon_3^{(1)}) = 0$, which shows that all three singularities of the orbit $\mathbf{e}_3^{(1)}$ are described by $x_2 = \bar{x}_3$.

(b) Plot of the function $y^2(a, b)$ with $\varepsilon_3^{(1)} = 0.3$. One can see that three separate exceptional cycles appear.

(c) For $\varepsilon_3^{(1)} = 0.4$, the function $y^2(a, b)$ shows that the exceptional cycles of the orbit $\mathbf{e}_3^{(1)}$ have merged.

Figure 23: Surfaces of $y^2(a, b, \varepsilon_3^{(1)}) = 0$ (left) and $y^2(a, b)$ with a fixed value for $\varepsilon_3^{(1)}$ (middle, right) of the hypersurface equation (4.83), with the exceptional cycle 3 of sector one being switched on.

interchange the fixed point orbits of the exceptional cycles $\mathbf{e}_3^{(1)}$, $\mathbf{e}_4^{(1)}$ and $\mathbf{e}_5^{(1)}$, cf. table 13. Hence, I will only discuss the case of $\mathbf{e}_3^{(1)}$. As for the respective exceptional cycles on the $\mathbb{Z}_2 \times \mathbb{Z}_6'$ orbifold, I have to compute correction terms to deform only one orbit at a time and to analyse global models. Unfortunately, I have not found these correction terms yet because the method that is explained in appendix A for the $\mathbb{Z}_2 \times \mathbb{Z}_6'$ orbifold has to be modified for this new orbifold in a highly non-trivial way. Nevertheless, I will have a look at the local structure of the deformations.
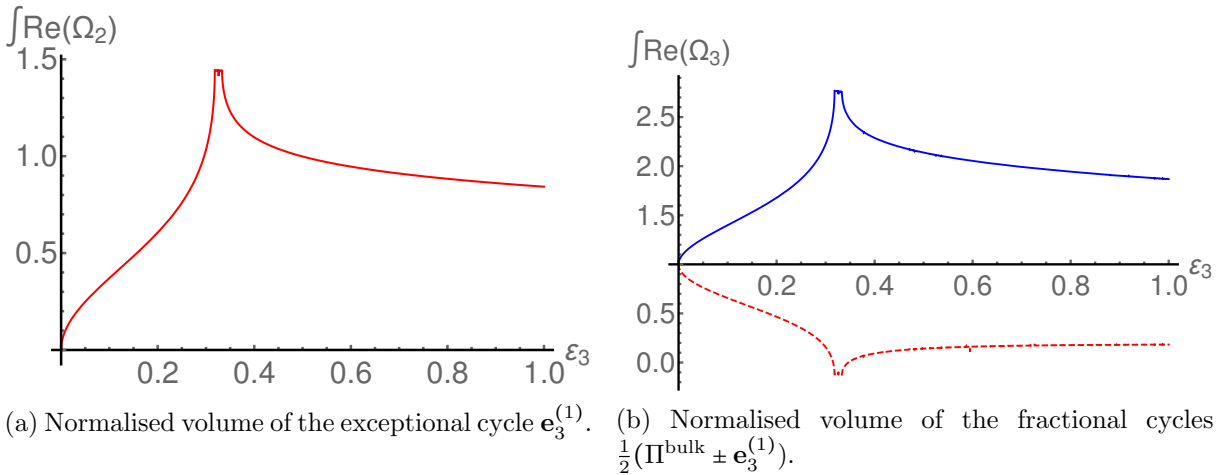
(a) Normalised volume of the exceptional cycle $\mathbf{e}_3^{(1)}$.

(b) Normalised volume of the fractional cycles $\frac{1}{2}(\Pi^{\text{bulk}} \pm \mathbf{e}_3^{(1)})$.

Figure 24: Exceptional and fractional cycles of sector one including $\mathbf{e}_3^{(1)}$. As expected from the considerations in figure 23, the deformation runs only in a controlled way for $\varepsilon_3^{(1)} \lesssim 0.3$.

99

(a) Normalised volume of the exceptional cycle $\mathbf{e}_2^{(1)}$.

(b) Normalised volumes of the fractional cycles $\frac{1}{2}(\Pi^{\mathrm{bulk}} \pm \mathbf{e}_2^{(1)})$.
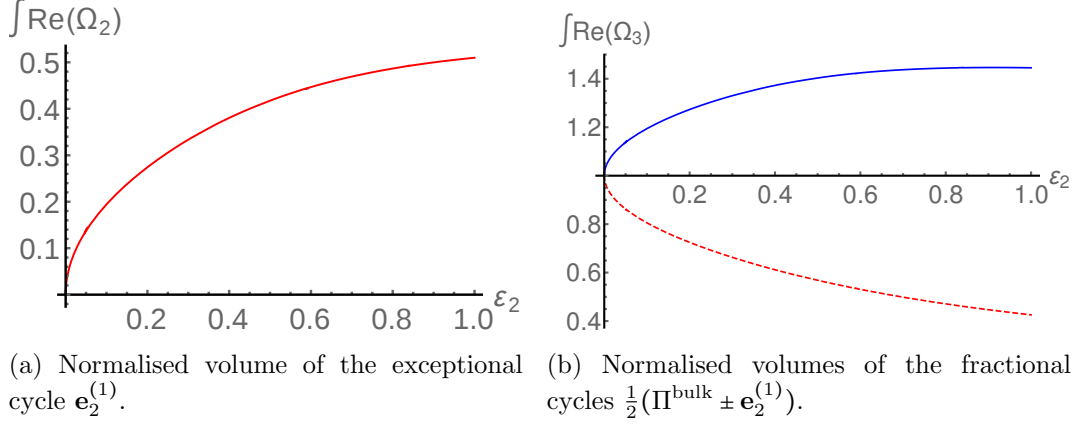
Figure 25: Exceptional and fractional cycles of sector one including $\mathbf{e}_2^{(1)}$. This deformation does not have any peculiarities besides the fact that they have to be accessed indirectly.

The main difference of $\mathbf{e}_3^{(1)}$ to the respective exceptional cycle of the $\mathbb{Z}_2 \times \mathbb{Z}_6'$ orbifold is the fact that the relation $x_2 = \bar{x}_3$ describes here all three fixed points that belong to the orbit of $\mathbf{e}_3^{(1)}$ (and additionally the fixed point (11), which is the only fixed point associated to the exceptional cycle $\mathbf{e}_0^{(1)}$). This fact can be observed in figure 23(b), where the exceptional cycle $x_2 = \bar{x}_3 = a + ib$ is inserted into equation (4.83), with deformation $\varepsilon_3^{(1)}$ of the first sector switched on. Moreover, one finds that only for $\varepsilon_3^{(1)} > 0$ an exceptional cycle of non-zero volume appears, and the plots in figures 23(b) and 23(c) reveal that only up to deformation parameters of about 0.3 the deformation behaves in a controlled way. This observation can also be made for the volumes of the exceptional and fractional cycles, see figure 24, which show for small values of $\varepsilon_3^{(1)}$ a behaviour as anticipated. More concretely, the integrals were computed by a separate integration of the exceptional and of the bulk part, similarly to the discussion for $\mathbb{Z}_2 \times \mathbb{Z}_6'$.

Exceptional cycle $\mathbf{e}_2^{(1)}$: This cycle has some similarities to the orbit $\mathbf{e}_1^{(1)}$, but the deformation parameters of table 13 have here different phases. Otherwise, the description works similarly as for the exceptional cycle $\mathbf{e}_2^{(1)}$ in the $\mathbb{Z}_2 \times \mathbb{Z}_6'$ orbifold, as discussed in section 4.5.3, which means that I have to access these cycles indirectly.

Exceptional cycle $\mathbf{e}_1^{(1)}$: This exceptional cycle behaves completely in the same manner as the exceptional cycle $\mathbf{e}_1^{(1)}$ on the $T^6/(\mathbb{Z}_2 \times \mathbb{Z}_6')$ orbifold, see the respective paragraph in section 4.5.3. Therefore, I will not further discuss it.

100
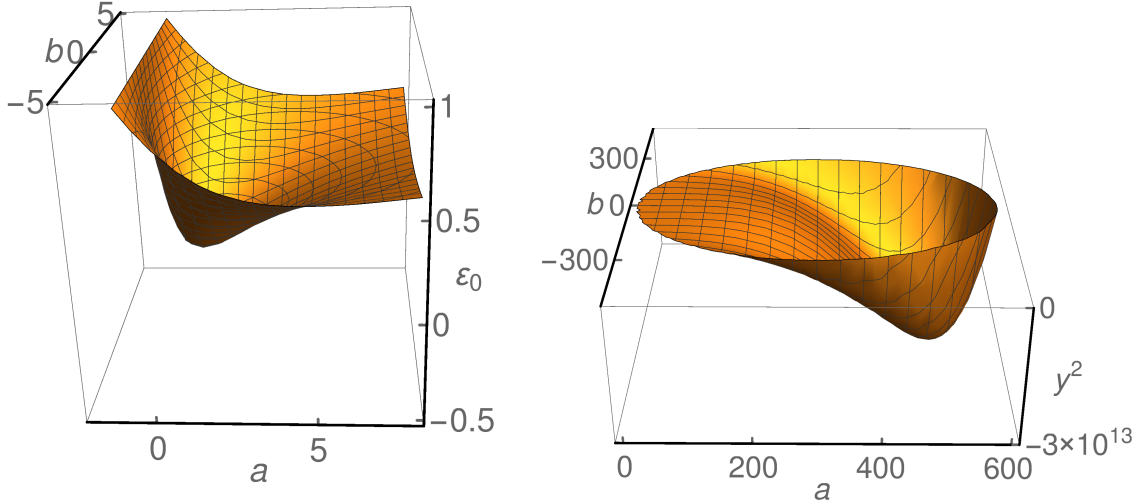
(a) Surface of the relation $y^2(a, b, \varepsilon_3^{(1)}) = 0$, which shows that the singularity (11) is the only one in the exceptional cycle $\mathbf{e}_0^{(1)}$, which is described by $x_2 = \bar{x}_3$.

(b) Plot of the function $y^2(a, b)$ for $\varepsilon_0^{(1)} = 1$. Note the huge values on the vertical axis.

Figure 26: Surfaces of $y^2(a, b, \varepsilon_0^{(1)}) = 0$ (left) and $y^2(a, b)$ with $\varepsilon_0^{(1)} = 1$ (right) of the hypersurface equation (4.83), with the exceptional cycle $\mathbf{e}_0^{(1)}$ of sector one being switched on.

Exceptional cycle $\mathbf{e}_0^{(1)}$: This exceptional cycle is especially simple because it involves only the fixed point labelled (11). Due to the fact that the cycle is at the origin of both tori, no fixed point orbit appears. As already mentioned, I can simply describe the exceptional cycle by $x_2 = \bar{x}_3$.

The integrals of the fractional and exceptional cycle are plotted in figure 27. Note that I could not use here the curve $\mathcal{C}_2$ as for the $\mathbb{Z}_2 \times \mathbb{Z}_6'$ orbifold because on $\mathbb{Z}_2 \times \mathbb{Z}_6$, $\mathcal{C}_2$ runs through the origin with fixed point (11), which is also deformed by the relation $x_2 = \bar{x}_3$. Hence, I used a different bulk cycle, where I chose a horizontal cycle close to the cycle **bIII** on the torus, and translated this curve via the Weierstrass function to the hypersurface description. For the exceptional cycle I could use an integration as for the exceptional cycle $\mathbf{e}_3^{(1)}$ in the orbifold $\mathbb{Z}_2 \times \mathbb{Z}_6'$, and no correction terms arise. The large integration boundaries can be read off from figure 26(b).

4.6.2 Sectors two and three ($\mathbb{Z}_2^{(2)}$ and $\mathbb{Z}_2^{(3)}$)

Since sector two and three show exactly the same properties, I consider here only sector three. For convenience I give the hypersurface equation for the third sector, where I restrict

(a) Normalised volume of the exceptional cycle $\mathbf{e}_0^{(1)}$.

(b) Normalised volumes of the fractional cycles $\frac{1}{2}(\Pi^{\text{bulk}} \pm \mathbf{e}_0^{(1)})$.
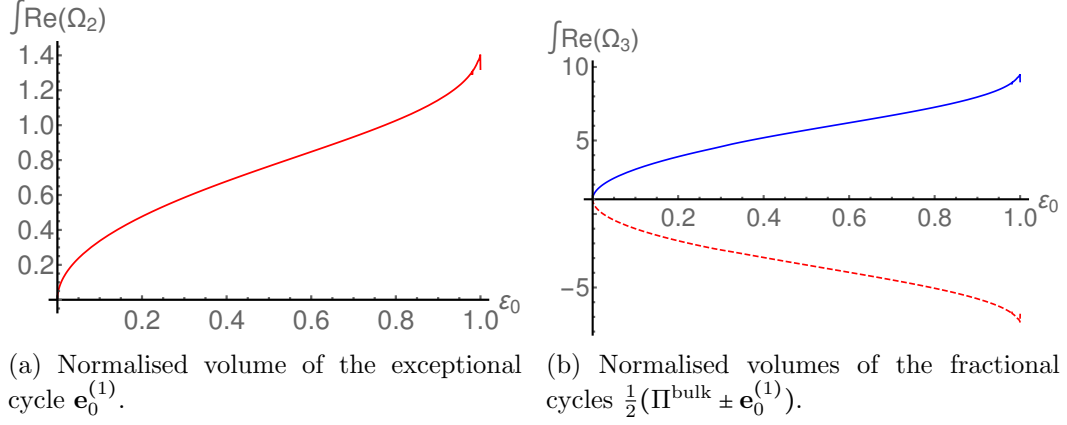
Figure 27: Volumes of the exceptional and fractional cycles of sector one that incorporate $\mathbf{e}_0^{(1)}$. The shape of the curves is as expected.

(a) Deformation parameter $\varepsilon_2^{(3)} = 0.03$. For small deformations, the deformed curves show approximately a hyperbolic shape, similarly to e.g. the $T^4/\mathbb{Z}_2$ orbifold.

(b) Deformation parameter $\varepsilon_2^{(3)} = 0.5$. One can see that for larger deformation parameters, not only the neighbouring cycles of the deformed singularity, but also the cycle $\mathbf{aIII} \otimes \mathbf{bI}$ and the non-$sLag$ cycle $\mathbf{aIII} \otimes \mathbf{bII}$ are strongly affected by the deformation.

Figure 28: Visualisation diagram of regions $\tilde{y}^2(x_1, x_2) > 0$ as defined in equation (4.84) for sector three of the $\mathbb{Z}_2 \times \mathbb{Z}_6$ orbifold, where the $sLag$ cycles with $\tilde{y}^2(x_1, x_2) > 0$ are highlighted in blue.

the first two-torus $T_{(1)}^2$ to have square shape, i.e. $\epsilon_2^{(1)} = 1$, $\epsilon_3^{(1)} = 0$, $\epsilon_4^{(1)} = -1$, and with the chart $v_i \equiv 1$. In addition, I factor out the terms with coordinates x_3, where in this sector

no orbifold fixed points appear. Therefore, I obtain

$$\tilde{y}^2(x_1, x_2) = x_1(x_1^2 - 1)(x_2^3 - 1)$$
$$+ 3\left(\varepsilon_1^{(3)} x_1^2(x_1^2 - 1) - \varepsilon_2^{(3)} x_1(x_1 + 1)^2 - \varepsilon_3^{(3)}(x_1^2 - 1) + \varepsilon_4^{(3)} x_1(x_1 - 1)^2\right), \quad (4.84)$$

and in line two no dependence on the coordinate x_2 is apparent, cf. equation (4.83).
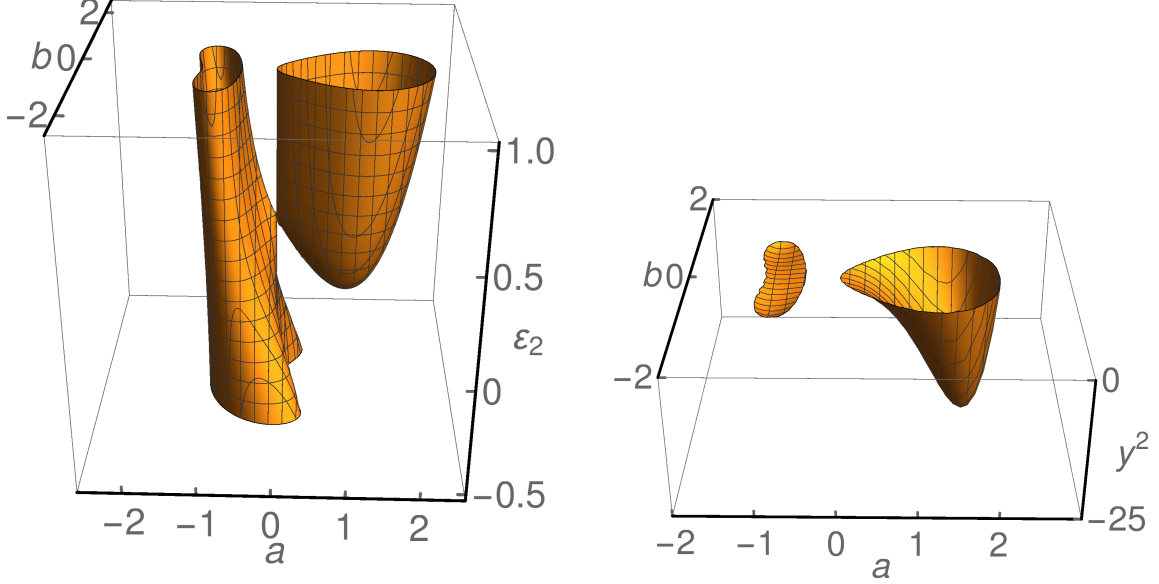
(a) This surface, which satisfies $y^2(a, b, \varepsilon_2^{(3)}) = 0$, reveals that for deformation parameters $\varepsilon_2^{(3)} > 0$, there grows indeed an exceptional cycle out of the singularity at $(a, b) = (1, 0)$. However, one directly sees that something goes wrong when leaving the local description because the left part is unexpected und should not be there.

(b) The plot of the function $y^2(a, b)$ for $\varepsilon_2^{(3)} = 1$ confirms that here arises an unexpected issue, i.e. the little area at the left side which is there for an arbitrary choice of $\varepsilon_2^{(3)} \in [0, 1]$.

Figure 29: Surfaces of $y^2(a, b, \varepsilon_2^{(3)}) = 0$ (left) and $y^2(a, b)$ with $\varepsilon_2^{(3)} = 1$ (right) of the hypersurface equation (4.84), with the exceptional cycle $\mathbf{e}_2^{(3)}$ of sector three being switched on.

As I stated in equation (4.36), on a square torus a shift of the fixed points is simply a suitable relabelling of all four fixed points. In addition, for all exceptional cycles the fixed point orbit on the second torus is the same, and therefore it is sufficient to consider only the exceptional cycle of fixed point (23) and its orbit that I call $\mathbf{e}_2^{(3)}$, which is described by the relation $x_1 = \bar{x}_2$. A plot in a similar manner as in figure 13 of the regions with $\tilde{y}^2(x_1, x_2) > 0$ as defined in equation (4.84), with x_1 and x_2 assumed to be real, is given in figure 28. There one can observe that for deformations of larger parameters ε, not only the cycles which pass through the deformed singularity feel the deformation, but also other cycles are strongly affected, see figure 28(b). Moreover, the surface plots in figure 29

make clear that, as already mentioned several times before, sectors two and three of the $T^6/(\mathbb{Z}_2 \times \mathbb{Z}_6')$ orbifold seem to have a different structure compared to the examples that were worked out before. Hence, it is clear that these sectors need a careful analysis in the future and probably different methods have to be developed in order to get over the just discovered difficulties.
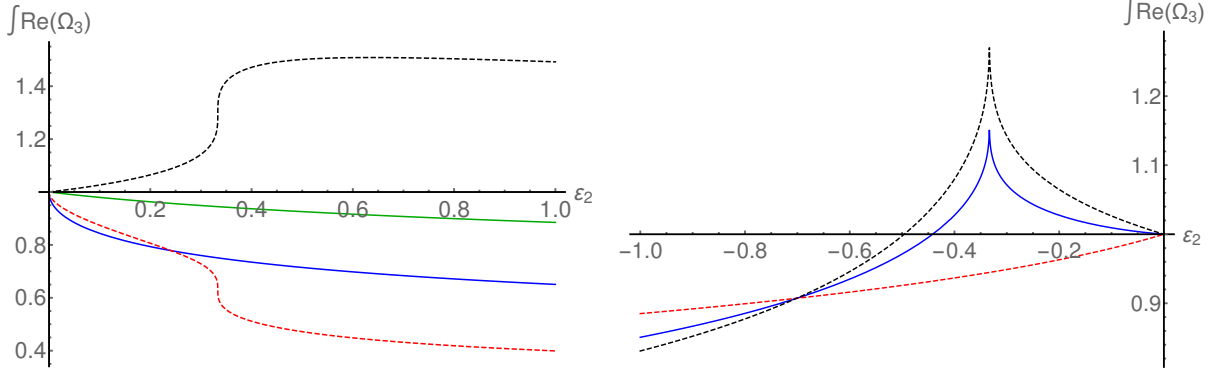
(a) Deformation $\varepsilon_2^{(3)} > 0$. The two upper curves correspond to the *sLag* cycles $\mathbf{aIII} \otimes \mathbf{bI}$ (black, dashed) and $\mathbf{aII} \otimes \mathbf{bII}$ (green, bold), which do not have an exceptional contribution and hence display a linear behaviour for small ε_2. On the other hand, the two lower curves that belong to the fractional cycles $\mathbf{aI} \otimes \mathbf{bI}$ (blue, bold) and $\mathbf{aIV} \otimes \mathbf{bII}$ (red, dashed) include, as expected, the exceptional cycle $\mathbf{e}_2^{(3)}$, and therefore the curves show a square-root like behaviour for small ε_2.

(b) Deformation $\varepsilon_2^{(3)} < 0$. All curves show a linear behaviour for small deformations, where the curves correspond top down to the *sLag* cycles $\mathbf{aII} \otimes \mathbf{bII}$ (black, dashed curve), $\mathbf{aI} \otimes \mathbf{bI} + \mathbf{aIV} \otimes \mathbf{bII}$ (blue, bold curve), and $\mathbf{aIII} \otimes \mathbf{bI}$ (red, dashed curve). The blue bold curve shows the integral over a merged cycles, which is made up of two formerly separated cycles. One also finds that the two upper curves are strongly influenced by the deformation for larger values of ε_2.

Figure 30: Integrals of all *sLag* cycles with real calibration (i.e. the shaded areas in figure 28) for deformations by the parameter $\varepsilon_2^{(3)}$.

The integrals over the fractional cycles depicted in figure 28 with a deformation of $\varepsilon_2^{(3)}$, where in the second torus only the undisplaced horizontal and vertical cycles $\mathbf{bI}$ and $\mathbf{bII}$ are considered, can be computed in a similar manner as in section 4.3.4 for the orbifold $T^4/\mathbb{Z}_2$, see equation (4.51). This is due to the fact these fractional cycles only have real values in the homogeneous coordinates x_1, x_2 (in the chart $v_i \equiv 1$). Therefore, the integral over one of these fractional *sLag* cycles reads

$$\int\limits_{\Pi^{\text{frac}}} \text{Re}\left(\Omega_2\right) = 2 \int\limits_{\epsilon_{k_i}^{(1)}}^{\epsilon_{k_f}^{(1)}} \mathrm{d}x_1 \int\limits_{-\infty}^{\infty} \mathrm{d}x_2 \, \frac{H[\tilde{y}^2(x_1, x_2, \varepsilon) > 0]}{\sqrt{\tilde{y}^2(x_1, x_2, \varepsilon)}} \,, \tag{4.85}$$

where the one-cycle in the first torus starts at the initial fixed point with value $\epsilon_{k_i}^{(1)}$ and ends at the final fixed point with value $\epsilon_{k_f}^{(1)}$. The results can be found in figure 30(a) for

104

deformations with positive parameter $\varepsilon_2^{(3)}$, and deformations in negative direction are given in figure 30(b). I also checked that upon deformation all cycles stay *sLag* by computing the imaginary part of the cycles, which is indeed zero for all values $\varepsilon_2^{(3)} \neq 0$.

I did not study yet explicitly the integrals with the shifted cycles **bIII** and **bIV** in the second torus, which I will leave for future work. I expect that one can shift these cycles onto the cycles **bI** and **bII**, respectively, and then integrate over these shifted cycles. Since for deformations on the orbifold $T^6/(\mathbb{Z}_2 \times \mathbb{Z}_6)$ there appeared already some unexpected technical difficulties, one has to analyse the deformations of these shifted cycles in more detail to obtain a concrete description.

5 Concrete Models

As done for the deformations, I start with model building on the $T^4/(\mathbb{Z}_2 \times \Omega\mathcal{R})$ orientifold, which I mostly present in order to explain the techniques of model building, before I come to the more complicated models on $T^6/(\mathbb{Z}_2 \times \mathbb{Z}_2 \times \Omega\mathcal{R})$ and on $T^6/(\mathbb{Z}_2 \times \mathbb{Z}_6' \times \Omega\mathcal{R})$. Note that the models on these latter orientifolds, which incorporate D6-branes and O6-planes and where I stabilise complex structure moduli via deformations, belong to type IIA string theory. On the other hand, the models on the $T^4/(\mathbb{Z}_2 \times \Omega\mathcal{R})$ orientifold are associated to type IIB string theory and are constructed with D7-branes and O7-planes, where actually Kähler moduli are stabilised using blow-ups.

Let me remind the reader that the volumes of the fractional cycles on which D-branes are wrapped are closely related to the physical gauge couplings by the relation

$$\frac{1}{g_{G_a}^2} \propto \mathrm{Vol}(\Pi_a) + \mathrm{Vol}(\Pi_{a'}) \qquad \text{with } G_a = U(N_a), \, USp(2N_a), \, SO(2N_a), \tag{5.1}$$

cf. equation (3.40). To this aim, it is interesting to study deformations in concrete models and to observe how the gauge couplings behave. In addition, I will study for which brane configurations complex structure moduli are stabilised by obtaining a *vev*, as discussed in section 3.2.3.

5.1 sLags on the deformed $T^4/(\mathbb{Z}_2 \times \Omega\mathcal{R})$ on square tori

The definitions of the different cycles from section 3.1.3 are here slightly modified in order to be compatible with the models on the $T^4/(\mathbb{Z}_2 \times \Omega\mathcal{R})$ orientifold, as already mentioned. Thus, the fractional two-cycles read

$$\Pi^{\text{frac}} := \frac{1}{2} \left(\Pi^{\text{bulk}} + \Pi^{\mathbb{Z}_2} \right), \tag{5.2}$$

and the bulk cycle has the simple form

$$\Pi^{\text{bulk}} := 2 \bigotimes_{i=1}^{2} \left(n_i \pi_{2i-1} + m_i \pi_{2i} \right). \tag{5.3}$$

The discrete displacements $\sigma^i \in \{0, 1\}$ per two-torus $T_{(i)}^2$ $(i = 1, 2)$ together with the integer torus wrapping numbers (n_i, m_i) determine the four fixed points through which the bulk cycle runs, and which therefore also appear in the exceptional *two*-cycle

$$\Pi^{\mathbb{Z}_2} := (-1)^{\tau^{\mathbb{Z}_2}} \cdot \left(e_{\alpha_0\beta_0} + (-1)^{\tau^1} e_{\alpha_1\beta_0} + (-1)^{\tau^2} e_{\alpha_0\beta_1} + (-1)^{\tau^1+\tau^2} e_{\alpha_1\beta_1} \right). \tag{5.4}$$

This definition is slightly different from the one of an exceptional *three*-cycle $\Pi^{\mathbb{Z}_2^{(k)}}$ of equation (3.21), which includes both exceptional two-cycles $e_{\alpha\beta}$ as well as torus one-cycles. $\Pi^{\mathbb{Z}_2}$ contains two of the fixed points $\alpha \in \{1, 2, 3, 4\}$ of the two-torus $T^2_{(1)}$, with α_0 being the reference point and α_1 the second fixed point, and similarly for the fixed points labelled β of $T^2_{(2)}$. At these fixed points $(\alpha\beta) \in T^4 \equiv T^2_{(1)} \times T^2_{(2)}$, the exceptional two-cycles $e_{\alpha\beta}$ arise, where the exceptional cycle $e_{\alpha_0\beta_0}$ at the reference point is only weighted with the global $\mathbb{Z}_2$ eigenvalue $(-1)^{\tau^{\mathbb{Z}_2}} = \pm 1$ (i.e. $\tau^{\mathbb{Z}_2} \in \{0, 1\}$). All other fixed points have additional sign factors from discrete Wilson lines $\tau^i \in \{0, 1\}$. Note that all these parameters have discrete values because the underlying space is an orbifold, and that the values are concretely specified for the following models. In analogy to equation (3.14), I will also often use the notation

$$\Pi^{\text{bulk}}_{IJ} = 2 \, \Pi^{\text{torus}}_{IJ} = 2 \, \pi_I \otimes \pi_J \tag{5.5}$$

for the basis two-cycles on the four-torus $T^2_{(1)} \times T^2_{(2)}$, with $I \in \{1, 2\}$ and $J \in \{3, 4\}$, and with positions on the untilted or tilted lattice as depicted in figure 1.

5.1.1 Models on untilted tori

My first example of a concrete (global) model, see also our publication [109], is known in the literature as the generalised T-dual of the **Gimon-Polchinski** model as presented 1996 in terms of D-branes [128], but which was actually developed by Bianchi and Sagnotti some years earlier [129]. This model was then taken up by Blumenhagen, Braun, Körs and Lüst in 2002 and reformulated in the language of two-cycles [53], which I will also use here. The concrete specifications of this model are summarised in table 14. Since the generalised T-dual of the Gimon-Polchinski model is supersymmetric for any choice of complex structure that describes the untilted two-tori $T^2_{(i)}$ ($i = 1, 2$), I can simply choose both tori to be of square shape.

The O7-plane $\Omega\mathcal{R}$ together with the second O7-plane $\Omega\mathcal{R}\mathbb{Z}_2$ is wrapped on the two-cycle

$$\Pi_{\text{O7}} = 2 \, \Pi^{\text{bulk}}_{13} - 2 \, \Pi^{\text{bulk}}_{24} , \tag{5.6}$$

where the reason for the factors of two is the following. Firstly, one has to take into account that the fixed point sets only wrap torus cycles Π^{torus}, but not bulk cycles Π^{bulk}, and secondly, that there are two parallel planes per torus $T^2_{(i)}$, which gives a total of $\frac{1}{2} \times 2 \times 2 = 2$. Due to table 14, the fractional cycles and their orientifold images have the following form,

$$
\begin{aligned}
\Pi^{\text{frac}}_a &= \tfrac{1}{2} \left(\Pi^{\text{bulk}}_{13} + \Pi^{\mathbb{Z}_2}_a \right) , &\quad \Pi^{\text{frac}}_{a'} &= \tfrac{1}{2} \left(\Pi^{\text{bulk}}_{13} - \Pi^{\mathbb{Z}_2}_a \right) , \\
\Pi^{\text{frac}}_b &= \tfrac{1}{2} \left(-\Pi^{\text{bulk}}_{24} + \Pi^{\mathbb{Z}_2}_b \right) , &\quad \Pi^{\text{frac}}_{b'} &= \tfrac{1}{2} \left(-\Pi^{\text{bulk}}_{24} - \Pi^{\mathbb{Z}_2}_b \right) ,
\end{aligned}
\tag{5.7}
$$

Model 1 (Gimon-Polchinski): $T^4/(\mathbb{Z}_2 \times \Omega\mathcal{R})$ on untilted tori							
x	n_i, m_i	$(\vec{\sigma})$	$\mathbb{Z}_2$	$(\vec{\tau})$	$\|$O7	N	Gauge group
a	$(1,0;1,0)$	(σ_a^1, σ_a^2)	$(-1)^{\tau_a^{\mathbb{Z}_2}}$	(τ_a^1, τ_a^2)	$\Omega\mathcal{R}$	16	$U(16)$
b	$(0,1;0,-1)$	(σ_b^1, σ_b^2)	$(-1)^{\tau_b^{\mathbb{Z}_2}}$	(τ_b^1, τ_b^2)	$\Omega\mathcal{R}\mathbb{Z}_2$	16	$U(16)$

Table 14: Concrete specifications of the generalised T-dual of the Gimon-Polchinski model on the $T^4/(\mathbb{Z}_2 \times \Omega\mathcal{R})$ orientifold on two untilted tori $T_{(i)}^2$ ($i = 1, 2$), where two stacks of D7-branes are wrapped on fractional cycles as defined in equation (5.2). The D7$_a$-branes are parallel to the orientifold plane O7 denoted by $\Omega\mathcal{R}$, and the D7$_b$-branes are parallel to the second O7-plane, which is called $\Omega\mathcal{R}\mathbb{Z}_2$. The displacements $\sigma_x^i \in \{0, 1\}$, the $\mathbb{Z}_2$ eigenvalues $(-1)^{\tau_x^{\mathbb{Z}_2}}$ with $\tau_x^{\mathbb{Z}_2} \in \{0, 1\}$, and the discrete Wilson lines $\tau_x^i \in \{0, 1\}$ can be chosen arbitrarily ($x = a, b$). The gauge group is $U(16)_a \times U(16)_b$.

and with all discrete displacements set to $\sigma_x^i = 0$, the exceptional contributions read

$$\Pi_a^{\mathbb{Z}_2} = (-1)^{\tau_a^{\mathbb{Z}_2}} \left[e_{11} + (-1)^{\tau_a^1} e_{21} + (-1)^{\tau_a^2} e_{12} + (-1)^{\tau_a^1 + \tau_a^2} e_{22} \right],$$
$$\Pi_b^{\mathbb{Z}_2} = (-1)^{\tau_b^{\mathbb{Z}_2}} \left[e_{11} + (-1)^{\tau_b^1} e_{41} + (-1)^{\tau_b^2} e_{14} + (-1)^{\tau_b^1 + \tau_b^2} e_{44} \right]. \tag{5.8}$$

This means that they are simply horizontal (for stack a) and vertical (for stack b) cycles running through the origin and therefore sitting on top of one of the O7-planes $\Omega\mathcal{R}$ or $\Omega\mathcal{R}\mathbb{Z}_2$, respectively. Equation (5.7) shows that the fractional cycles are not invariant under the antiholomorphic involution $\mathcal{R}$, and therefore a gauge group enhancement from $U(N_{a,b})$ to one of the groups $USp(2N_{a,b})$ or $SO(2N_{a,b})$ is not possible.

Moreover, one can check that the R-R tadpole cancellation condition, which is a necessary condition to obtain a global model, is satisfied,

$$\sum_{x=a,b} N_x \left(\Pi_x^{\text{frac}} + \Pi_{x'}^{\text{frac}} \right) - 8\,\Pi_{\text{O7}} = 0, \tag{5.9}$$

where the sum over the fractional cycles and their orientifold images cancels the exceptional contributions and only the bulk part remains,

$$\Pi_a^{\text{frac}} + \Pi_{a'}^{\text{frac}} = \Pi_{13}^{\text{bulk}}, \qquad \Pi_b^{\text{frac}} + \Pi_{b'}^{\text{frac}} = -\Pi_{24}^{\text{bulk}}. \tag{5.10}$$

Thus, the gauge couplings, as given in equation (5.1), obey the relations

$$\frac{1}{g_{U(16)_a}^2} \propto \Pi_{13}^{\text{bulk}}, \qquad \frac{1}{g_{U(16)_b}^2} \propto -\Pi_{24}^{\text{bulk}}, \tag{5.11}$$

and should therefore not be influenced by deformations of the exceptional cycles. This furthermore implies that one can parallelly shift parts of the D7-branes away from the

fixed points such that they are not invariant under $\mathcal{R}$ and $\mathbb{Z}_2$ anymore and hence, the gauge group is broken to $USp(16)_a \times USp(16)_b$. A different possibility is to split each stack of 16 D7-branes into two stacks of eight D7-branes and moves these apart, which results in the gauge group $\Pi_{i=1}^2 USp(8)_{a_i} \times \Pi_{j=1}^2 USp(8)_{b_j}$ of the Bianchi-Sagnotti model [129].

5.1.2   Models on tilted tori

As a global model for tilted tori, I use four stacks of D7-branes which are either parallel to the orientifold-plane $\Omega\mathcal{R}$ or to $\Omega\mathcal{R}\mathbb{Z}_2$, cf. table 15 for details. In this model, supersymmetry is preserved upon any choice of complex structure which leads to tilted tori. Again I choose a square torus lattice, as presented in figure 1, for concrete calculations. This model was considered by me and my collaborators in [109], but since I use here a different choice of basis one-cycles, I had to redefine the specifications of table 15 compared to our article. Also note that here the discussion for the deformations of $T^4/\mathbb{Z}_2$ orbifolds on tori with square **a**-type lattices applies, cf. section 4.3, because the cycles that are considered here can all be described by the additional cycles on square tori that are inherited from the *(s)Lag* lines on square **b**-type lattices, see section 4.1 and table 9.

Model 2: $T^4/(\mathbb{Z}_2 \times \Omega\mathcal{R})$ on tilted tori							
x	n_i, m_i	$(\vec{\sigma})$	$\mathbb{Z}_2$	$(\vec{\tau})$	$\|O7$	N	Gauge group
a_1 a_2	$(1,0;1,0)$	$(1,0)$	$+$ $-$	$(1,0)$	$\Omega\mathcal{R}$	2	$USp(4)$
b_1 b_2	$(-1,2;1,-2)$	$(0,1)$	$+$ $-$	$(0,1)$	$\Omega\mathcal{R}\mathbb{Z}_2$	2	$USp(4)$

Table 15: D7-brane specifications of a global model for the $T^4/(\mathbb{Z}_2 \times \Omega\mathcal{R})$ orientifold on tilted tori with four stacks of $N = 2$ D7-branes and with gauge group $USp(4)^4$.

Concretely, the four fractional cycles and their identical $\mathcal{R}$-images have the form

$$\Pi_{a_1}^{\text{frac}} = \frac{1}{2}\left(\Pi_a^{\text{bulk}} + \Pi_a^{\mathbb{Z}_2}\right) = \Pi_{a_1'}^{\text{frac}} ,$$

$$\Pi_{a_2}^{\text{frac}} = \frac{1}{2}\left(\Pi_a^{\text{bulk}} - \Pi_a^{\mathbb{Z}_2}\right) = \Pi_{a_2'}^{\text{frac}} ,$$

(5.12)

$$\Pi_{b_1}^{\text{frac}} = \frac{1}{2}\left(\Pi_b^{\text{bulk}} + \Pi_b^{\mathbb{Z}_2}\right) = \Pi_{b_1'}^{\text{frac}} ,$$

$$\Pi_{b_2}^{\text{frac}} = \frac{1}{2}\left(\Pi_b^{\text{bulk}} - \Pi_b^{\mathbb{Z}_2}\right) = \Pi_{b_2'}^{\text{frac}} ,$$

(5.13)

and with the fixed points as given in figure 3, the bulk and exceptional parts read

$$\Pi_a^{\text{bulk}} = \Pi_{13}^{\text{bulk}}, \qquad\qquad\qquad \Pi_a^{\mathbb{Z}_2} = [e_{41} - e_{21} + e_{43} - e_{23}], \qquad (5.14)$$

$$\Pi_b^{\text{bulk}} = -\Pi_{13}^{\text{bulk}} + 2\Pi_{14}^{\text{bulk}} + 2\Pi_{23}^{\text{bulk}} - 4\Pi_{24}^{\text{bulk}}, \qquad \Pi_b^{\mathbb{Z}_2} = [e_{14} + e_{34} - e_{12} - e_{32}]. \qquad (5.15)$$

The displacements $(\vec{\sigma}_x)$ and the discrete Wilson lines $(\vec{\tau}_x)$ obey for all stacks x the condition $\sigma_x^1 \tau_x^1 \neq \sigma_x^2 \tau_x^2$. Together with the fact that all bulk cycles are parallel to O7-branes, this relation yields that all D7-branes are orientifold invariant and thus the gauge group enhances to $USp(4)_{a_1} \times USp(4)_{a_2} \times USp(4)_{b_1} \times USp(4)_{b_2}$.

At the singular orbifold point, the cycles of all stacks x have the same volume as their orientifold image x', but as soon as deformations are switched on they can be different. This behaviour is expected to translate as well to the tree-level gauge couplings due to the close relation to the volumes of cycles.

5.2 sLags on the deformed $T^6/(\mathbb{Z}_2 \times \mathbb{Z}_2 \times \Omega\mathcal{R})$ on square tori

Model 3: $T^6/(\mathbb{Z}_2 \times \mathbb{Z}_2 \times \Omega\mathcal{R})$ on untilted tori							
x	n_i, m_i	$\parallel$O7	$(\vec{\sigma})$	$\mathbb{Z}_2^{(i)}$	$(\vec{\tau})$	N	Gauge group
a	$(1,0;0,-1;0,1)$	$\Omega\mathcal{R}\mathbb{Z}_2^{(1)}$	$(\vec{0})$	$(+++)$	$(\tau_a^1, \tau_a^2, \tau_a^3)$	4	$USp(2N_a)$ if $\eta_{\Omega\mathcal{R}\mathbb{Z}_2^{(1)}} = -1$ $U(N_a)$ else

Table 16: D7-brane specifications of a local toy model for the $T^6/(\mathbb{Z}_2 \times \mathbb{Z}_2 \times \Omega\mathcal{R})$ orientifold on untilted tori with either $USp(2N_a)$ or $U(N_a)$ gauge group, depending on the choice of the exotic O6-plane.

The definitions of the three-cycle, wrapped by D6-branes and O6-planes, that I use in this and in the following section are as introduced in section 3.1.3. For the O6-plane charges I form the combination

$$\eta_{(i)} \equiv \eta_{\Omega\mathcal{R}} \cdot \eta_{\Omega\mathcal{R}\mathbb{Z}_2^{(i)}}, \qquad (5.16)$$

with $i = 1, 2, 3$. For the example on untilted tori as specified in table 16, I use only one stack of four D6-branes a, which is parallel to the orientifold plane $\Omega\mathcal{R}\mathbb{Z}_2^{(1)}$. Considering the orientifold images of the exceptional three-cycles as specified in our article [109],

$$\Omega\mathcal{R}(E_{\alpha\beta}^{(i)}) = \eta_{(i)} \left(-E_{\alpha'\beta'}^{(i)}\right), \qquad \Omega\mathcal{R}(\tilde{E}_{\alpha\beta}^{(i)}) = \eta_{(i)} \tilde{E}_{\alpha'\beta'}^{(i)}, \qquad (5.17)$$

the fractional cycle and its orientifold image have the form

$$\Pi_a^{\text{frac}} = \frac{1}{4}\left(-\Pi_{146}^{\text{bulk}} + \Pi^{\mathbb{Z}_2^{(1)}} - \Pi^{\mathbb{Z}_2^{(2)}} + \Pi^{\mathbb{Z}_2^{(3)}}\right), \tag{5.18}$$

$$\Pi_{a'}^{\text{frac}} = \frac{1}{4}\left(-\Pi_{146}^{\text{bulk}} - \eta_{(1)}\Pi^{\mathbb{Z}_2^{(1)}} + \eta_{(2)}\Pi^{\mathbb{Z}_2^{(2)}} + \eta_{(3)}\Pi^{\mathbb{Z}_2^{(3)}}\right), \tag{5.19}$$

where $m_2 = -1$ had to be taken into account for the correct signs in front of $\Pi^{\mathbb{Z}_2^{(2)}}$, and the exceptional contributions (for $(\vec{\sigma}_a) = (\vec{0})$) are given by

$$\Pi^{\mathbb{Z}_2^{(1)}} = \left(E_{11}^{(1)} + (-1)^{\tau_a^2}E_{41}^{(1)} + (-1)^{\tau_a^3}E_{14}^{(1)} + (-1)^{\tau_a^2+\tau_a^3}E_{44}^{(1)}\right),$$

$$\Pi^{\mathbb{Z}_2^{(2)}} = \left(\tilde{E}_{11}^{(2)} + (-1)^{\tau_a^1}\tilde{E}_{21}^{(2)} + (-1)^{\tau_a^3}\tilde{E}_{14}^{(2)} + (-1)^{\tau_a^1+\tau_a^3}\tilde{E}_{24}^{(2)}\right), \tag{5.20}$$

$$\Pi^{\mathbb{Z}_2^{(3)}} = \left(\tilde{E}_{11}^{(3)} + (-1)^{\tau_a^1}\tilde{E}_{21}^{(3)} + (-1)^{\tau_a^2}\tilde{E}_{14}^{(3)} + (-1)^{\tau_a^1+\tau_a^2}\tilde{E}_{24}^{(3)}\right).$$

Taking the sum of the fractional cycle with its orientifold image,

$$\Pi_a^{\text{frac}} + \Pi_{a'}^{\text{frac}} = \begin{cases} \frac{1}{2}\left(-\Pi_{146}^{\text{bulk}} + \Pi^{\mathbb{Z}_2^{(1)}}\right) & \text{if } \eta_{\Omega\mathcal{R}} = -1 \\ 2\,\Pi_a^{\text{frac}} & \text{if } \eta_{\Omega\mathcal{R}\mathbb{Z}_2^{(1)}} = -1 \\ \frac{1}{2}\left(-\Pi_{146}^{\text{bulk}} - \Pi^{\mathbb{Z}_2^{(3)}}\right) & \text{if } \eta_{\Omega\mathcal{R}\mathbb{Z}_2^{(2)}} = -1 \\ \frac{1}{2}\left(-\Pi_{146}^{\text{bulk}} + \Pi^{\mathbb{Z}_2^{(2)}}\right) & \text{if } \eta_{\Omega\mathcal{R}\mathbb{Z}_2^{(3)}} = -1 \end{cases}, \tag{5.21}$$

one can see that for the choice $\eta_{\Omega\mathcal{R}\mathbb{Z}_2^{(1)}} = -1$ of the exotic O6-plane $\Pi_a^{\text{frac}} = \Pi_{a'}^{\text{frac}}$ is obtained, while all other possibilities result in $\Pi_a^{\text{frac}} \neq \Pi_{a'}^{\text{frac}}$.

5.3 sLags on the deformed $T^6/(\mathbb{Z}_2 \times \mathbb{Z}_6' \times \Omega\mathcal{R})$ on hexagonal tori

The models that I present in this section were already discussed by me and my collaborators in [110]. For these models, I will always use the lattice of **AAA** orientation and set $\Omega\mathcal{R}$ as the exotic orientifold plane such that $(\eta_{\Omega\mathcal{R}}, \eta_{\Omega\mathcal{R}\mathbb{Z}_2^{(1)}}, \eta_{\Omega\mathcal{R}\mathbb{Z}_2^{(2)}}, \eta_{\Omega\mathcal{R}\mathbb{Z}_2^{(3)}}) = (-1, 1, 1, 1)$. Using the definition of equation (5.16), I obtain for the given choice of exotic O-plane $\eta_{(i)} = -1$ for $i = 1, 2, 3$. The bulk and twisted R-R tadpole cancellation conditions, which have to be satisfied for the following global models, were first derived in [66] and summarised in [110], as well as the supersymmetry conditions on the $T^6/(\mathbb{Z}_2 \times \mathbb{Z}_6' \times \Omega\mathcal{R})$ orientifold. One obtains from these conditions the following *orientifold-even* bulk and exceptional wrapping numbers for a stack of N_a D6-branes,

$$[2X_a + Y_a], \quad 2\hat{x}_{\rho,a}^{(i)} + \hat{y}_{\rho,a}^{(i)} \text{ for } \rho = 1, 2, 3, \quad \hat{y}_{4,a}^{(i)} - \hat{y}_{5,a}^{(i)}, \quad 2(\hat{x}_{4,a}^{(i)} + \hat{x}_{5,a}^{(i)}) + (\hat{y}_{4,a}^{(i)} + \hat{y}_{5,a}^{(i)}), \tag{5.22}$$

and similarly the *orientifold-odd* bulk and exceptional wrapping numbers

$$Y_a, \qquad \hat{y}_{\rho,a}^{(i)} \quad \text{for } \rho = 1,2,3\,, \qquad \hat{y}_{4,a}^{(i)} + \hat{y}_{5,a}^{(i)}\,, \qquad 2(\hat{x}_{4,a}^{(i)} - \hat{x}_{5,a}^{(i)}) + (\hat{y}_{4,a}^{(i)} - \hat{y}_{5,a}^{(i)})\,. \qquad (5.23)$$

The quantities X_a and Y_a are the $\mathbb{Z}_3$ invariant bulk wrapping numbers as defined in [66, 67], which are combinations of the bulk wrapping numbers n_i, m_i, given by

$$X_a \equiv n_a^1 n_a^2 n_a^3 - m_a^1 m_a^2 m_a^3 - \sum_{(ijk)=(123) \text{ cyclic}} n_a^i m_a^j m_a^k\,, \qquad (5.24)$$

$$Y_a \equiv \sum_{(ijk)=(123) \text{ cyclic}} \left(n_a^i n_a^j m_a^k + n_a^i m_a^j m_a^k\right)\,. \qquad (5.25)$$

As explained in section 3.1.3, the exceptional wrapping numbers appear as integer factors in the exceptional contributions of the fractional three-cycles, see equations (3.20) and (3.21), which I rewrite here for convenience,

$$\Pi^{\text{frac}} := \frac{1}{4} \left(\Pi^{\text{bulk}} + \sum_{k=1}^{3} \sum_{\alpha=\alpha_0,\alpha_1} \sum_{\beta=\beta_0,\beta_1} \left(\hat{x}_{\alpha\beta}^{(k)} E_{\alpha\beta}^{(k)} + \hat{y}_{\alpha\beta}^{(k)} \tilde{E}_{\alpha\beta}^{(k)} \right) \right)\,, \qquad (5.26)$$

with the exceptional three-cycles $E_{\alpha\beta}^{(k)}$ and $\tilde{E}_{\alpha\beta}^{(k)}$ defined in equation (3.19), which reads

$$E_{\alpha\beta}^{(k)} := 2 \sum_{q=0}^{M-1} \omega^q \left(e_{\alpha\beta}^{(k)} \otimes \pi_{2k-1} \right)\,, \qquad \tilde{E}_{\alpha\beta}^{(k)} := 2 \sum_{q=0}^{M-1} \omega^q \left(e_{\alpha\beta}^{(k)} \otimes \pi_{2k} \right)\,. \qquad (5.27)$$

I anticipate that the orientifold-odd exceptional wrapping numbers will play an important role in the context of deformations, since they are supposedly in direct correspondence with the number of stabilised twisted complex structure moduli. The reason for that is the fact that for stacks of N_a D6-branes which are *not invariant* under the orientifold involution $\Omega\mathcal{R}$, and which therefore have non-vanishing *orientifold-odd* exceptional wrapping numbers (see equation (5.23)), I find the gauge group $U(N_a)$. Since $U(1) \subset U(N_a)$, I expect that for these stack the twisted complex structure moduli can be stabilised, see section 3.2.3. On the other hand, if the *orientifold-odd* exceptional wrapping numbers vanish, the respective D6-brane stack is *invariant* under the orientifold involution $\Omega\mathcal{R}$, and the gauge groups enhance to either $SO(2N_a)$ or to $USp(2N_a)$. In this case, my expectation is that the moduli are not stabilised, but can varied continuously in flat directions of the moduli space.

5.3.1 Models with $USp(8)^4$ and $SO(8)^4$ gauge groups

To construct models with $SO(2N)$ or $USp(2N)$ gauge groups, one has to use stacks of D6-branes that are either parallel or perpendicular with respect to the O6-planes, and therefore invariant under $\Omega\mathcal{R}$. The bulk R-R tadpole cancellation conditions then imply as simplest setup four stacks $a_{1,\ldots,4}$ of D6-branes, where each stack consists of $N_a = 4$ D6-branes, and one can show that the models of table 18 also satisfy the twisted R-R tadpole conditions.

	n_i, m_i	X	Y	$(\vec{\sigma})$	$\mathbb{Z}_2^{(i)}$	$(\vec{\tau})$	N	Gauge group
Model 4: D6-brane configurations with $USp(8)^4$ or $SO(8)^4$ gauge group								
	n_i, m_i	X	Y	$(\vec{\sigma})$	$\mathbb{Z}_2^{(i)}$	$(\vec{\tau})$	N	Gauge group
Model 4a								
$a_{1\ldots4}$	$(1,0;1,0;1,0)$	1	0	$(0,0,0)$	$(+++)$ $(+--)$ $(-+-)$ $(--+)$	(τ^1, τ^2, τ^3)	4	$USp(8)$
Model 4b								
$\tilde{a}_{1\ldots4}$	$(1,0;1,0;1,0)$	1	0	$(1,1,1)$	$(+++)$ $(+--)$ $(-+-)$ $(--+)$	$(1,1,1)$	4	$SO(8)$
Model 4c								
$\hat{a}_{1\ldots4}$	$(1,0;1,0;1,0)$	1	0	$(1,1,0)$	$(+++)$ $(+--)$ $(-+-)$ $(--+)$	$(0,0,\tau)$	4	$USp(8)$

Table 17: D6-brane configurations of three models on the orientifold $T^6/(\mathbb{Z}_2 \times \mathbb{Z}_6' \times \Omega\mathcal{R})$, which give rise to either $USp(8)^4$ or $SO(8)^4$ gauge groups. Each model consists of $N = 4$ $\Omega\mathcal{R}$-invariant D6-brane stacks, where the stacks only differ in their $\mathbb{Z}_2^{(i)}$ eigenvalues. The parameters n_i, m_i are the torus wrapping numbers, and X, y are the $\mathbb{Z}_3$ invariant bulk wrapping numbers given in equation (5.24). One can see that the three models only differ in their discrete displacements $(\vec{\sigma})$ and in the discrete Wilson lines $(\vec{\tau})$, which determine the gauge groups on a certain stack.

Exceptional wrapping numbers of Model 4a

	$\hat{x}_1^{(1)}$	$\hat{x}_2^{(1)}$	$\hat{x}_3^{(1)}$	$\hat{x}_4^{(1)}$	$\hat{x}_5^{(1)}$	$\hat{y}_{1,\dots,5}^{(1)}$
a_1	$(-1)^{\tau^2}$	$(-1)^{\tau^3}$	$(-1)^{\tau^2+\tau^3}$	0	0	0
a_2	$(-1)^{\tau^2}$	$(-1)^{\tau^3}$	$(-1)^{\tau^2+\tau^3}$	0	0	0
a_3	$(-1)^{\tau^2+1}$	$(-1)^{\tau^3+1}$	$(-1)^{\tau^2+\tau^3+1}$	0	0	0
a_4	$(-1)^{\tau^2+1}$	$(-1)^{\tau^3+1}$	$(-1)^{\tau^2+\tau^3+1}$	0	0	0

	$\hat{x}_1^{(2)}$	$\hat{x}_2^{(2)}$	$\hat{x}_3^{(2)}$	$\hat{x}_4^{(2)}$	$\hat{x}_5^{(2)}$	$\hat{y}_{1,\dots,5}^{(2)}$
a_1	$(-1)^{\tau^3}$	$(-1)^{\tau^1}$	$(-1)^{\tau^3+\tau^1}$	0	0	0
a_2	$(-1)^{\tau^3+1}$	$(-1)^{\tau^1+1}$	$(-1)^{\tau^3+\tau^1+1}$	0	0	0
a_3	$(-1)^{\tau^3}$	$(-1)^{\tau^1}$	$(-1)^{\tau^3+\tau^1}$	0	0	0
a_4	$(-1)^{\tau^3+1}$	$(-1)^{\tau^1+1}$	$(-1)^{\tau^3+\tau^1+1}$	0	0	0

	$\hat{x}_1^{(3)}$	$\hat{x}_2^{(3)}$	$\hat{x}_3^{(3)}$	$\hat{x}_4^{(3)}$	$\hat{x}_5^{(3)}$	$\hat{y}_{1,\dots,5}^{(3)}$
a_1	$(-1)^{\tau^1}$	$(-1)^{\tau^2}$	$(-1)^{\tau^1+\tau^2}$	0	0	0
a_2	$(-1)^{\tau^1+1}$	$(-1)^{\tau^2+1}$	$(-1)^{\tau^1+\tau^2+1}$	0	0	0
a_3	$(-1)^{\tau^1+1}$	$(-1)^{\tau^2+1}$	$(-1)^{\tau^1+\tau^2+1}$	0	0	0
a_4	$(-1)^{\tau^1}$	$(-1)^{\tau^2}$	$(-1)^{\tau^1+\tau^2}$	0	0	0

Table 18: For the exceptional wrapping numbers of Model 4a, only the numbers $\hat{x}_1^{(i)}$, $\hat{x}_2^{(i)}$, and $\hat{x}_3^{(i)}$ (in all sectors $i = 1, 2, 3$) have non-zero entries, which are according to equation (5.22) orientifold-even exceptional wrapping numbers. Hence, only deformations $\varepsilon_1^{(i)}$, $\varepsilon_2^{(i)}$, and $\varepsilon_3^{(i)}$ can be switched on, cf. table 12.

Since I demand that for fractional cycles not only the bulk part, but also the exceptional cycles have to be invariant under the orientifold action, I obtain the additional restrictions

$$(\eta_{(1)}, \eta_{(2)}, \eta_{(3)}) = (-1, -1, -1) \overset{!}{=} \left(-(-1)^{\sigma^2\tau^2+\sigma^3\tau^3}, -(-1)^{\sigma^1\tau^1+\sigma^3\tau^3}, -(-1)^{\sigma^1\tau^1+\sigma^2\tau^2}\right), \quad (5.28)$$

which imply for all i the same value of $\sigma^i \cdot \tau^i$. An analysis of the beta-function coefficients as done in [130, 67] reveals that

$$\sigma^i \cdot \tau^i = \begin{cases} 1 & SO\text{-type gauge groups} \\ 0 & USp\text{-type gauge groups} \end{cases}. \quad (5.29)$$

Exceptional wrapping numbers of Model 4b

	$\hat{x}_1^{(1)}$	$\hat{x}_2^{(1)}$	$\hat{x}_3^{(1)}$	$\hat{x}_4^{(1)}$	$\hat{x}_5^{(1)}$	$\hat{y}_1^{(1)}$	$\hat{y}_2^{(1)}$	$\hat{y}_3^{(1)}$	$\hat{y}_4^{(1)}$	$\hat{y}_5^{(1)}$
$\tilde{a}_1$	0	0	−1	−1	0	0	0	0	1	−1
$\tilde{a}_2$	0	0	−1	−1	0	0	0	0	1	−1
$\tilde{a}_3$	0	0	1	1	0	0	0	0	−1	1
$\tilde{a}_4$	0	0	1	1	0	0	0	0	−1	1

	$\hat{x}_1^{(2)}$	$\hat{x}_2^{(2)}$	$\hat{x}_3^{(2)}$	$\hat{x}_4^{(2)}$	$\hat{x}_5^{(2)}$	$\hat{y}_1^{(2)}$	$\hat{y}_2^{(2)}$	$\hat{y}_3^{(2)}$	$\hat{y}_4^{(2)}$	$\hat{y}_5^{(2)}$
$\tilde{a}_1$	0	0	−1	−1	0	0	0	0	1	−1
$\tilde{a}_2$	0	0	1	1	0	0	0	0	−1	1
$\tilde{a}_3$	0	0	−1	−1	0	0	0	0	1	−1
$\tilde{a}_4$	0	0	1	1	0	0	0	0	−1	1

	$\hat{x}_1^{(3)}$	$\hat{x}_2^{(3)}$	$\hat{x}_3^{(3)}$	$\hat{x}_4^{(3)}$	$\hat{x}_5^{(3)}$	$\hat{y}_1^{(3)}$	$\hat{y}_2^{(3)}$	$\hat{y}_3^{(3)}$	$\hat{y}_4^{(3)}$	$\hat{y}_5^{(3)}$
$\tilde{a}_1$	0	0	−1	−1	0	0	0	0	1	−1
$\tilde{a}_2$	0	0	1	1	0	0	0	0	−1	1
$\tilde{a}_3$	0	0	1	1	0	0	0	0	−1	1
$\tilde{a}_4$	0	0	−1	−1	0	0	0	0	1	−1

Table 19: In Model 4b, one can easily check that all orientifold-odd exceptional wrapping numbers given in equation (5.23) vanish. Firstly, the numbers $\hat{y}_1^{(i)}$, $\hat{y}_2^{(i)}$, and $\hat{y}_3^{(i)}$ are in all sectors $i = 1, 2, 3$ zero, secondly, the combination $\hat{y}_4^{(i)} + \hat{y}_5^{(i)}$ always vanishes, and thirdly, one finds that $2(\hat{x}_4^{(i)} - \hat{x}_5^{(i)}) + (\hat{y}_4^{(i)} - \hat{y}_5^{(i)}) = 0$ for all three sectors. The non-vanishing orientifold-even exceptional wrapping numbers, cf. equation (5.22), are $2\hat{x}_3^{(i)}$, $\hat{y}_4^{(i)} - \hat{y}_5^{(i)}$, and $2(\hat{x}_4^{(i)} + \hat{x}_5^{(i)})$.

Furthermore, the chosen setup of D6-branes together with the R-R tadpole cancellation conditions is only consistent if all 16 D6-branes have the same Wilson lines $\vec{\tau}$ and displacements $\vec{\sigma}$. The specifications for three concrete models with these properties are displayed in table 17. The parameters $\vec{\tau}$, $\mathbb{Z}_2^{(i)}$, and $\vec{\sigma}$ are incorporated in the exceptional wrapping numbers in non-trivial ways, where the concrete equations can be found in [66]. The exceptional wrapping numbers of these models are listed in tables 18 to 20, and one can check that all orientifold-odd combinations summarised in equation (5.23) vanish due to the orientifold invariance imposed on all D6-branes. Thus, only flat directions should be

<table>
<caption>Exceptional wrapping numbers of Model 4c</caption>
</table>

	$\hat{x}_1^{(1)}$	$\hat{x}_2^{(1)}$	$\hat{x}_3^{(1)}$	$\hat{x}_4^{(1)}$	$\hat{x}_5^{(1)}$	$\hat{y}_1^{(1)}$	$\hat{y}_2^{(1)}$	$\hat{y}_3^{(1)}$	$\hat{y}_4^{(1)}$	$\hat{y}_5^{(1)}$
$\hat{a}_1$	-1	0	0	0	$(-1)^{\tau+1}$	0	0	0	$(-1)^{\tau+1}$	$(-1)^{\tau}$
$\hat{a}_2$	-1	0	0	0	$(-1)^{\tau+1}$	0	0	0	$(-1)^{\tau+1}$	$(-1)^{\tau}$
$\hat{a}_3$	1	0	0	0	$(-1)^{\tau}$	0	0	0	$(-1)^{\tau}$	$(-1)^{\tau+1}$
$\hat{a}_4$	1	0	0	0	$(-1)^{\tau}$	0	0	0	$(-1)^{\tau}$	$(-1)^{\tau+1}$

	$\hat{x}_1^{(2)}$	$\hat{x}_2^{(2)}$	$\hat{x}_3^{(2)}$	$\hat{x}_4^{(2)}$	$\hat{x}_5^{(2)}$	$\hat{y}_1^{(2)}$	$\hat{y}_2^{(2)}$	$\hat{y}_3^{(2)}$	$\hat{y}_4^{(2)}$	$\hat{y}_5^{(2)}$
$\hat{a}_1$	0	-1	0	$(-1)^{\tau}$	$(-1)^{\tau}$	0	0	0	0	0
$\hat{a}_2$	0	1	0	$(-1)^{\tau+1}$	$(-1)^{\tau+1}$	0	0	0	0	0
$\hat{a}_3$	0	-1	0	$(-1)^{\tau}$	$(-1)^{\tau}$	0	0	0	0	0
$\hat{a}_4$	0	1	0	$(-1)^{\tau+1}$	$(-1)^{\tau+1}$	0	0	0	0	0

	$\hat{x}_1^{(3)}$	$\hat{x}_2^{(3)}$	$\hat{x}_3^{(3)}$	$\hat{x}_4^{(3)}$	$\hat{x}_5^{(3)}$	$\hat{y}_1^{(3)}$	$\hat{y}_2^{(3)}$	$\hat{y}_3^{(3)}$	$\hat{y}_4^{(3)}$	$\hat{y}_5^{(3)}$
$\hat{a}_1$	0	0	-1	-1	0	0	0	0	1	-1
$\hat{a}_2$	0	0	1	1	0	0	0	0	-1	1
$\hat{a}_3$	0	0	1	1	0	0	0	0	-1	1
$\hat{a}_4$	0	0	-1	-1	0	0	0	0	1	-1

Table 20: In Model 4c, all orientifold-odd exceptional wrapping numbers vanish, cf. equation (5.23), which can be easily checked. According to equation (5.22), for the orientifold-even exceptional wrapping numbers, which have to be considered separately for the three sectors, one finds $2\hat{x}_1^{(1)}$, $2\hat{x}_2^{(2)}$, and $2\hat{x}_3^{(3)}$, as well as $\hat{y}_4^{(1)} - \hat{y}_5^{(1)}$, $\hat{y}_4^{(3)} - \hat{y}_5^{(3)}$, and $2(\hat{x}_4^{(i)} + \hat{x}_5^{(i)})$ (for $i = 1, 2, 3$).

observed for all $5 + 5 + 5$ deformations, i.e. I expect that no moduli are stabilised at the orbifold point.

Model 4a: In the first model, all fractional cycles that are wrapped by D6-branes (cf. equation (5.26)) are purely horizontal and run through the origin. Therefore, the bulk cycles are the *sLag* cycles $\mathbf{aI} \otimes \mathbf{aI} \otimes \mathbf{aI}$, and also all exceptional three-cycles $E_{13}^{(i)}$, $E_{31}^{(i)}$, and $E_{33}^{(i)}$, see equation (5.27), are already *sLag* by themselves, cf. also table 18. Hence, all fractional cycles in this model stay *sLag* under deformations. The deformations with the parameters ε_1, ε_2, ε_3, give rise to volumes as in figures 21(b) and 22(a), where the factors

from the respective wrapping numbers have to be taken into account.

Model 4b: Here, the fractional cycles are also horizontal, but all displaced. Therefore the bulk part is the *sLag* cycle **aIII** ⊗ **aIII** ⊗ **aIII**, and the exceptional three-cycles are $E_{24}^{(i)}$, $E_{42}^{(i)}$, $E_{22}^{(i)}$, and $E_{44}^{(i)}$. Due to the choice of discrete displacements, one can compute that also in this model all exceptional cycles are *sLag* when the $\mathbb{Z}_3$ orbifold images are taken into account, see table 19. Thus, the deformation parameters $\varepsilon_3^{(i)}$ and $\varepsilon_{4+5}^{(i)}$ can be switched on, and the volumes of these fractional cycles behave as displayed in figures 21(a) and 21(b).

Model 4c: In this model, the two horizontal one-cycles in the first two tori are displaced, while the horizontal one-cycle in the third torus is not. This implies that the exceptional contributions depend on the $\mathbb{Z}_2^{(i)}$ sector under consideration, but as for Model 4b, the relative signs are arranged such that under the orbifold image of $\mathbb{Z}_3$ only *sLag* cycles remain. The exceptional wrapping numbers for this model are listed in table 20, and one finds that in all sectors deformations $\varepsilon_{4+5}^{(i)}$, can be applied, while the other allowed deformations depend on the sector, namely $\varepsilon_1^{(1)}$, $\varepsilon_2^{(2)}$, and $\varepsilon_3^{(3)}$. The volumes of the fractional cycles (with the corresponding wrapping numbers assigned) change under the deformations as depicted in figures 21(a), 21(b), and 22(a).

5.3.2 A Pati-Salam model with gauge groups $U(N)$

The model that I discuss in this section was developed in [67] and consists of five D6-brane stacks, which are all not orientifold-invariant, contrary to the SO- and USp-type models of the last section. Therefore, one obtains $U(N)$ gauge groups on all brane stacks, for which one finds non-trivial D-terms for those fractional D6-branes which run over a deformed singularity. In [67] it was shown that this model is globally consistent and provides three generations of particles. The five factors $U(1) \subset U(N)$ acquire masses due to the so-called Stückelberg mechanism, see e.g. [9] for more information on that. The details of this model with gauge group $U(4) \times U(2)^4$ are summarised in table 21.

The exceptional wrapping numbers of this model can be found in table 22, where one can read off the following properties,

$$(\hat{x}_2^{(1)}, \hat{y}_2^{(1)}) = (\hat{x}_2^{(2)}, \hat{y}_2^{(2)}) = (\hat{x}_2^{(3)}, \hat{y}_2^{(3)}) = (\hat{x}_1^{(3)}, \hat{y}_1^{(3)}) = (0, 0) \,, \tag{5.30}$$

$$(\hat{x}_3^{(3)}, \hat{y}_3^{(3)}) = (\pm 1, 0) \,. \tag{5.31}$$

	n_i, m_i	X	Y	$\mathbb{Z}_2^{(i)}$	$(\vec{\tau})$	$(\vec{\sigma})$	N	Gauge group
	Model 5: D6-brane configuration of a global Pati-Salam model							
a	(0,1;1,0;1,-1)	1	0	(+ + +)	(0,0,1)	(1,1,1)	4	$U(4)$
b	(0,1;1,0;1,-1)	1	0	(− − +)	(0,1,1)	(1,1,1)	2	$U(2)_L$
c	(0,1;1,0;1,-1)	1	0	(− + −)	(1,0,1)	(1,1,1)	2	$U(2)_R$
d	(-1,2;2,-1;1,-1)	3	0	(− − +)	(0,0,1)	(1,1,1)	2	$U(2)_d$
e	(1,0;1,0;1,0)	1	0	(+ − −)	(1,1,1)	(1,1,0)	2	$U(2)_e$

Table 21: D6-brane configuration of a globally defined Pati-Salam model on the orientifold $T^6/(\mathbb{Z}_2 \times Z_6' \times \Omega\mathcal{R})$ with five stacks of D6-branes that are all not invariant under the orientifold involution $\Omega\mathcal{R}$. The gauge group is $\mathrm{SU}(4)_a \times \mathrm{SU}(2)_b \times \mathrm{SU}(2)_c \times \mathrm{SU}(2)_d \times \mathrm{SU}(2)_e \times \mathrm{U}(1)^5_{\mathrm{massive}}$.

For these $1 + 1 + 3$ exceptional cycles in the three $\mathbb{Z}_2^{(i)}$ sectors ($i = 1, 2, 3$) I expect flat directions and therefore no stabilisation of the respective moduli. In particular, while there is no coupling of the D6-brane stack to the cycles of equation (5.30), I expect for the exceptional cycle in equation (5.31), I can adjust the gauge coupling in a smooth way by changing the volume of the cycle. This makes the deformation $\varepsilon_3^{(3)}$ particularly interesting for model building because, due to the exceptional wrapping numbers $\hat{x}_{3,a}^{(3)}$ displayed in table 22, one finds that upon deformation the volume of the $U(4)$ branes is reduced, while the volume of the $U(2)_{L/R}$ branes is enhanced.

Contrary to these cycles, I expect for the other $4 + 4 + 2$ directions supersymmetry breaking upon deformation and therefore stabilised moduli at the orbifold point.

The considerations of this section 5.3 can be straightforwardly applied to models on $T^6/(\mathbb{Z}_2 \times \mathbb{Z}_6 \times \Omega\mathcal{R})$ orientifolds. Indeed, me and my collaborators already worked out the exceptional wrapping numbers for several models [112], which were taken from [69, 70]. Naively, we expect for these models that, as for the just presented Pati-Salam model, the twisted complex structure moduli should be stabilised for non-vanishing orientifold-odd wrapping numbers. On the other hand, in case that an exceptional cycle has non-zero orientifold-even, but vanishing orientifold-odd wrapping numbers, we expect that the gauge coupling can be varied with changes in the volume of the exceptional cycle. If both the orientifold-even and -odd exceptional wrapping numbers are zero, the brane stack does not couple to the corresponding deformation, and one should find a flat direction in the moduli space. These expectations have to be checked in future investigations.

Exceptional wrapping numbers of Model 5									
	$\hat{x}_1^{(1)}$	$\hat{x}_2^{(1)}$	$\hat{x}_3^{(1)}$	$\hat{x}_4^{(1)}$	$\hat{x}_5^{(1)}$	$\hat{y}_1^{(1)}$	$\hat{y}_2^{(1)}$	$\hat{y}_3^{(1)}$	$\hat{y}_4^{(1)}$	$\hat{y}_5^{(1)}$
a	0	0	1	1	-2	0	0	0	-1	1
b	0	0	-1	1	0	0	0	0	-1	1
c	0	0	-1	-1	2	0	0	0	1	-1
d	0	0	1	-3	2	0	0	-2	3	-1
e	-1	0	0	0	1	2	0	0	-1	-1

	$\hat{x}_1^{(2)}$	$\hat{x}_2^{(2)}$	$\hat{x}_3^{(2)}$	$\hat{x}_4^{(2)}$	$\hat{x}_5^{(2)}$	$\hat{y}_1^{(2)}$	$\hat{y}_2^{(2)}$	$\hat{y}_3^{(2)}$	$\hat{y}_4^{(2)}$	$\hat{y}_5^{(2)}$
a	0	0	1	-1	0	0	0	0	-1	1
b	0	0	-1	1	0	0	0	0	1	-1
c	0	0	-1	1	0	0	0	0	-1	1
d	0	0	-1	1	0	0	0	2	1	-3
e	1	0	0	0	-1	-2	0	0	1	1

	$\hat{x}_1^{(3)}$	$\hat{x}_2^{(3)}$	$\hat{x}_3^{(3)}$	$\hat{x}_4^{(3)}$	$\hat{x}_5^{(3)}$	$\hat{y}_1^{(3)}$	$\hat{y}_2^{(3)}$	$\hat{y}_3^{(3)}$	$\hat{y}_4^{(3)}$	$\hat{y}_5^{(3)}$
a	0	0	-1	1	0	0	0	0	-1	-1
b	0	0	1	1	-2	0	0	0	-1	1
c	0	0	1	1	2	0	0	0	-1	-1
d	0	0	-1	-1	0	0	0	0	1	1
e	0	0	1	-1	0	0	0	0	1	-1

Table 22: For the exceptional wrapping numbers of Model 5, I find that $\hat{y}_2^{(i)}$ (with $i = 1, 2, 3$), $\hat{y}_1^{(3)}$, and $\hat{y}_3^{(3)}$, as well as the numbers $\hat{x}_2^{(i)}$ and $\hat{x}_1^{(3)}$ are zero for all stacks. Further implications of the exceptional wrapping numbers like their contributions to the orientifold-even and -odd wrapping numbers of equations (5.22) and (5.23) are discussed in the main text.

6 Conclusions and Outlook

In this thesis, I presented explicit complex structure deformations of fractional *special Lagrangian* cycles on which D6-branes are wrapped, where the $\mathbb{Z}_2$ singularities of different type IIA/$\Omega\mathcal{R}$ orientifolds were deformed. As explicit examples, I studied the orientifolds $T^6/(\mathbb{Z}_2 \times \mathbb{Z}_{2M} \times \Omega\mathcal{R})$ of $2M = 2, 6, 6'$ with discrete torsion. I also discussed the local deformations $\mathbb{C}^2/\mathbb{Z}_2$ and $\mathbb{C}^3/(\mathbb{Z}_2 \times \mathbb{Z}_2)$ and the toy model of $T^4/(\mathbb{Z}_2 \times \Omega\mathcal{R})$, which actually belongs to type IIB string theory and which incorporated fractional D7-branes. While the orientifolds with $2M = 2, 6'$, the local models, and the toy model $T^4/(\mathbb{Z}_2 \times \Omega\mathcal{R})$ were studied together with my collaborators Jun.-Prof. Dr. Gabriele Honecker and Dr. Michael Blaszczyk, see [109–111], the discussion of the orientifold with $2M = 6$ is completely new. In the examples that I presented here in my thesis, I gave often much more details than appeared in the publications with my collaborators, which makes the description partly rather technical. The aim is here to give the reader the possibility to easily reproduce my results, and maybe to further develop them or to apply them to different orbifold setups in the future. Therefore, I also give a short summary in appendix B on which functions I used in Mathematica.

Based on the idea of Vafa and Witten [108], we developed for the first time an explicit formalism for the complex structure deformations of the $\mathbb{Z}_2$ orbifold fixed points. For this purpose, we used the language of hypersurfaces in weighted complex projective spaces that already appeared in the context of heterotic string theories, see the discussion and references in the introductory chapter. As I showed in my thesis in explicit calculations, in this language one cannot only directly switch on certain deformations, but one can also study their impact on physical quantities like the gauge couplings and supersymmetry breaking. In addition, I could concretely analyse which complex structure moduli were stabilised by certain deformations, where the mechanism of Fayet-Iliopoulos terms in the context of D-terms was used.

As a starting point, we studied the concrete expressions of Lagrangian one-cycles on the two-torus in this description [109, 110], where my main contribution was a detailed analysis of the properties and symmetries of all possible *sLag* cycles. In addition, we translated the shift symmetry on the two-torus, which makes it possible to exchange singularities (and also fractional cycles) with different singularities (cycles), to the hypersurface language. The shifts proved later to be a useful tool in cases where explicit descriptions were hard to find, and where for example a shift of the respective object onto the real axis could lead to a tractable formulation. In my thesis, I presented these findings in great detail in section 4.1.

Next, I treated the local deformations $\mathbb{C}^2/\mathbb{Z}_2$ and $\mathbb{C}^3/(\mathbb{Z}_2 \times \mathbb{Z}_2)$ in section 4.2. This was done in order to familiarise the reader with the procedure of concrete deformations and to show how the exceptional cycles on the orbifolds can be described locally, where the discussion is similar to the one in [109]. I also presented a plot of the volume of the exceptional cycle of $\mathbb{C}^2/\mathbb{Z}_2$ as a function of the deformation parameter, where the volume was obtained by integrating the holomorphic two-form over the exceptional cycle. Since the singularities of the orbifolds that I deformed in the following sections are locally of the form $\mathbb{C}^2/\mathbb{Z}_2$, the square-root shape of this integral reappeared many times and was the characteristic property to see if a certain fractional cycle has an exceptional contribution. I showed the relation between deformations in positive and negative direction and the calibration of the exceptional cycles.

After that, I turned to the toy model of the $T^4/\mathbb{Z}_2$ orbifold that I studied together with my collaborators in [109]. In section 4.3, I presented our hypersurface formalism for the orbifold setup $T^4/\mathbb{Z}_2$ (which can easily be generalised to orbifolds $T^4/\mathbb{Z}_{2M}$). As in [109], I restricted in this section the description to square torus lattices, which simplifies the hypersurface equation considerably, and which is sufficient for most applications. As an extra, I studied pure bulk cycles in more detail, where I introduced two different constructions and commented on how much the different cycles are affected by deformations. In a next step I analysed the exceptional cycles, where I found new pictorial representations of a deformation that give a good intuitive understanding of which exceptional cycles are deformed and how they behave. I also showed the direct integration of a deformed exceptional cycle, which, for small values of the deformation parameter, indeed has the same shape as the local deformation on $\mathbb{C}^2/\mathbb{Z}_2$. Finally, I presented the concrete integrals over all fractional *sLag* cycles on the square torus, which can be nicely visualised in a two-dimensional diagram. The integrals were obtained by directly integrating over the fractional cycle, and the plots revealed by either linear or square-root-like behaviour if an exceptional contribution was present and with which sign it appeared. These plots together with a detailed analysis of the concrete deformations were my main contributions to the publication [109].

In section 4.4, I treated the $T^6/(\mathbb{Z}_2 \times \mathbb{Z}_2 \times \Omega\mathcal{R})$ orientifold on square torus lattices that also appeared in our publication [109]. In this section, I discussed the modifications in the hypersurface equation compared to the toy model $T^4/\mathbb{Z}_2$ and discussed the meaning of each term. After that, I commented on the cycle structure, which implies that if only one of the three sectors is deformed, the deformations can be easily deduced from the $T^4/\mathbb{Z}_2$ orbifold. More general deformations turned out to be difficult to compute for several reasons, but some specific deformations could be constructed [109]. I did not reproduce these results in my thesis, but instead I refer the interested reader to our article.

The treatment of the phenomenologically appealing $T^6/(\mathbb{Z}_2 \times \mathbb{Z}_6' \times \Omega\mathcal{R})$ orientifold on tilted

torus lattices, which all have necessarily hexagonal shape, is similar to our publication [110], and is discussed in my thesis in section 4.5. To find the hypersurface formalism of this orientifold, we used the description of $\mathbb{Z}_2 \times \mathbb{Z}_2$ and imposed an additional $\mathbb{Z}_3$ symmetry on the hypersurface equation, which leads to a hexagonal torus lattice. Furthermore, certain fixed points and deformation parameters are identified and can be grouped into orbits, as I found together with my collaborators. Similarly to the toy model of $T^4/(\mathbb{Z}_2 \times \Omega\mathcal{R})$, I started with the description of different bulk cycles. After an analysis of many different bulk cycles and their behaviour under deformations, performed by me and Dr. Michael Blaszczyk, one especially suitable candidate could be found, as already presented in [110]. For the subsequent analysis of the exceptional cycles in my thesis, I extended the results that I obtained together with my collaborators in [110] by many computational details. In addition, I studied in this section the behaviour of the exceptional cycles by using my new pictorial tool, which indeed improved the understanding of the structure of the deformations considerably. With these pictures it was evident why at some places correction terms had to be included into the hypersurface equation in order to keep the undeformed singularities singular, and it could be checked qualitatively if the computed correction terms had the desired properties. The correction terms were first derived by Dr. Michael Blaszczyk, but I cross-checked the results and gave the step-by-step calculations in appendix A. Due to some technical issues, it was not possible to calculate all integrals over fractional cycles directly. Therefore, me and my collaborators approached these cycles by either integrating over bulk and exceptional parts separately and then combining the results, or by accessing the exceptional cycle indirectly by subtracting suitable cycles from each other.

Finally, in section 4.6 I showed my first new results for the phenomenologically very attractive orientifold $T^6/(\mathbb{Z}_2 \times \mathbb{Z}_6 \times \Omega\mathcal{R})$, where unexpected technical issues arose. I could write down the hypersurface equation and identify the fixed point orbits and restrictions on the deformation parameters, where a closer look revealed that only one deformation in the first sector had the same structure as on the $\mathbb{Z}_2 \times \mathbb{Z}_6'$ orbifold. All other deformations had to be analysed anew in detail. In particular, in sector one I was able to observe the local behaviour of all exceptional cycles, but I could not find the correction terms that would be necessary to perform global deformations. In the sectors two and three, which behave completely analogously to each other, and which are a mixture of one rectangular and one hexagonal torus, I could directly integrate all *sLag* cycles. I found that due to the different structure of the two tori, also the deformations behave less symmetrically and e.g. also some cycles that are distant from the deformed singularity are highly affected by the deformation (in contrast to the $T^6/(\mathbb{Z}_2 \times \mathbb{Z}_2)$ and $T^6/(\mathbb{Z}_2 \times \mathbb{Z}_6')$ models which exhibit symmetries between all three $\mathbb{Z}_2$ sectors).

Since the focus of my thesis was mainly to develop a language for concrete deformations

and to study concrete deformations in different orbifold setups, I did not construct new models in chapter 5, but I took them from our publications [109] and [110]. The main purpose of the concrete models that I presented in this section was to check if our method of complex structure deformations behaves as expected and to give a physical motivation. More concretely, on the one hand I studied models of either $SO(2N)$ and $USp(2N)$ gauge groups, for which, as expected, all fractional cycles stayed *sLag* under deformations. Thus, no moduli were stabilised, but they could be varied smoothly, and therefore also the gauge coupling constants changed. On the other hand, in the models with $U(N)$ gauge groups, it was indeed possible to stabilise several or all complex structure moduli for those fractional cycles which lost their *sLag* property under deformations, i.e. which developed an imaginary contribution to the integral.

In the future, one could apply this method to more concrete models, especially to phenomenologically appealing ones with Standard Model or GUT spectrum. For example, the orbifold $T^6/(\mathbb{Z}_2 \times \mathbb{Z}_6)$, which was not studied before in the context of deformations, would be an interesting candidate. Unfortunately, this orbifold will need further investigation due to unexpected technical difficulties. Hence, the idea is, after some more research, to publish my new findings together with my collaborators Jun.-Prof. Dr. Gabriele Honecker and Dr. Wieland Staessens in another article, where my collaborators will contribute the gauge threshold corrections for this orbifold [112], and we will compare the sizes of the different effects on the gauge couplings.

A further application is to study dual models in the heterotic $E_8 \times E_8$ string theory. Due to the conjectured M-theory duality, as mentioned in the introductory chapter 1, one should find such dual models after deformation and blow-up to a completely smooth type IIA string theory background, where I assume that the models under consideration are supersymmetric. As a first ansatz one could study D6-brane models which only contain $SO(2N)$ and $USp(2N)$ gauge groups, where the expectation is that under the deformation all codimension three singularities vanish and therefore a smooth background remains. A useful tool for such a systematic analysis could be the data base http://orbifolder.hepforge.org/, in which (by the duality relation) the same orbifolds with the same gauge groups as in type IIA string theory should be searched for. In a next step, one could also compare the particle spectra in type IIA and in the heterotic $E_8 \times E_8$ string theory for generic $\Pi_i SU(N_i)$ groups, or study which parameters in the $E_8 \times E_8$ string theory are involved in the process of the deformation.

A Calculation of the correction terms on $T^6/(\mathbb{Z}_2 \times \mathbb{Z}_6')$

A.1 Calculation of the correction term $\varepsilon_3(\varepsilon_{4+5})$

The starting point for the calculation of the correction terms is the condition $f = \mathrm{d}f = 0$ for the existence of singularities in the hypersurface f. From $\partial f/\partial y$ I obtain the constraint $y = 0$, and together with $f = 0$ I find $f \equiv \tilde{y}^2 = 0$, where $\tilde{y}^2$ is given in equation (4.69) for the hypersurface. I take a configuration with $\varepsilon_1 = \varepsilon_2 = \varepsilon_{4-5} = 0$ and choose $v_i \equiv 1$ such that equation (4.69) reads

$$\tilde{y}^2(x_2, x_3, \varepsilon_3, \varepsilon_{4+5}) = \left(x_2^3 - 1\right)\left(x_3^3 - 1\right) - \varepsilon_3\left(1 + x_2^2 x_3 + x_2 x_3^2\right) - \varepsilon_{4+5}\left(2 - x_2^2 x_3 - x_2 x_3^2\right), \quad \text{(A.1)}$$

which preserves the symmetry $x_2 \leftrightarrow \overline{x_3}$. As a first step, I insert the exceptional cycle $x_2 = \overline{x_3} = a + ib$ into that, which leads to a purely real expression for $\tilde{y}^2(a, b, \varepsilon_3, \varepsilon_{4+5}) = 0$ that can be rewritten as a function $\varepsilon_3(a, b, \varepsilon_{4+5})$. By finding expressions for the coordinates a, b that depend on ε_3, ε_{4+5}, I will obtain the correction term $\varepsilon_3(\varepsilon_{4+5})$.
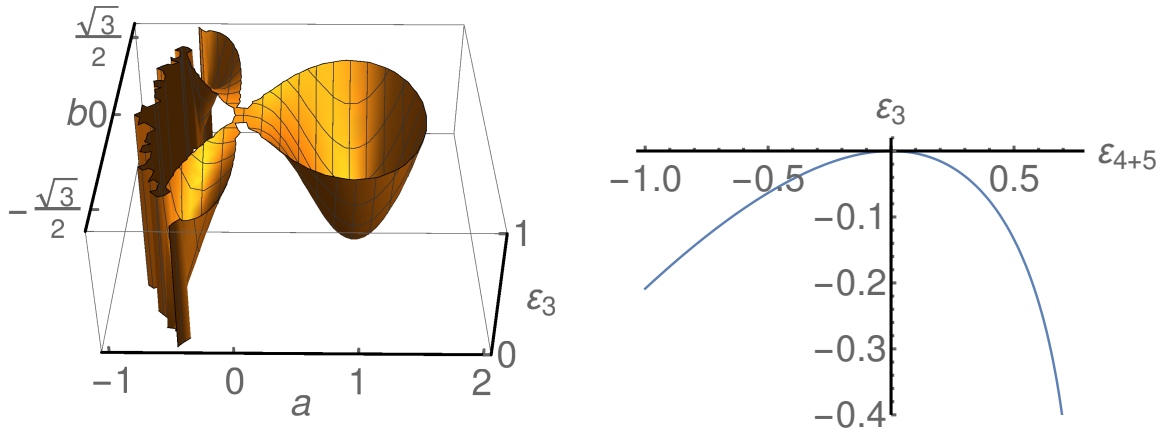
(a) Surface of the function $\varepsilon_3(a, b)$ for parameter $\varepsilon_{4+5} = 0$. For the fixed points $(33),(42),(24)$ at $(a, b) = (1, 0), \left(-\frac{1}{2}, -\frac{\sqrt{3}}{2}\right), \left(-\frac{1}{2}, +\frac{\sqrt{3}}{2}\right)$, respectively, which are local minima of the depicted surface, on finds $\varepsilon_3(a, b) = 0$.

(b) Correction term to the deformation parameter ε_3 as a function of ε_{4+5}.

Figure 31: Illustrations to the correction term $\varepsilon_3(\varepsilon_{4+5})$.

The plots of the function $\varepsilon_3(a, b, \varepsilon_{4+5})$ with respect to a, b and with different fixed values for ε_{4+5} make it possible to observe how the size of the parameter ε_3 changes at the singularity (33) with position $(a, b) = (1, 0)$, as exemplarily done in figure 31(a) for $\varepsilon_{4+5} = 0$. Actually, ε_3 should not change at all at the singularities and stay zero when ε_{4+5} is varied, but the plots reveal that this is not the case. Having had a look at several plots for $\varepsilon_3(1, b)$, I

suggest that there is no change in this direction, while for $\varepsilon_3(a,0)$ the minimum has a negative value and is slightly shifted in its position, i.e. $a = a(\varepsilon_3, \varepsilon_{4+5})$.

Since the condition $f = \mathrm{d}f = 0$ directly translates to the new coordinates a, b, I confirm this assumption by solving $\frac{\partial \varepsilon_3(a,b,\varepsilon_{4+5})}{\partial b} = 0$ for b, which provides indeed a solution $b = 0$. With the restriction $b = 0$ it is now possible to solve $\frac{\partial \tilde{y}^2(a,0,\varepsilon_3,\varepsilon_{4+5})}{\partial a} = 0$, which yields the result $a = (1 + \varepsilon_3 - \varepsilon_{4+5})^{1/3}$. Finally, one can solve $\tilde{y}^2(a(\varepsilon_3, \varepsilon_{4+5}), 0, \varepsilon_3, \varepsilon_{4+5}) = 0$ to arrive at the correction term

$$
\begin{aligned}
\varepsilon_3(\varepsilon_{4+5}) &= -\frac{3}{2} + \varepsilon_{4+5} + \frac{1}{2}\sqrt{9 - 12\varepsilon_{4+5}} \\
&= -\frac{1}{3}\varepsilon_{4+5}^2 - \frac{2}{9}\varepsilon_{4+5}^3 + \mathcal{O}(\varepsilon_{4+5}^4)
\end{aligned}
\tag{A.2}
$$

that is also presented in the plot of figure 31(b). One should note that the analytic expression is only valid up to $\varepsilon_{4+5} \leq \frac{3}{4}$ because otherwise the expression has imaginary values.

A.2 Calculation of the correction term $\varepsilon_{4+5}(\varepsilon_3)$

The calculation of the correction term $\varepsilon_{4+5}(\varepsilon_3)$ is somewhat more involved. The same approach as in the previous section turned out to be difficult because the fixed points (42), (24) change their position in both variables a and b when the deformation ε_3 is switched on. Therefore, I will first shift fixed point (42), which shall stay singular, to the position of (33), and (24) to (11), as explained in section 4.1. I use again equation (A.1) and apply the shift transformation λ_2 on the coordinate x_2 and λ_4 on x_3 as defined in equation (4.18). After that I insert the equation for the exceptional cycle, $x_2 = \overline{x_3} = a + ib$ as above. Together with the condition $\tilde{y}^2(a,b,\varepsilon_3,\varepsilon_{4+5}) = 0$ for the singularities I can write $\varepsilon_{4+5}(a,b,\varepsilon_3)$, which is illustrated in figure 32(a).

The following steps are similar to the one of section A.1. Using figure 32(a) with different values $\varepsilon_3 \neq 0$, I find that the coordinate a does not feel the deformation, while b depends on ε_3. Solving $\frac{\partial \varepsilon_{4+5}(1,b,\varepsilon_3)}{\partial b} = 0$ for b, I get

$$
b^6\varepsilon_3 + b^5(-9 - 3\varepsilon_3) + \varepsilon_3 + b^4(9 + 6\varepsilon_3) + b^3(-27 - 7\varepsilon_3) + b^2(9 + 6\varepsilon_3) + b(-9 - 3\varepsilon_3) = 0, \tag{A.3}
$$

which means that b is given by a root expression and cannot simply be resolved as a function of ε_3. Thus, for this correction I cannot find an analytic expression, but nevertheless I can write down the series expansion

$$
\varepsilon_{4+5} = -\frac{1}{9}\varepsilon_3^2 - \frac{1}{81}\varepsilon_3^3 + \mathcal{O}(\varepsilon_3^5), \tag{A.4}
$$

which is presented in the plot in figure 32(b).

126
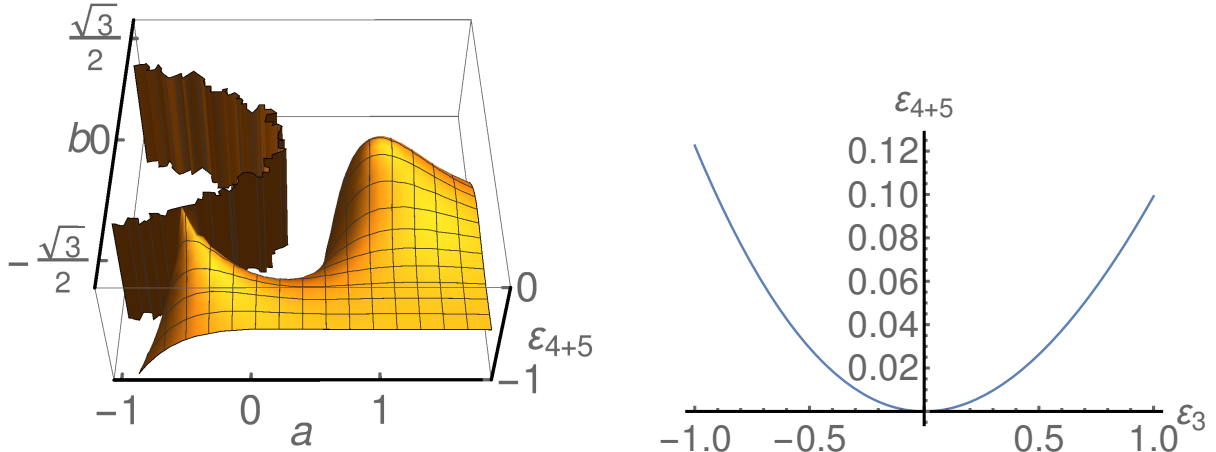
(a) After the shift $\lambda_2(x_2) = \lambda_4(\overline{x_3})$ I find the singularities (33) and (42) of the function $\varepsilon_{4+5}(a, b)$ at $(a, b) = (-\frac{1}{2}, -\frac{\sqrt{3}}{2})$ and $(1, 0)$, respectively. For the parameter $\varepsilon_3 = 0$, I find the value $\varepsilon_{4+5}(a, b) = 0$ at these points.

(b) Correction term of the deformation parameter ε_{4+5} as a function of ε_3.

Figure 32: Illustrations of the correction term $\varepsilon_{4+5}(\varepsilon_3)$.

B   Implementation in Wolfram Mathematica

In this appendix, I will explain how I concretely implemented the results of my thesis in Wolfram Mathematica. In case that the reader tries to perform some explicit calculations by him/herself or to reproduce my figures, it will be of some help to have these details already at hand. More details on the built-in functions that I describe in the following can be found in the Wolfram Documentation directly in the Mathematica "Help" menu or at http://reference.wolfram.com/language/.

Figures 2 and 3 in section 4.1, which depict the real and imaginary part of the Weierstrass $\wp$-function (see equation (2.31)) imposed on torus lattices of different shape, incorporate several built-in Mathematica functions. Firstly, I used

$$\text{ContourPlot3D}[f == g, \{x, x_{\min}, x_{\max}\}, \{y, y_{\min}, y_{\max}\}, \{z, z_{\min}, z_{\max}\}], \qquad \text{(B.1)}$$

where for x and y I inserted the range of the lattice vectors (in particular, for y only the value of the imaginary part of the second lattice vector), and with appropriate values for z on the vertical axis (usually of the order of ten). Secondly, I utilised the built-in Mathematica function

$$\text{WeierstrassP}[z, \{g_2, g_3\}], \qquad \text{(B.2)}$$

127

where g_2, g_3 are the Weierstrass invariants, defined in equation (2.34), which were set to $\{4, 0\}$ for the square and to $\{0, 4\}$ for the hexagonal torus lattice. The complex coordinate z simply specifies the position on the torus lattice, as in $\wp(z)$. For $f == g$ (where the symbol "==" stands for equality in Mathematica) I inserted Re[WeierstrassP[$z, \{g_2, g_3\}$]]$-z == 0$ (or analogously the imaginary part). Also the similar function WeierstrassPPrime[$z, \{g_2, g_3\}$] exists that computes the derivative $\wp'(z)$ (as well as functions for the invariants and half lattice vectors). Thirdly, the option MeshFunctions of ContourPlot3D[...] together with the option "Mesh $\rightarrow \{\{0\}\}$" gave me the possibility to depict certain Lagrangian one-cycles on the surface of the Weierstrass function $\wp(z)$.

In figure 10 of section 4.3.2, I depicted arbitrary torus one-cycles in the hypersurface language, which were parametrised by $x(t)$ as defined in equation (4.40). This can be easily implemented in Mathematica by making use of ParametricPlot[$\{f_x, f_y\}, \{t, t_{\min}, t_{\max}\}$], which in my case schematically reads

$$\text{ParametricPlot}\big[\big\{\,\text{Re}\,(\text{WeierstrassP}[x(t), \{g_2, g_3\}]),$$
$$\{\,\text{Im}\,(\text{WeierstrassP}[x(t), \{g_2, g_3\}])\}\big\}, \{t, 0, 1\}\big]\,. \tag{B.3}$$

It is clear that in this way also the *(s)Lag* lines in figures 4, 5, and 6 can be depicted.

Beginning from section 4.3, I inserted the relations $x_1 = a + ib$, $x_2 = \pm(a - ib)$ into a certain hypersurface equation, which means into the function $y^2(x_1, x_2)$ of e.g. equation (4.34) or (4.53) (which also depend on all deformation parameters ε_i), in order to describe a purely exceptional cycle. For this replacement I employed the built-in Mathematica function ReplaceAll[rules], which was also utilised for the shift transformations. In this context also Simplify[expr], FullSimplify[expr], and ComplexExpand[expr] were helpful from time to time to find a suitable form of the expression under consideration, either for further calculations or to better understand the structure of the expression. For the purely exceptional cycles, I showed figures of "surfaces" of the relation $y^2(a, b, \varepsilon) = 0$, which were created with Mathematica's built-in function

$$\text{ContourPlot3D}\big[f == g, \{a, a_{\min}, a_{\max}\}, \{b, b_{\min}, b_{\max}\}, \{\varepsilon, \varepsilon_{\min}, \varepsilon_{\max}\}\big], \tag{B.4}$$

where obviously $y^2(a, b, \varepsilon) = 0$ was inserted for $f == g$, and where the coordinates were relabelled and restricted in an appropriate way (in particular, $\varepsilon \in [-1, 1]$). Similarly, I implemented the functions $y^2(a, b)$ with a fixed value of ε by making use of

$$\text{Plot3D}\big[f, \{a, a_{\min}, a_{\max}\}, \{b, b_{\min}, b_{\max}\}\big] \tag{B.5}$$

to plot the function $y^2(a, b)$ as a two-dimensional surface, depending on the coordinates a and b of a certain range. Helpful options were PlotRange (to specify the depicted values on

the vertical axis), Ticks (to show only the important parameter values), and "ClippingStyle $\rightarrow$ None", which yielded a better overview.

For the concrete integrations in chapter 4, which gave me the volumes of fractional, bulk, or exceptional cycles, I used Mathematica's numerical integration

$$\text{NIntegrate}[f, \{x_1, x_{1,\min}, x_{1,\max}\}, \{x_2, x_{2,\min}, x_{2,\max}\}] \tag{B.6}$$

with the option "WorkingPrecision $\rightarrow$ 10". For the variables x_1, x_2, I used the respective homogeneous coordinates in the hypersurface equations, see e.g. equation (4.34) or (4.53), whose concrete values specified which (two-)cycle was integrated over (and analogously for three-cycles). The concrete functions f for the integration can be found at the respective places in chapter 4. To study the behaviour of the volumes in dependence of a deformation parameter ε, I simply utilised

$$\text{Plot}[\text{NIntegrate}[f, \{\ldots\}, \{\ldots\}], \{\varepsilon, \varepsilon_{\min}, \varepsilon_{\max}\}]. \tag{B.7}$$

Unfortunately, some of these computations were quite time consuming, i.e. up to several hours or even days. Hence, for convenience I often used the built-in function

$$\text{DiscretePlot}[\text{expr}, \{\varepsilon, \varepsilon_{\min}, \varepsilon_{\max}, d\varepsilon\}], \tag{B.8}$$

where only specific points in steps $d\varepsilon$ were depicted (for instance $d\varepsilon = 0.2$). This plot was in most cases sufficient to see if the graph has the expected shape, and in the next step, to plot the complete curve using the expression in equation (B.7). A further built-in Mathematica function that is incorporated in my integrations is

$$\text{Boole}[\text{expr}] = \begin{cases} 1 & \text{if expr is true} \\ 0 & \text{if expr is false} \end{cases}, \tag{B.9}$$

which gives me a realisation of the Heaviside step function that was defined in equation (4.46).

The two-dimensional diagrams in the real x_1,x_2-plane, which show schematically the fractional cycles that appear in a certain orientifold, can be found in figures 13, 14 and 28. For arbitrary fixed values of one or several deformation parameters ε_i, these diagrams were built with Mathematica's function

$$\text{RegionPlot}[\text{pred}, \{x_1, x_{1,\min}, x_{1,\max}\}, \{x_2, x_{2,\min}, x_{2,\max}\}], \tag{B.10}$$

where for the prediction the condition $y^2(x_1, x_2) > 0$ (with the assumption $x_1, x_2 \in \mathbb{R}$) was inserted, which holds true for *sLag* cycles with real calibration. This made it possible to

directly distinguish between *sLag* cycles of real or imaginary calibration. Similarly, one could apply ContourPlot[...], where the relation $y^2(x_1, x_2) = 0$ had to be inserted, and where only the lines which border the cycles were apparent. Let me remark that the labels of the cycles could be nicely inserted into this diagram by making use of

$$\text{Epilog} \rightarrow \{\text{Inset}[\text{Graphics}[\text{Text}[\text{Style}[\text{"}<\text{label}>\text{"}, \text{Large}, \text{Bold}]]], \{x_1, x_2\}]\}, \quad \text{(B.11)}$$

and by combining this with the actual plot by employing Show$[g_1, g_2, \ldots]$.

As a fast method to check explicitly for a certain model which singularities were deformed and which ones stayed singular if one or several deformation parameters ε_i were switched on, I calculated

$$\begin{aligned} \text{Solve}[\{y^2(v_1, v_2, \varepsilon_1, \varepsilon_2, \ldots) &== 0, \\ D[y^2(v_1, v_2, \varepsilon_1, \varepsilon_2, \ldots), v_1] &== 0, \\ D[y^2(v_1, v_2, \varepsilon_1, \varepsilon_2, \ldots), v_2] &== 0\}, \{v_1, v_2\}], \end{aligned} \quad \text{(B.12)}$$

corresponding to equation (4.65) in the chart $x_i \equiv 1$. Below equation (4.65), I also explained why the coordinates v_i were here more favourable. The results directly showed which singularities were not deformed (i.e. still apparent) and if they also changed their position depending on the deformation parameters. In case that more singularities vanished than expected, one needed to calculate correction terms to keep them singular, as for example done in appendix A.

References

[1] M. B. Robinson, K. R. Bland, G. B. Cleaver, and J. R. Dittmann, "A Simple Introduction to Particle Physics. Part I - Foundations and the Standard Model," `arXiv:0810.3328 [hep-th]`.

[2] S. Braibant and G. Giacomelli, *Particles and fundamental interactions*. Undergraduate lecture notes in physics. Springer, Dordrecht, Netherlands, 2012. `http://www.springer.com/978-94-007-2463-1`.

[3] J. C. Maxwell, "On Physical Lines of Force," *Philosophical Magazine Series 4* **21, 23** (1861) .

[4] S. L. Glashow, J. Iliopoulos, and L. Maiani, "Weak Interactions with Lepton-Hadron Symmetry," *Phys. Rev.* **D2** (1970) 1285–1292.

[5] A. Salam, "Weak and Electromagnetic Interactions," *Conf. Proc.* **C680519** (1968) 367–377.

[6] S. Weinberg, "A Model of Leptons," *Phys. Rev. Lett.* **19** (1967) 1264–1266.

[7] K. Becker, M. Becker, and J. Schwarz, *String theory and M-theory: A modern introduction*. Cambridge University Press, 2007.

[8] L. E. Ibáñez and A. M. Uranga, *String theory and particle physics: An introduction to string phenomenology*. Cambridge University Press, 2012.

[9] R. Blumenhagen, D. Lüüst, and S. Theisen, *Basic concepts of string theory*. Theoretical and Mathematical Physics. Springer, Heidelberg, Germany, 2013.

[10] B. Zwiebach, *A first course in string theory*. Cambridge University Press, 2 ed., 2009.

[11] E. Witten, "String theory dynamics in various dimensions," *Nucl. Phys.* **B443** (1995) 85–126, `arXiv:hep-th/9503124 [hep-th]`.

[12] T. Kaluza, "Zum Unitätsproblem in der Physik," *Sitzungsberichte der Preussischen Akademie der Wissenschaften* **July-Dec 1921** (1918) 966–972.

[13] O. Klein, "Quantentheorie und fünfdimensionale Relativitätstheorie," *Zeitschrift für Physik* **37** (1926) 895–906.

[14] G. Veneziano, "Construction of a crossing - symmetric, Regge behaved amplitude for linearly rising trajectories," *Nuovo Cim.* **A57** (1968) 190–197.

[15] M. A. Virasoro, "Alternative constructions of crossing-symmetric amplitudes with regge behavior," *Phys. Rev.* **177** (1969) 2309–2311.

[16] J. A. Shapiro, "Narrow-resonance model with regge behavior for pi pi scattering," *Phys. Rev.* **179** (1969) 1345–1353.

[17] A. Neveu and J. H. Schwarz, "Factorizable dual model of pions," *Nucl. Phys.* **B31** (1971) 86–112.

[18] A. Neveu and J. H. Schwarz, "Quark Model of Dual Pions," *Phys. Rev.* **D4** (1971) 1109–1111.

[19] P. Ramond, "An Interpretation of Dual Theories," *Nuovo Cim.* **A4** (1971) 544–548.

[20] J. Scherk and J. H. Schwarz, "Dual Models for Nonhadrons," *Nucl. Phys.* **B81** (1974) 118–144.

[21] T. Yoneya, "Connection of Dual Models to Electrodynamics and Gravidynamics," *Prog. Theor. Phys.* **51** (1974) 1907–1920.

[22] M. B. Green and J. H. Schwarz, "Anomaly Cancellation in Supersymmetric D=10 Gauge Theory and Superstring Theory," *Phys. Lett.* **B149** (1984) 117–122.

[23] P. Candelas, G. T. Horowitz, A. Strominger, and E. Witten, "Vacuum Configurations for Superstrings," *Nucl. Phys.* **B258** (1985) 46–74.

[24] M. B. Green, J. Schwarz, and E. Witten, *Superstring Theory: Volume 1, Introduction.* Cambridge Monographs on Mathematical Physics. Cambridge University Press, 1987.

[25] M. B. Green, J. Schwarz, and E. Witten, *Superstring Theory: Volume 2, Loop Amplitudes, Anomalies and Phenomenology.* Cambridge Monographs on Mathematical Physics. Cambridge University Press, 1987.

[26] D. J. Gross, J. A. Harvey, E. J. Martinec, and R. Rohm, "The Heterotic String," *Phys. Rev. Lett.* **54** (1985) 502–505.

[27] D. J. Gross, J. A. Harvey, E. J. Martinec, and R. Rohm, "Heterotic String Theory. 1. The Free Heterotic String," *Nucl. Phys.* **B256** (1985) 253.

[28] D. J. Gross, J. A. Harvey, E. J. Martinec, and R. Rohm, "Heterotic String Theory. 2. The Interacting Heterotic String," *Nucl. Phys.* **B267** (1986) 75–124.

[29] L. J. Dixon, J. A. Harvey, C. Vafa, and E. Witten, "Strings on Orbifolds," *Nucl. Phys.* **B261** (1985) 678–686.

[30] L. J. Dixon, J. A. Harvey, C. Vafa, and E. Witten, "Strings on Orbifolds. 2.," *Nucl. Phys.* **B274** (1986) 285–314.

[31] K. S. Narain, "New Heterotic String Theories in Uncompactified Dimensions < 10," *Phys. Lett.* **B169** (1986) 41–46.

[32] K. S. Narain, M. H. Sarmadi, and E. Witten, "A Note on Toroidal Compactification of Heterotic String Theory," *Nucl. Phys.* **B279** (1987) 369–379.

[33] L. E. Ibanez, J. E. Kim, H. P. Nilles, and F. Quevedo, "Orbifold Compactifications with Three Families of SU(3) x SU(2) x U(1)**n," *Phys. Lett.* **B191** (1987) 282–286.

[34] L. E. Ibanez, J. Mas, H.-P. Nilles, and F. Quevedo, "Heterotic Strings in Symmetric and Asymmetric Orbifold Backgrounds," *Nucl. Phys.* **B301** (1988) 157–196.

[35] A. Font, L. E. Ibanez, and F. Quevedo, "Z(N) x Z(M) ORBIFOLDS AND DISCRETE TORSION," *Phys.Lett.* **B217** (1989) 272.

[36] K. Hori, S. Katz, A. Klemm, R. Pandharipande, R. Thomas, C. Vafa, R. Vakil, and E. Zaslow, *Mirror symmetry*, vol. 1 of *Clay mathematics monographs.* AMS, Providence, USA, 2003.
http://www.claymath.org/library/monographs/cmim01.pdf.

[37] J. H. Schwarz, "The power of M theory," *Phys. Lett.* **B367** (1996) 97–103, arXiv:hep-th/9510086 [hep-th].

[38] J. Polchinski, "Dirichlet Branes and Ramond-Ramond charges," *Phys. Rev. Lett.* **75** (1995) 4724–4727, arXiv:hep-th/9510017 [hep-th].

[39] J. Polchinski, *String theory. Vol. 1: An introduction to the bosonic string.* Cambridge Monographs on Mathematical Physics. Cambridge University Press, 1998.

[40] J. Polchinski, *String theory. Vol. 2: Superstring theory and beyond.* Cambridge Monographs on Mathematical Physics. Cambridge University Press, 1998.

[41] C. Angelantonj and A. Sagnotti, "Open strings," *Phys. Rept.* **371** (2002) 1–150, arXiv:hep-th/0204089 [hep-th]. [Erratum: Phys. Rept.376,no.6,407(2003)].

[42] M. Berkooz, M. R. Douglas, and R. G. Leigh, "Branes intersecting at angles," *Nucl. Phys.* **B480** (1996) 265–278, arXiv:hep-th/9606139 [hep-th].

[43] C. Bachas, "A Way to break supersymmetry," arXiv:hep-th/9503030 [hep-th].

[44] R. Blumenhagen, L. Görlich, B. Körs, and D. Lüst, "Noncommutative compactifications of type I strings on tori with magnetic background flux," *JHEP* **10** (2000) 006, `arXiv:hep-th/0007024 [hep-th]`.

[45] R. Blumenhagen, L. Görlich, B. Körs, and D. Lüst, "Magnetic flux in toroidal type I compactification," *Fortsch. Phys.* **49** (2001) 591–598, `arXiv:hep-th/0010198 [hep-th]`. [,1197(2000)].

[46] G. Aldazabal, S. Franco, L. E. Ibáñez, R. Rabadán, and A. Uranga, "Intersecting brane worlds," *JHEP* **0102** (2001) 047, `arXiv:hep-ph/0011132 [hep-ph]`.

[47] R. Blumenhagen, M. Cvetič, P. Langacker, and G. Shiu, "Toward realistic intersecting D-brane models," *Ann.Rev.Nucl.Part.Sci.* **55** (2005) 71–139, `arXiv:hep-th/0502005 [hep-th]`.

[48] R. Blumenhagen, B. Körs, D. Lüst, and S. Stieberger, "Four-dimensional String Compactifications with D-Branes, Orientifolds and Fluxes," *Phys.Rept.* **445** (2007) 1–193, `arXiv:hep-th/0610327 [hep-th]`.

[49] M. Cvetič, G. Shiu, and A. M. Uranga, "Chiral four-dimensional N=1 supersymmetric type 2A orientifolds from intersecting D6 branes," *Nucl.Phys.* **B615** (2001) 3–32, `arXiv:hep-th/0107166 [hep-th]`.

[50] M. Cvetič, G. Shiu, and A. M. Uranga, "Three family supersymmetric standard - like models from intersecting brane worlds," *Phys.Rev.Lett.* **87** (2001) 201801, `arXiv:hep-th/0107143 [hep-th]`.

[51] L. E. Ibáñez, F. Marchesano, and R. Rabadan, "Getting just the standard model at intersecting branes," *JHEP* **0111** (2001) 002, `arXiv:hep-th/0105155 [hep-th]`.

[52] R. Blumenhagen, B. Körs, D. Lüst, and T. Ott, "The standard model from stable intersecting brane world orbifolds," *Nucl. Phys.* **B616** (2001) 3–33, `arXiv:hep-th/0107138 [hep-th]`.

[53] Ralph Blumenhagen and Volker Braun and Boris Körs and Dieter Lüst, "Orientifolds of K3 and Calabi-Yau manifolds with intersecting D-branes," *JHEP* **0207** (2002) 026, `arXiv:hep-th/0206038 [hep-th]`.

[54] Ralph Blumenhagen and Lars Görlich and Tassilo Ott, "Supersymmetric intersecting branes on the type 2A $T^6/\mathbb{Z}_4$ orientifold," *JHEP* **0301** (2003) 021, `arXiv:hep-th/0211059 [hep-th]`.

134

[55] G. Honecker and T. Ott, "Getting just the supersymmetric standard model at intersecting branes on the $\mathbb{Z}_6$ orientifold," *Phys.Rev.* **D70** (2004) 126010, `arXiv:hep-th/0404055 [hep-th]`.

[56] G. Honecker, "Chiral N=1 4-D orientifolds with D-branes at angles," *Mod.Phys.Lett.* **A19** (2004) 1863–1879, `arXiv:hep-th/0407181 [hep-th]`.

[57] D. Bailin and A. Love, "Towards the supersymmetric standard model from intersecting D6-branes on the Z-prime(6) orientifold," *Nucl.Phys.* **B755** (2006) 79–111, `arXiv:hep-th/0603172 [hep-th]`.

[58] Florian Gmeiner and Dieter Lüst and Maren Stein, "Statistics of intersecting D-brane models on $T^6/\mathbb{Z}_6$," *JHEP* **0705** (2007) 018, `arXiv:hep-th/0703011 [hep-th]`.

[59] F. Gmeiner and G. Honecker, "Mapping an Island in the Landscape," *JHEP* **0709** (2007) 128, `arXiv:0708.2285 [hep-th]`.

[60] F. Gmeiner and G. Honecker, "Millions of Standard Models on Z-prime(6)?," *JHEP* **0807** (2008) 052, `arXiv:0806.3039 [hep-th]`.

[61] D. Bailin and A. Love, "Constructing the supersymmetric Standard Model from intersecting D6-branes on the Z(6)-prime orientifold," *Nucl.Phys.* **B809** (2009) 64–109, `arXiv:0801.3385 [hep-th]`.

[62] G. Honecker and J. Vanhoof, "Towards the field theory of the Standard Model on fractional D6-branes on T6/Z6': Yukawa couplings and masses," *Fortsch.Phys.* **60** (2012) 1050–1056, `arXiv:1201.5872 [hep-th]`.

[63] Stefan Förste and Gabriele Honecker and Ralph Schreyer, "Supersymmetric $\mathbb{Z}_N \times \mathbb{Z}_M$ orientifolds in 4-D with D branes at angles," *Nucl.Phys.* **B593** (2001) 127–154, `arXiv:hep-th/0008250 [hep-th]`.

[64] G. Honecker, "Chiral supersymmetric models on an orientifold of $\mathbb{Z}_4 \times \mathbb{Z}_2$ with intersecting D6-branes," *Nucl.Phys.* **B666** (2003) 175–196, `arXiv:hep-th/0303015 [hep-th]`.

[65] D. Bailin and A. Love, "Intersecting D6-branes on the $\mathbb{Z}_{12}$-II orientifold," *JHEP* **1401** (2014) 009, `arXiv:1310.8215 [hep-th]`.

[66] S. Förste and G. Honecker, "Rigid D6-branes on $T^6/(\mathbb{Z}_2 \times \mathbb{Z}_{2M} \times \Omega\mathcal{R})$ with discrete torsion," *JHEP* **1101** (2011) 091, `arXiv:1010.6070 [hep-th]`.

[67] G. Honecker, M. Ripka, and W. Staessens, "The Importance of Being Rigid: D6-Brane Model Building on $T^6/\mathbb{Z}_2 \times \mathbb{Z}'_6$ with Discrete Torsion," *Nucl.Phys.* **B868** (2013) 156–222, `arXiv:1209.3010 [hep-th]`.

[68] G. Honecker and W. Staessens, "D6-Brane Model Building and Discrete Symmetries on $T^6/(\mathbb{Z}_2 \times \mathbb{Z}_6 \times \Omega\mathcal{R})$ with Discrete Torsion," *PoS* **Corfu2012** (2013) 107, `arXiv:1303.6845 [hep-th]`.

[69] J. Ecker, G. Honecker, and W. Staessens, "Rigour and rigidity: Systematics on particle physics D6-brane models on $\mathbb{Z}_2 \times \mathbb{Z}_6$," *Fortsch.Phys.* **62** (2014) 981–1040, `arXiv:1409.1236 [hep-th]`.

[70] J. Ecker, G. Honecker, and W. Staessens, "D6-Brane Model Building on $\mathbb{Z}_2 \times \mathbb{Z}_6$: MSSM-like and Left-Right Symmetric Models," *arXiv:1509.00048[hep-th]* (2015) , `arXiv:1509.00048 [hep-th]`.

[71] R. Blumenhagen, M. Cvetič, F. Marchesano, and G. Shiu, "Chiral D-brane models with frozen open string moduli," *JHEP* **0503** (2005) 050, `arXiv:hep-th/0502095 [hep-th]`.

[72] C. Vafa, "Modular Invariance and Discrete Torsion on Orbifolds," *Nucl.Phys.* **B273** (1986) 592.

[73] E. Palti, "Model building with intersecting D6-branes on smooth Calabi-Yau manifolds," *JHEP* **0904** (2009) 099, `arXiv:0902.3546 [hep-th]`.

[74] D. Joyce, "Lectures on Calabi-Yau and special Lagrangian geometry," *math/0108088* (2001) , `arXiv:math/0108088 [math-dg]`.

[75] D. Joyce, "Lectures on special Lagrangian geometry," *math/0111111* (2001) , `arXiv:math/0111111 [math-dg]`.

[76] M. R. Douglas, "The Statistics of string / M theory vacua," *JHEP* **05** (2003) 046, `arXiv:hep-th/0303194 [hep-th]`.

[77] C. Vafa, "The String landscape and the swampland," `arXiv:hep-th/0509212 [hep-th]`.

[78] D. Lüst, "String Landscape and the Standard Model of Particle Physics," `arXiv:0707.2305 [hep-th]`.

[79] A. N. Schellekens, "The String Theory Landscape," *Adv. Ser. Direct. High Energy Phys.* **22** (2015) 155–217.

[80] M. Graña, "Flux compactifications in string theory: A Comprehensive review," *Phys. Rept.* **423** (2006) 91–158, `arXiv:hep-th/0509003 [hep-th]`.

[81] P. G. Camara, A. Font, and L. E. Ibáñez, "Fluxes, moduli fixing and MSSM-like vacua in a simple IIA orientifold," *JHEP* **09** (2005) 013, `arXiv:hep-th/0506066 [hep-th]`.

[82] G. Aldazabal, P. G. Camara, A. Font, and L. E. Ibáñez, "More dual fluxes and moduli fixing," *JHEP* **05** (2006) 070, `arXiv:hep-th/0602089 [hep-th]`.

[83] D. Bailin and A. Love, "Stabilising the supersymmetric Standard Model on the $\mathbb{Z}_6'$ orientifold," *Nucl.Phys.* **B854** (2012) 700–737, `arXiv:1104.3522 [hep-th]`.

[84] T. Hübsch, *Calabi-Yau Manifolds - A Bestiary for Physicists*. World Scientific, 1992.

[85] P. Griffiths and J. Harris, *Principles of Algebraic Geometry*. Wiley-Interscience, 1 ed., 1994.

[86] T. Eguchi, P. B. Gilkey, and A. J. Hanson, "Gravitation, Gauge Theories and Differential Geometry," *Phys. Rept.* **66** (1980) 213.

[87] P. S. Aspinwall, "(2,2) Superconformal Field Theories Near Orbifold Points," *Commun. Math. Phys.* **128** (1990) 593.

[88] P. S. Aspinwall, "Resolution of orbifold singularities in string theory," `arXiv:hep-th/9403123 [hep-th]`.

[89] D. Lüst, S. Reffert, E. Scheidegger, and S. Stieberger, "Resolved Toroidal Orbifolds and their Orientifolds," *Adv.Theor.Math.Phys.* **12** (2008) 67–183, `arXiv:hep-th/0609014 [hep-th]`.

[90] S. Reffert, "Toroidal Orbifolds: Resolutions, Orientifolds and Applications in String Phenomenology," `arXiv:hep-th/0609040 [hep-th]`.

[91] S. Reffert, "The Geometer's Toolkit to String Compactifications," `arXiv:0706.1310 [hep-th]`.

[92] M. Cvetič, T. Liu, and M. B. Schulz, "Twisting $K3 \times T^2$ orbifolds," *JHEP* **0709** (2007) 092, `arXiv:hep-th/0701204 [hep-th]`.

[93] S. Groot Nibbelink, M. Trapletti, and M. Walter, "Resolutions of C**n/Z(n) Orbifolds, their U(1) Bundles, and Applications to String Model Building," *JHEP* **0703** (2007) 035, `arXiv:hep-th/0701227 [hep-th]`.

[94] S. Groot Nibbelink, T.-W. Ha, and M. Trapletti, "Toric Resolutions of Heterotic Orbifolds," *Phys. Rev.* **D77** (2008) 026002, `arXiv:0707.1597 [hep-th]`.

[95] S. Groot Nibbelink, D. Klevers, F. Ploger, M. Trapletti, and P. K. S. Vaudrevange, "Compact heterotic orbifolds in blow-up," *JHEP* **04** (2008) 060, `arXiv:0802.2809 [hep-th]`.

[96] S. Groot Nibbelink, J. Held, F. Rühle, M. Trapletti, and P. K. Vaudrevange, "Heterotic Z(6-II) MSSM Orbifolds in Blowup," *JHEP* **0903** (2009) 005, `arXiv:0901.3059 [hep-th]`.

[97] M. Blaszczyk, S. Groot Nibbelink, F. Rühle, M. Trapletti, and P. K. Vaudrevange, "Heterotic MSSM on a Resolved Orbifold," *JHEP* **1009** (2010) 065, `arXiv:1007.0203 [hep-th]`.

[98] M. Blaszczyk, S. Groot Nibbelink, and F. Rühle, "Gauged Linear Sigma Models for toroidal orbifold resolutions," *JHEP* **1205** (2012) 053, `arXiv:1111.5852 [hep-th]`.

[99] S. P. Martin, "A Supersymmetry primer," `arXiv:hep-ph/9709356 [hep-ph]`. [Adv. Ser. Direct. High Energy Phys.18,1(1998)].

[100] M. Dine, N. Seiberg, and E. Witten, *Fayet-Iliopoulos Terms in String Theory*, vol. B289. Nucl. Phys., 1987.

[101] J. J. Atick, L. J. Dixon, and A. Sen, "String Calculation of Fayet-Iliopoulos d Terms in Arbitrary Supersymmetric Compactifications," *Nucl. Phys.* **B292** (1987) 109–149.

[102] R. Blumenhagen, G. Honecker, and T. Weigand, "Non-Abelian brane worlds: The Open string story," in *2nd Southeastern European Workshop on Challenges Beyond the Standard Model (BW2005) Vrnjacka Banja, Serbia, Nis, Serbia, May 19-23, 2005*. 2005. `arXiv:hep-th/0510050 [hep-th]`.

[103] R. Blumenhagen, G. Honecker, and T. Weigand, "Supersymmetric (non-)Abelian bundles in the Type I and SO(32) heterotic string," *JHEP* **08** (2005) 009, `arXiv:hep-th/0507041 [hep-th]`.

[104] L. B. Anderson, J. Gray, A. Lukas, and B. Ovrut, "Stabilizing the Complex Structure in Heterotic Calabi-Yau Vacua," *JHEP* **02** (2011) 088, `arXiv:1010.0255 [hep-th]`.

[105] L. B. Anderson, J. Gray, A. Lukas, and B. Ovrut, "Stabilizing All Geometric Moduli in Heterotic Calabi-Yau Vacua," *Phys. Rev.* **D83** (2011) 106011, `arXiv:1102.0011 [hep-th]`.

[106] L. B. Anderson, J. Gray, A. Lukas, and B. Ovrut, "The Atiyah Class and Complex Structure Stabilization in Heterotic Calabi-Yau Compactifications," *JHEP* **10** (2011) 032, `arXiv:1107.5076 [hep-th]`.

[107] L. B. Anderson, J. Gray, A. Lukas, and B. Ovrut, "Vacuum Varieties, Holomorphic Bundles and Complex Structure Stabilization in Heterotic Theories," *JHEP* **07** (2013) 017, `arXiv:1304.2704 [hep-th]`.

[108] C. Vafa and E. Witten, "On orbifolds with discrete torsion," *J.Geom.Phys.* **15** (1995) 189–214, `arXiv:hep-th/9409188 [hep-th]`.

[109] M. Blaszczyk, G. Honecker, and I. Koltermann, "Circling the square: deforming fractional D-branes in type II/$\Omega\mathcal{R}$ orientifolds," *JHEP* **07** (2014) 124, `arXiv:1403.2394 [hep-th]`.

[110] M. Blaszczyk, G. Honecker, and I. Koltermann, "Deformations on Tilted Tori and Moduli Stabilisation at the Orbifold Point," *JHEP* **11** (2015) 019, `arXiv:1507.07568 [hep-th]`.

[111] I. Koltermann, M. Blaszczyk, and G. Honecker, "Deforming D-brane models on $T^6/(\mathbb{Z}_2 \times \mathbb{Z}_{2M})$ orbifolds," *Fortsch. Phys.* **64** (2016) 412–413, `arXiv:1511.03549 [hep-th]`.

[112] G. Honecker, I. Koltermann, and W. Staessens, "work in progress." 2016.

[113] B. R. Greene, "String theory on Calabi-Yau manifolds," in *Fields, strings and duality. Proceedings, Summer School, Theoretical Advanced Study Institute in Elementary Particle Physics, TASI'96, Boulder, USA, June 2-28, 1996*, pp. 543–726. 1996. `arXiv:hep-th/9702155 [hep-th]`.

[114] V. Bouchard, "Lectures on complex geometry, Calabi-Yau manifolds and toric geometry," in *Proceedings of the Modave Summer School in Mathematical Physics 2005*. Solvay Institute, 2007. `arXiv:hep-th/0702063 [hep-th]`.

[115] M. Nakahara, *Geometry, topology and physics*. Graduate Student Series in Physics. CRC Press, 2 ed., 2003.

[116] P. Candelas, "Lectures on complex manifolds," in **TRIESTE 1987, PROCEEDINGS, SUPERSTRINGS '87**, pp. 1–88. 1987.

[117] E. Calabi, "On Kähler manifolds with vanishing canonical class," *Algebraic geometry and topology. A symposium in honor of S. Lefschetz* (1957) 78–89.

[118] S. T. Yau, "On the Ricci curvature of a compact Kähler manifold and the complex Monge-Ampere equation. I," *Communications on Pure and Applied Mathematics* (1978) 339–411.

[119] W. Chow, "On Compact Complex Analytic Varieties," *American Journal of Mathematics* **71** no. 4, (1949) 893–914.

[120] K. Chandrasekharan, *Elliptic functions*, vol. 281 of *Grundlehren der mathematischen Wissenschaften.* Springer Berlin Heidelberg, 1985.

[121] S. Lang, *Elliptic Functions*, vol. 112 of *Graduate Texts in Mathematics.* Springer-Verlag New York, 2 ed., 1987.

[122] R. Blumenhagen and E. Plauschinn, "Introduction to conformal field theory," *Lect. Notes Phys.* **779** (2009) 1–256.

[123] A. N. Schellekens, "Introduction to conformal field theory," *Fortsch. Phys.* **44** (1996) 605–705.

[124] L. J. Dixon, "INTRODUCTION TO CONFORMAL FIELD THEORY AND STRING THEORY," in *Boulder ASI 1989:509-560*, pp. 509–560. 1989.

[125] P. H. Ginsparg, "APPLIED CONFORMAL FIELD THEORY," in *Les Houches Summer School in Theoretical Physics: Fields, Strings, Critical Phenomena Les Houches, France, June 28-August 5, 1988.* 1988. `arXiv:hep-th/9108028 [hep-th]`.

[126] M. R. Gaberdiel, "An Introduction to conformal field theory," *Rept. Prog. Phys.* **63** (2000) 607–667, `arXiv:hep-th/9910156 [hep-th]`.

[127] L. J. Dixon, D. Friedan, E. J. Martinec, and S. H. Shenker, "The Conformal Field Theory of Orbifolds," *Nucl. Phys.* **B282** (1987) 13–73.

[128] E. G. Gimon and J. Polchinski, "Consistency conditions for orientifolds and d manifolds," *Phys.Rev.* **D54** (1996) 1667–1676, `arXiv:hep-th/9601038 [hep-th]`.

[129] M. Bianchi and A. Sagnotti, "On the systematics of open string theories," *Phys.Lett.* **B247** (1990) 517–524.

[130] G. Honecker, "Kähler metrics and gauge kinetic functions for intersecting D6-branes on toroidal orbifolds - The complete perturbative story," *Fortsch.Phys.* **60** (2012) 243–326, `arXiv:1109.3192 [hep-th]`.